January 2015

INTELLIGENT SENSOR SYSTEM FOR SELECTED ENVIRONMENTAL SAFETY APPLICATION

CHEN-LIN SONG
Purdue University

Graduate School Form 30
Updated 1/15/2015

PURDUE UNIVERSITY
GRADUATE SCHOOL
Thesis/Dissertation Acceptance

This is to certify that the thesis/dissertation prepared

By CHEN-LIN SONG

Entitled
INTELLIGENT SENSOR SYSTEM FOR SELECTED ENVIRONMENTAL SAFETY APPLICATION

For the degree of Master of Science

Is approved by the final examining committee:

Suranjan Panigrahi
Chair

Robert J Herrick

Ronald F Turco

To the best of my knowledge and as understood by the student in the Thesis/Dissertation Agreement, Publication Delay, and Certification Disclaimer (Graduate School Form 32), this thesis/dissertation adheres to the provisions of Purdue University's "Policy of Integrity in Research" and the use of copyright material.

Approved by Major Professor(s): Suranjan Panigrahi

Approved by: Kathryne A Newton 6/24/2015
Head of the Departmental Graduate Program Date

INTELLIGENT SENSOR SYSTEM FOR SELECTED ENVIRONMENTAL SAFETY APPLICATION

A Thesis

Submitted to the Faculty

of

Purdue University

by

Chen-Lin Song

In Partial Fulfillment of the

Requirements for the Degree

of

Master of Science

December 2015

Purdue University

West Lafayette, Indiana

ACKNOWLEDGEMENTS

The Author would like to thank his major advisor and his thesis committee member for their effort and time:

Dr. Panigrahi

Prof. Herrick

Dr. Turco

The author also wants to thank Dr. Jennifer Freeman for providing her lab space (Freeman Lab, Lilly Hall in Purdue University). Also, the author appreciated the help and time from Sara E Wirbisky, the lead of the laboratory in Lilly Hall at Purdue University. In addition, the author wants to thank friends who supported and encouraged throughout this process. Finally, the author would like to thank his parents. Without them, the author would not be able to have the opportunity to start the journey in the United States and also obtain the professional knowledge in past seven years.

TABLE OF CONTENTS

Page

Page

LIST OF TABLES

Table Page

Table Page

LIST OF FIGURES

Figure Page

Figure Page

Figure Page

Figure Page

Figure Page

Figure Page

Figure Page

Figure Page

ABSTRACT

Song, Chen-Lin. M.S., Purdue University, December 2015. Intelligent Sensor System for Selected Environmental Safety Applications. Major Professor: Suranjan Panigrahi

This study focuses on two objectives. The first objective is to develop an integrated sensor system, called electronic nose (E-nose). E-nose has the ability to detect selected gases in the air. In this study, the interests of gas are Volatile organic compound (VOC), Ammonia and Carbon dioxide. The second object is to evaluate a system that can discriminate arsenic contamination levels in water, the researchers call it Electronic tongue (E-tongue). The system is based on using interdigitated dielectric sensing mode. Finally, demonstrating both systems (E-nose and E-tongue) are capable of detecting the specific targets (pollutant/ contaminant) in selected environments (air/water).

CHAPTER 1. INTRODUCTION

In chapter 1, the problem, the scope, and the significance are introduced. Also, the technical term used in this study would be defined. Lastly, there are the assumption, delimitations and limitations.

1.1 Statement of Problem

Nowadays countries have built many industries in order to diversify and strengthen their economies. However, those factories emit various toxic gases and industrial waste that endanger our environment. Acid rain, eutrophication and global climate change are the consequences of air pollution. According to NASA, these industrial activities have raised the atmospheric carbon dioxide level from 280 parts per million to 379 parts per million in the last 150 years. That's also one of the reasons why the average of the global temperature has been gradually increasing since two to three decades ago. On the other hand, United States Environmental Protection Agency (U.S. EPA) estimates, 1.2 trillion gallons of untreated sewage and industrial waste is dumped into U.S. waters annually. Approximately, 700 million people globally drink contaminated water.

As a result of the pollution, human health begins to drive a huge topic of discussion in today's media. According to the study, air/water pollution can cause different levels of effects on human health, such as nausea, difficulty in breathing, ski

irritation and cancer. The World health Organization (WHO) reported that a total of 7 million people, one-eighth of the world's total population, died because of air pollution exposure. Out of the 7 million, 6.7 million died of outdoor air pollution and 4.3 million died of indoor air pollution. Furthermore, according to UNICEF more than 3,000 children die every day all over the world due to consumption of contaminated drinking water.

1.2 Significant

The world population has increased tremendously over the past decade, and many human-made activities resulted in an increase in high demand for ease of living, such as increased reliance on automobiles, chemical applications in the household, high-tech manufacturing, agricultural products etc. However, these activities cause a large amount of chemical pollutants in air and water. Usually, compounds that harm a human's health are odorless, colorless and tasteless, so it is really hard for human to be aware of them. People inhale and drink these contaminants from air and water without a clue. Thesis contaminants could potentially lead to Lung disease, allergies, cancer and other illnesses. Recently, this has become a serious focus around the globe.

Human beings have the ability to smell, but cannot quantify odors and contaminants in water. Thus, a system to monitor the level of pollution in the air and water is needed to prevent people from over inhaling/ injecting harmful contaminants.

1.3 Research Question

The research question of this study is:

Is it possible to detect contaminants in air and water using an intelligent olfactory and gustatory system?

1.4 Scope

Today, people are very conscious about life quality and health. People want to live in places with uncontaminated air and water but are also conscious about whether or not they are exposed to hazardous gases and wastes. However, most detection instruments are for laboratory use and not for household use. The prices of these instruments are not affordable for the general public.

The long-term goal of our research group is to develop portable intelligent sensor system for selected environmental safety applications. This research (thesis) focuses on developing intelligent sensor system for selected air and water contaminants. For air pollutants, we will target selected air pollutants: volatile organic compound (VOC), carbon dioxide and ammonia. For water contaminants, we will focus on Arsenic, a heavy metal with multiple adverse health effects.

This research project was designed from a system's perspective while focusing on the usability of the developed system in real-world scenario. This frame work involves synergy between multiple domains (i.e. material handling, electronic hardware, computational software, user interface design and specific application domain related expertise/information) of cross cutting scientific area/disciplines.

From a practical consideration, it would be very difficult or could take more time for a typical student enrolled in a M.S. program. Thus, key and a majority of the concepts and techniques conceived by the major professor (Dr. Panigrahi) were communicated to the student as a form of training. The student was given opportunity to exercise his skills in electrical and computational related hardware and software skills to develop and

evaluate the system for specific application. This approach of training has many advantages and prepares the student well for solving real world problems.

Thus, the followings are associated specific objectives:

1. Develop, adapt and evaluate an integrated electronic sensor system for assessment of air quality in selected application domain.
2. Integrate and evaluate a proof-of-the concept of E-tongue (electronic tongue) system for detection of contaminates in liquid. In this study, the research used arsenic contamination in water as a specific application.

1.5 Definitions

This section defines the key terminology used through this research:

Arsenic – "Arsenic is a chemical element with symbol "As" and atomic number 33. Arsenic occurs in many minerals, usually in conjunction with sulfur and metals, and also as a pure elemental crystal."

Electronic nose -"an instrument which comprises an array of electronic chemical sensors with partial specificity and appropriate pattern recognition system, capable of recognizing simple or complex odors" (Gardner & Bartlett, 1994, p. 115).

Intelligent sensor system- an intelligent sensor system has the following basic characteristics:

1. It can be adaptive to the environment with high detection performance and communication and low power consumption (Swanson, 2000).
2. It has the ability to acquires raw data and analyze it either pre-programmed or self-learned (Swanson, 2000).

3. It has self-awareness ability through calibration, internal process control check, and measurements in different operation (Swanson, 2000).
4. It has re-programmable ability and allows external access all levels of processed data (Swanson, 2000).
5. It not only can do pattern recognition but also perdition of future patterns (Swanson, 2000).

Transducers (sensors) - it is a device provides the information of physical, chemical, and biological properties of an object or process.

CHAPTER 2. LITERATURE REVIEW

The goal of building an intelligent olfactory and gustatory sensor system for environment is based on safety and sustainability application that requires an understanding of the development of an electrical nose and how the technology can best be applied in reality. The concept of an electronic nose and tongue has been widely adopted in various applications such as industry, healthy, food and safety. In this research, the literature review focuses on the system description of an electronic nose and tongue for both hardware and software, and the applications that are used with the technology.

2.1 System Description – Electronic Nose and Tongue

The electronic nose consists of "an array of chemical gas sensors with a broad and partly overlapping selectivity for measurement of volatile compounds within the headspace over a sample combined with computerized multivariate statistical data processing tools" (Gardner & Bartlett, 1994, p. 115). The block diagram of the electronic nose is shown in Figure 2.1.

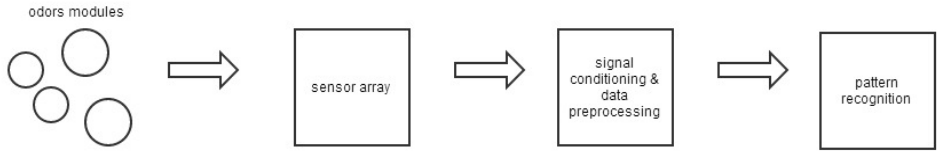

Figure 2.1 The block diagram of electronic nose (Arshak, Moore, Lyons, Harris & Clifford , 2004)

2.1.1 Sensor, Data acquisition, related Hardware

2.1.1.1 Transducer

There are different kinds of gas/taste sensors that can be implemented into a sensor system: metal oxide semiconductors (MOS), metal oxide semiconducting field effect transistors (MOSFET), conducting polymer (CP), oscillating sensors, and optical sensor.

A MOSFET sensor operates at certain range of temperature (100~200°C) (Lundstrom, Spetz, Winquist, Ackelid, & Sundgren, 1990). The operation of MOSFET based on "a change of potential in the sensor due to electrical polarization when molecules react on the catalytic surface" (Haugen & Kvaal, 1998, p. 234). The other type of gas sensor is MOS, the principle is "the reaction between adsorbed oxygen on the oxide surface with incoming molecules" (Haugen & Kvaal, 1998 , p.234) with a specific operating temperature (200-500°C) (Gardner, Shurmer, & Corcoran, 1991). For both sensors, their selectivity and sensitivity are changed by the temperature and the choice of metal used (Haugen & Kvaal, 1998).

Next, the concept of conducing polymer is depended on the conductivity of the polymers when volatiles interface with the polymers. The sensitivity and selectivity are relied on the different doping ions and the structure of the polymer. One advantage is that

there is no specific temperature range for using this kind of sensor (Haugen & Kvaal, 1998).

The principle of an oscillating sensor, then, is that "the adsorption of molecules onto the sensing layer result in a decrease in frequency due to increased mass and sometime a changed viscosity of the sensing layer" (Haugen & Kvaal, 1998, p. 296). Two types of oscillating sensors include quartz crystal microbalance sensor (QCM) and surface acoustic wave (SAW) sensor. By changing the composition of the coasted sensing layer and the operation frequency, the selectivity and sensitivity can be altered (Haugen & Kvaal, 1998). The operation frequency for a SAW sensor is 50-1000MHz and 5-30 MHz for a QCM sensor (Hao, Tang, Ku, Chao, Li, Yang & Yao, 2009).

Comparing among of the sensors mentioned above, the most common sensor for commercial electronic sensor is a metal oxide semiconductor and conducting organic polymers due to the simple electrical properties and interface circuit (Pearce, Schiffman, Nagle & Gardner, 2003). Moreover, there are more recent instruments that use an oscillating sensor due to high sensitivity, fully reversible behavior and high S/N ratio (Hao et al., 2009).

2.1.1.2 Interface circuitry

Interface circuitry is to generate an electrical signal from the sensor response. There are various ways to interface with the sensor. This subsection only focuses on the interface circuitry for MOS senor, MOSFT sensor and oscillating sensor.

For a conductance sensor, the existence of odors changes the sensor resistance. Two types of resistance measurements are voltage divider and Wheatstone bridge. The

circuit structure of a voltage divider is that the sensor is placed in series with a load resistor and a DC voltage source. The load resistor should be selected to maximize the sensitivity of the circuit. The equation of voltage divider is shown in equation 2.1, (Pearce et al., 2003):

$$V_L = \frac{Vcc}{Rs+RL} \times RL \qquad \text{(Equation. 2.1)}$$

Based on the equation 2.1, the resistance of the sensor is changed with respect to the voltage across the sensor (Pearce et al., 2003). Moreover, the voltage divider is popular to use in an analog field due to its simplicity, but there are some disadvantages. Firstly, it is not suitable if the relationship between sensor resistance and output voltage is nonlinear. Secondly, it is only applicable for a sensor with large among of resistance change. In order to solve the limitation, a Wheatstone bridge is one method to measure the small resistance change. The principle is to subtract the offset voltage with the sensor voltage. Equation 2.2 shows this (Pearce et al., 2003).

$$Vout = Vcc\left(\frac{RL}{Rs+RL} - \frac{R2}{R1+R2}\right) \qquad \text{(Equation. 2.2)}$$

The R1, R2 and RL are selected based on the sensor baseline resistance.

The instrumentation designs for SAW and QCM sensors are oscillator circuits, vector voltmeters, and network analyzers. An oscillator circuit consists of a RF amplifier and a frequency counter (Pearce et al., 2003). The benefits are low cost, simplicity and good frequency stability, but the limitation is that it only provides the frequency velocity without amplitude measurement (Pearce et al., 2003). The vector voltmeters, however, overcome the problem, and can measure the velocity and amplitude. Nevertheless, the disadvantage is that it is expensive and not suitable for portable sensor system. The

network analyzer has more detail than the previous two options, but the price is not affordable for most applications.

For the field-effect gas sensor (e.g., MOSFET), the measurement can be achieved by using constant-voltage circuits or constant-current (Pearce et al., 2003). Like the previous review on the MOSFET sensor, it operates at certain high temperature ranges, so it requires the circuit that can efficiently control the temperature.

2.1.1.3 Processor

Processor is another indispensable part in an electronic nose and tongue. The purpose is to process the signal from the sensor and classify the data to become meaningful information to a human. Because there are varieties of processors to choose from, the criteria for the selection of a processor are based on the processing time (i.e., desired speed), the environment, and the budget of the project. Many researchers used a PC as the processor for the electronic nose and tongue because it has the fastest processing time, but the disadvantages are extensive power consumption, high expense, and the lack of portability (Chiu & Tang , 2013). Microprocessors have been used in an electronic nose and tongue for couple of years (Chiu & Tang , 2013). The advantages are low cost, compact size, low power consumption, and portability (Chiu & Tang , 2013). The drawbacks are the processing time is slower than PC and the designer needs to integrate external peripherals (i.e., ADC converter, memory etc.) with the processor to become a completed sensor system.

Next, some recent researchers have used a microcontroller for electronic nose, which provides advantages that are similar to that of a microprocessor except that the

designer does not need to integrate external peripherals because most of them already have the peripherals built into the system. The disadvantage however results from the relatively incompetent speed performance compared to the PC. Moreover, recent research has focused on the integration between an array of odor sensors and System on a Chip (SoC) technology (Chiu , Wang, Lin, Chang, Chen & Tang, 2012). The definition of SoC is an integrated circuit that combines all the components of a computer into a chip. It is quite similar to a microcontroller, but the processing speed and physical size is much better than a microprocessor or microcontroller. For example, the processor used in a smartphone is applied SoC technology.

2.1.2 Software (Pattern recognition)

The software of an electronic nose and tongue implies preprocessing and multivariate pattern recognition (Pearce et al., 2003). The purpose of preprocessing is to take out applicable information from the sensor and make sure that the data is compatible for subsequent pattern recognition. Preprocessing is divided into three stages- baseline manipulation, compression, and normalization (Pearce et al., 2003). The multivariate pattern recognition has two categories. One is statistical methods and the other one is biological methods.

2.1.2.1 Preprocessing

For artificial nose, the first stage of preprocessing is baseline manipulation. It controls the output of the sensor relative to the baseline (Gutierrez-Osuna, 2002). There are three common methods to compensate for the baseline (Table 2.1). Fractional change has the best performance for pattern recognition for metal oxide sensors and the

differential measurement is commonly used by surface acoustic wave and MOSFETS sensor (Pearce et al., 2003).

Table 2.1 *Baseline manipulation method (Nord, 2006)*

Method	Equation	Purpose
Difference	$X_{ij} = R_s - R_o$	Remove additive error
Relative	$X_{ij} = \frac{R_s}{R_o}$	Remove multiplicative error and dimension number
Fractional	$X_{ij} = \frac{R_s - R_o}{R_o}$	Overcome restricted concentration range of relative method

X_{ij} is the i^{th} baseline manipulated value in vector j.

R_s is the i^{th} value in vector j.

R_o is the baseline value of vector j.

Compression is the second stage of preprocessing. Fundamentally, it produces an illustrative constant by squeezing the response of sensor. Three algorithms are sub-sampling, parameter extraction and model fitting. The metal oxide semiconductor and conducting polymer are commonly compressed using sub-sampling or model fitting, and parameter extraction frequently employs in metal insulated semiconductor field-effect transistor (Gutierrez-Osuna, 2002). The compression can improve selectivity, reduce acquisition time and increase sensor lifetime (Pearce et al., 2003).

The last stage of preprocessing is normalization, an action that prepares the processed vector for later pattern analysis (Gutierrez-Osuna, 2002). There are two classes: local method and global method. The local method, also called vector normalization, is "the feature vector of each individual "sniff" is divided by its norm and is forced to lie on

a hyper-sphere of unit radius" (Gutierrez-Osuna, 2002, p. 14). It is used when odors have different concentrations, and the judgment is not based on the odor quality but instead intensity (Gutierrez-Osuna, 2002). Global methods, on the other hand, are used to protect the comparability of the sensor magnitude (Gutierrez-Osuna, 2002). Sensor auto scaling and sensor normalization are the most common global methods for an electronic nose (Gutierrez-Osuna, 2002).

Similar preprocessing techniques are used for the electronic tongue as well.

2.1.2.2 Multivariate pattern

Pattern recognition in an electronic nose and tongue is to let users have detailed understanding of the relationship between the response from the array of sensors versus the odor's class and concentration (Pearce et al., 2003). There are two classes: parametric and non-parametric. Parametric is commonly referred to as a statistical approach. In most cases, the data set is normally distributed with a constant mean and variance. These methods include multiple linear regression (MLR), partial least square (PLS), principal component analysis (PCA), cluster analysis (CA), discriminant function analysis (DFA), linear discriminant analysis (LDA), and principle component regression (PCR) (Pearce et al., 2003). Haugen and Kvaal (1998) suggested that starting with PLS and PCR is a good way to learn the data structure. Marcelloni (2001) found out that PCA can conceivably lower collinearity between volatiles but also increases classification error. In essence, both of PLS and fuzzy C-means with KNN can significantly improve the accuracy of classification (Marcelloni, 2001; Schiffman et al., 2001).

The biological method, also called non-parametric, doesn't require any assumption before use, so it applies more generally (Pearce et al., 2003). The algorithms under non-parametric are self-organizing maps (SOM), multi-layer perception (MLP), probabilistic neural network (PNN), radial basis function (RBF), learning vector quantization (LVQ), fuzzy inference system (FIS), fuzzy neural network (FNN), fuzzy c-means (FCM), adaptive resonance theory (ART), fuzzy ARTMAP, genetic algorithm (GA), neural fuzzy system (NFS), and wave transformations (Pearce et al., 2003). Hines (2003) said that ANN has more advantage than parametric pattern recognition because it carries the ability to do parallel signal processing and higher resilience to the shifting and unwanted signals. In addition, using fuzzy with NN can enhance the quality of classification (Gutierrez-Osuna, 2002; Liu et al., 2001). Lastly, fuzzy ARTMAP can do real-time learning without forgetting what has been learned, which is suitable for field instruments (Hines et al., 2003). In figure 2.2, during supervised learning, known odors are grouped and saved in the knowledge base in the system. After learning is finished, an unknown sample would be tested and classified against the knowledge base. Unsupervised learning, alternatively, doesn't have known data to train, and the algorithms are able to cluster the data into different classes.

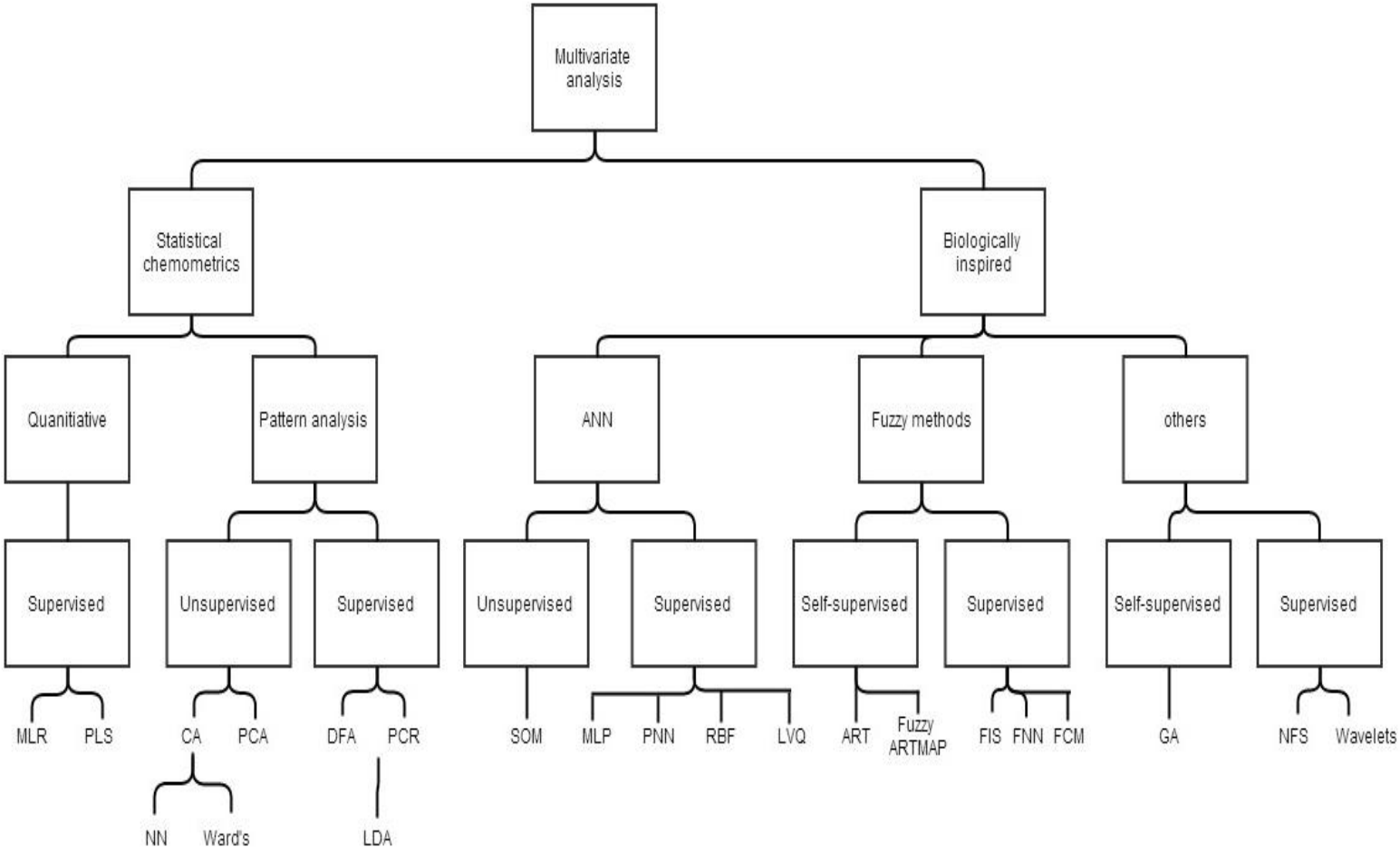

Figure 2.2 Pattern recognition paradigm classification (Hines et al., 2003)

2.1.2.3 Validation

The purpose of validation is to make sure the PARC models are valid. The validation for an electronic nose and tongue has the three methods: Hold out, K-fold cross validation and Bootstrapping (Gutierrez-Osuna, 2002). The Hold out method divides the data into two sets; one is for training and the other one is for testing. K-fold cross validation uses the fraction (1/K) for validation and the fraction (1-1/k) for model training (Nord, 2006). The data sets are recalculated every time, so the accuracy is the average of K. Bootstrapping is similar to K-fold cross validation; the only differences are the data sets are replaced in each cycle.

2.2 Application

According to Tang et al., (2010) and Zhang et al., (2007), the electronic nose and tongue has been a continuously growing analytical technology in a multiplicity of applications (e.g., air quality, health care, safety and security, environment, quality control, agriculture etc.) for 15 years. In the following sections, popular applications are reviewed based on the types of sensors, processors and pattern recognitions.

2.2.1 Food industries

Food safety becomes serious problem for the public. There were 325,000 instances of hospitalization and 5,000 deaths per year in United States due to the food poisoning (Panigrahi, Balasubramanian, Gu, Logue & Marchello, 2006). However, the biggest problem with the recent existence of food detections is its time consuming nature (Panigrahi et al., 2006). Therefore more researchers have developed detectors with different methods.

In research from North Dakota State University, Panigrahi et al. (2006) developed an intelligent sensor system to evaluate the quality and safety of meat. The system consisted of an array of nine MOS sensors that had different odor sensing capabilities and a laptop computer for signal processing. LDA and QDA were used to classify models from the responses of sensors. Then leave-1-out cross validation and bootstrapping were the methods for validating the models. The result showed that the accuracy of the system was more than 80 percent (Panigrahi et al., 2006).

The study from National Tsing Hua University talked about the potential of using an electronic nose to discriminate fruits (Tang et al., 2010). The system consisted of an array seven MOS sensors with different target gases, a DAQ on a PCB, a 8051 microprocessor, a keyboard and an LCD display (Tang et al., 2010). Six different algorithms were used for classification, including NN, KNN, SVM, PNN, PKNN and PSVM (Tang et al., 2010). In the end, the system was able to achieve accuracy above 95 percent Also, the authors suggested there was a need to have more sensors with different varieties in order to improve classification accuracy.

Moreover, the investigation of fish freshness in real-time was proposed by El Barbri et al. (2007). In the system, there were six tin-oxide based Taguchi gas sensors and a microcontroller as a data acquisition system (El Barbri, Llobet, El Bari, Correig & Bouchikhi, 2007). Moreover, a laptop was the processor for pattern recognition. PCA and support vector machines analysis (SVM) were used to analyze the data (El Barbri et al., 2007). The result, by using SVM method, showed the success rate was 93.75 percent and when the fish were stored less than or equal to three days, the success rate was 100percent for identification (El Barbri et al., 2007).

In addition, research from the University of Bologna developed a method that was able to classify Pecorino Chesses according to their ripening time and manufacturing techniques (Cevoli et al., 2011). The result of the proposed method was compared with exiting commercial equipment (GC-MS). The system was based on an array of six MOS sensors with ANN method (Cevoli et al., 2011). PCA reduced the dimensionality of data set and ANN classified the models from the sensor response. The authors compared between PC score, feature extraction and GC-Ms analysis; the proposed methods had higher effective classification than GC-MS analysis (Cevoli et al., 2011).

2.2.2 Environmental application

Ninety percent of the cancer risk and lung disease are associated with air pollution. Health impact from diesel pollution exposure costs $22 billion statewide in 2004. And, the average world temperature is increasing every year. Moreover, the change in food chain of aquatic animals and the increment of human sickness are partially because of water pollution. Those facts are related to human-made activities such as transportation, chemical application in the household, dumping waste in water and land, etc. Various proposed projects related to an electronic nose and tongue have targeted the environment, such as indoor air quality, health of rice plant, water pollution etc.

Zampolli et al. (2003) developed a low cost and compact-size electronic nose consisting of an array of metal oxide solid state gas sensors and RH sensors (humanity measurement) for monitoring pollution levels inside buildings. The device was designed to target, identify and qualify carbon monoxide and nitrogen dioxide. The authors used a fuzzy- logic system for pattern recognition (Zampolli et al., 2003). The experience showed that the device was able to differentiate and classify concentrations as low as 20

ppb for nitrogen dioxide and 5 ppm for carbon monoxide (Zampolli et al., 2003). In another design by Zhang et al. (2012), the electronic nose consisted of an array of four MOS sensors, a module combined with a temperature sensor and humidity sensor, and a 12-bit analog-digital converter (Zhang et al., 2012) for similar application as Zampolli et al. (2003) did. The processor was the Field Programmable Gate Array with a synchronous Dynamic Access Memory for storage. On the software side, Zhang et al. (2012) used a back-propagation neural network for classification and chaotic sequence for optimization. The result was built on the comparison between chaotic sequence and standard particle warm (Zhang et al., 2012). The outcome was that both optimizations were effective for weights optimization and 26.03percent prediction error decreased after applied chaotic sequence (Zhang et al., 2012).

Furthermore, a portable electronic nose system was able to measure and inspect the presence of sulphate-reducing bacteria (SRB) by Tan and Abdul Halim (2011). The rationale for this system was that old methods to detect SPB were inefficient in terms of time (Tan & Halim, 2012). They used a metal oxide gas sensor to detect specific gas and analyzed the data by applied neural network algorithm on FPGA and statistical method (i.e. ANOVA) (Tan & Halim, 2012). The hardware interface consisted of an 8 bit analog-digital converter and bus transceiver to regulate the voltage (Tan & Halim, 2012). The indication of the result was greater than 94percent accuracy and the future work was to decrease other parameters affected by the sensor reading such as temperature, humidity and pH (Tan & Halim, 2012).

Moreover, Zhou and Wang (2010) developed an olfactory system for the health of rice plants by determining the possibility of detecting Nilaparvata lugens infestation. The

device equipped with 10 MOS sensors (Zhou & Wang, 2010). PCA and LDA were used for classification and dimension reduction, and SDA and 3-layer BPNN were adopted for the data training (Zhou & Wang, 2010). The result showed that the discrimination rates were over 92.5percent for BPNN and 70percent for using SDA (Zhou & Wang, 2010).

2.2.3 Medical application

It has been found that particular volatile organic compounds within human breath are associated with specific human diseases, such as respiratory diseases (Akyar, 2011). Some volatile metabolites are often released within a few hours to a few days before the appearance of the actual symptom (Akyar, 2011). An electronic nose can be applied to health monitoring and molecular marker distinction in the early stages of illnesses.

Research from Shih, Lin, Lee, Chien and Drake (2009) developed an electronic nose based on an array of 24 piezoelectric quartz crystal microbalance sensors with different coatings for monitoring the exhaled breath of patients. The main focus was to use MDA to detect and classify bacteria inflections for the patients in intensive care units (Shih, Lin, Lee, Chien & Drake, 2010). The result showed that six different bacterial pathogens were recognized and were classified with 98 percent accuracy.

Additionally, Tang, Chiu, Chang, Hsieh and Shyu (2011) proposed and built personal healthcare application using an electronic nose. The study was the first application using SoC technology, which integrated the sensor array and signal processing circuit (Tang, Chiu, Chang, Hsieh & Shyu, 2011). There were an array of eight conducting polymer materials and an 8051 microprocessor as the processor with SRAM for storage in the system (Tang et al., 2011). The algorithm the system used was KNN (Tang et al., 2011). In conclusion, the power consumption was 1.05mW at1.8V

digital/1V supply voltage and the chip successfully identified four various samples (Tang et al., 2011).

2.2.4 Safety application

Border safety has been a serious issue for every country; many nations are seeking a way to insure public safety and improve the level of security. One of the methods is to upgrade the technology. Therefore, the electronic nose may get more and more attention in the field such as detection for illicit drug, gas leakage and fire (Zhang et al., 2007).

Sadeghifard, Anjomshoa and Esfandiari (2011) developed a portable electronic nose for fire detection. Fire is one of main problem in our life now. It brings the damage not only on the property assets but also physical and mental injuries of the people. It is significant to improve the reliability of fire alarm system (Sadeghifard at el., 2011). The electronic nose consisted of three main components – sample handing, detection and data processing system. They used several distinct metal oxide gas sensors to acquire data and a microcontroller to analyze the data with neural network (i.e., back propagation algorithm) (Sadeghifard at el., 2011). In conclusion, the electronic nose had the ability to detect smoke at early stage with greater than 97percent accuracy (Sadeghifard at el., 2011). In order to improve the accuracy and reliability, the author suggested that adding more kinds of sensors to the system (Sadeghifard at el., 2011).

In 2010, a portable electronic nose detected organic vapor based on a novel chemical surface acoustic wave array and readout electronics. It was developed and tested by Hao et al. (2010). Humans are not able to sense the organic vapors that might be fatal and corrosive if inhaled. Thus, vapor detection is essential for different

environments. The authors used a polymer-coat surface acoustic wave (SAW) array to acquire data and studied data by using an 89C51 microprocessor (Hao et al. 2010). Hao et al. (2010) used Spearman's Rank Correlation coefficient with average-linkage to cluster the data and *Cluster*, "a hierarchical cluster program obtained from the Eisen Laboratory" (Hao et al. 2010), to do the analysis. The total time of one cycle was about 10 minutes (Hao et al. 2010). At the end, the system could differentiate vapors by the combination of an array of multiple sensors and appropriate recognition algorithm (Hao et al. 2010).

Wongchoosuk, Lutz and Kerdcharoen (2009) designed an electronic nose that could detect and identify the odor of the human armpit. Recently, there had been more attention paid to the application of E-nose for human body odor measurement (Wongchoosuk, Lutz & Kerdcharoen, 2009).The system included a sensor chamber, airflow system data acquisition and measurement circuit measurement (Wongchoosuk et al., 2009). The sensors used MOS; the signal from the sensors would send to DAQ-card and measurement circuit board (Wongchoosuk et al., 2009). Since this kind of sensor was sensitive to humidity, the authors examined the results in different humidity in percentage (Wongchoosuk et al., 2009). Wongchoosuk et al. (2009), then, used a *t*-test and PCA to inspect and identify the measurements respectively. In conclusion, the background humanity was 75percent for the best sensor performance and the system was able to differentiate different human odors (Wongchoosuk et al., 2009). For the improvement, Wongchoosuk et al. (2009) would like to add more different type of sensors for a variety of volatile compounds.

In the study by Haddi et al. (2010), the portable electronic nose system has been built and tested for classify different types of drugs. The system consisted of six MOS

sensor, a humidity sensor, a temperature sensor, a microcontroller for data acquisition, and a laptop for data analysis (Haddi et al., 2010). The pattern recognition methods for this system were PCA, multivariate analysis of variance (MANOVA) and SVM (Haddi et al., 2010). The PCA and MANOVA successfully classified the different drugs ($p<0.0001$) (Haddi et al., 2010). In addition, when SVM classifier was applied, the accuracy reached to 98.5percent (Haddi et al., 2010).

2.3 Summary

In this chapter, the system description of electronic nose was reviewed based on the perspectives of hardware and software. Also, the applications of electronic nose that have been developed were presented in this section. Even though this technology has been investigated for many years, there are still few studies that prove the potential of improvement in classification accuracy, portability and sustainability.

CHAPTER 3. PROCESS AND METHODOLOGY

3.1 Computational System Development for Sensors

The purpose of the computational system is to control the gas flow, collect data from sensors, and analyze the data in the processor. The overall block diagram consists of an electromechanical system, an acquisition interface, a power supply, a signal analysis block and a display. This is illustrated in Figure 3.1 and presented in the next four subsections as follows:

- Electromechanical system
- Sensor integration
- Centralized power
- System integration

Each of the parts were designed, fabricated, and tested individually. All system components were then integrated and preliminary experiments were conducted

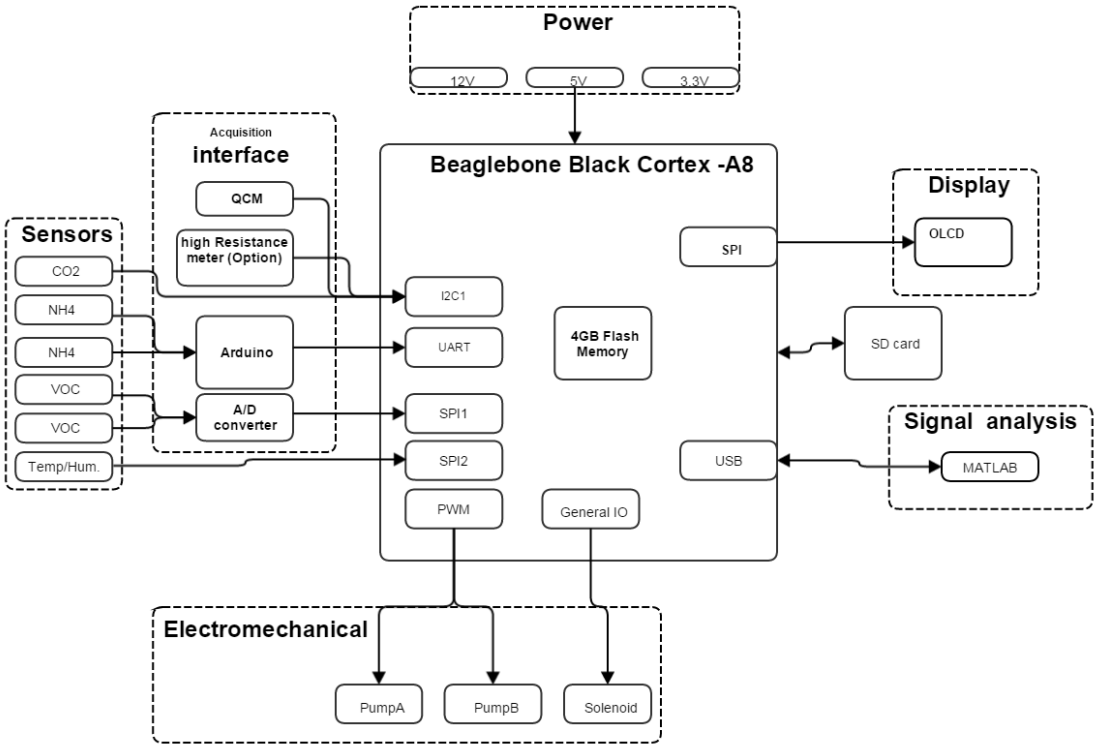

Figure 3.1 Overall block diagram of the integrated sensor system.

3.1.1 Electromechanical Gas handling System

The electromechanical gas handling system was used to control the gas flow and to safely transfer the gas to the transducer sensor. This design was a modification of a similar design conceived by Dr. Suranjan Panigrahi. The system consisted of a sensing chamber, two pumps, and a three-way solenoid valve. The block diagram of the electromechanical gas handling is presented in Figure 3.2. The chamber was designed using *SolidWorks*- a software program for solid modeling computer-aided design (CAD) and computer-aided engineering (CAE) - and fabricated using Teflon material. The prototype is presented in Figure 3.3. The holes on the top of the chamber are for the sensors and the center holes on both sides of the chamber are for connecting the tubing.

The dimensions of the chamber are 107.03mm x 71.88mm x 47mm. The fabrication of the chamber was done at the Artificial and Fabrication Lab (AFL) located in Armstrong Hall, Purdue University. An image of the product is presented in Figure 3.4. Furthermore, the two pumps and the solenoid valve were purchased from KNF and Parker. The specifications of the pump and solenoid valve are presented in Appendix A. The flow rate of the pump at atmospheric pressure is 0.4 Liter/min on a 5V DC supply and the type of valve the system used was the Diaphragm isolation valve with an operating pressure of 20 psig.

The basic operations of the system are displayed in Table 3.1. During T1, the system conducts air flushing, which is an operation where the valve changes the source from gas sample to air by sucking the air from the chamber using Pump A in order to bring in the fresh air to reset the environment. Next, Pump A stops running for a period during T2. Finally, the last stage of the system operation involved the valve changing the source from air back to the gas sample using Pump B to push the gas sample into the chamber for a period during T3.

In order to control the pumps and the valve following the logic mentioned in Table 3.1, drivers for pump and solenoid were incorporated (Jianwen, 2006) and they are shown in Figure 3.5. A low side switch was used to control the “on/off” operation, and the schematic of the two types of drivers are presented in Figure 3.6. In the figure, R1 and R3 in the circuits were to improve electrostatic discharge and R2 and R4 were acting as pull-down resistors in the circuit (Jianwen, 2006). The transistors for the pumps and the solenoid valve are NPN MOSFET and FQR30N06L, and both were purchased from Digi-Key.

Initial test for driver

The procedure of the test is listed below.

- Connected the drain of the MOSFET to a power supply (Agilent E3630 A).
- Adjusted the power supply to specific voltage (Pump driver – 5 volts. Solenoid drive – 12 volts)
- Connected the input of the driver to another power supply (Agilent E3630 A):simulation the SOC-Beaglebone black
- Adjusted the voltage to 3.3 volts DC (voltage required by Beaglebone Balck)
- Measured the DC voltage between the power supply and the drain of the MOSFET using a multimeter, FLUKE 115

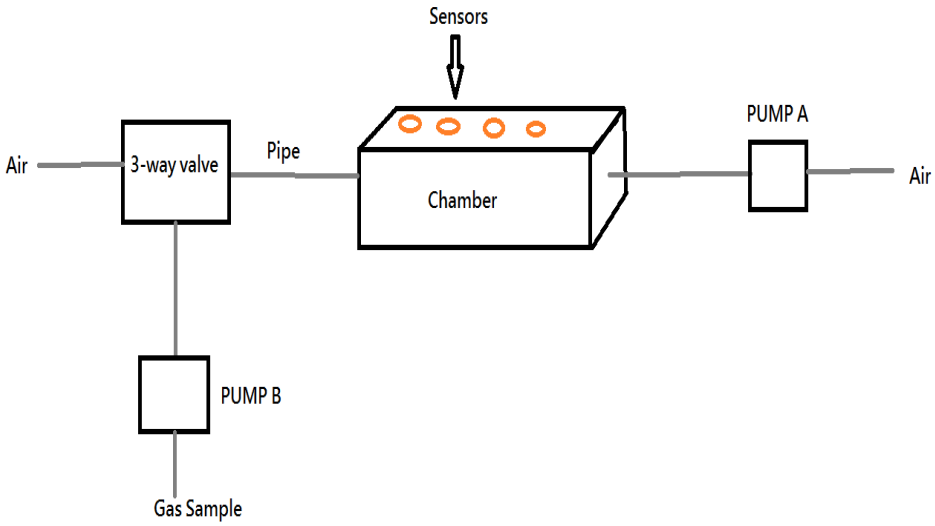

Figure 3.2 Design of the electromechanical gas handlingsystem with flow directions.

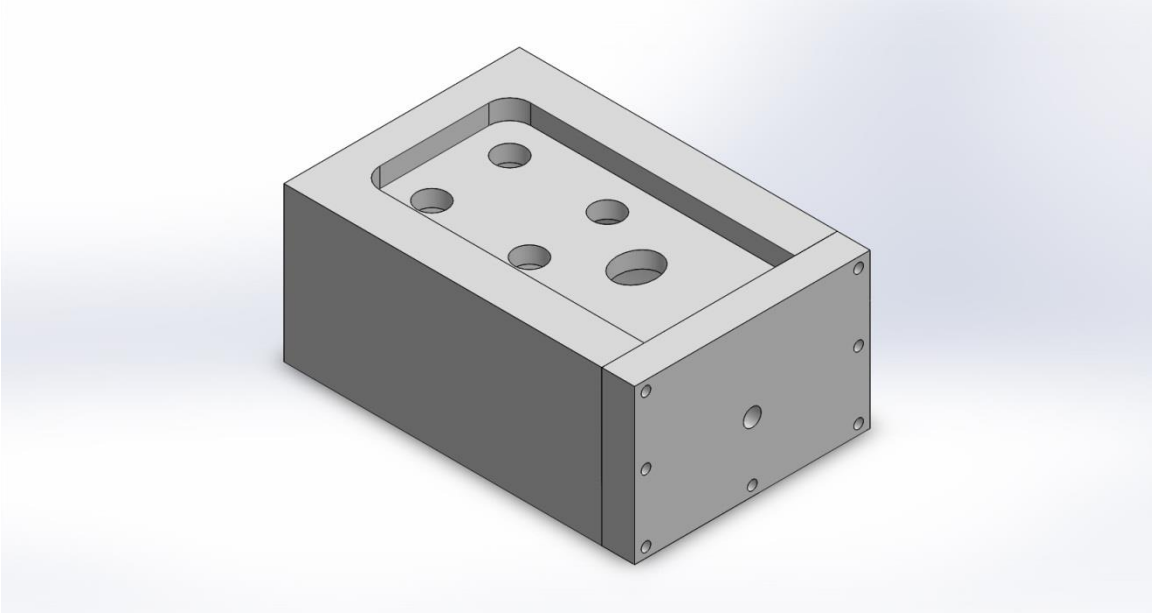

Figure 3.3 SolidWorks image of the chamber prototype.

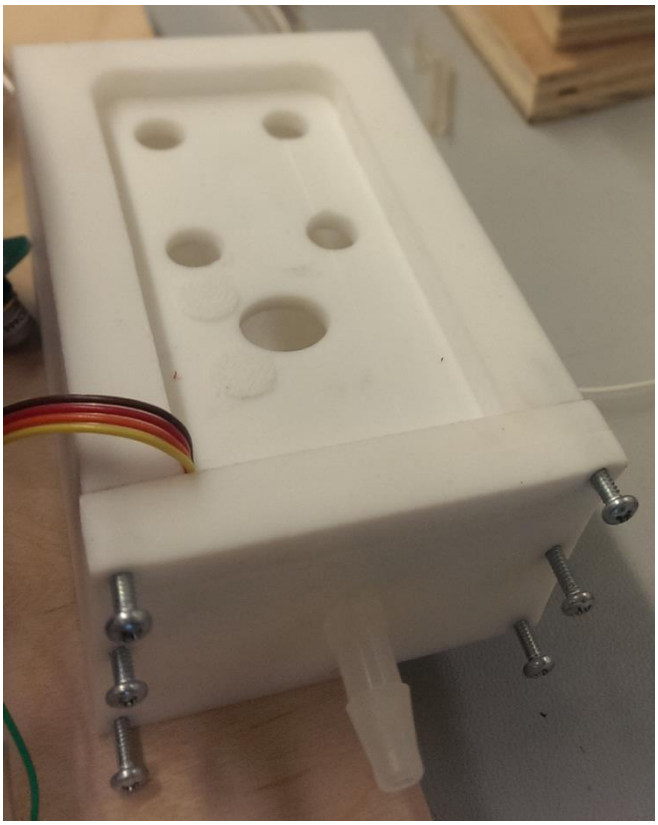

Figure 3.4 Finished product of the chamber.

Table 3.1 *Operation table of the system*

Time	**Pump A**	**Pump B**	**Solenoid valve***	**Operation**
	(5V)	(5V)	(12V)	
T1	ON	OFF	Close	Air flushing & expelling from chamber
T2	OFF	OFF	Close	Collecting Air reference Path (A→C)
T3	OFF	ON	Open	Gas filling/ data collecting Path (B→C)

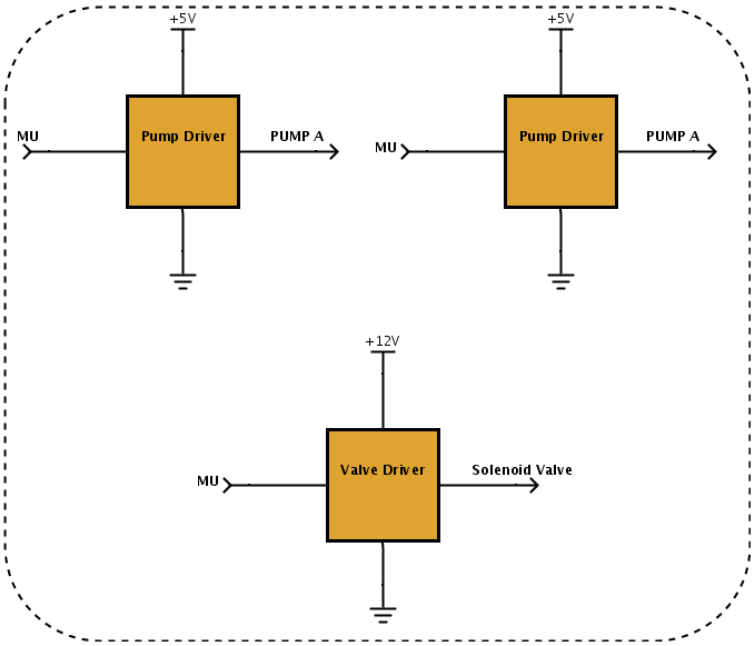

Figure 3.5 Pump and solenoid valve drivers. (Jianwan, 2006)

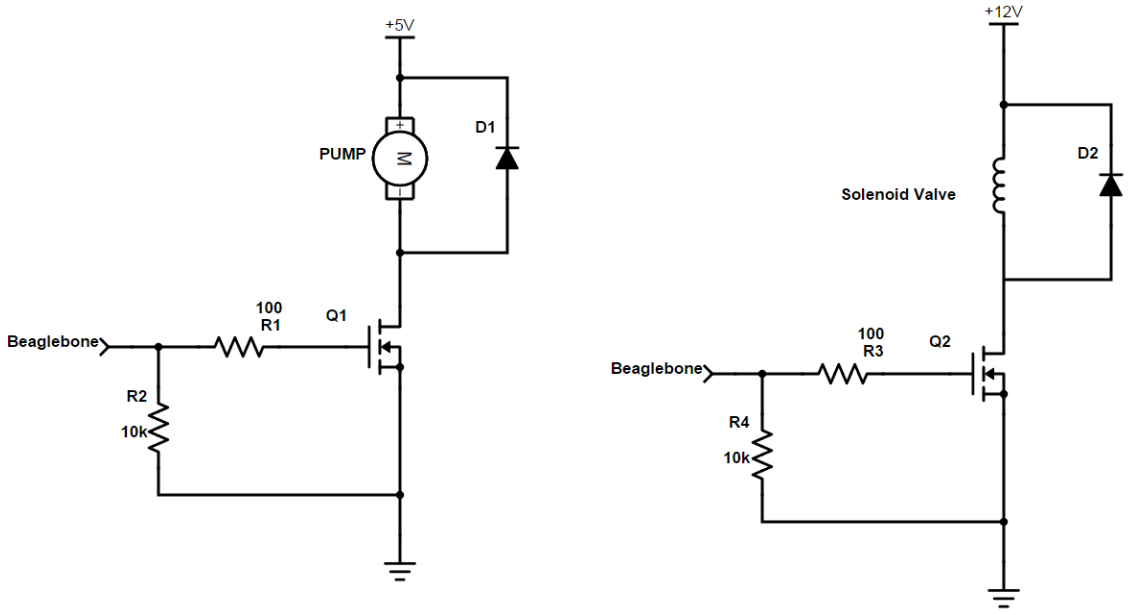

Figure 3.6 Schematic of driver. (a) for the pump and (b) for the solenoid valve.(Jianwen, 2006)

3.1.2 Sensor Integration

This section covered the specification and the hardware/software interface of each sensor. The three sensors that were used in this system are the volatile organic compound sensor, ammonia sensor, and Carbon dioxide sensor.

3.1.2.1 Volatile Organic Compound (VOC) Sensor

The VOC sensor used was the TGS 2620, a hydrocarbon vapors sensor made by Figaro. It has the high sensitivity on alcohol, methane, carbon monoxide and other volatile vapors. The sensor must be warmed up for at least 2 minutes in order to get the desired accuracy according to the datasheet. Figure 3.7 shows the hardware interface of the sensor. This type of sensor is intended to be used as a voltage divider because the goal is to get the resistance of the sensor. Pin1 and Pin4 are exchangeable and can be connected to either the 5V power or ground. Pin 3 was connected to a 5V power source

and Pin 2 was connected to the load, the combination of R3 and R4. According to the datasheet, the R3 resistor was used to ensure the power in the sensor never exceeds the maximum rating of 15 milliwatts. The RC circuit shown in Figure 3.7 was used to prevent a false high voltage output and also to reduce noise (Beard, 2007). Resistor R4 was a potentiometer with a maximum value of 50k ohms and was used to adjust the sensitivity of the sensor. The relationship between sensor resistance, R_s, and the load,R_L $(R3 + R4)$, is presented in the following equation

$$R_s = \frac{Vc - V_{out}}{V_{out}} \times R_L \qquad \text{(Equation 3.1)}$$

Where Vc is the power supply (5V).

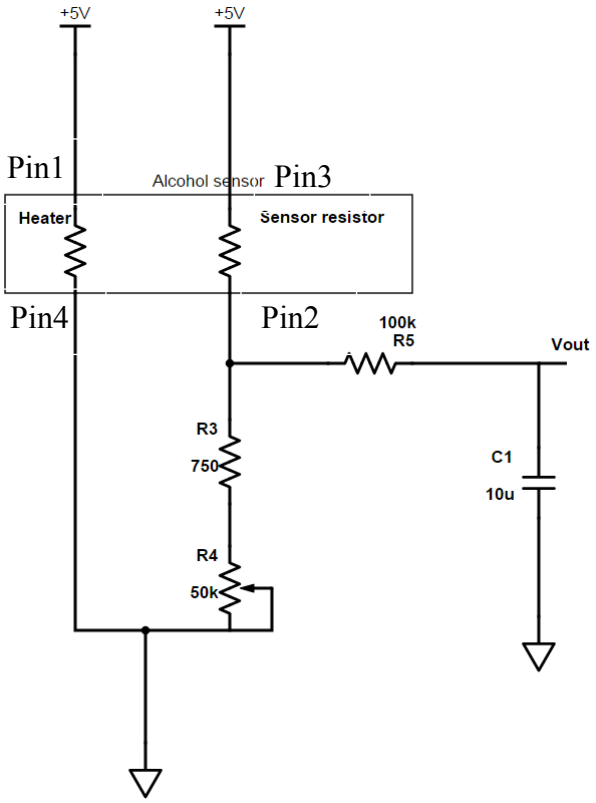

Figure 3.7 Hardware interface of TGS 2620 VOC sensor referred to the datasheet ("TGS2620-for the detection of solvent vapors", 2005)

Initial test for VOC sensor

The Vout port of the VOC sensor was then connected to an Arduino Uno microprocessor for the initial test. Due to lack of information in the datasheet, the test was based on the discovering the characteristic of the sensor that included the sensor's response time, recovered time, and sampling time as well as the Vout voltage range. The procedures of the test are listed below:

1. Conditioned the sensor for 7 days if it wasn't started for at least a week (according to the datasheet).
2. Powered the sensor and waited for the sensors to reach equilibrium stage (response to air).
3. Recorded Vout for air (reference) for 20 seconds.
4. Dipped a cotton ball with Alcohol liquid.
5. Placed cotton ball near the sensor head until the signal got equilibrium.
6. Removed the cotton ball and kept recording Vout until the reading were back to the reference (air value).

Each sensor was tested once and the voltage respected to the time was plotted by using Excel. Finally, the response time, recovered time and the Vout range were determined from the plot.

3.1.2.2 Ammonia Sensor

The TGS 2444 ammonia sensor made by Figaro USA, INC was the other sensor implemented in the system. Its fundamental operation was similar to the TGS 2620 VOC sensor presented in section 3.1.1.1. However, there are specific heating cycle (VH) and

control cycle (VC) due to the possibility of migration within the sensor. Figure 3.8 presents the overall timing char for the heater and the circuit voltage. The period of both was 250 milliseconds and the pulse widths of heater and control cycle were 14 milliseconds and 5 milliseconds respectively. In addition, there was a 2 milliseconds delay for the VC after triggering the VH. More detail on the timing of VH and VC can be referred to in Figure 3.9.

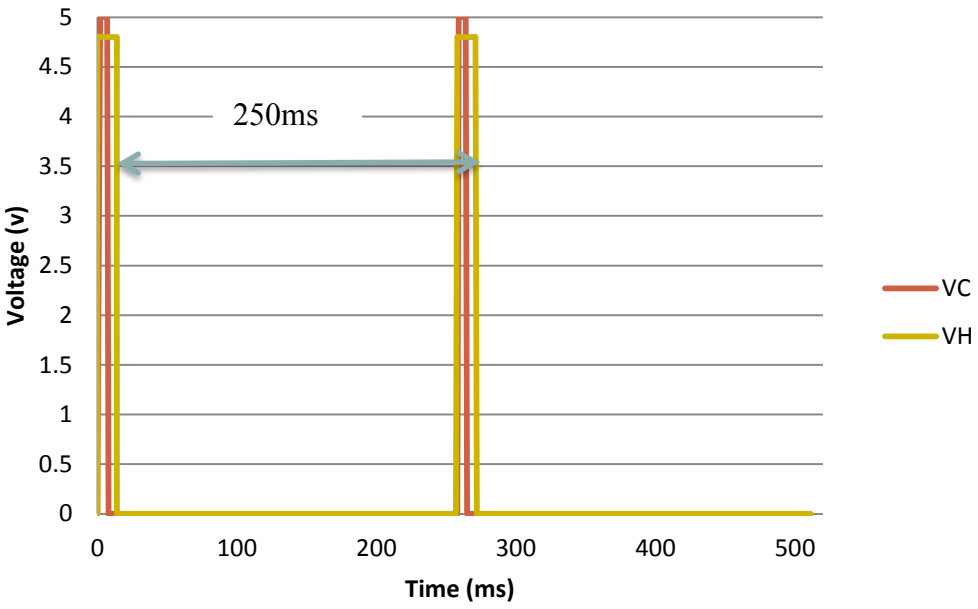

Figure 3.8 Timing chart of the heating cycle (VH) and the control cycle (VC).

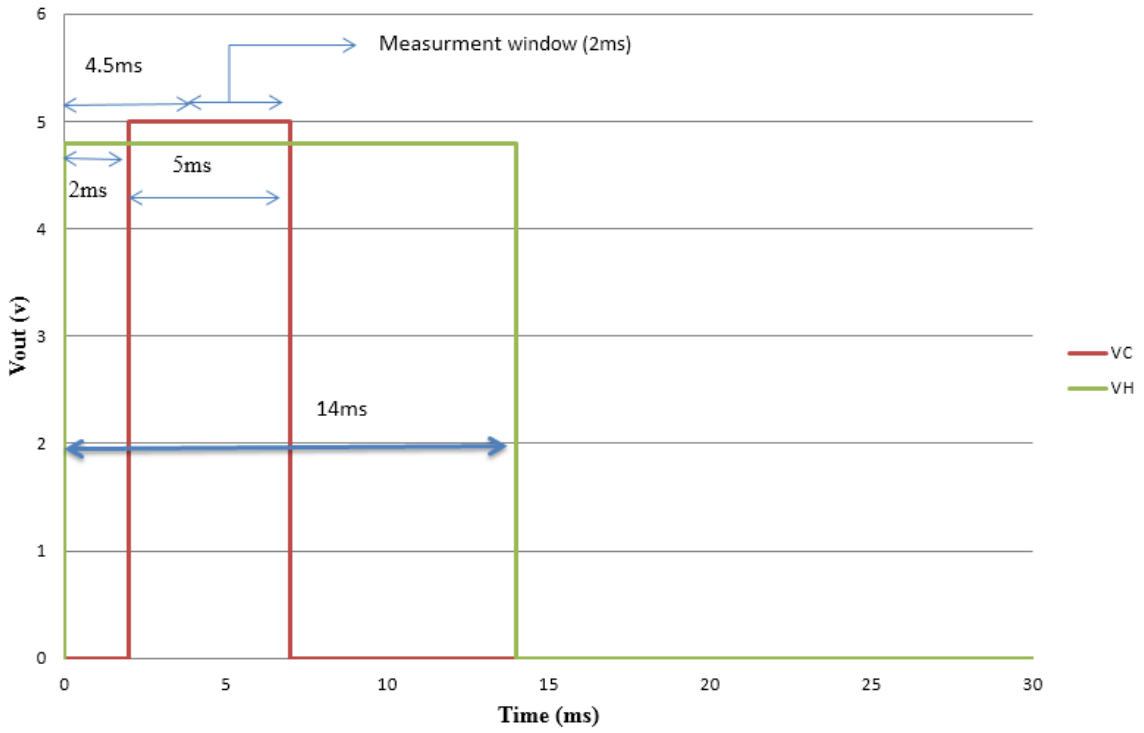

Figure 3.9 Detail timing diagram for 14ms of one cycle

In Figure 3.10, the hardware interface for operating the sensor is displayed. The circuit inside the dashes box is referred to the datasheet in Appendix A. To control the heater's on/off, the high side compound pair switch was used because initally the microprocessor for the intial sensor test was Beaglebone black which generates 0 to 3.3V signal. Due to the difficulty of hardware issue, the research substituted Beaglebone black to Arduino Uno for this specfic sensor. The values of resitors R1, R2, R3 and R4 were calculated based on changing the transistor into switch mode. On the other hand, a low side switch controls the control voltage VC, and the resistor placed between microcontroller and the transistor was used to limit the current going into the transistor. Moverover, in order to get the information of the sensor resistance (Rs), the resistance of resistor RL (R6 and R7) was measrued. Like the TGS2620 VOC sensor circuit, the

resistor R7 in the ammonia sensor circuit was the power limiting resisor used to ensure that the power never exceeded the maximum rating. The user can change the sensitivity of the sensor by modefying the resistance of potentimeter R6 (325-50k ohms). The relationship between Rs and RL (R6 + R7) is

$$R_s = \frac{V_c \times RL}{V_{out}} - RL \qquad \text{(Equation 3.2)}$$

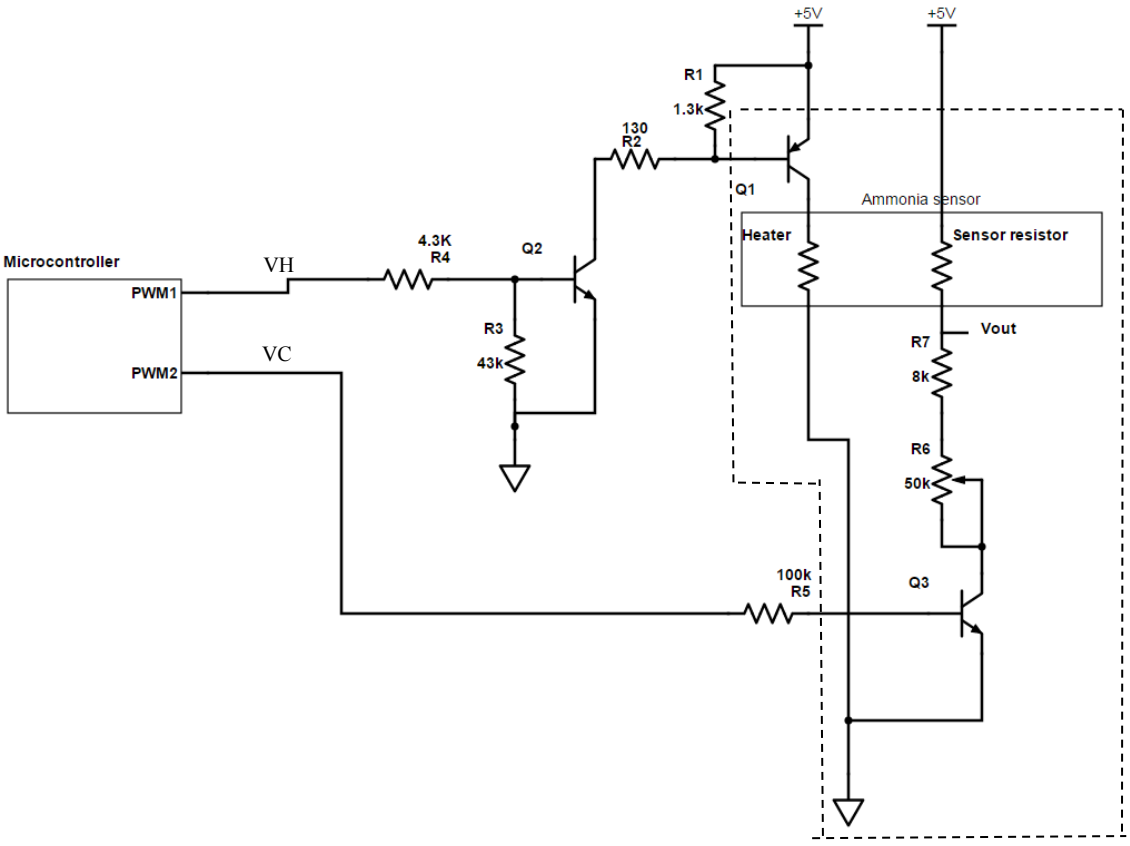

Figure 3.10 Instrumentation interface for TGS 2444 ammonia sensor with Arduino Uno. The circuit inside dash box was referred to the datasheet. ("TGS2420- for the detection of Ammonia", 2011)

Determination of measurement window (timing)

According to the the ideal timing diagram in Figure 3.9 and the specifcations listed in the application note in Appendix A, the data sampling window should be greater than 4.5ms and smaller than 7ms. Also, it is deliberated that the sampling window should

stays away from the edge where the transection of VC from 5V to 0V .Thus, it was decided to keep 0.5 ms timing distance from the edge. Therefore, the researcher acquired the data for both ammonia sensors at 5ms and 6 ms of one cycle. In other words, both sensors acquired data within a window of 2ms (between 4.5 and 6.5 ms).

Procedure for prelimitary test

The timing cycles to the ammonia sensor was generated by the Arduino timer interrupt. The interrupt service routine ran every millisecond to update the signals. The sampling rate of the Arduino is 10ksps (i.e. 0.001sec/reading). Therefore, in 2 millseconds, 20 sample(data) are collected for each cycle. This tranlsates to the sensor's sampling rate of 80 samples per second.

The procedure of testing ammonia senosr is really simliar to the test for ammonia sensor. The procedures are shown below:

1. Conditioned the sensor for 48 hours if it wasn't started for at least a week (according to the datasheet).
2. Powered the sensor and waited for the sensors to reach equilibrium stage (response to air).
3. Recorded Vout for air (reference) for 20 seconds.
4. Dipped a cotton ball with ammonia liquid.
5. Placed cotton ball near the sensor head until the signal got equilibrium.
6. Removed the cotton ball and kept recording Vout until the reading were back to the reference (air value).

Each sensor was tested once and , and the Vout was plotted with respect to the time. The response time, recovered time and the vout range were determined.

3.1.2.3 Carbon Dioxide Sensor

The Carbon dioxide sensor manufactured by TELAIRE (Pennsylvania, USA) was purchased from Digi-key. The measurement range of the sensor was from 0 to 5000 ppm with an accuracy of ±3%. There are different ways to obtain the CO_2 concentrations from this sensor (e.g. I2C, PWM and USART). The I2C was chosen for its easy implementation and simple wiring configuration. Figure 3.11 illustrates the I2C wiring setup. Pin1 and Pin2 were, respectively, SDA and SCL, which connected to the master. Pin 3 and Pin 4 were the power and ground pins. Pin 6 was connected to ground in order to configure the sensor to I2C communication referred to datasheet specifications in Appendix A. The master in the communication was Bealgebone Black, a low cost embedded system developed by Texas Instruments. Details on Bealgebone Black are discussed in a later section. Moreover, a level shifter, converts one digital signal from one logic standard to another, was theoretically needed in the both the SDA and SCL lines because of the voltage limitation (3.3V) of GPIO (General purpose of input/output) on the Beaglebone Black system, but this specific CO_2 sensor was compatible for both 3.3 volts logic level and 5 volts logic level so the level shifter was not required.

CO_2 Program class and initial test

The CO_2 class was developed and displayed in the Figure 3.12. In this class, there are three main methods, “readRegister”, “gas_reading”, and “gas_reading_in_a_loop”. “readResgiter” was used to display the firmware version of the sensor as well as the status of the sensor. The “gas_reading” was used to read the register that stores the data of CO_2 concentration. Lastly, the “gas_reading_in_a_loop” has similar functionality as “gas_reading”. The main difference between the two was that the user can use the

"gas_reading_in_a_loop" class to define how many loops (5 seconds interval) the program going to run. After the CO_2 class was developed, the testing for the main coding was written with the integration of the CO_2 class. In Figure 3.13, the test main program defined an object of class and checked the status and displayed the CO_2 concentration in ppm on PC screen.

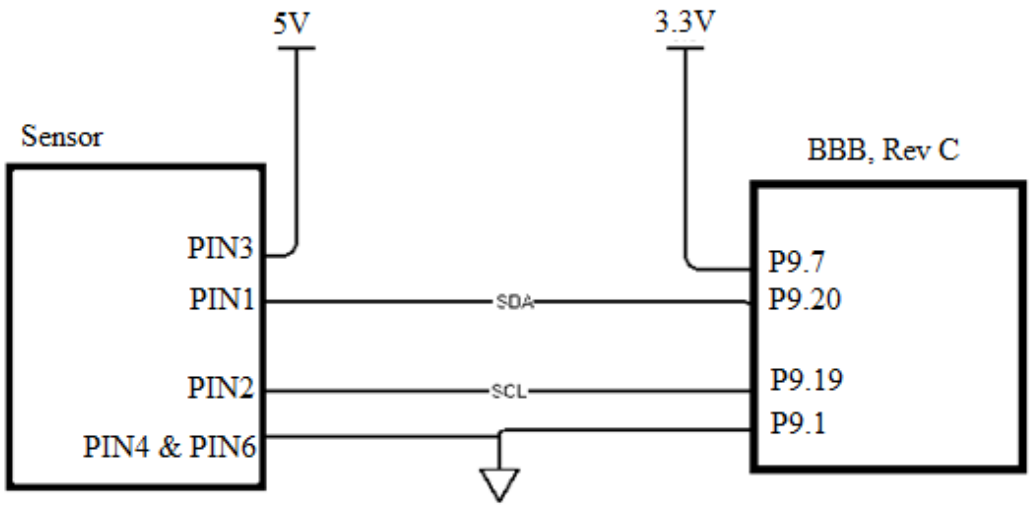

Figure 3.11 Wiring between the CO_2 sensor and a host

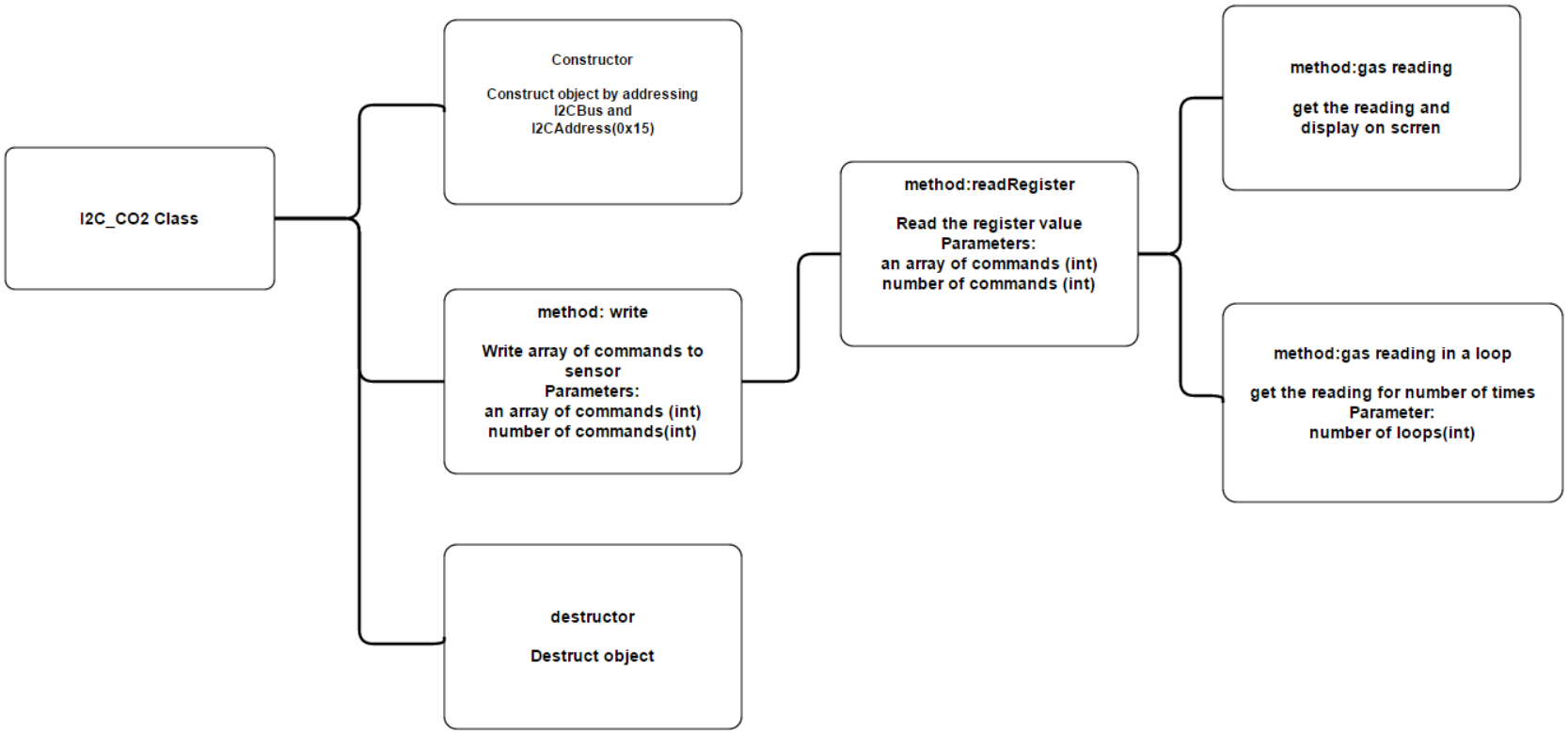

Figure 3.12 Class diagram of CO_2 sensor

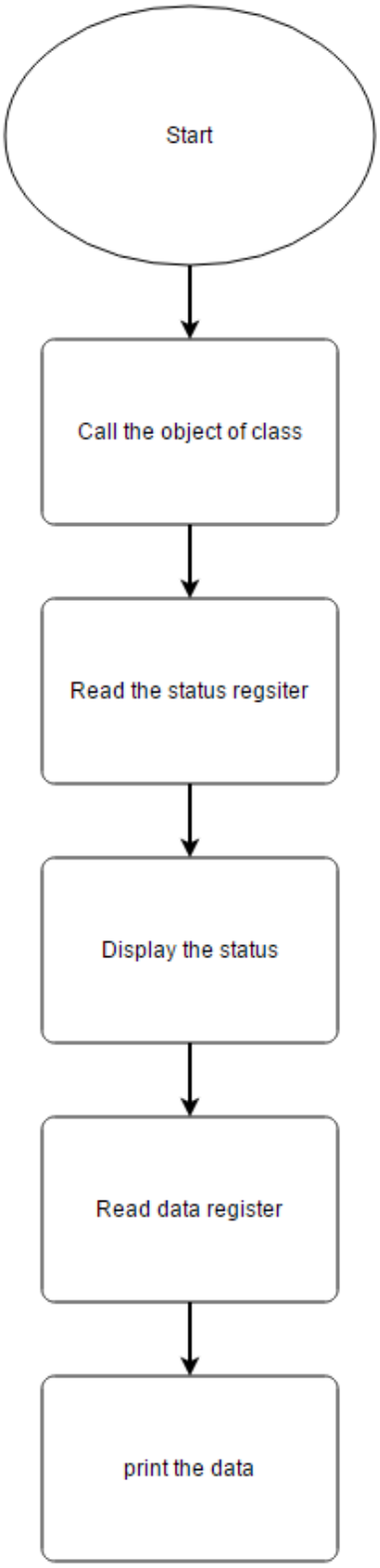

Figure 3.13 Flow chart of test main file

3.1.2.4 Temperature and Humidity Sensor

The temperature and humidity sensors, from Adafruit, of the system used were an assembled breakout board called Adafruit HTU21D-F Temperature & Humidity Sensor Breakout Board. The sensor was based on HTU21D-F with humidity accuracy of ± 2% and temperature accuracy of ± 1° C. The dimensions of the board were 18mm x 16mm x 2mm. In addition, a 3.3 volts regulator and I2C shifting circuit are included on the board to enable the developer to easily connect to either a 3.3 volts or a 5.5volts microcontroller. As shown in Figure 3.14, the hardware configuration of the temperature and humidity sensor was similar to the configuration of the CO_2 sensor. The VIN pin was connected to a 3.3 volts power supply. The SDA and SCL pins were directly connected to the host, the Beaglebone Black. The host and slave were connected to a common ground.

Temperature and humidity program class and initial test

Figure 3.15 illustrates the class chart for the temperature & humidity sensor. The class has three methods: begin(), readTemp(), and readHumidity(). The begin() method was used to reset the system and wait for 150 milliseconds. In the readTemp() and readHumidity() method, the sensor received the specific commands from the host and sent a 16 bits of data (8 bits temperature + 8 bits humidity) that did not include CRC, an error-detecting code, back to the master. The temperature and humidity values were calculated using the equations referred to the datasheet in Appendix A below:

$$Temp(in\ Celsius) = -48.65 + (175.72\ \times \frac{t}{2^{16}}) \quad \text{(Equation 3.3)}$$

Where t is the binary temperature data from the sensor.

$$Humidity = \ -6 + (125 \times \frac{h}{2^{16}}) \quad \text{(Equation 3.4)}$$

Where h is the binary humidity data from the sensor.

The testing flow chart for the temperature and humidity sensor is shown in Figure 3.16. The program first declared the object of the class and then started the begin method. After return0, the program was set in a loop that sequentially called readTem() and readHumidity() to get and display the data for every second.

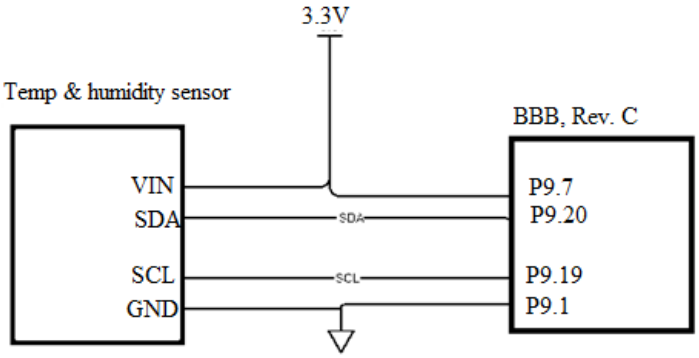

Figure 3.14 Hardware configuration of temperature and humidity sensor

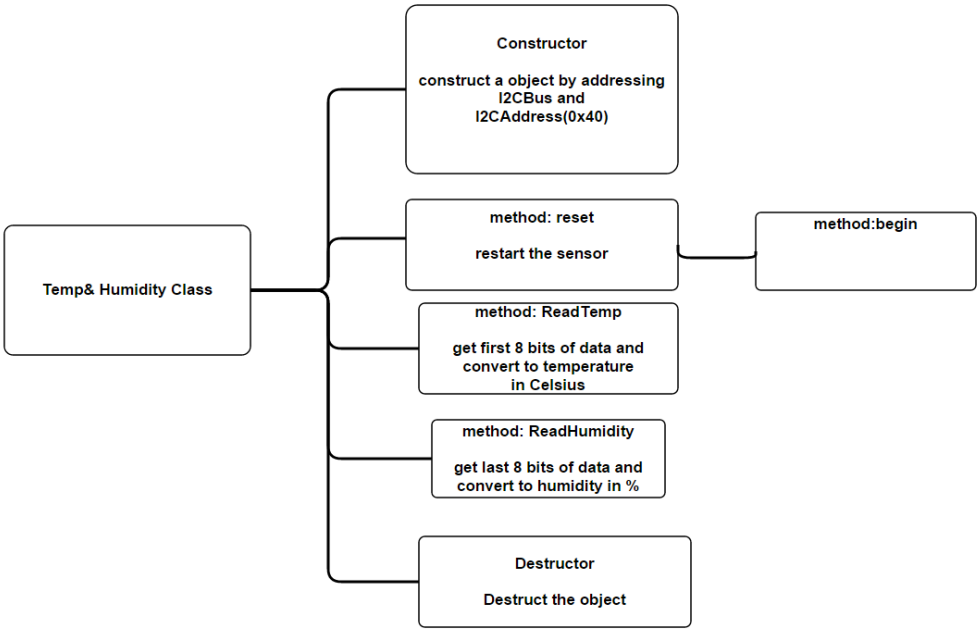

Figure 3.15 Class diagram of temperature and humidity sensor

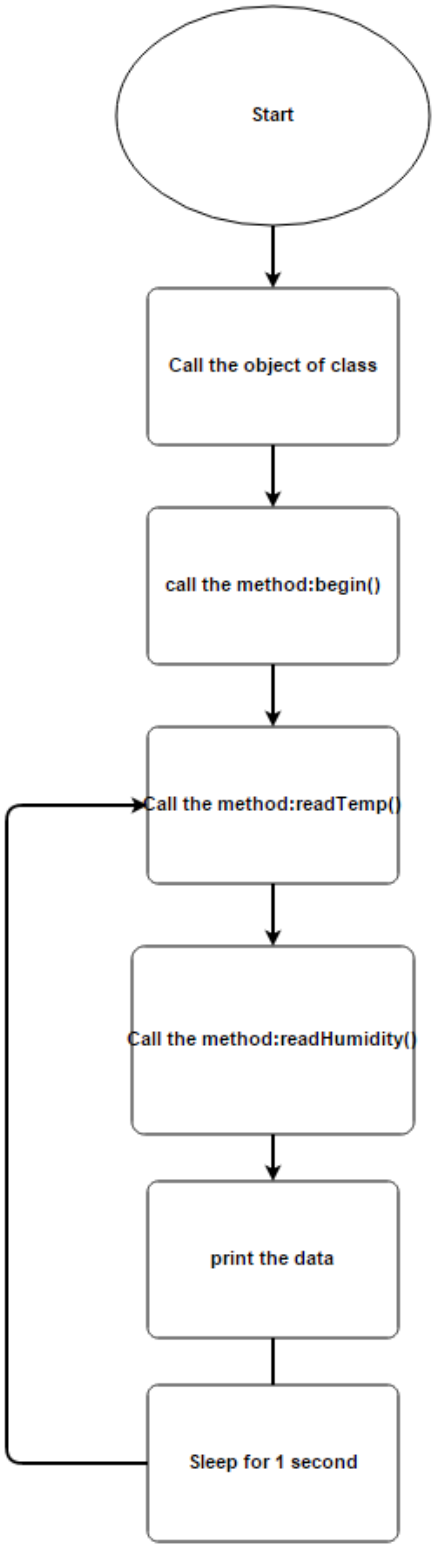

Figure 3.16 Flow chat of temperature and humidity sensor testing program

3.1.3 Centralized Power System

The goal of this section was to develop a power system. Due to the complexity of the loads in the system, the power system was designed based on power centralization. The benefit of having such a power system in the application was for convenient debugging and maintenance. Also, the power system designed this way can avoid electrical interference to other hardware circuits (i.e. sensor interface, communication bus). The next two subsections focused on the classification of the loads and the design of power blocks corresponding to the voltages.

3.1.3.1 Loads

Before designing the power system, the required current and voltage of each component in the system must be known. Therefore, the first step was to find the sinking current of each load. Table 3.2 lists the required voltages of different components. The required voltages for E-nose system were 12 volts, 5 volts and 3.3 volts. The 12 volts and 3.3 volts settings required only one load, and the number of load required for the 5 volts setting was nine. A 20% safety factor was applied to current (load). The final sinking currents (amperage) was 253.2 milliamps for 12 volts, 1,383.84 milliamps for 5 volts, and 36 milliamps for 3.3volts As a result, the total sinking current (amperage) of the full system was 1673.04 milliamps.

3.1.3.2 Design

Regarding the chip selection for the central power system, the POWER WEBENCH by Texas Instrument was used. The user-interface of WEBENCH is shown in Figure 3.17. After entering the required output voltage, 5 volts with a current of1.4

amp, the Texas Instruments TPS562209-5 and Texas Instruments LM2678-5.0 were chosen as the 5 volts switch regulator due to the minimized footprint and affordable price. These two chips are able to give fixed 5V output with maximum current at 1.5 amps. The schematics of TPS562209 and LM2678 are shown in Figures 3.18 and 3.19. For the 3.3 volts chip selections, a Texas Instruments LP2950-3.3 a linear regulator was selected for its ease of assembling and extremely low quiescent current. Figure 3.20 shows the schematic of LP2950.

The block diagram of the centralized power system was designed and this is shown in Figure 3.21. The 12 volts was the power source of the central power system because it was the highest required voltage among the loads and also the chip selection for step-down IC was wider than the boot IC. The corresponding load current for each voltage was referred from Table 3.2. The power source for the system was an AC/AC wall plug. As mentioned before, 12 volts was the voltage that was applied to the power systems, therefore a 12 volts AC to DC adapter was implemented to convert 120 volts AC 60 Hz from the wall to a fixed 12 volts DC voltage.

3.1.3.3 Centralized Power System Test Procedure

The test conducted was to examine the current limitation of the chip and the consistency of the output voltage. The expectation was that the voltage output for both of the LM2678 and the TPS562209 was 5 volts with maximum sourcing current of 1.5 amps. The expectation for the LP2950-3.3 was 3.3 volts with current limitation of 100mA. For each regulator, the current and voltage were measured with respect to different loads and

recorded. Then the LM2678 and TPS562209 were compared based on the performance, footprint size, and the cost of the two ICs.

Table 3.2 *Design of power supply for integrated sensor system*

	Specification		Factor safety (spec*20%)
Voltage (V)	Component	Current (mA)	Current (mA)
12	solenoid Valve	211	253.2
5	BBB	500	600
5	Pump A	250	300
5	Pump B	250	300
5	VOC-1 sensor	46	55.2
5	VOC-2sensor	46	55.2
5	Ammonia-1 sensor	10.6	12.72
5	Ammonia -2sensor	10.6	12.72
5	CO2 A	20	24
5	CO2 B	20	24
3.3	LCD	30	36
Total Design Load			
Voltage		Current (mA)	Current (mA)
12		211	253.2
5		1153.2	1383.84
3.3		30	36
Total		1394.2	1673.04

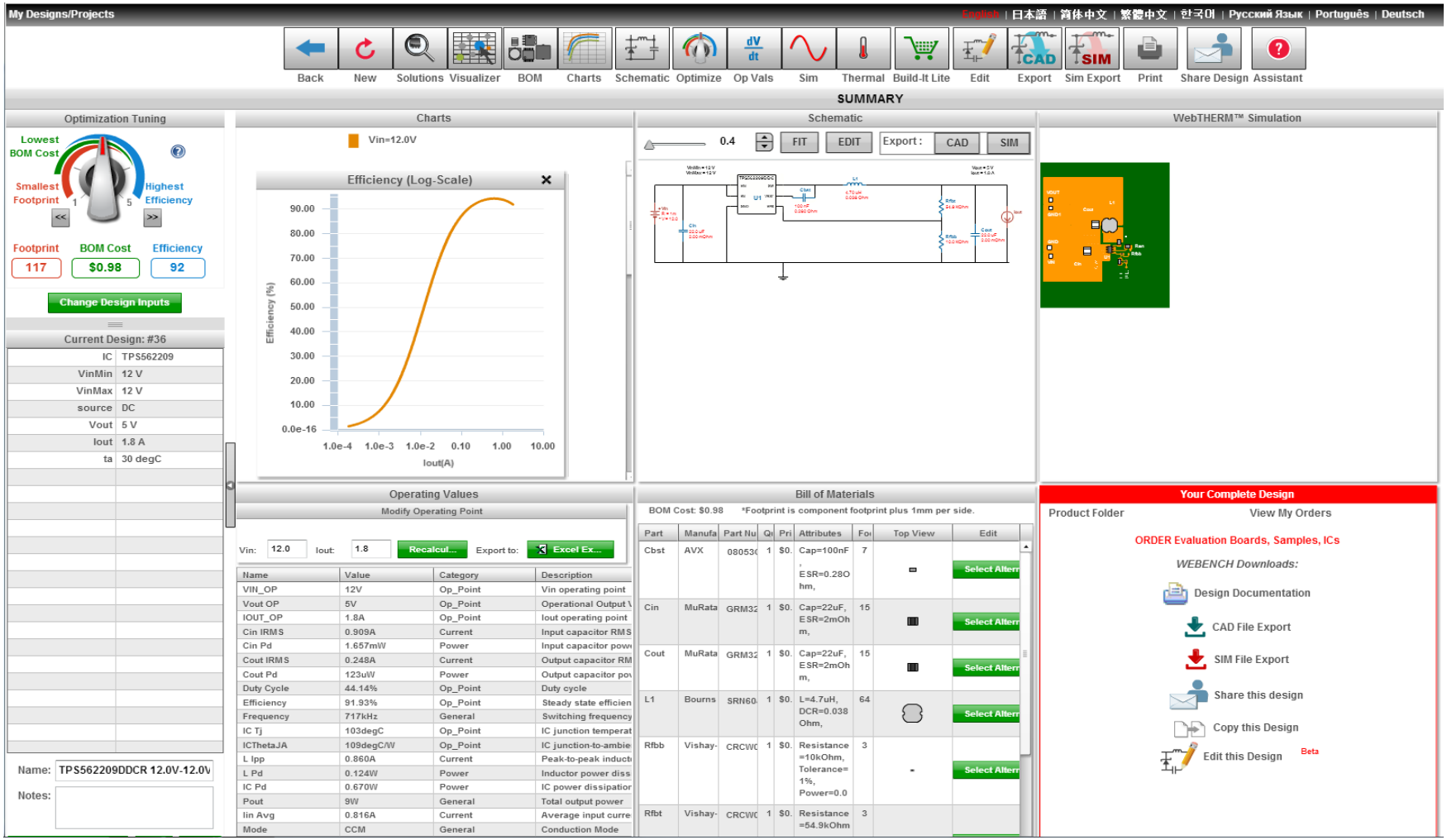

Figure 3.17 User-interface of WEBENCH by Texas Instrument

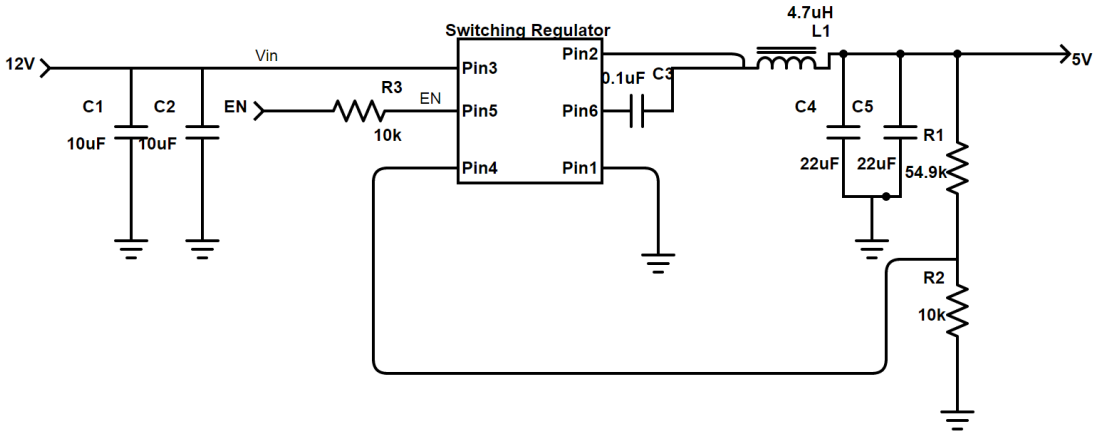

Figure 3.18 Schematic of TPS562209 LM2678-5.0(referred to Power WEBENCH by Texas Instruments)

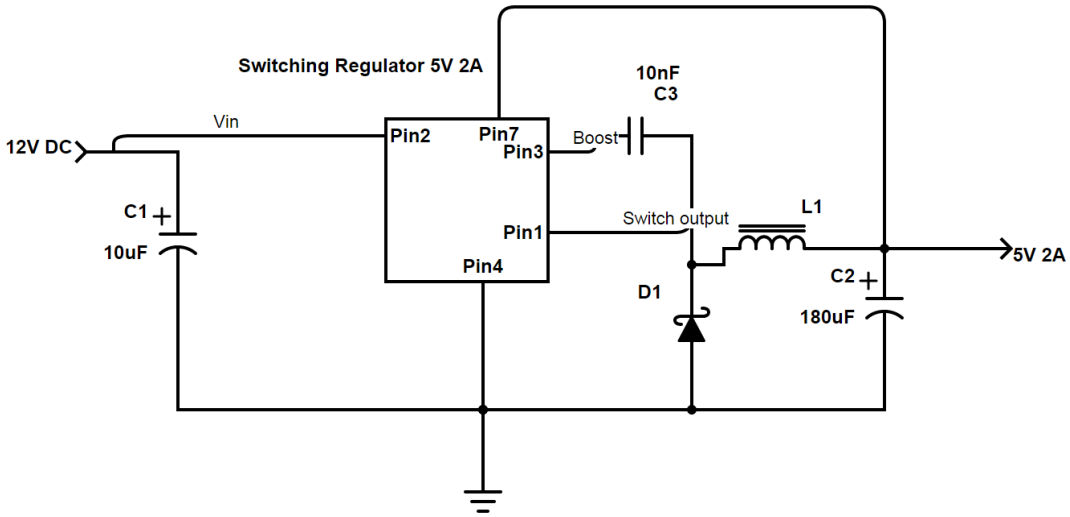

Figure 3.19 Schematic of LM2678-5.0(referred to Power WEBENCH by Texas Instruments)

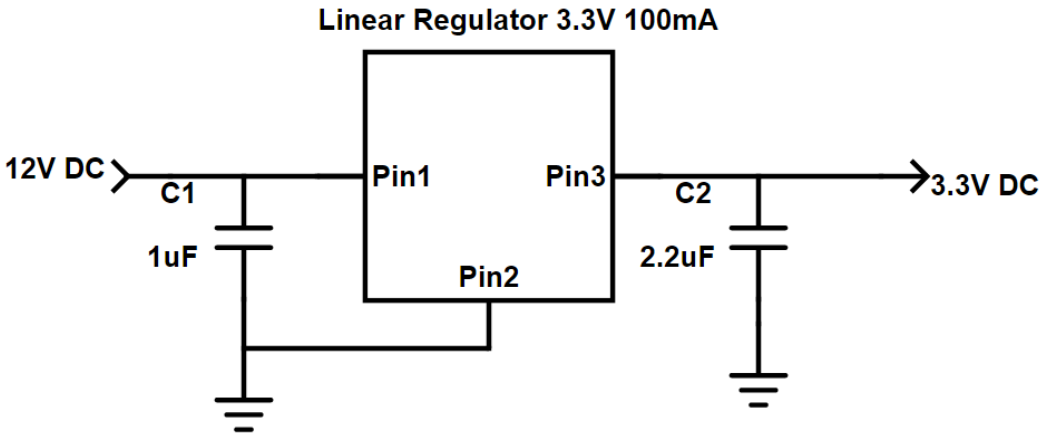

Figure 3.20 Schematic of LP2950-3.3(referred to Power WEBENCH by Texas Instruments)

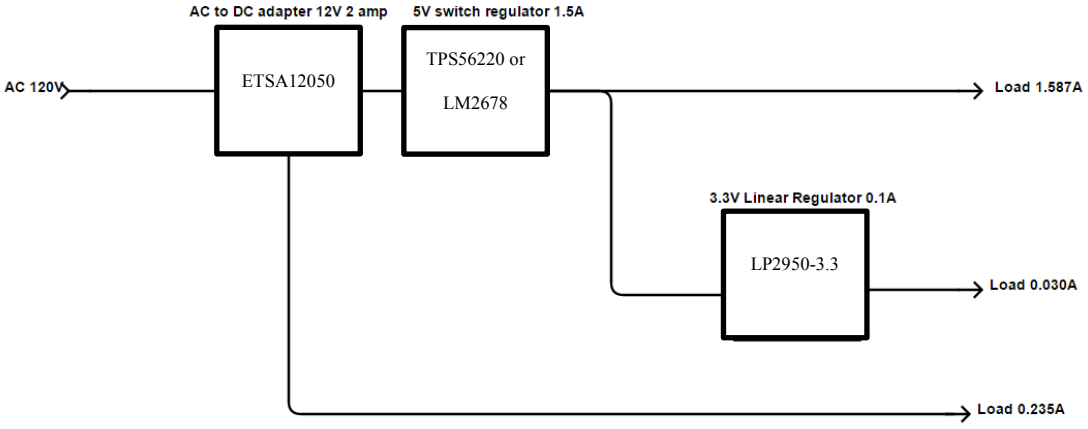

Figure 3.21 Block diagram of centralized power system (referred to Power WEBENCH by Texas Instruments)

3.1.4 System Integration

The last step of developing the E-nose system involved integrating the systems mentioned in the previous sections (i.e. electromechanical system, sensor system and centralized power system) with the computing platform. This section was broken down into four subsections: comparison of the computing platform, peripheral integration, hardware integration, and software integration.

3.1.4.1 Computing Platform Comparison

In order to select the most suitable computing platform for the system, a comparison of the most popular computing platforms was necessary. After recent products on the market were surveyed and the products' reviews were checked, the latest and most used single board computers were selected. The selected single board computers were the Beaglebone Black Rev. C, Raspberry Pi Generation 2 Model B, and Intel Galileo. The parameters that were compared among these three platforms are shown as following:

a. CPU
b. Memory type/ size
c. Debug support
d. Power consumption
e. Dimension of the board
f. Number of GPIO pin
g. Peripherals
h. SD card compatibility
i. ADC configuration
j. Number of timers/PWM

Beaglebone Black Rev. C

Beaglebone black was a low-cost, community-supported development platform that can be adapted to many electronic applications such as robot control, real time application, and environmental sensing ("beagleboard.org", 2015). The processor used was a 1GHz ARM Cortex with 512MB RAM, 4GB on-board flash storage and NEON

floating-point accelerator. The power consumption was 210-460 mA at 5V. Additionally, the Beablebone Black contained 65 GPIO pins with high logic level of 3.3 volts. There are also seven 12 bits ADC pins, and the maximum accepted voltage was 1.8 volt. Moreover, the Beaglebone Black has the standard communication peripherals such as I2C, SPI, UART, UBS and CAN. The physical size of the board was 86.36mm x 53.35mm. Software wise, the Debian Linux distro has been installed before the product was shipped, and the user can install a wide variety of other systems, such as Android or other real time operation systems. The information above was referred to from begleboard.org. (www.beagleboard.org)

Raspberry Pi Model B+

The following information is according to the official website of Raspberry Pi, the Raspberry Pi was a compact size single board computer that was developed by the Raspberry Pi foundation in UK. It was based on Broadcom BCM 2835 system on a chip, which used an ARM11 family 700M Hz ARM1176JZF-S microprocessor. Additionally, the Raspbetrry Pi contained its own graphic processing unit (GPU). The memory size was 512 Megabytes. For the peripherals, I2C, SPI, UART, USB and 8 GPIO pins were included with the platform. The board's power consumption was 700 mA with 5V power Supply. The dimensions of the board were 85.60mm x 53.98mm. Software wise, an operating system was not preinstalled. The developers must prepare their own SD card that contains an operating system (OS). The most popular OS for the Raspberry Pi was Raspbian, which was based on Debian, one of Linux distribution. (www.raspberrypi.org)

Intel Gallieo

The Intel Gallieo was a microcontroller board based on the Intel Quark SoC X1000, 400M Hz. The memory size was 256MB. The board's power dissipation was in the range of 80mA to 800mA with a 5V DC power source. The peripherals of the Intel Gallieo were I2C, SPI, UART, six 12-bit ADC pins, and 14 GPIO pins with high logic level at 3.3V DC. The physical size of the board was 100mm x 70mm. The software that the Intel Gallieo was able to run was Microsoft Windows, Mac OS, and Linux OS. The board also brought the simplicity of the Arudino integration development Environment Software on board. This information above is referred to the office website of Intel. (www.intel.com)

The result of comparison

As shown in Table 3.3, the Bealgebone Black was more suitable in this specific application due to several reasons. First, it contained the fastest processor speed among these three computing platforms. Second, it contained the largest on-board memory (4GB). Third, the Bealgebone Black contained more GPIO pins (65) than the Raspberry Pi (40) and the Intel Gallieo (14). Fourth, the amount of peripherals (i.e. Serial communication ports, timers, pwm) on the Bealgebone black was more abundant. However, the drawback of the Beaglebone black was the board's resources, which were limited to sources on Internet. But several guide books have been published recently. The Raspberry Pi had the largest community support among the three platforms.

Table 3.3 *Comparison of Computing platform*

Parameters	Beaglebone Black Rev. C	Raspberry Pi Mode B+	Intel galileo
Processor	Sitara AM3358BZCZ100 1GHz,2000 MIPS	700 MHz ARM1176JZF-S core	X1000 (16K Cache, 400MHz)
DRAM	512MB DDR3L 800MHZ	512MB	256MB DDR3-800MHZ
FLASH	2GB, 8bit Embedded MMC	[redacted]	[redacted]
SRAM	[redacted]	[redacted]	512KB
Debug Support	Onboard 20-pin CTI JTAG (OPTIONS), Serial Header		
POWER	210-460mA @5V = 2.3W	700 mA (3.5 W)@ 5V	80mA -800mA@5V = 4W
PCB SIZE	86.36mm x 53.34mm	85.60 × 53.98 mm	100mm x 70mm
I/O pin	65(3.3V)	8 GPIO(3.3V)	14(3.3V or 5V) Providing 10mA(Max), receiving 25mA(MAX), Internal Pull-up resistor of 5.6k to 10k
USB	USB2.0 Client Port - Aceess to USB0, Client mode via miniUSB Host port- Aceess to USB1, Type A socket, 500mA LS/FS/HS	2 USB2.0 PORTs	3 USB PORTS (USB 2.0)

Table 3.3 *continued*

PCI express	[redacted]		a mPCIe(e.g. wifi, bluetooth or cellular connectivity)
Serial Port	UART0 ACCESS via 6 pin 3.3V TTL		UART1 RS-232 XCVR
Ethernet	10/100, RJ45	10/100 Ethernet (RJ45)	10/100, RJ45
WIFI	VIA USB (may need extension cable to move away from the PCB)		Via PCI express
SD	microSD, 3.3V,32Gbyte	microSD, 3.3V,32Gbyte	microSD,32Gbyte , SD Library
User Input	Reset, Boot, Power		Reboot,reset
Video Out	HDMI 1280X1024(MAX)	Composite RCA, HDMI	[redacted]
Audio	Stereo, Via HIDM	3.5 mm jack, HDMI	
Communications	4xUART,2x SPI,2x I2C, 2xCAN,	UART, I C bus, SPI bus	I2C,TWI, SPI
ADC	7 AIN (1.8V MAX) 12 bits	[redacted]	6x -12 bits
TIMER	4x	1x	Not able to find the information
PWM	8x	1x	6x
weight	1.4 oz(39.69 g)		
Support Interface	LCD, GPMC, MMC		
Others		Broadcom VideoCore IV, OpenGL ES 2.0, 1080p30 h.264/MPEG-4 AVC high-profile decoder	RTC, lots of peripherial libraries

3.1.4.2 Peripheral component Integration

After the platform was decided on, the next stage involved integration of all the components. This subsection was targeted on the peripheral integration. An external ADC, digital potentiometer, OLED (organic LED) display, and communication transmission buses are discussed in this section.

External Analog to Digital Converter (ADC)

An external ADC will be useful for E-nose expansion of sensor in E-nose system. Also, due to the limited available ADC channels (7) on the Beaglebone Black board and the board's voltage range being 0 volts to 1.8 volts, an external 12 bits ADC was used. The external 12 bits ADC was the TLV2543IN from Texas Instrument that contained 11 channels with a sample rate of 66kS/s. The communication protocol used was SPI with a transmission speed rate at 4MHz. The hardware configuration is shown in Figure 3.22. As previously mentioned, the Beaglebone Black was only capable of 3.3V logic level. The external ADC accepted both 3.3V and 5V logic level. Figure 3.22 indicated that the signal direction of the signal on CK (clock), MOSI(Master out slave in) and CS (chip select) were directly from the Beaglebone black to the external ADC. On the other hand, the signal direction of EOC and MISO (Master in slave out) were from the external ADC to the Beaglebone black, which required the implementation of a level shifter for these two signals. A level shifter are used to convert digital signals from one voltage domain to another. In this case, the level shifter transformed the signals of EOC and MISO from 5V logic standard to 3.3V logic standard.

ADC Program class

For the ADC software interface, an ADC class was written and the class diagram is shown in Figure 3.23. There are three main public methods in the class: (1) “read_one”, (2) “read_one_with_sample_size”, and (3) “read_mutiple_with_sample_size”. The function of “read_one” was to return a voltage reading on a chosen channel. The “read_one_with_sample_size” method was similar to the previous method but here the user can define the sample size. The returned value was the mean of the samples recorded. The last method in the class was the “ read_mutiple_with_sample_size”. This method allowed the user to select the number of channels used. The starting channel was always starting from channel 0. Also, similar to the previous method, the “read_multiple_with_sample_size” also allowed the user to define the sample size.

Testing of the functionality of ADC

The test program defined the object of the program and called the “read_mutiple_with_sampel_size (a, b)”, where ‘a’ is the channel number to which the function stop reading (start at Channel0). ‘b’ is number of sample. In the testing program, ‘a’ is 13 and ‘b’ is 10 (random choice). The program reads 11 channels (0-10) and other reference channels (+ref,-ref and median of ref) for ten times and calculated the average of each channel. The flowchart of the program is shown in Figure 3.24. The program ran in a continuous loop until the CTL + c command was detected.

The hardware setup for the test is shown in Figure 3.22. Channels 0 to channel 4 were connected to power supplies with random voltages of 1 volt, 2.5 volts, 5 volts, 3.3 volts and 4 volts respectively. The rest of channels were connected to ground. The

positive reference was connected to 5 volts and the negative reference was connected to ground.

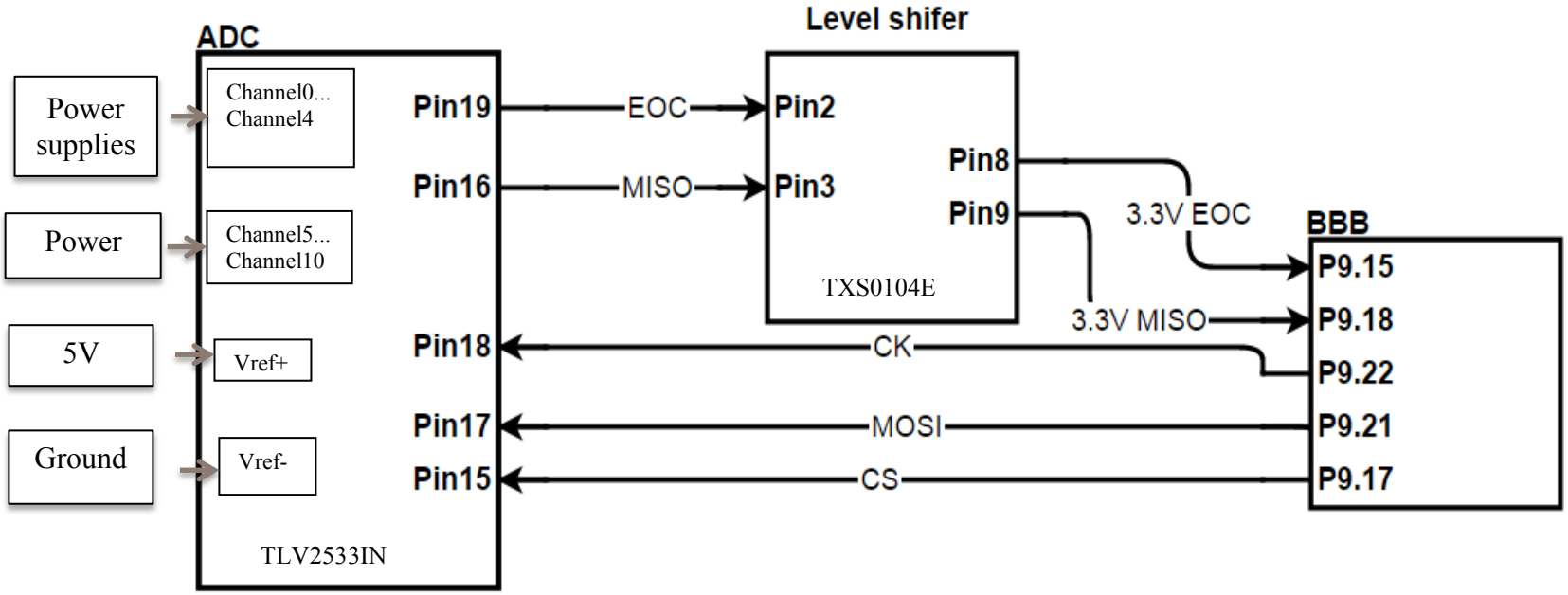

Figure 3.22 Hardware configuration of external ADC (referred to the TLV2533IN datasheet)

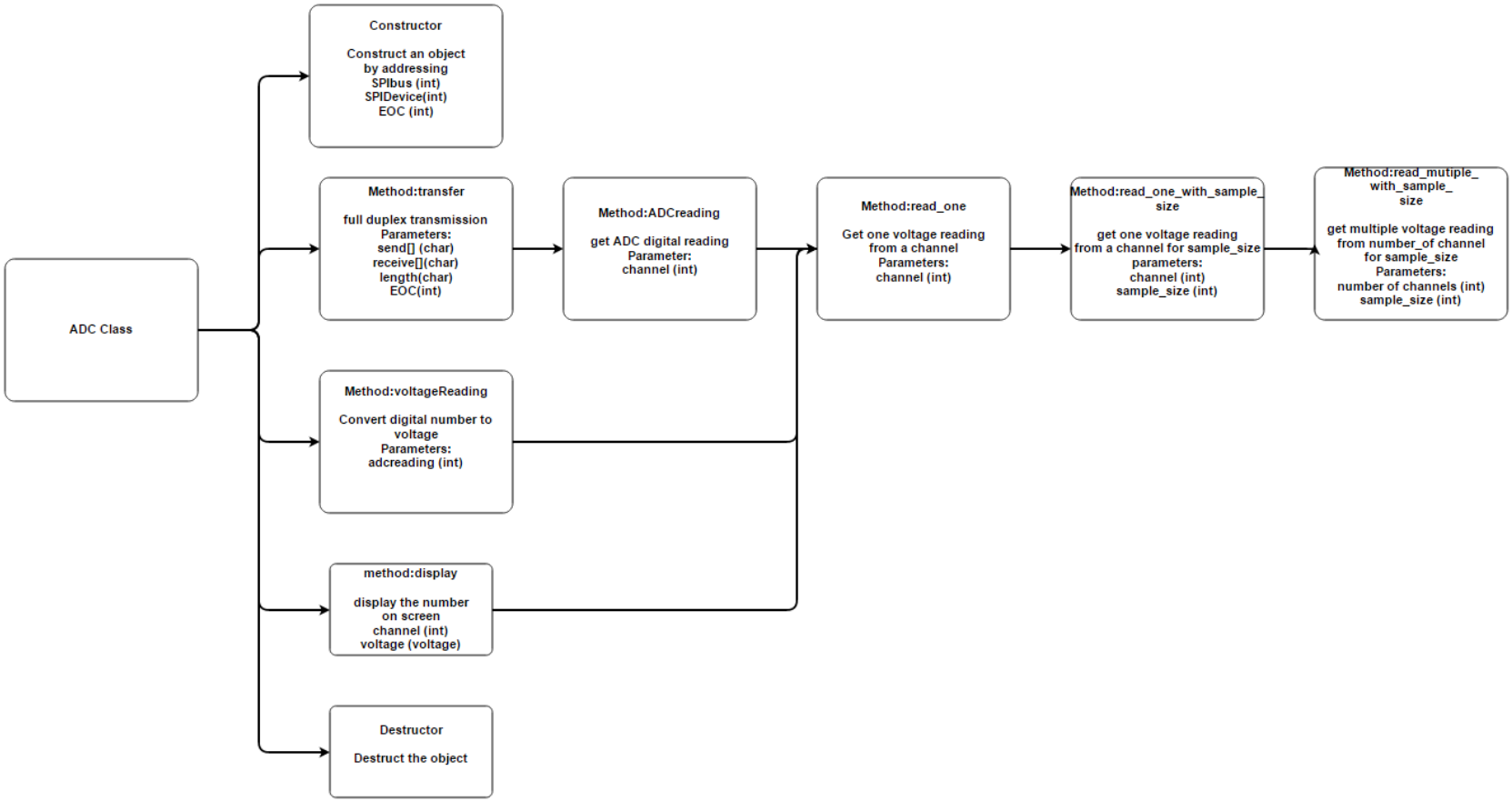

Figure 3.22 The class chart of external ADC

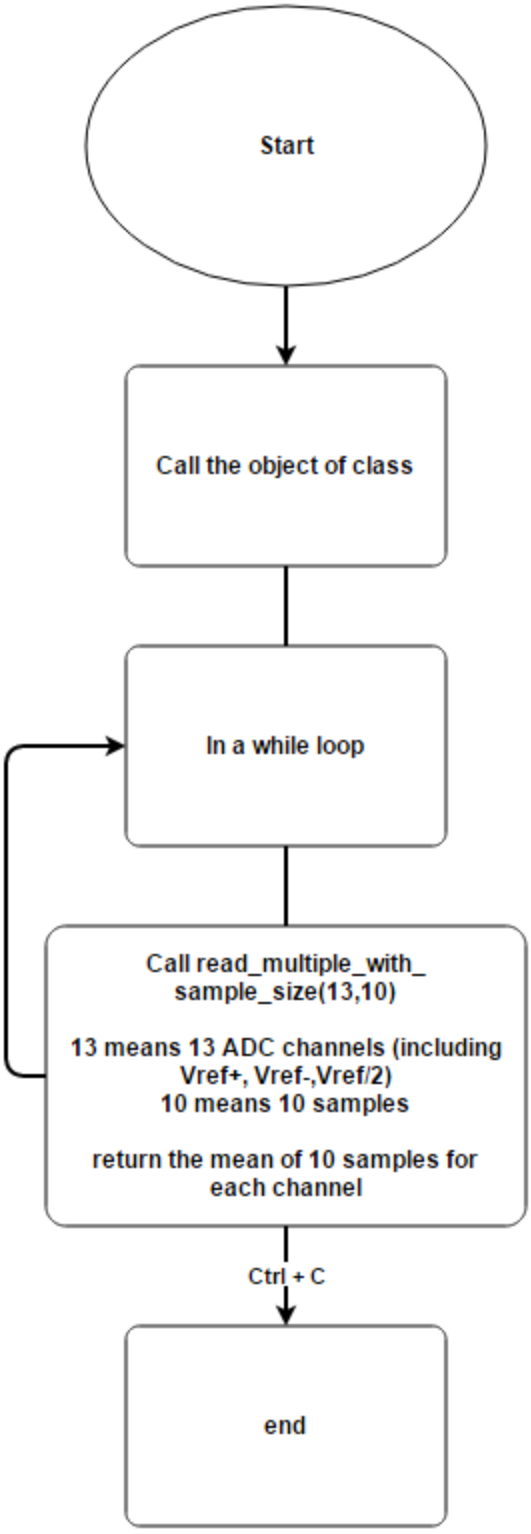

Figure 3.23 Flow chart of ADC testing program

Digital Potentiometer

As mentioned in the previous sections on the VOC and ammonia sensors, a potentiometer was used to adjust for sensor sensitivity. Two MCP4205 programmable potentiometer chip with a range of 3.3 ohms to 50k ohms by Microchip were implemented in the circuit. The resistances changed inversely proportional to the value from 0 to 255. Two potentiometers in each chip and the communication protocol used was 3-wire SPI.

The hardware configuration for the digital potentiometer was shown in Figure 3.25. POT1 and POT2 represent the potentiometer chips. As mentioned above, the chip has two potentiometers. POT1 was adjusting the sensitivities of two VOC sensors in the system. POT2 was used to change the sensitivity for the other two ammonia sensors. From the datasheet, MCP42050 has Daisy-Chain configuration, which meant that the SO pin from one device (POT1) connected to the SI pin on the next device (POT2). The data on the SO pin was the output of the 16-bit shift register. This configuration allowed the host to connect to multiple devices without using a separate CS line for each device.

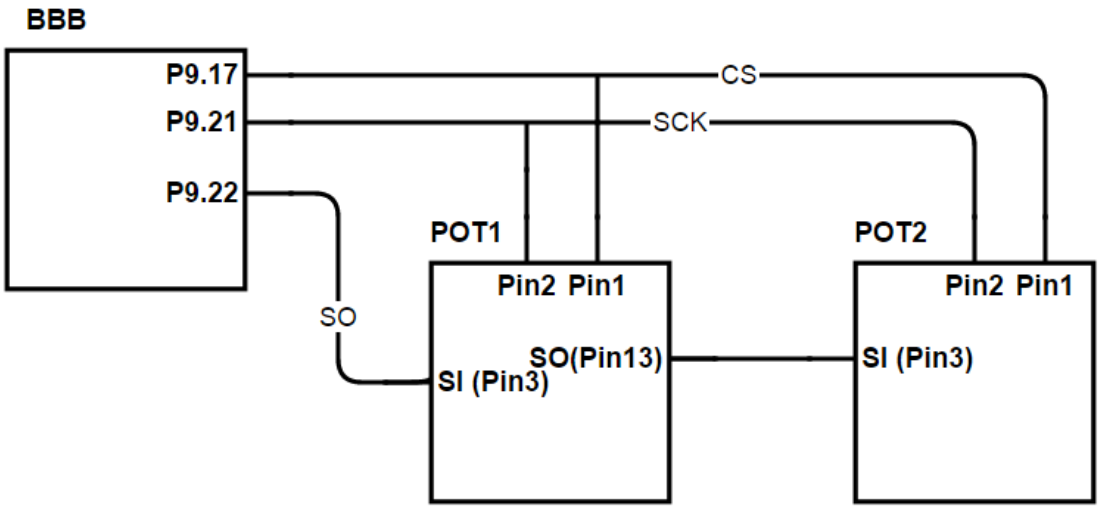

Figure 3.24 Hardware configuration of programmable potentiometer for VOC and ammonia sensors

POT Class and initial test procedures

The POT class was one of the child classes from the SPI class. Two main methods of the POT class were named “TWO_POTs” and “FOUR_POTS”. “TWO_POT” function was used to change the value of potentiometers on one device, and the “FOUR_POTS” function simultaneously modified the value of potentiometers on both devices. The class diagram was shown in Figure 3.26. The test was established by first changing the value of potentiometer and then using a multimeter to measure the resistance of each potentiometer. The measured values were compared with the expected values.

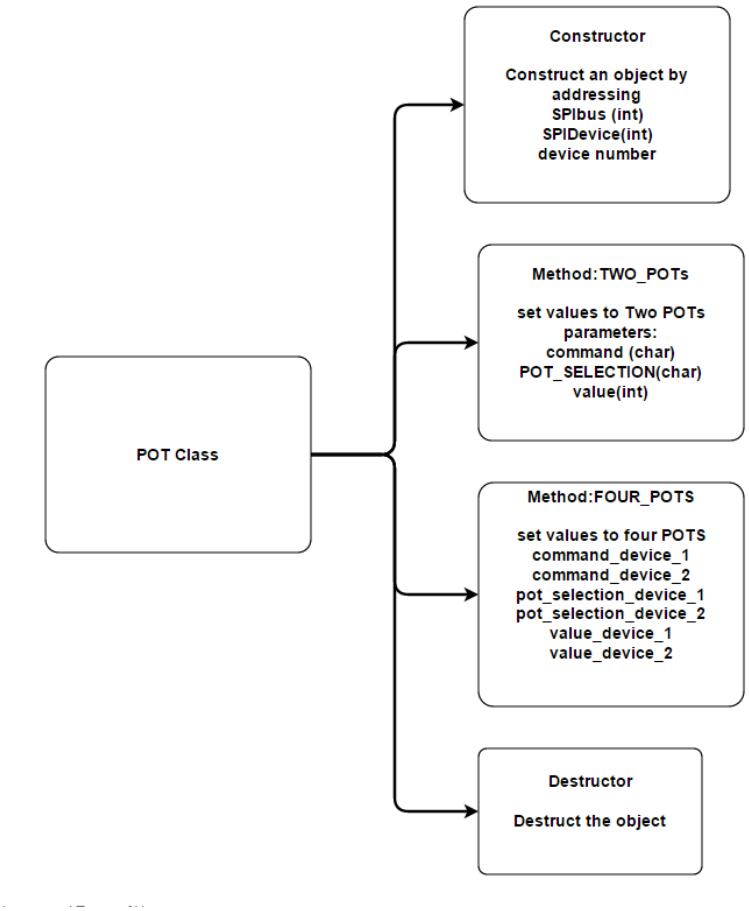

Figure 3.25 Class chart of POT class

Display- Monochrome 0.96" 128x64 OLED graphic display

The display monitor, UG-2864HSWEG01 made by Univision Technology Inc. in Taiwan, employed a small 1” diagonal OLED with high contrast. The screen has 128x32 individual white pixels, and does not have a backlight that would need more power. This specific display used 3- wire SPI plus two GPIO pins as a communication protocol.

Figure 3.27 showed the hardware configuration for the OLED. The power for the OLED was supplied from the 3.3 volts regulator on the Bealgebone Black. DATA, CLK and CS were part of the SPI specification. RST was the reset signal and the D/C was the DATA /Command switch. According to the datasheet, when D/C was pulled HIGH, the

DATA signal was treated as data. On the other hand, when D/C is pulled LOW, the DATA signal was transferred as command to the command register.

The display program was written using python script and used an embedded python library to eexculte the program within C++ environment. Figure 3.28 shows the flow chart on how the python script was ran using the c++ program. The figure 3.29 was the python script for controlling the OLED display.

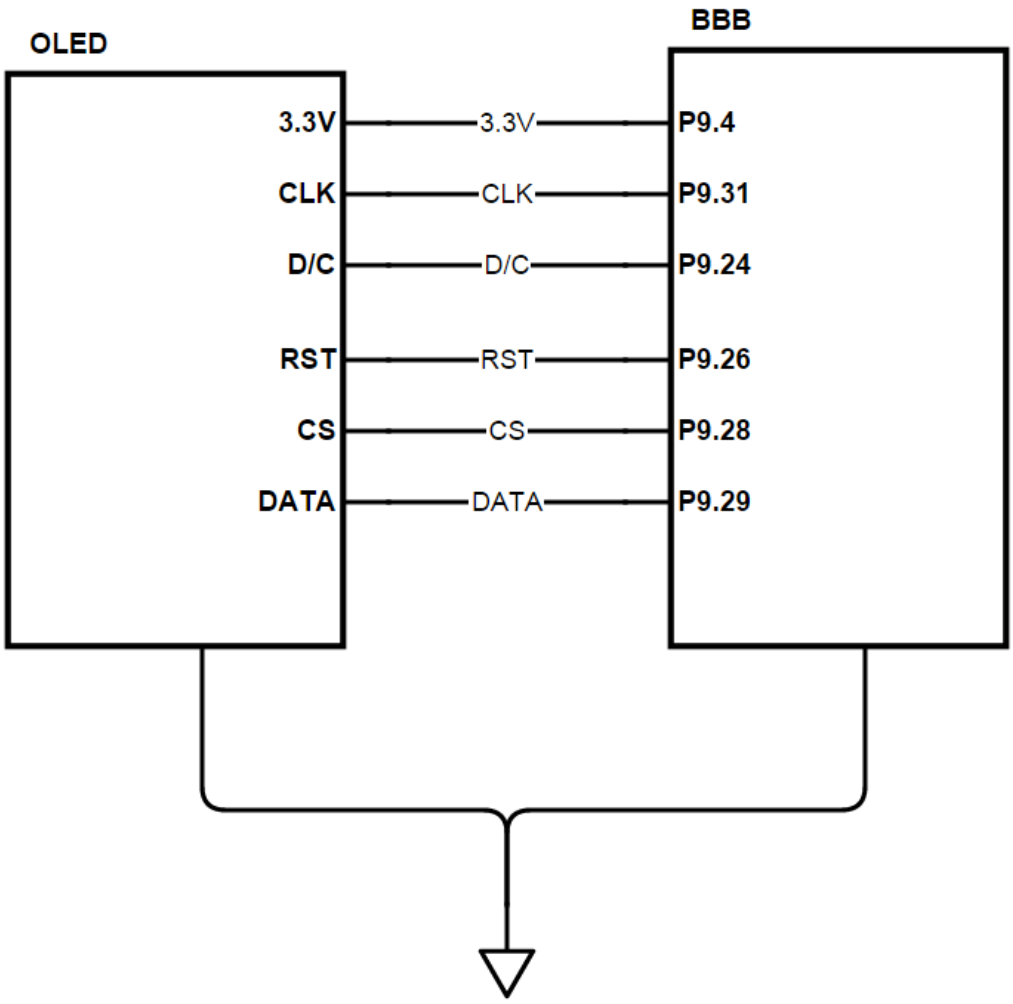

Figure 3.26 Hardware configuration of OLED display

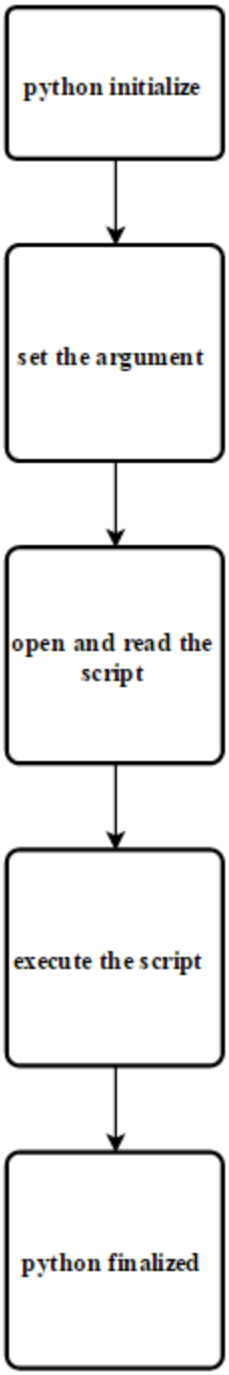

Figure 3.27 Flow chart of executing python script in C++ environment

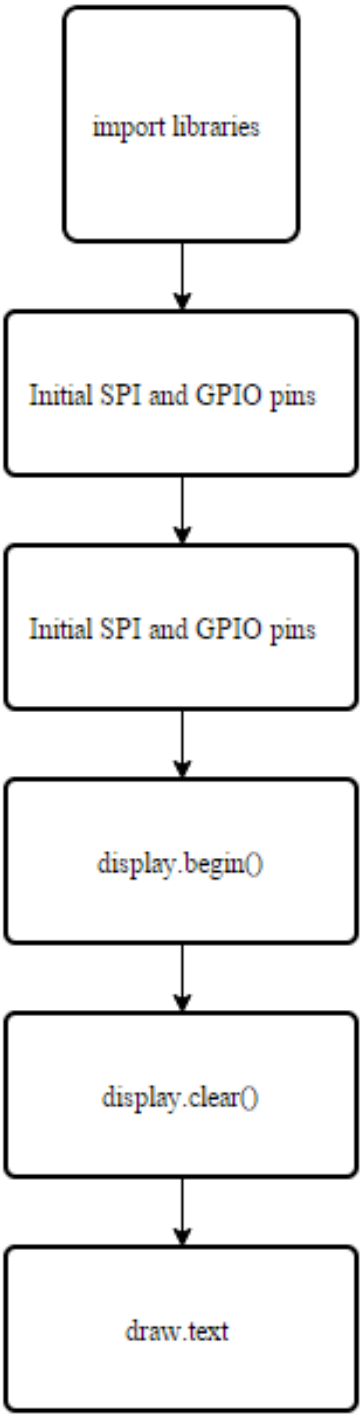

Figure 3.28 Flow chart of OLED interface using python

Transmission Buses for device communication

The integrated sensor system contained three SPI devices and two I2C devices, but the serial communications on the Bealgebone Black were limited-(two SPI buses and two I2C buses). Therefore, the circuit was modified to let multiple devices operate under the same bus lines. Figure 3.30 shows the logic circuit for interfacing the ADC and the programmable potentiometers using gates (Molloy, 2015). In most of the circuit configurations were same. The only difference was the configuration of the CS signal and an addition of a GPIO pin (P9.16). The first slave device, ADC, got the CS signal from output of the OR gate (U1) where one input was connected to the CS and the other input was connect to a GPIO pin on Beaglebone Black. The second device, the potentiometers, received the CS signal from the other output of the OR gate (U2) where one input was connected to the CS and the other input was connect to the GPIO that was inverted using U3 gate. This configuration ensured that only one slave device is active during communication. Figures 3.31 and 3.32 illustrate the logic of in circuity OR gate and NOT gate, in high and low condition respectively.

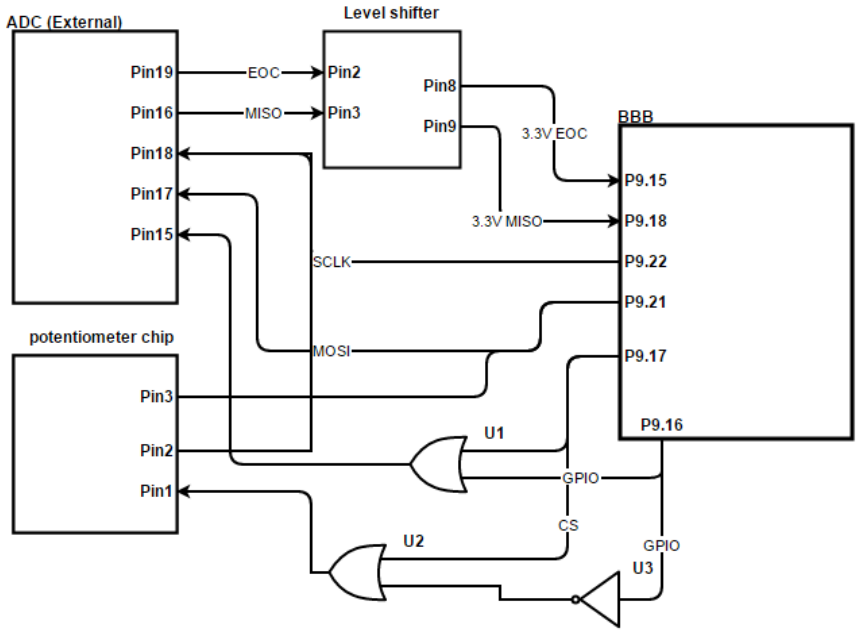

Figure 3.29 Circuit diagram for interfacing ADC & potentiometer with SPI (Molly, 2015)

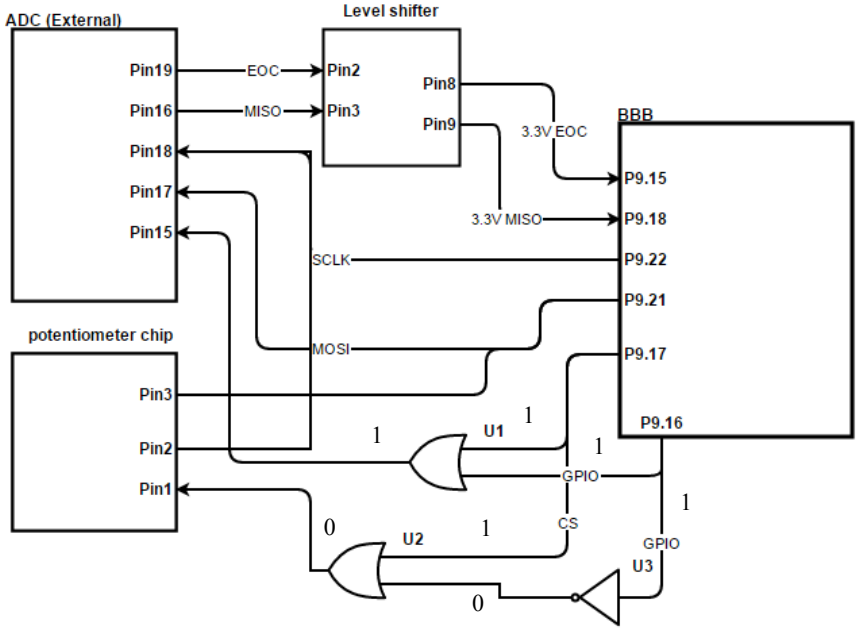

Figure 3.30 Communicating between BBB and ADC when P9.16 is HIGH

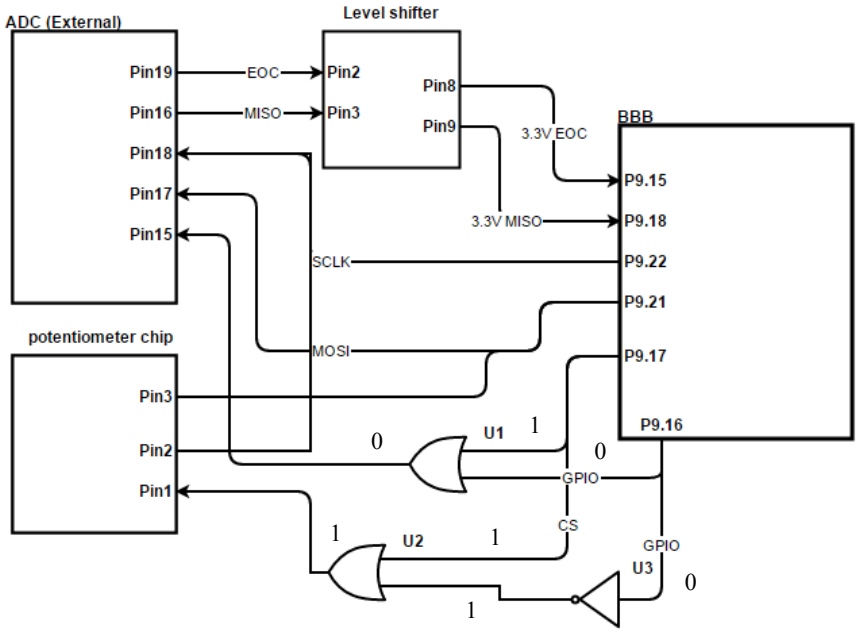

Figure 3.31 Communicating between BBB and potentiometer when P9.16 is LOW

3.1.4.3 Hardware Integration

PCBs

All the acquisition circuitries of the sensors, the external ADC circuitry, the centralized power system, and the pump/solenoid drivers were transferred to PCB using EAGLE software by CADSOFT. The design file was sent to a commercial PCB manufacturing facility, Advance Circuits. Two PCBs (Central power and sensor acquisition) were designed. The pump driver and solenoid driver were included on the centralized power system PCB. This is shown in Figures B.1 and B.2. The second PCB contained the acquisition interface and external ADC circuit. This is displayed in Figures B.3, B.4, and B.5. Figure 3.33 shows the schematic of the PCBs for the integrated system. The dimensions of the PCB were 105.41mm x 55.88mm. The bottom left of the figure is the combination of the CO_2 hardware interface and the ADC components. At the top left

of figure, the ammonia interface is located and the VOC sensor circuit is located at middle of the figure.

System layout

The enclosure for the integrated sensor system was designed and built using the 3D printers in the Boilermaker lab located in Knoy hall. The enclosure consists of three layers. The bottom layer contained the power system PCB and the transmission bus point to point board. The acquisition interface PCB was in the middle layer, and the top layer was for the Beaglebone Black. Those three layers were interconnected via the holes on the two sides of the enclosure. The layout of the integrated system is shown in Figure 3.34. Lastly, the whole system was mounted on a wooden plate, shown in Figure 3.35 and 3.36.

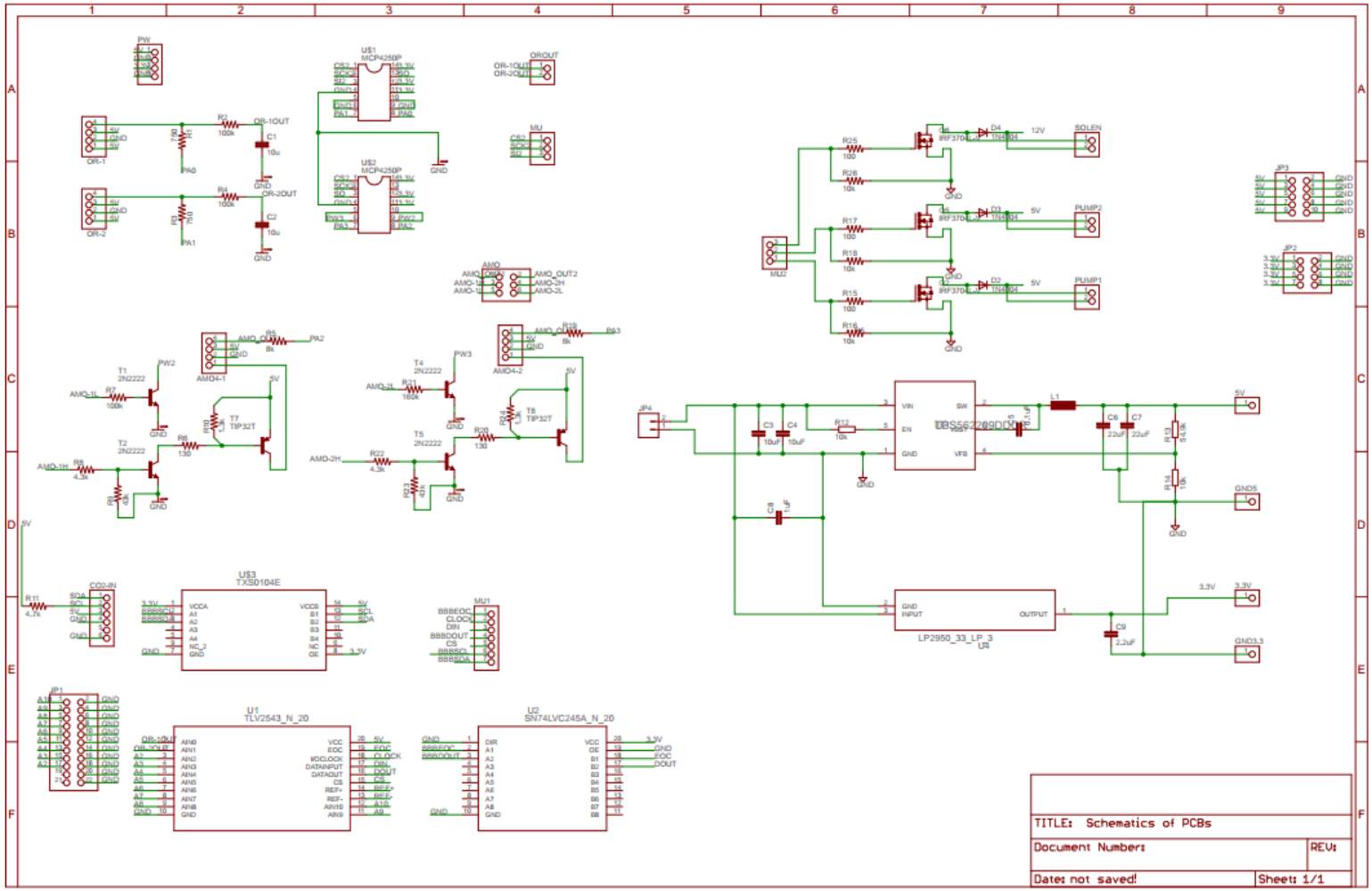

Figure 3.32 Schematic of all PCBs

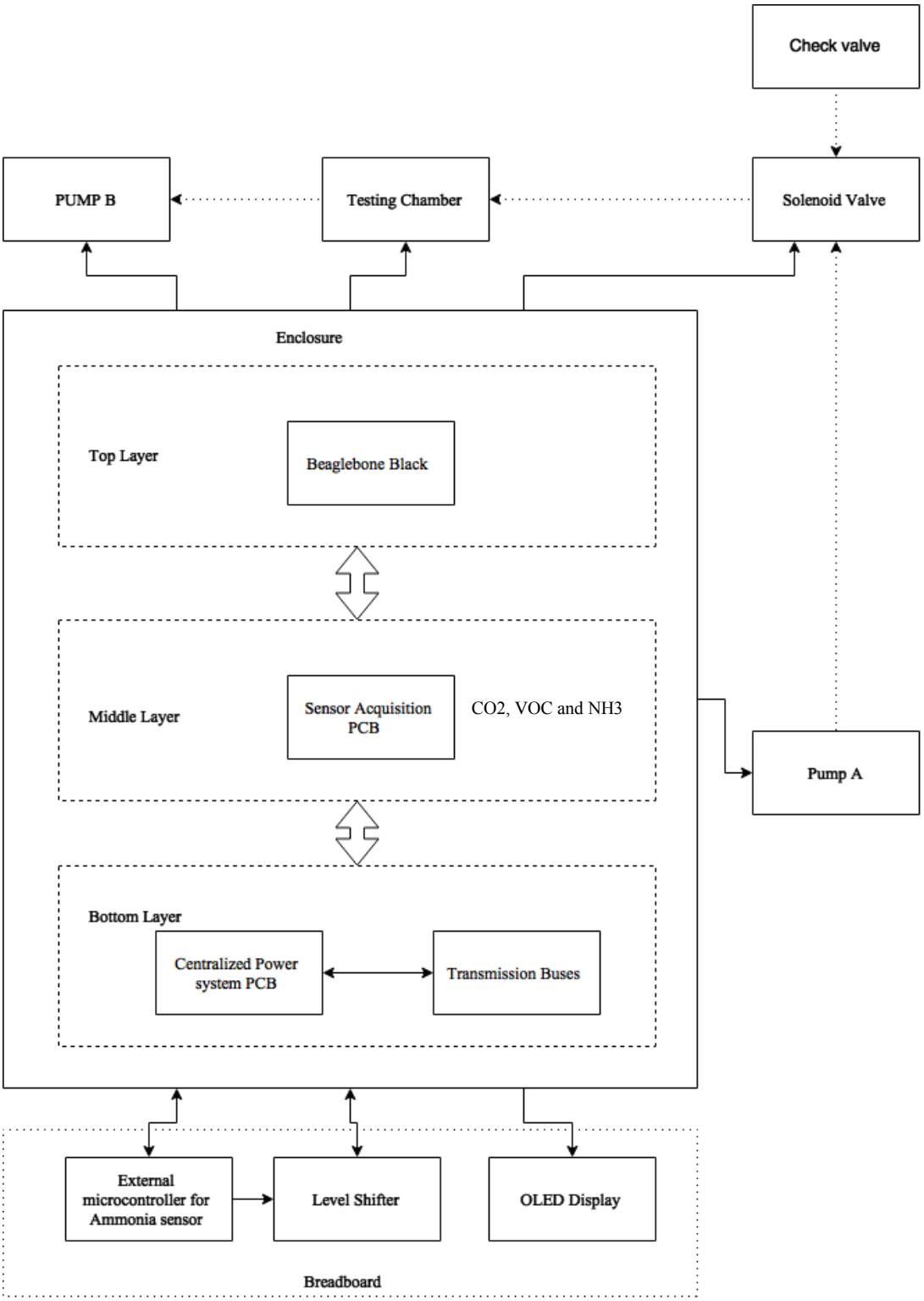

Figure 3.33 Layer layout of the integrated sensor system. Dashed arrow is the air direction.

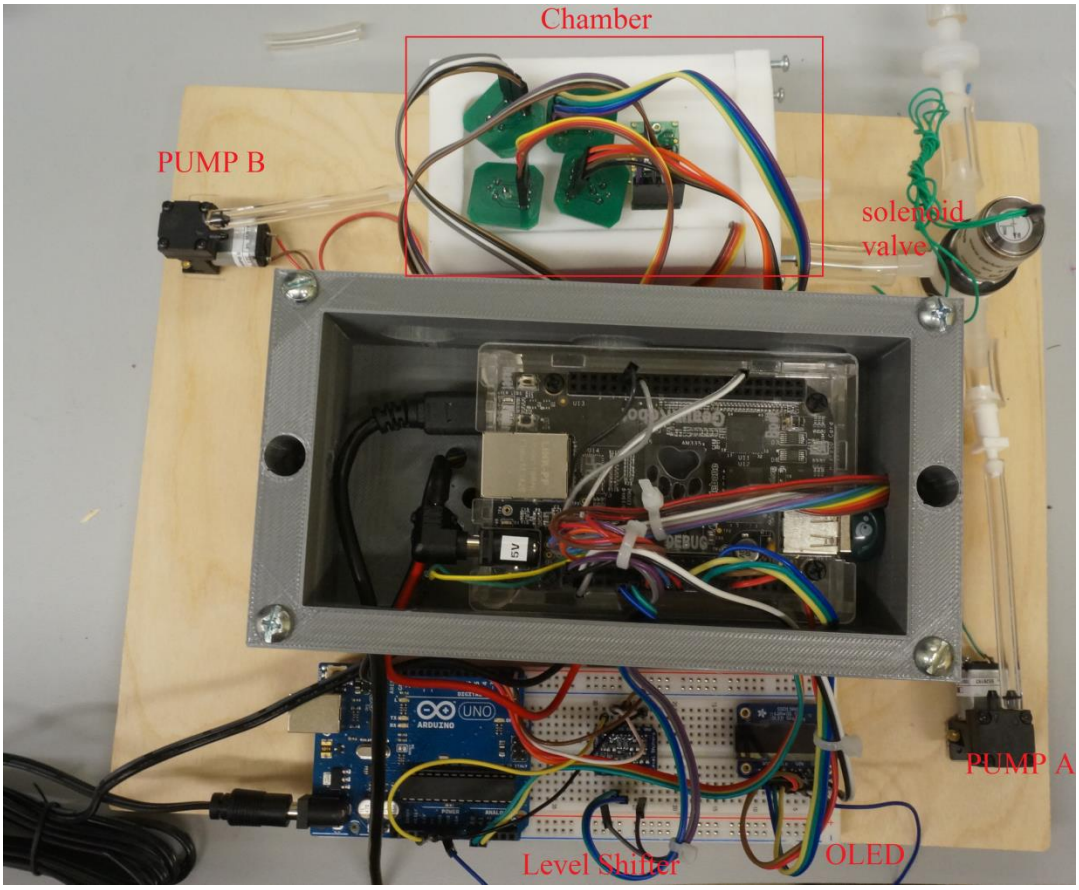

Figure 3.34 Top view of the integrated Sensor System

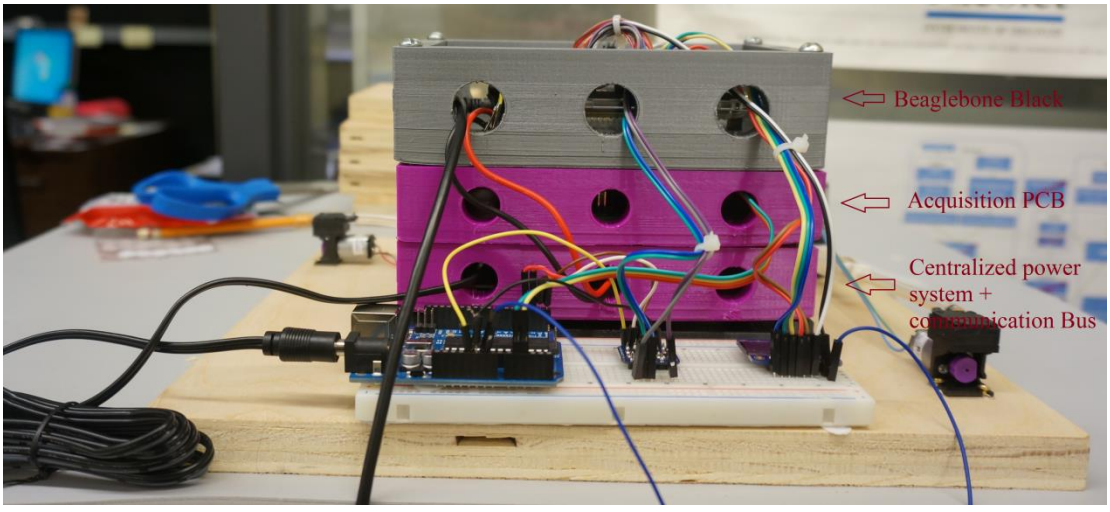

Figure 3.35 Side view of the integrated sensor system

3.1.4.4 Software Integration

The last section of the integration was the software integration. This subsection explained the programs included the operation of the system, the data acquisition, and the signal processing.

Operation of the system

There are five stages in the program. The flow chart for the main program is shown in Figure 3.37(a) and its source code is in Appendix E. This main program incorporates several external library/classes – Python.h, SPI-ADC.h, PWM.h, GPIO.h, I2C_CO2.h, and I2C_Temp_Humidity.h. GPIO class is to easily export, convert and modify the GPIO pins on Beaglebone Black. PWM class makes PWM pins to run, stop and adjust the PWM characteristics (i.e. period, polarity, duty cycle, and frequency) efficiently. These two classes were written in "Exploring Beaglebone" by Molly (2014). The functionality of SPI-ADC, I2C_CO2 and I2C_Temp_Humidity are described in previous sections of the thesis.

The five stages were (1) initialization, (2) air flush, (3) reference collecting, (4) gas injection, and (5) data collection. The first step in the program was to initialize all the objects of the classes as well as the necessary parameters on the Bealgebone black (i.e. pin configuration, serial communication enable, PWM enable). Next, the system went into the air flush stage. The time of air flushing was determined by the equations below:

$$T_f = \frac{V_a}{Q_m} \times 1.2 \qquad \text{(Equation 3.5)}$$

$$V_a = semi\ circle\ cylinder + rectangular\ prism \qquad \text{(Equation 3.6)}$$

$$Q_m = 400\ \frac{cm^3}{min}\ at\ 5\ volts\ DC\ rate \qquad \text{(Equation 3.7)}$$

$$where\ V_a\ is\ the\ volume\ of\ the\ chamber\ that\ air\ occupied\ and$$

$$Q_m is\ the\ delivery\ rate\ of\ motor\ in\ atmospher\ pressure.$$

After the calculations were made using the above equations, the resulting V_a value was 152.34 cm^3 and the approximated time was 28 seconds. During this period, the air was sucked by the pump, and fresh air got into the chamber. The next stage was to store the reference (air) data for T, a changeable time variable in seconds. In this time the data from each sensor (alcohol, ammonia, CO_2, humidity and temperature) were collected by the Bealgebone Black with different time intervals. The timing flow chart for collected data from each sensor is shown in Figure 3.37(b). In Figure 3.38, the timing was control by the combination of thread, a smallest unit of processing that can be executed asynchronously, and timer. The time between sample collections for the alcohol sensor was 50 milliseconds. For the ammonia sensor, the time interval between sample collections was 500 milliseconds. The data from the temperature and humidity sensor and the CO_2 sensor were collected every 5 seconds. Right after T, the interest of gas was injected and the processor was kept collecting data from the sensors for another T. Once the time was up, a signal was sent to all the thread functions to ask for exit. Next, all the data files were saved and closed. Lastly, the pump and the valve operations were stopped.

Signal processing

The signal processing was based on using MATLAB. The following are the procedure for signal processing:

1. Sent the collected data to the host PC
2. Stored the data into the cell. (The functionality of cell is similar to array in MATLAB)

3. For VOC sensor and ammonia sensor, converting the voltage to sensor resistance by using the equations that described in the sensor sections
4. For VOC sensor and ammonia sensor, normalization was implemented using the equation below:

$$R_n = \frac{R_s - R_f}{R_f} \quad \text{(Equation 3.8)}$$

Where R_s is the resistance of the sample and R_f is the resistance of the reference.

5. For VOC sensor and ammonia sensor, the normalized values of each observation and the mean of normalized values for all observations were plotted with respect to time.
6. For CO_2 sensor and Temperature and Humidity sensor, the data was plotted along with the time in seconds.

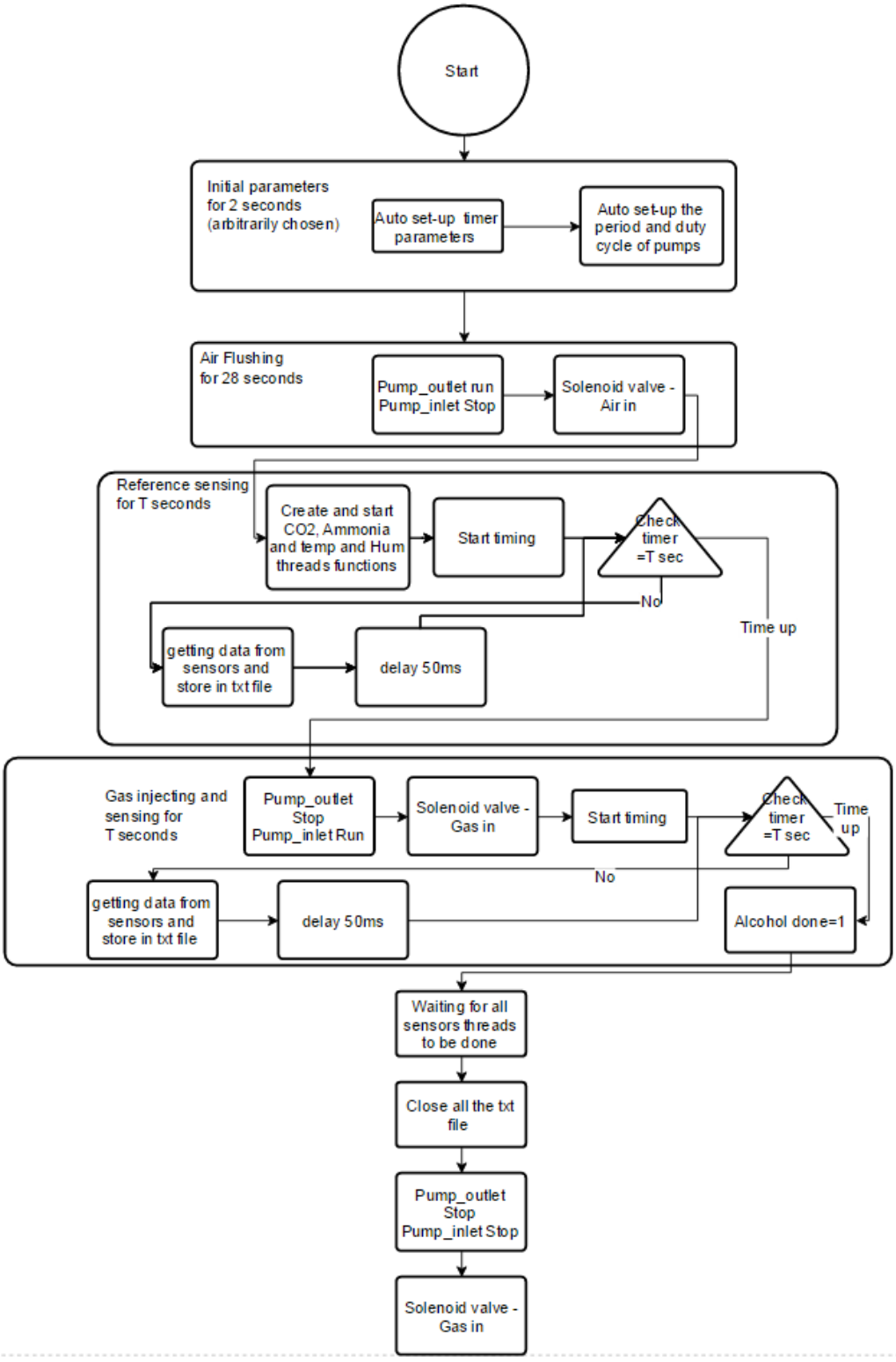

Figure 3.36 (a) Flow chart of the operation program, hosted on Beaglebone black.

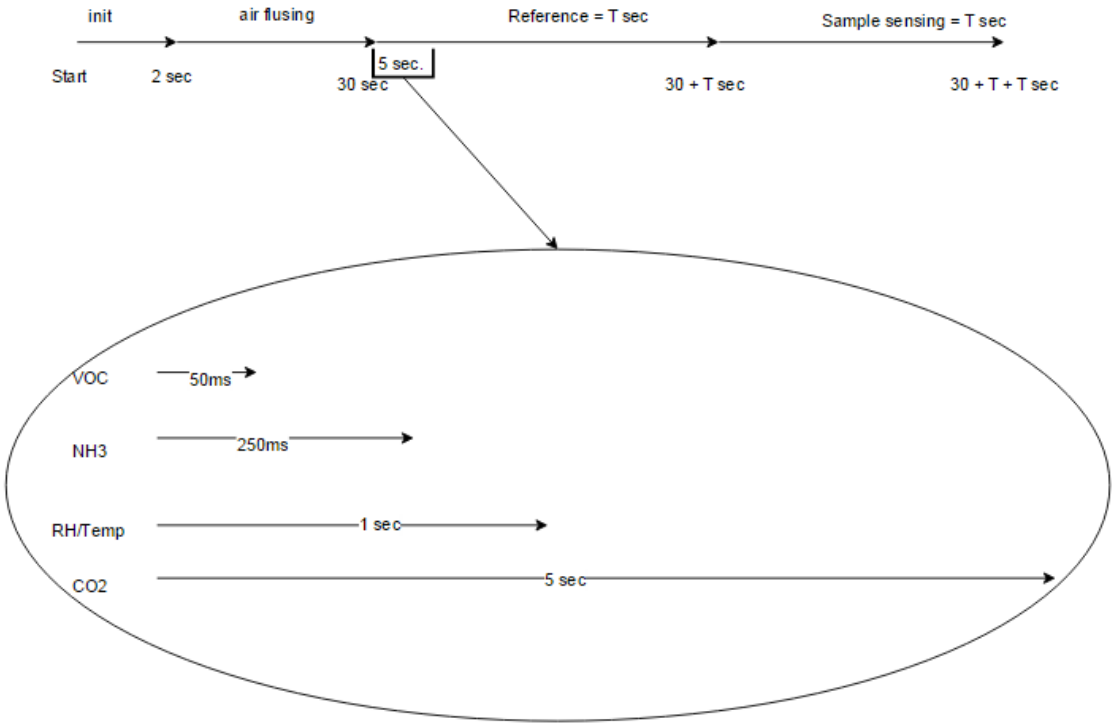

Figure 3.37 (b) The timing chart for collecting data from the sensors. (Beaglebone Black gets data from VOC sensors for every 50ms, from NH3 sensors for every 250ms, from Temp/RH sensors for every 1 second, and from CO2 sensor for every 5 seconds.)

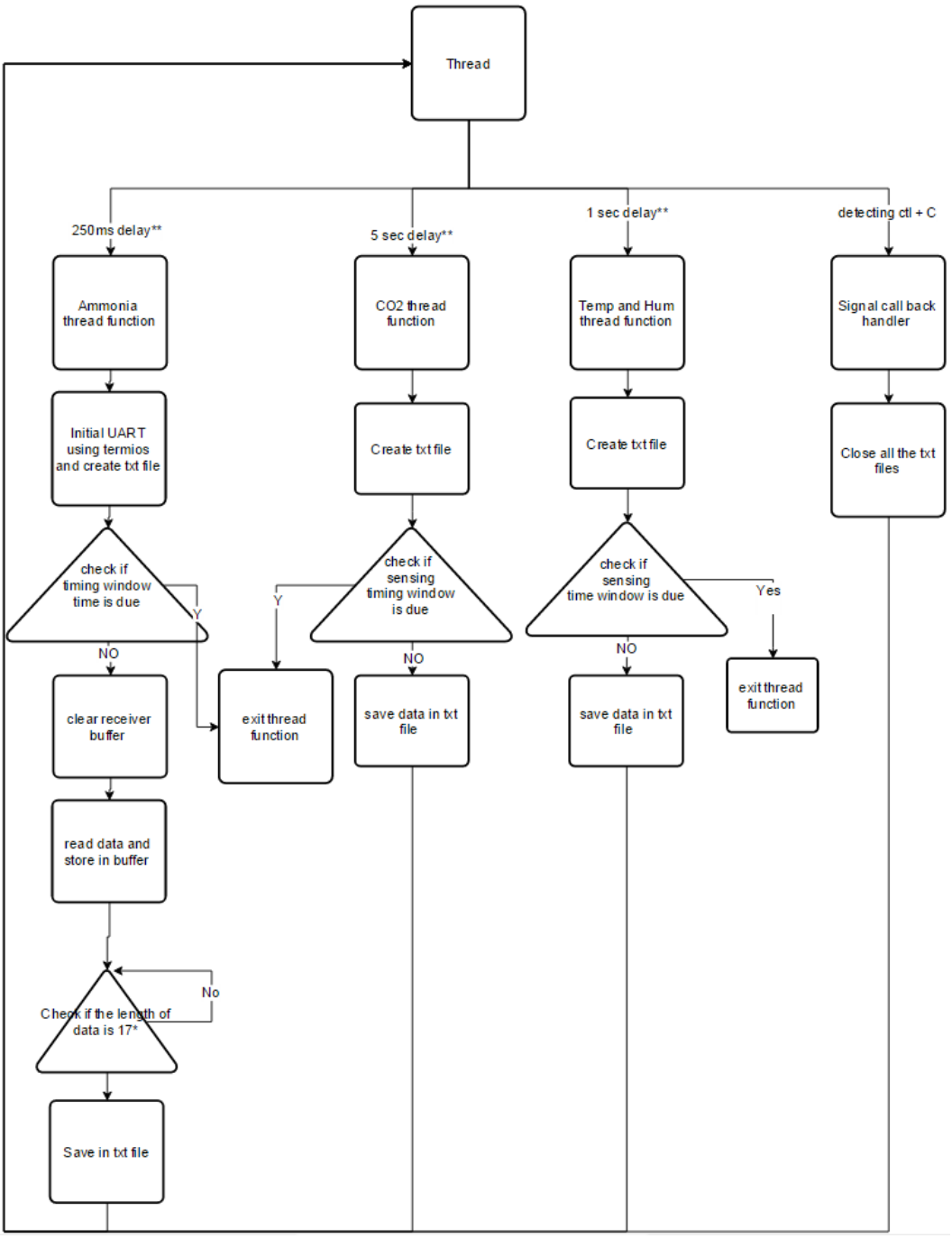

*Ammonia data format -"x.xxx.xxx.xxx.xx"("x.xx" is the structure of one data at either 5ms or 6ms, the first 6 numbers represents the data at 5ms and 6ms from first ammonia sensor and the rest are from second ammonia sensor.) The number of the characters is 17.

**CO_2-5s 1data.NH3-250ms-2 data. Temperature-5s-1data. Humidity-5s-1data

Figure 3.37 Flow chart of the sensor (thread) functions. *

3.1.4.5 Preliminary test

Due to the time constraint and the difficulty of obtain the gas sample, the experiment were conducted under preliminary testing that focused on only the presence of the gas of interest and not on the concentration of the gas. The test was separated into two parts. The first part was to compare the reference (air) and the interest of gas along with the time. Also, the sensor output was compared at between outside and inside of lab (Purdue MGL 1236). For sample preparation, CO_2 sample was prepared by the combination of baking soda and vinegar. The procedures were shown as below:

1. Took 25 ml of distilled vinegar into 100ml flask.
2. Added one third of spoon of baking soda into the flask.
3. Waited for the reaction (30 seconds).
4. Plugged the stopper with a hole to the flask.
5. Plug the plastic tube into the flask via the hole.
6. Ran the program

For VOC gas and ammonia gas, a bottle of 91% Isopropyl Alcohol was purchased from Walmart and household ammonia liquid was purchased from local store. The in-house built universal sensor gas characterization system controlled by LABVIEW (Panigrahi et al., 2008) was used to evaluate this test. The picture of the system is shown in Figure 3.39. The system consisted of a testing chamber with a heater surrounding, a thermocouple sensor, an Arduino and a laptop installed with LABVIEW. After the hardware setup was completed, the following protocol was conducted:

1. Turned on the heater of the gas characterization system and waited until the temperature of inside chamber got expected temperature.

2. Injected the Alcohol into the testing chamber
3. Turned on the blades by using LABVIEW interface
4. Executed the script in integrated sensor system

All of the data from the sensor was saved in the Beaglebone Black. The .txt files were processed using the procedures described in the section of signal processing.

The second part of the test was to evaluate the integrated sensor system in the field. The test was taken at Purdue poultry farm, located at Animal Sciences Research Center and Education Center. Due to the limitation of environmental setup, the connection supposed to connect to the gas sample was opened, which made the reference entry and the gas sample entry were from the same source. The procedures were listed below:

1. Warned up the system for 10 minutes
2. Measured the air in office (confined space) for five observations.
3. Measured the air at outside of the office (open space) for five observations.
4. Measured the air in the poultry farm (sample) for five observations.
5. Ran the signal processing that mentioned in previous section.
6. Plotted the result with respect to time.

Figure 3.38 Picture of the in-house built universal sensor gas characterization system (Panigrahi et al,. 2008)

3.2 E-tongue

E-tongue is otherwise known an electronic tongue. The basic functionality of E-tongue is to detect or predict the concentration of a given compound in a liquid medium. Thus, E-tongue is also otherwise known an artificial tongue or artificial taste sensor. Hence, E-tongue is generally considered as a complementary to artificial nose or E-nose.

In this case, we focused on developing and assessing an E-tongue system for detection of contamination in water or liquid medium. In this study, we focused on detecting arsenic in water as an example.

Many reports have described multiple ways to realize the development of an E-tongue system. In this study, we focused on assessing two methods to develop E-tongue system, and they are (1) Quartz crystal microbalance and (2) interdigitated dielectric sensing mode.

3.2.1 Quartz Crystal Microbalance (QCM)

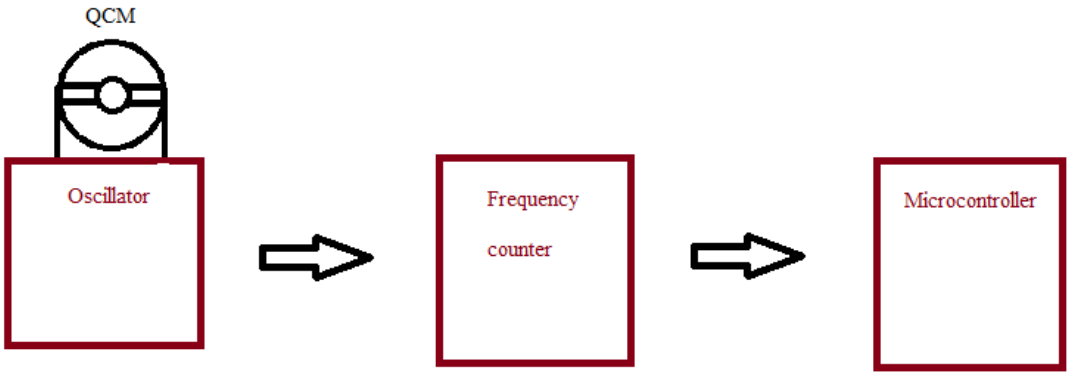

Figure 3.39 Schematic of a QCM system.

Figure 3.39 illustrates the system diagram of the QCM envisioning system. The principle was to read the frequency of the QCM using a microcontroller. This study focused on the development of a frequency counter that converted the frequency of QCM to a digitalized numerical number that a microcontroller/microprocessor can acquire and process. The stages of the QCM acquisition system procedure is shown in Figure 3.40. The QCM sensor was connected to a commercial oscillator, QCM lever oscillator by International Crystal Manufacturing CO, INC (ICM). The output was amplified and connected to a prescaler (flip flop). The next stage was to convert the raw frequency data to digital numbers. There are various ways to do the conversion. The easiest way was to directly connect the signal to a microcontroller. However, there were a few problems must be considered. First, the input signal must be conditioned so that a signal must sweep between the high and low thresholds of the microcontroller. For example, the input signal must sweep between 0 to 5 volts for the Arduino Uno. Second, the speed with which a microcontroller acquires the signal was critical. Due to these considerations, a frequency counter circuit as described in to by Michael et al. (2010) was designed. In the

paper (Michael et al., 2010), a USTI (universal sensors and transducers interface), as an alternative to using a high cost commercial frequency counter, was selected. The USTI is a 28 pin single programmable chip with two-channel frequency-to-digital converter with an operating frequency range of 0.05 Hz to 9 MHz. This range can be extended to 144 MHz using prescaling method. The accuracy of the frequency converter can be programed from 0.001 to 1% accuracy. The output in ASCII format can be sent to microcontroller by either UART or I2C protocol.

According to the datasheet of the lever oscillator we used, the output was 400 millivolts peak to peak. But the input requirement of USTI was 5 volts peak to peak. In order to amplify the signal from the oscillator to meet the 5 Volts peak to peak requirement, an amplifier circuit was designed. Initially, a non-inverting amplifier circuit was constructed with an AD817 operational- amplifier. However, the output of the amplifier reduced when the frequency was increased to 10 MHz. This indicated that the bandwidth of AD817 op-amp was not large enough to amplify a signal at high frequency. Therefore, the Analog Device ADA4891 amplifier, a low cost CMOS, high speed, rail-to-rail signal-supply amplifier was chosen instead. The bandwidth of the ADA4891 amplifier was 220 MHz with slew rate of 170V/microsecond.

Presented in Figure 3.41, the amplifier circuit consisted of three cascading stages. The gain of each stage was 2.2 with a 2.5 volts DC offset. An offset was added to the system because the input of USTI cannot accept negative voltage and also the amplifer has a signal power supply. It can cause the negative signal of input to be clipped.

Additionally, the QCM had a resonant frequency of 10 MHz, which exceeded the highest frequency (9 MHz) the USTI can measure. To overcome this problem, a prescaler

was implemented between the amplifier and the USTL. A flip-flop was used as prescaler in the circuit (Figure 3.42). When the J, K, reset, and preset pins were pulled high, the output frequency was scaled to half frequency detected on the clock pin. The signal from the amplifier was connected to the clock pin of the flip-flop and the flip-flop's output Q pin was attached to the USTI. Using the I2C protocol, the digitalized frequency was sent to a device that is able to do serial communications (i.e. UART, I2C, SPI, CAN).

After designing the circuit shown in Figure 3.41, it was fabricated into a PCB. EAGLE by CADSOFT was used to generate the gerber files. Figure 3.42 is shown the schematic of frequency counter PCB. In Figure 3.43, BNC connector was used at the input of the frequency counter and the size of the board was 70mm x 57mm.

The frequency counter was tested to measure the frequency three times from 1M Hz to 15M Hz in two types of accuracies, accuracy of 1% and accuracy of 0.005%. The input was simulated using a function generator supplying an output signal of 400 millivolts peak to peak and 0 VDC offset. The Arduino UNO was the microcontroller used for this test and it also supplied the power to the frequency counter. The measurements were recorded. The schematic of frequency counter test is shown in Figure 3.44. The complete Arduino code is attached in Appendix E.

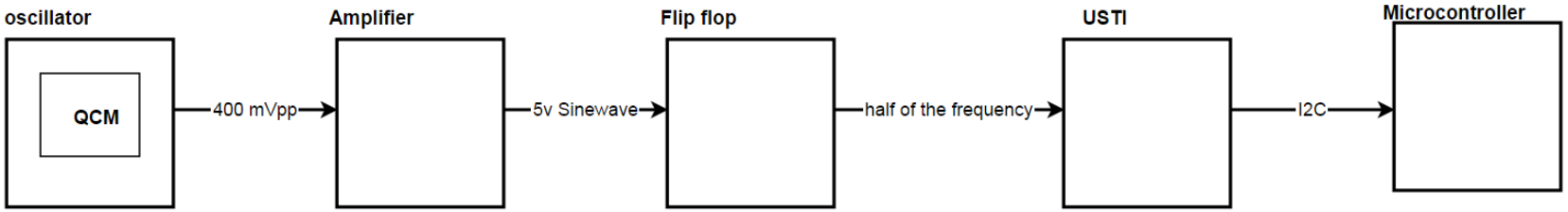

Figure 3.40 Stage of QCM acquisition system

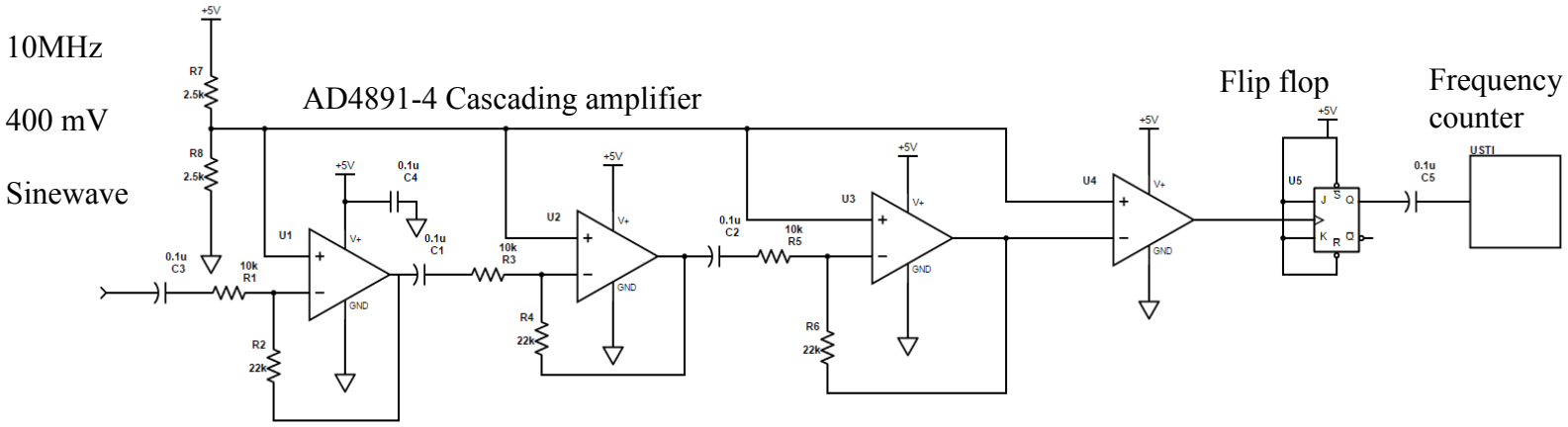

Figure 3.41 Schematic of frequency counter in QCM

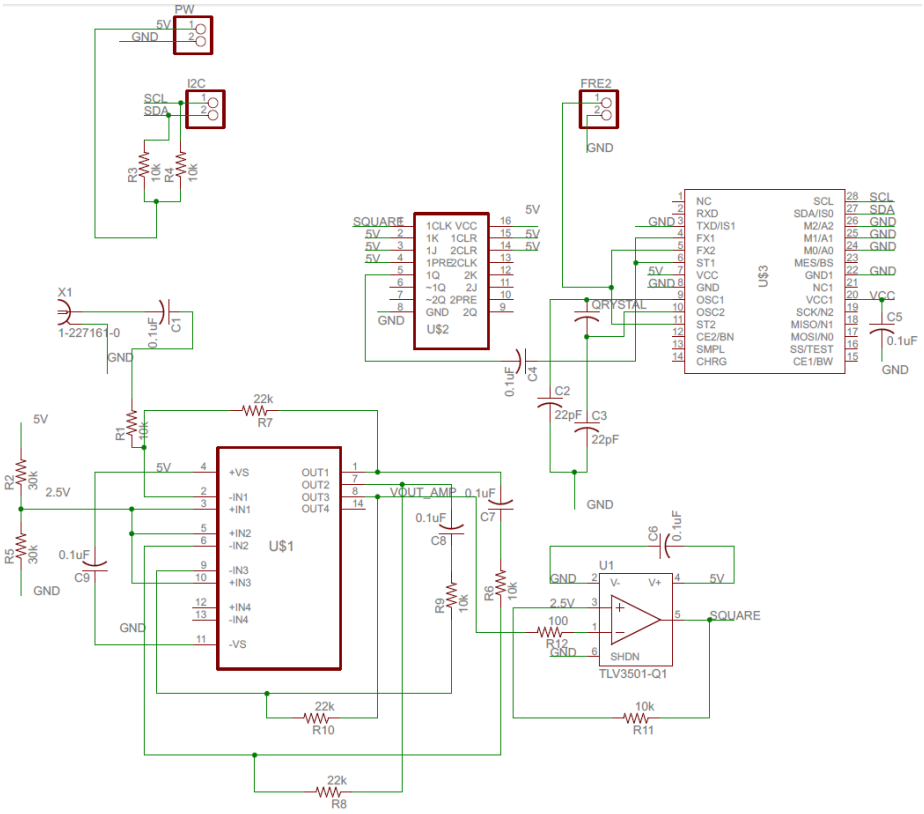

Figure 3.42 Schematic of frequency counter PCB

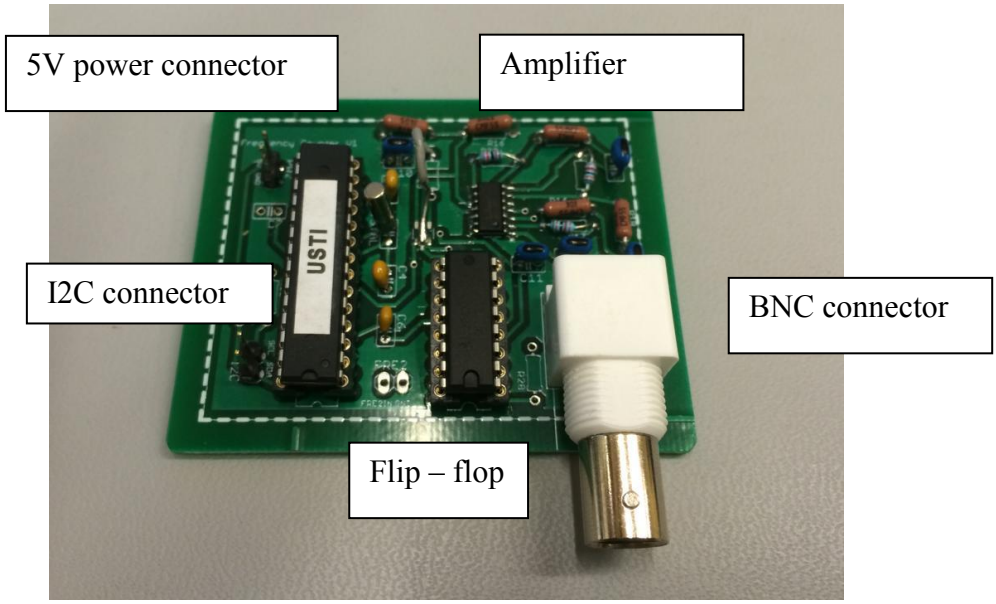

Figure 3.43 PCB of the frequency counter

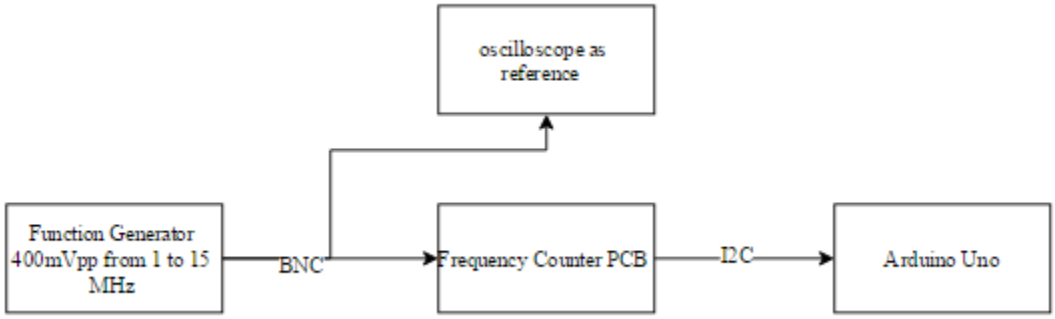

Figure 3.44 Schematic of frequency counter test

3.2.2 Interdigitated Capacitance

Interdigitated capacitance (with dielectric)

Multiple methods have been used for determination of arsenic in water. There is a need of developing a sensor/detection system that will rapid and cost-effective for possible used in low resource settings. In this study, a novel concept of adapting the interdigitated capacitance method (conceived by Dr. Panigrahi) was evaluated. This interdigitated capacitance has been used by Angawisittoan and Manasri (2012) for determination of sugar content of sugar solution. The concept was further adapted for arsenic application using a different configuration of interdigitated electrode (thin film gold electrode 8mm x8mm on silicon substrate) and procured from a commercial source.

Electrode Cleaning

Several preliminary and exploration experiments with different configurations and cleaning methods for detection classification of arsenic in water were conducted. In this report, the following method that involved cleaning the method with acetone is described. The researchers believe that this method is more suitable for this study.

The protocol of washing the electrode is described below:

1. Immersed the electrode into 60 mL acetone liquid and the container was on the top of a magnetic stirrer. It was stirred for 3 minutes.
2. The acetone in the cleaning container was replaced with DI water and again stirred for 3 minutes.
3. The interdigitated electrode was removed and rinsed with DI water for three times using a pipette.

The electrode was washed using the above protocol for testing each category of arsenic contaminated water (e.g. 10, 50, and 100ppb)

Sample preparation

All the samples and treatments were prepared in the Freeman Laboratory, cooperated partner, in Lilly Hall at Purdue University, West Lafayette.

Hardware setup

The measurement circuit consisted of an AC power source, an electrode, and a 5.1k ohms resistor. This setup is shown in Figure 3.45 and was used in a research study by Angkawisittoan (2012). The Vout displayed in the figure 3.45 was the voltage peak-peak across the 5.1k ohms resistors. The circuit was soldered on a point-to-point board with two BNC connectors on both at the AC input end and Vout pin side. A picture of the setup is shown in Figure 3.46. From Figure 3.46, the input BNC connector was connected to the function generator and the Vout BNC connector was connected to the oscilloscope. One end of the customized shield cable was soldered on the point to point board (at the source end) and the other end was connected to the interdigitated electrode. Lastly, the sensor was tapped on the inside wall of a 100ml container which shown in Figure 3.46.

So that the electrode was fixed in a vertical position. It was ensured that the liquid does not reach the two pads of the electrode.

The frequency range of the experiment was set from 10k Hz to 700K Hz because the researcher postulated that the sensor output had a significant response in this specific range from the initial test. The two pads of the electrode were connected via wire-bonding method. On each pad, 4 wires were used. The connector leads of the wire bond package were connected with shielded cable.

Experiment protocols

The protocol of the experiment is represented four observations in Figure 3.47. First, the voltages were measured in air four times in a row while tapped on the inside wall of the container. Then, 11 to 12 mL of treatment (treatments indicates water with arsenic contamination and without arsenic contamination) was filled into the container to cover the sensing area of the sensor

The protocol of measuring the voltage across the 5.1k ohms resistor shown in Figure 3.46 is listed below.

1. Connected the input source to the CH.1 of the oscilloscope.
2. Turned on the function generator and make sure the input signal (10VPP, 50K Hz)
3. Turned off the generator and connect the input source to the circuit
4. Turned on the function generator
5. Measured and recorded the results
6. After done measuring, turned off the function generator
7. Poured the sample into the waste container

In addition, the electrode was cleaned between the samples of 10ppb, 50ppb and 100ppb arsenic water. The cleaning protocol is listed below:

1. Put into 60mL DI water on magnetic stirrer for 3 minutes.
2. The interdigitated electrode was rinsed with DI water for three times.

In this experiment, there are four treatments and they are DI water (no Arsenic), Water with Arsenic (10ppb), Water with Arsenic (50 ppb) and water with Arsenic (100 ppb). In addition, four observations per treatment in each experiment. The researcher conducted 3 separate experiments. Thus, for each treatment, the researcher obtained 4x3=12 observation. In total, these 3 experiments have 48 observations (12x4) per each frequency value. It is to be noted that the above mentioned observations refer to a single frequency value. The researcher collected data for 16 difference frequency over a range (10 KHz – 700 KHz) in the experiment. These 16 frequency are 10, 20, 30, 40, 50, 100, 150, 200, 250, 300, 350, 400, 450, 500, 550, 600, 650 and 700 KHz.

Moreover, within the observations, the sample was changed by pouring out the old sample and adding new 11 to 12 mL of sample into the container. The order of the treatment is displayed below.

1. DI water
2. 10ppb arsenic water (11~ 12 mL)
3. 50ppb arsenic water (11~ 12 mL)
4. 100ppb arsenic water (11~ 12 mL)

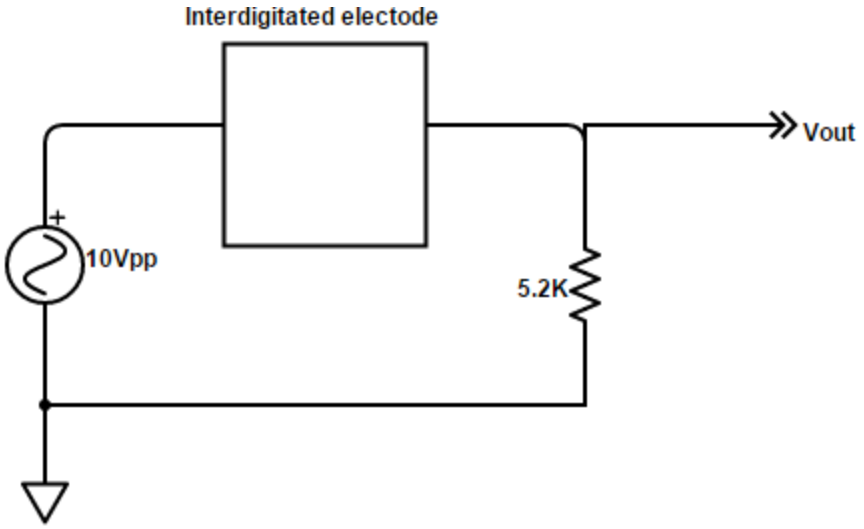

Figure 3.45 Schematic of instrumentation circuit

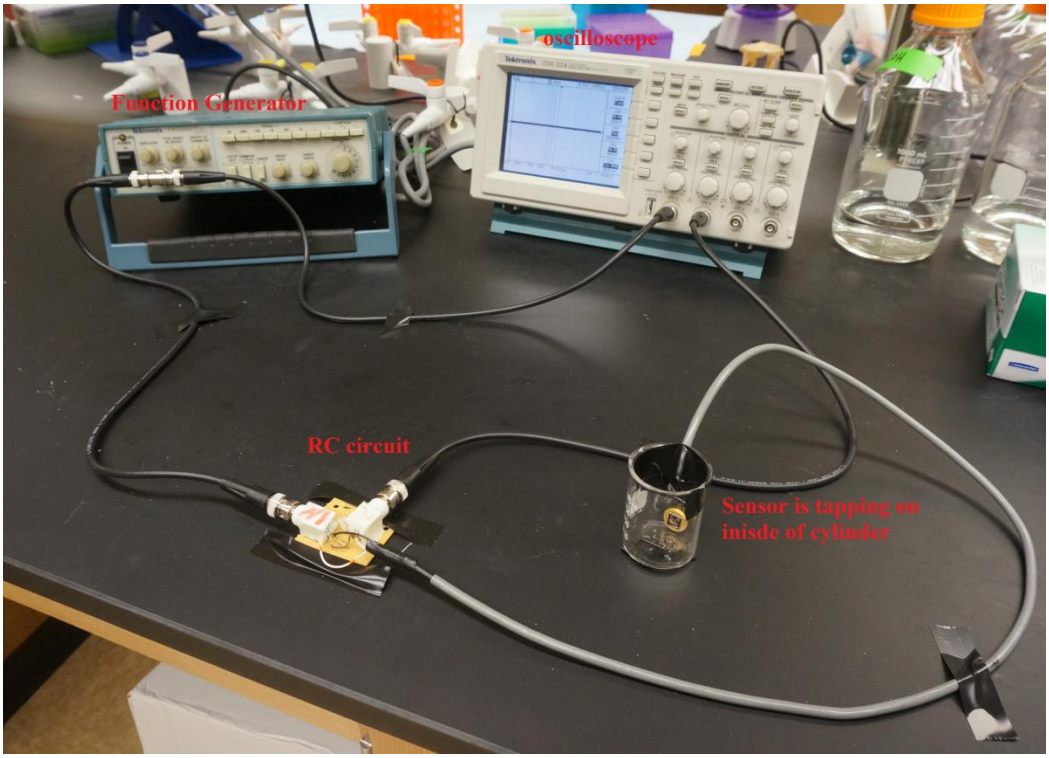

Figure 3.46 Experiment setup for arsenic detection

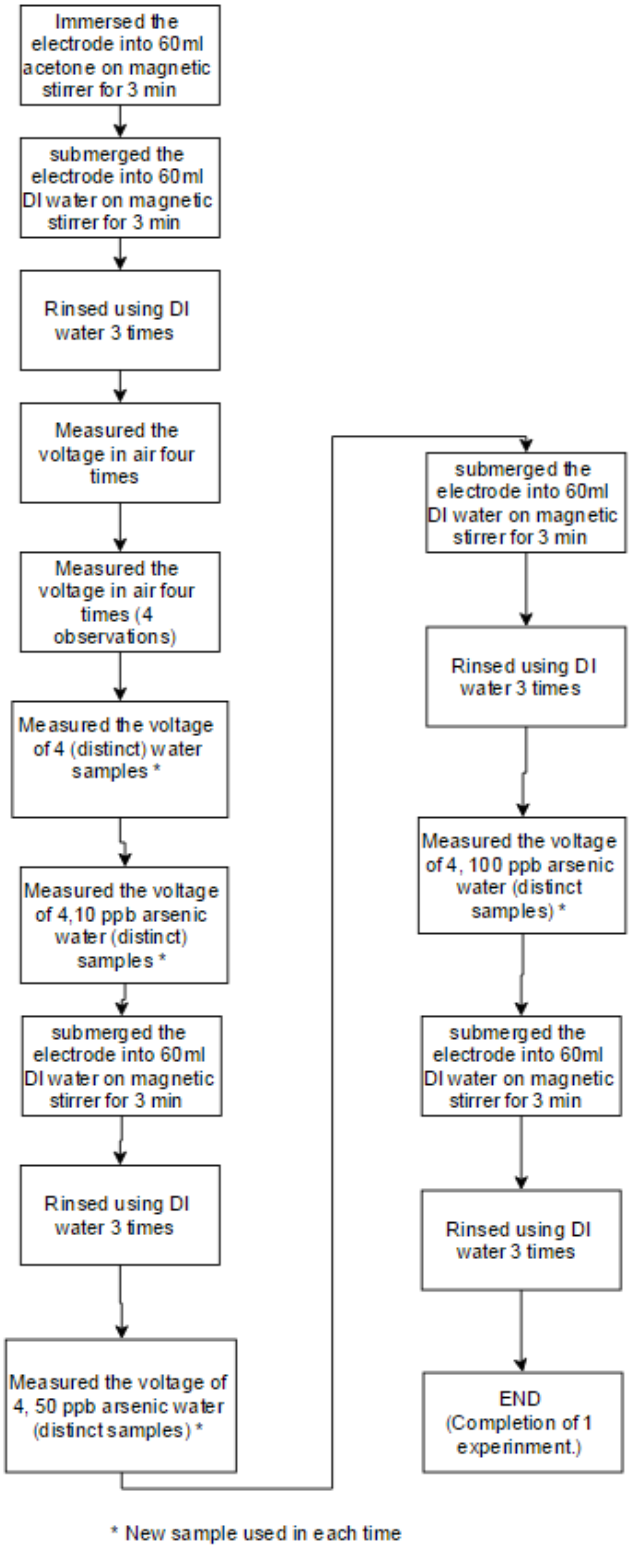

Figure 3.47 Flow chart of the protocol for arsenic detection experiment

CHAPTER 4. RESULTS AND DISCUSSION

Chapter 4 comprises of the results and discussions of E-nose and E-tongue related experiments. Under E-nose, the preliminary sensor test results of the integrated system are firstly discussed. Second, the electrical test results of external components in the system are deliberated. The result and discussion for trail experiments are later presented. Finally, the test result of frequency counter and the results of arsenic measurement in water are also discussed.

4.1 E-nose

E-nose consists of an electromechanical system, six sensors (two VOC sensors, two ammonia sensors, one Carbon dioxide sensor and a temperature & humidity sensor), a centralized power system and the various peripherals of the system. The entire system was tested and its performance was compared between the expected value and measured result. Next, the integration test was based on data understanding from two experiments, which are the laboratory test and the poultry room experiment.

4.1.1 Preliminary sensor test results

The test of VOC sensor, ammonia sensor, CO_2 sensor and Temperature and Humidity sensor were done as the system was integrated. The sample of gases (Alcohol,

ammonia, CO_2) were prepared as the description mentioned in Chapter 3.The individual sensor was tested based on the characteristics of the sensor as well as the sensor output comparison between observations taken inside and outside of building.

4.1.1.1 VOC sensor

The evaluation of two VOC sensors (model number- TGS2620), was established by finding out the characteristics of the sensor- the response time and the recovery time. The test setup was based on the description mentioned in chapter 3. Figure 4.1 and Figure 4.2 illustrates the characteristics of two sensors. In Both Figure 1 and Figure 2, the indicators on the bottom represent the timing for the three stages and the indicators on the top express the response time and recovery time. The definition of the response time in this test is to measure the time period between the gas injection and the point where the signal is in equilibrium with the environment of the gas. As shown in Figure 4.1 and Figure 4.2, the response time for VOC-1 and VOC-2 were 20 seconds and 24 seconds respectively. The definition of the recovery time in this test is to measure the time period after the cotton ball was removed until the response of the sensor was restored to the air reference. As shown in Figure 4.1 and Figure 4.2, the recovery times were 219 seconds and 180 seconds for VOC-1 and VOC-2 correspondingly. The average of Vout readings when Alcohol was injected, are 4.92 volts and 4.73 volts for VOC-1 and VOC-2 corresponding. The average in air reference for VOC-1 and VOC-2 are 2.74 volts and 5.74 volts. Those parameters are shown in Table 4.1.

The second test was conducted by comparing the air reading inside the room (Room 1236 in Purdue MGL) and outside of Purdue MGL building, using VOC sensor.

The measuring time of the test was 66 seconds which consisted of 1000 data points, thus resulting in a sampling rate of 66 milliseconds per sample. Figures 4.3 and 4.4 show the results of VOC-1 and VOC-2 inside the room and outside the building. The averages of VOC-1 and VOC-2 in outdoor environment were 1.807 volts and 1.836 volts respectively. The Vout reading in indoor environment, the average of VOC-1 and VOC-2 were 2.153 and 2.181 volts respectively.

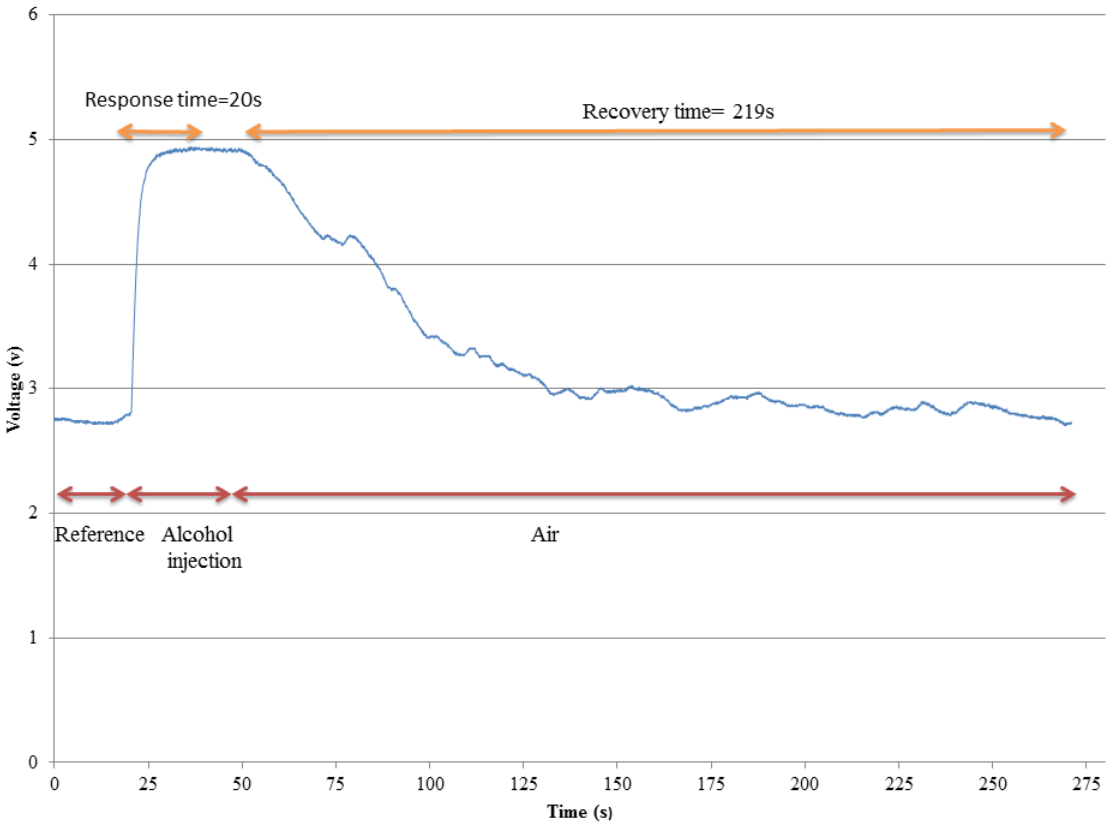

Figure 4.1 Characteristic test of VOC -1. The response time is 20 seconds and the recovery time was 219 seconds

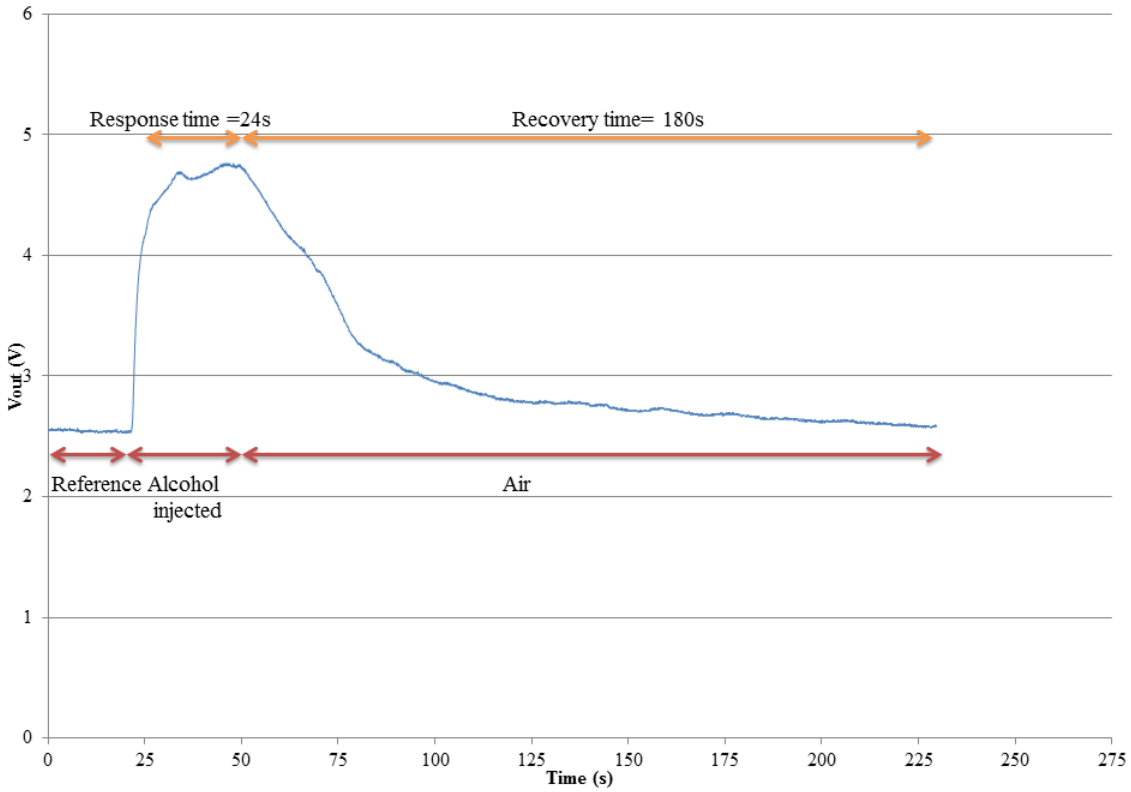

Figure 4.2 Characteristic test of VOC -2. The response time is 24 seconds and the recovery time was 180s seconds

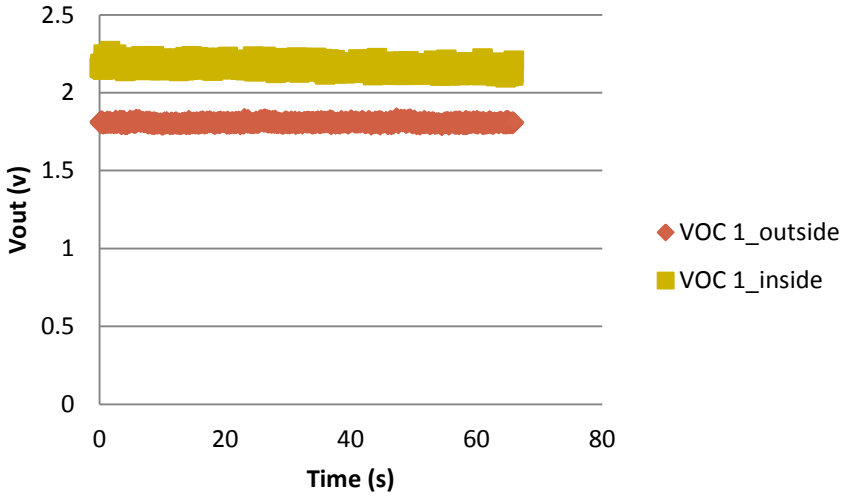

Figure 4.3 Comparison between inside and outside of the building for VOC-1

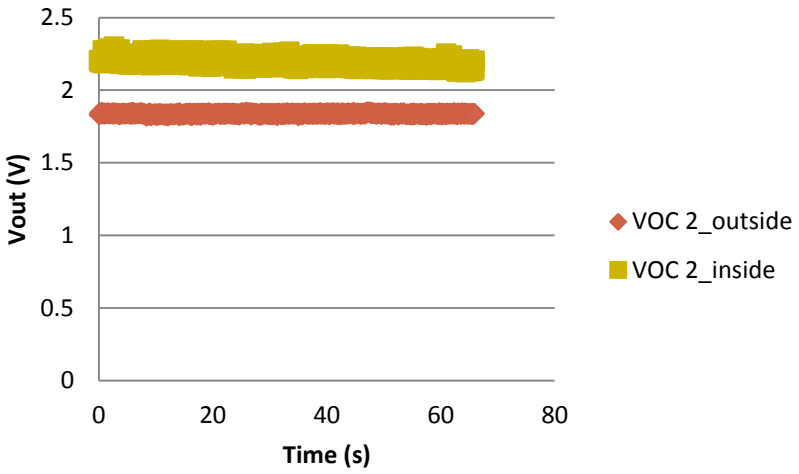

Figure 4.4 Comparison between inside and outside of the building for VOC-2

4.1.1.2 Ammonia sensor

Similar to the setup of VOC sensor, the two ammonia sensors (Ammonia-1 and Ammonia-2) were testing. The characteristics of the sensors were evaluated as well as the reading comparison between inside and outside of building. Due to the timing issue that was mentioned in section 3, the data was only collected at 5 milliseconds and 6 milliseconds of a cycle (250 milliseconds). Figures 4.5 and 4.6 present the characteristic of both sensors. The arrows on the bottom of the figures represent the time of the stages, which are the same indicators discussed in last section. From Figures 5 and 6, the response time and recovery time of Ammonia-1 were found to be 79 seconds and 1624 seconds correspondingly. For Ammonia-2, the response time was 75 seconds and the recovery time was about 1624 seconds. The equilibrium voltage for Vout of for Ammonia-1 and Ammonia-2 sensors were 4.29 volts and 4.6 volts respectively. The voltages in air (reference) of Ammonia-1 and Ammonia-2 were 1.44 volts and 1.93 volts respectively. Table 5 shows the time and the average value in the gas and air.

Like the test for VOC sensor, the air readings inside of the building and outside of the building were measured, and the result is shown in Figures 4.7 and 4.8. The response in Figure 4.7 and Figure 4.8 were the mean of reading at 5 milliseconds and 6 milliseconds. Identical performance to the VOC sensor, the reading from outdoor environment is higher than the reading inside of the building. The mean reading inside the building for Ammonia-1 was 2.153 volts and Ammonia-2 was 2.181 volts. From outside of the building the means for Ammonia- 1 and Ammonia-2 were 0.64 volts and 0.83 volts.

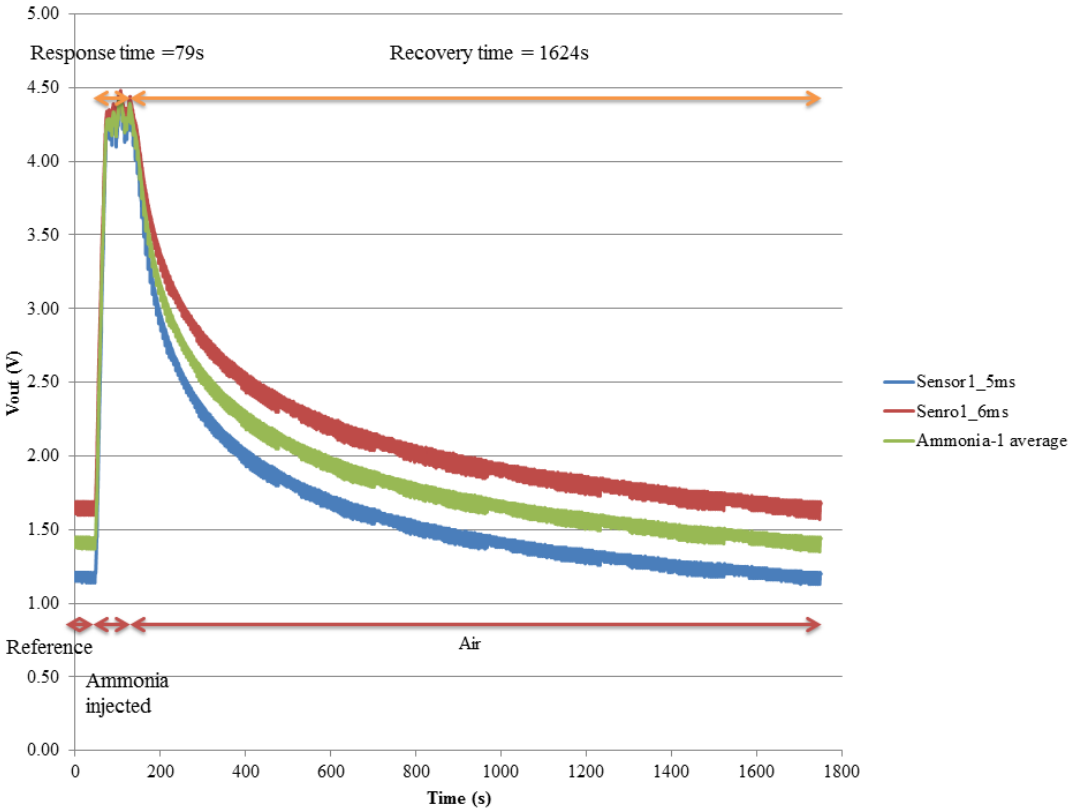

Figure 4.5 Characteristic test of Ammonia-1. The response time was 79 seconds and the recovery time was 1624 seconds

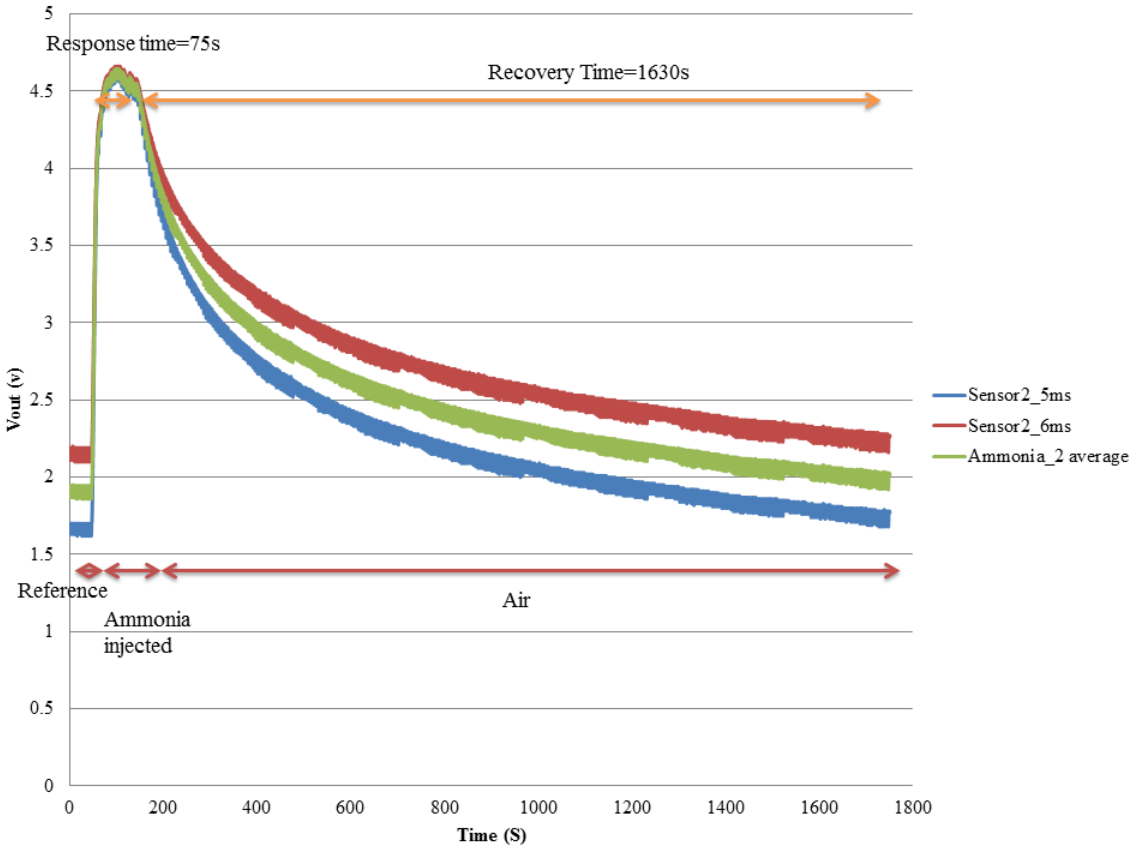

Figure 4.6 Characteristic test of Ammonia-2. The response time was 75 seconds and the recovery time was 1630 seconds

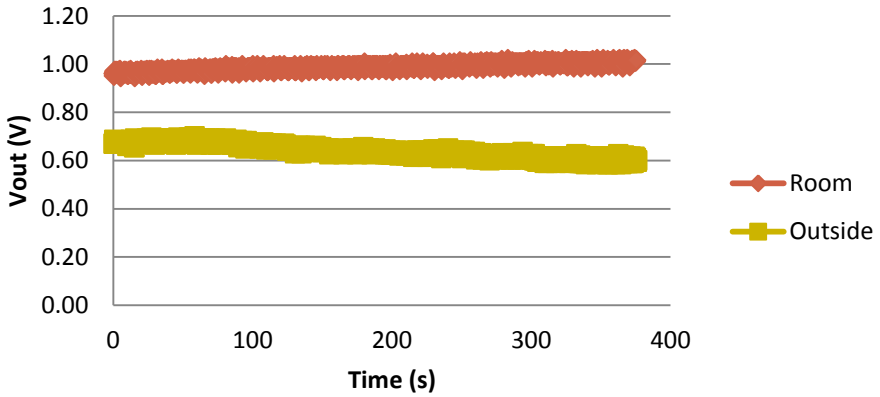

Figure 4.7 Comparison between inside and outside of building for Ammonia-1

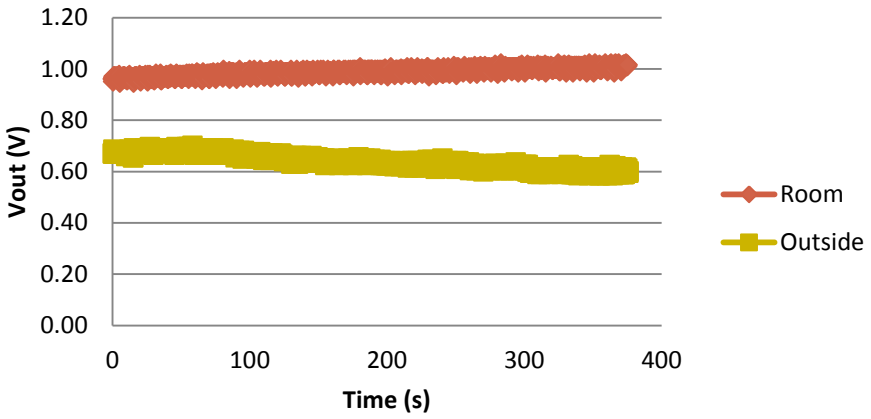

Figure 4.8 Comparison between inside and outside of the building for Ammonia-2

4.1.1.3 Carbon dioxide sensor

In Carbon dioxide sensor, the initial characteristics test was performed by injecting sample gas to the chamber for 180 seconds. The sample gas was made by combining baking soda and distilled vinegar. Figure 4.9 illustrates the response of the sensor. The total time of measurement was 540 seconds and the data was collected every 5 seconds due to the limitation of data updating in the sensor ("TElaire 6713 Series CO_2 Module", 2014). In this case, the response time was measured from the time when the gas was injected until the response reached on equilibrium. The recovery time was measured from the point where the system started flushing until the response of the sensor was restored to the reference (air). Both the response time and recovery time were about 140 seconds in Figure 4.9. The highest CO_2 level of this experiment was 3301 ppm and the reference level was about 384.61 ppm.

Additionally, the comparison between inside and outside of the building was conducted. The test was run for 120 seconds and data sampling was 5 seconds. From

Figure 4.10, the mean of CO_2 concentration in room was 395 ppm and the mean of CO_2 (atmosphere) in West Lafayette was 416ppm. The CO_2 (atmosphere) level of the day (June 3, 2015) was 403.33 ppm according to the CO2now.org. The error percentage between the CO_2 concentration at outside of the building and that from website is 3.48%, which is smaller than 5%.

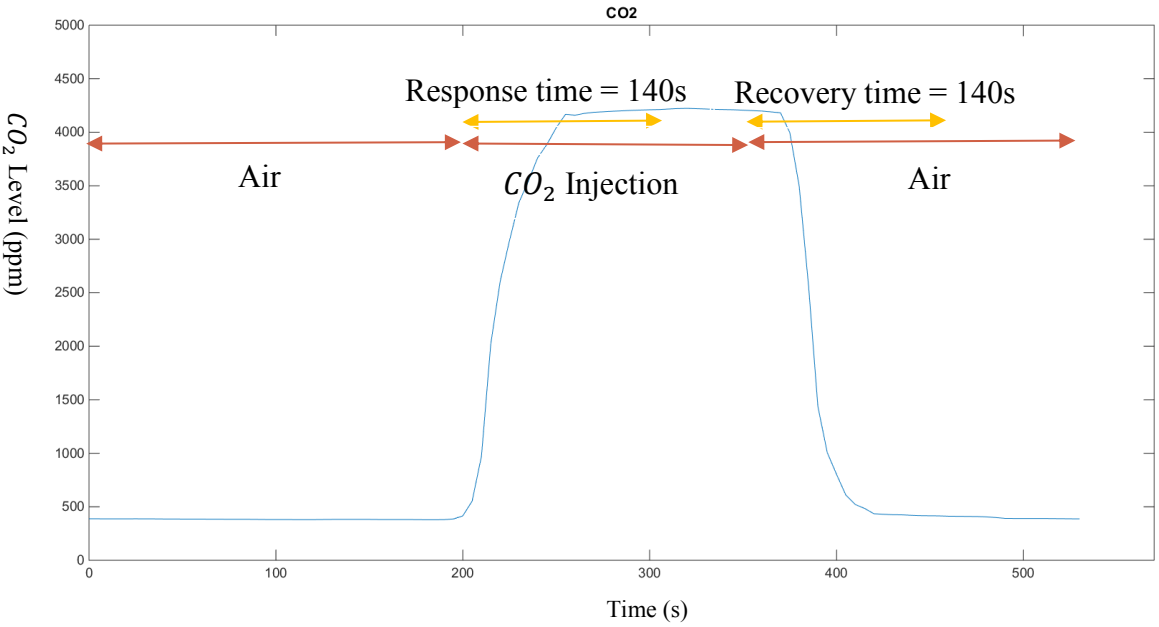

Figure 4.9 Characteristics test of CO_2 sensor. The response time and recovery time were 140 seconds

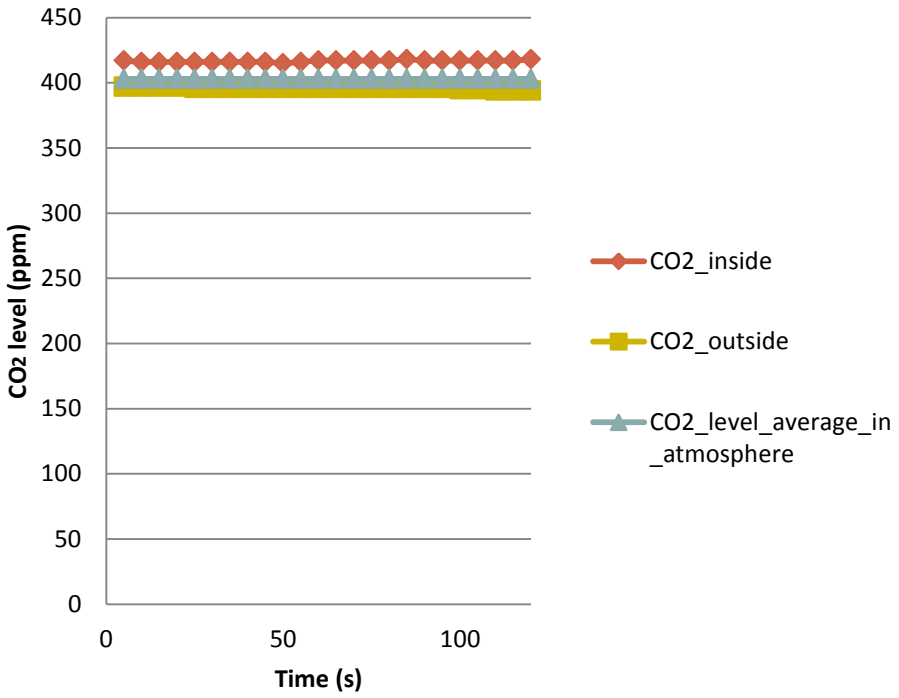

Figure 4.10 Comparison between room and outside of building for CO_2sensor

4.1.1.4 Temperature and humidity sensor

The last sensor test was for HTU21D-F, temperature and humidity sensor. The inspection was established by comparing the temperature and humidity between inside and outside of the building.

Figure 4.11 illustrates the temperature readings inside and outside of the building. The total time of the measurement was 120 seconds and the data was collected every 5 seconds. The reading from Rosewill REGD-TN439L0 Non-Contact Digital Infrared Thermometer was used as reference data. The data sampling rate for the infrared thermometer was the same as for HTU21D-F, 5 seconds. Table 4.1 shows the mean of the room temperature and outside temperature. The means of expected value of room and outside temperature. The error percentages of room and outside environment are 0.9% and 3.4%.

The result for the humidity is shown in Figure 4.12. The average humidity reading in the room was 60.98%. The average humidity at the outside of the numidity on specific day (June 4, 2015) was 39.48%. The expected value was acquired from Weather.com. The Website showed that humidity level on June 4, 2015 at West Lafayette was 48%. The error between the measurement at outside of building and the average of the day is 17.75%, shown in Table 2.

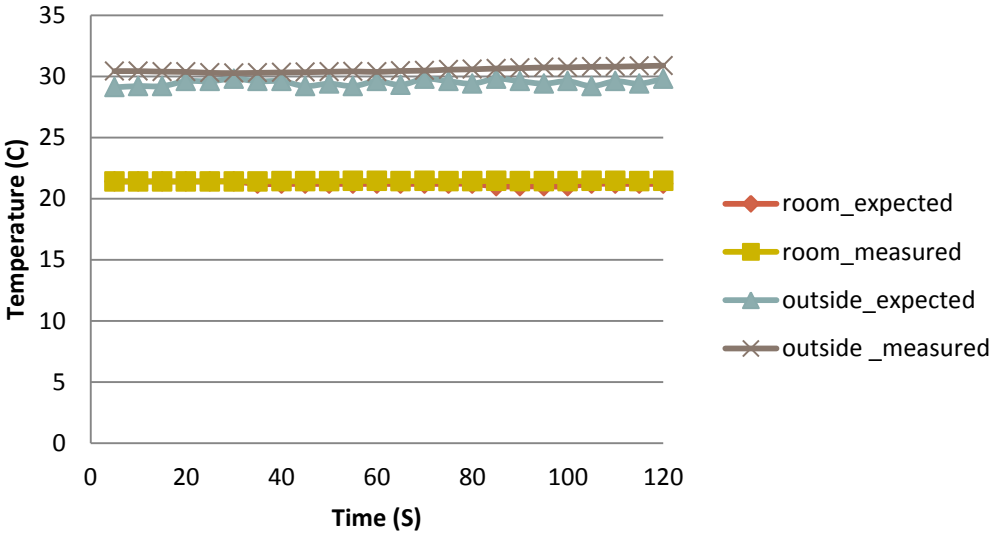

Figure 4.11 Comparison of temperature at room and the temperature at outdoor environment

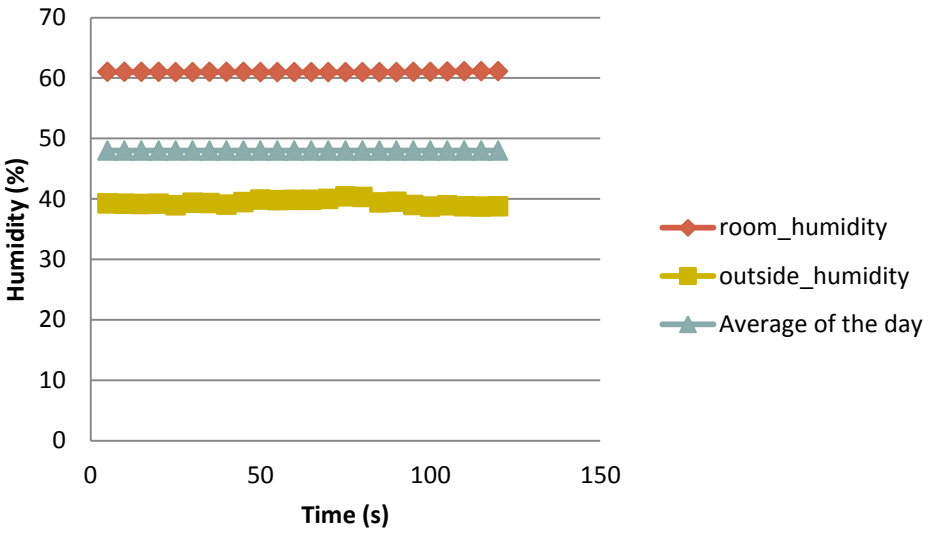

Figure 4.12 Humidity comparison between inside and outside of building

Table 4.1 *Temperature measurements at both room and outside of the building*

	Expected average (Celsius)	Measured average (Celsius)	Error percentage (%)
Room	21.21	21.42	0.9
Outside	29.48	30.51	3.4

Table 4.2 *Humidity Comparison*

	Expected average	Measured average	Error percentage
Room	N/A	60.98%	
Outside	48%	39.48%	17.75

Discussion

Table 4.3 illustrates the recovery time and response time of VOC sensors and ammonia sensors. The average response time of two VOC sensors were 22 seconds and the average of two ammonia sensors were 77 seconds. The response time of VOC sensor (55 seconds) was faster than that of ammonia sensor. The average recovery time for VOC sensors and ammonia sensors were 199.5 seconds and 1627 seconds respectively. The recovery time for VOC sensor was 1427.5 seconds quicker than ammonia.

In addition, the standard deviations for both VOC sensors and ammonia sensors were closer to 0 among the sensors in Table 4.4. This indicates the variance was significantly smaller than others sensors. Moreover, Figures 4.3, 4.4, 4.7 and 4.8 imply that the sensor value for VOC and ammonia in the room were higher than those readings outside the building due to the better ventilation at outside of building than at room.

For CO_2 sensor, the result from the sensor was consistent, which are 416.625ppm with standard deviation of 0.711 and 395.333ppm with standard deviation of 0.864 for CO2 atmosphere level outside of the building and inside of the building respectively.

As shown in Figures 4.11 and 12, the room temperature and humidity and the outside temperature were consistent throughout the test. Referred to Table 4.3, the standard deviations are 0.19 and 0.0126 for outside temperature and room temperature respectively. The standard deviations of humidity for inside and outside of building are 0.481 and 0.048.

Furthermore, the room humidity is higher than the humidity at outside environment on the specific day according to Figure 4.12. Lastly, greater than 5% error between expected humidity and measured humidity is reasonable. The expected value

from the Weather.com is the average of the day and the measured humidity was only measured at specific time of the day. Also, the location where the sensor tested was different. That's why the error was significantly large between the expected value and measured value.

Table 4.3 *Characteristic of VOC sensors and ammonia Sensors*

	Response time	Recovery time	Equilibrium in gas sample	Equilibrium in Reference (air)
	Seconds	Seconds	volts	Volts
VOC-1	20	219	4.92	2.74
VOC-2	24	180	4.73	2.54
Ammonia-1	79	1624	4.29	1.44
Ammonia-2	75	1630	4.60	1.93

Table 4.4 *Means and standard deviations of sensors*

	Mean	Standard Deviation
VOC 1_outside	1.807V	0.008
VOC 1_room	2.153V	0.024
VOC 2_outside	1.836V	0.005
VOC 2_room	2.181V	0.024
Ammonia 1_outside	0.64V	0.03
Ammonia 1_room	0.99V	0.01
Ammonia 2_outside	0.83V	0.05
Ammonia 2_room	1.44V	0.02
CO2_outside	416.625ppm	0.711
CO2_room	395.833ppm	0.868
Temperature_outside	30.51ºC	0.190
Temperature_room	21.42 ºC	0.0126
Humidity_outside	39.43%	0.481
Humidity_room	60.98%	0.048

4.1.2 External components of the system

In this section, electromechanical system, centralized power supply system and Peripherals in the system are discussed. Each system was test as the whole system was integrated. The results of the test were then compared with the expected values.

4.1.2.1 Electromechanical system

The electromechanical system was tested to analyze the operation of the pump including the timing of each mechanical movement as referred in Table 4.5. In addition, electrical inspection of the solenoid valve driver and pump driver was done and the results have been recorded in Table 4.5

Technically, when the processor (Begalebone Black) gives logic high signal (3.3 volts), the drains of the MOSFET for the pump and the solenoid valve are at 5 volts and 12 volts respectively and thus resulting in energizing them. As shown in Table 4.5, when the input (one of GPIOs from the processor) is high (3.3V) the output (the drain of the MOSFET) is at ON position (5V for the pump and 12V for the solenoid valve). On the other hand, when the input is low (0V), the output (the drain of the MOSFET) is at OFF position (0V for the pump and solenoid valve).

The second measurement of the electromechanical system is to measure the elapsed time for each stage. As mentioned earlier in Chapter 3, there are three stages. The first stage was air flushing. In reference to the calculation made in section 3, the air flushing time was found to be 28 seconds. The next stage was to obtain reference for three minutes (180 seconds), where the time was user defined. The last stage was to inject the gas to the chamber while the processor was still collecting the data for another three

minutes. “time.h”, one of the libraries defined in Linux, was used to measure time by the processor. The unit of measuring the time was in seconds. Table 4.6 exhibits the results of the measurement. The experiment was run three times. The last column of the table is the average of 3 observations. From the Table 4.5 and Table 4.6 in this subsection, the mean of measured time and the driver test are the same as expected.

Table 4.5 *Result of drive test*

	PUMP Drive test		Solenoid Drive test	
	INPUT	OUTPUT	INPUT	OUTPUT
ON	3.3V	5V	3.3V	12V
OFF	0V	0V	0V	0V

Table 4.6 *Time measurements of mechanical operations*

	Expected time in second	The average of measured time in second
Air flushing	28	28
Reference collection	180	180
Gas injecting/ data collection	180	180

4.1.2.2 Centralized power supply

The next segment is the results of the centralized power system. The setup of the test was described in Chapter 3. The first section of the test is to examine the current limitation of the chip and the consistency of output voltage. The expectation was that the voltage output for both of the LM2678 and the TPS562209 was expected to be 5 volts

with maximum sourcing current at 1.8 amps. Also, the LP2950-3.3 is 3.3 volts with current limitation at 100mA.

For LM2678, TPS562209, and LP2950-3.3, the currents and voltages were measured with respect to different loads and recorded in Tables 4.7, 4.8 and 4.9 respectively. The percent error of the voltages and the current from the loads of 14 ohms to 131 ohms were less than 5%. Loads of 2 ohms to 6 ohms were out of 5% error range because the resistance value of the load box used in test was not exact the same as the expected resistance value. Even though they had significant current differences, the voltage was around 5 volts. It implies the regulator was still in operation. The load of 2 ohms was to test the shutdown functionality. The chip was shut down when the current was over the current limitation- 1.8 amps for LM2678 and TPS562209. Similarly, Table 4.9 illustrates the LP2950-3.3 had about 3.3 volts output with respect to different loads. However, the output voltage at 16 ohms load was 2.707 volts because the current was over the limit of the chip- 0.110 amps.

The performance comparison between LM2678 and TPS562209, both chips met the requirements, which were approximately 5 volts at output with the maximum sourcing current at 1.8 amps. Tables 4.7 and 4.8 emphasize the sum of TPS562209 voltage errors for the loads were smaller than the sum of LM2678 voltage errors. That explains all the outputs corresponding to different loads on TPS562209 were closer to 5 volts comparing to the outputs on LM2678. The same comparison can be applied to the error in current between Tables 4.7 and 4.8. The sum of current error percentage in Table 4.7 is larger than the sum in Table 4.8. Size perspective, after populating the components on PCB, the footprint of TPS562209 is more compact than the size of LM2678. Because

of those factors mentioned above, the TPS562209-5 was a switch regulator for the power system.

Due to lack of output pin on PCB, the second version of PCB was fabricated. The same power measurement was run again, and the measurements are shown in Tables 4.10 and 4.11. All the voltage outputs were similar to the previous test. The TPS562209 shut down when the current is beyond the limitation, and the 3.3 volts linear regulator (LP2950) was not functional once the current was larger than 0.139 amps.

Table 4.7 *Measurement result of LM2678*

Power measurement for LM2678						
Load (ohms)	Expected Current (A)	Measured Current (A)	Expect Voltage (v)	Measured voltage (V)	% Error in voltage	% Error in current
131	0.038	0.038	5.000	4.939	1.220	0.419
63	0.079	0.078	5.000	4.938	1.240	1.714
30	0.167	0.169	5.000	4.937	1.260	1.441
14	0.350	0.354	5.000	4.933	1.340	1.143
6	0.830	0.768	5.000	4.922	1.560	7.470
4	1.250	1.072	5.000	4.911	1.780	14.240
2	2.500	0.2	Shut down	0.56	N/A	N/A
Total					8.400	26.427

Table 4.8 *Measurement result of TPS562209 (Ver.1)*

Power measurement for TPS562209						
Load (ohms)	Expected Current (A)	Measured Current (A)	Expect Voltage (v)	Measured voltage (V)	% Error in voltage	Error in current
131	0.038	0.038	5.000	4.986	0.280	0.419
63	0.079	0.080	5.000	4.985	0.300	0.806
30	0.167	0.170	5.000	4.983	0.340	2.041
14	0.350	0.351	5.000	4.980	0.400	0.286
6	0.830	0.777	5.000	4.974	0.520	6.386
4	1.250	1.097	5.000	4.969	0.620	12.240
2	2.500	0.354	Shut down	0.570	N/A	N/A
Total					2.460	22.178

Table 4.9 *Measurement for LP2950-3.3 (Ver.1)*

Power measurement for LP2950 -3.3V						
Load (ohms)	Expected Current (A)	Measured Current (A)	Expect Voltage (v)	Measured voltage (V)	% Error in voltage	Error in current
131	0.025	0.025	3.300	3.288	0.364	0.754
63	0.052	0.053	3.300	3.287	0.394	1.184
47	0.070	0.069	3.300	3.286	0.424	1.709
39	0.085	0.081	3.300	3.286	0.424	4.255
33	0.100	0.091	3.300	3.285	0.455	9.000
30	0.110	0.112	3.300	3.291	0.273	1.818
16	0.200	0.121	Not functional	2.707	N/A	N/A

Table 4.10 *Measurement result of TPS562209 (Ver.2)*

Power measurement for TPS562209						
Load (ohms)	Expected Current (A)	Measured Current (A)	Expect Voltage (v)	Measured voltage (V)	% Error in voltage	error in current
131	0.038	0.040	5.000	5.035	0.700	2.244
63	0.079	0.082	5.000	5.032	0.640	1.517
30	0.167	0.174	5.000	5.026	0.520	2.039
14	0.350	0.363	5.000	5.007	0.140	1.643
6	0.830	0.791	5.000	4.972	0.560	3.555
4	1.250	1.097	5.000	4.950	1.000	71.163
2	2.500	0.215	Shut down	0.515	N/A	N/A

Table 4.11 *Measurement result of LP2950-3.3 (Ver.2)*

Power measurement for LP2950 -3.3V						
Load (ohms)	Expected Current (A)	Measured Current (A)	Expect Voltage (v)	Measured voltage (V)	% Error in voltage	error in current
131	0.025	0.026	3.300	3.288	0.364	1.500
63	0.052	0.054	3.300	3.287	0.394	2.282
47	0.070	0.071	3.300	3.286	0.424	1.311
39	0.085	0.061	3.300	3.286	0.424	24.082
33	0.100	0.098	3.300	3.285	0.455	1.439
24	0.208	0.139	3.300	3.291	0.273	2.536
16	0.200	0.163	Not functional	2.707	N/A	N/A

4.1.2.3 Peripherals

In the peripherals test section, two components were tested. They are (1) analog to digital converter (ADC) and (2) digital programmable potentiometer.

The test for ADC was based on connecting the channels to individual power supply and comparing the reading values with the expected values. Channels 0, 1, 2, 3 and 4 were connected to individual power supply of 1, 2.5, 5, 3.3 and 4 volts respectively. Channels 5 and 6 were open, and were not connected to anything. The rest of the channel was connected to the ground. In this specific IC, the channel 11 represents the positive side of reference voltage and channe12 indicates the negative side of reference voltage. The last channel represents the result of dividing the sum of positive reference and negative reference by two. The software program described in Figure 3.24 was run three times, and the data is shown in Table 4.12.

Table 4.12 illustrates that the error percentage of each channel for three observations are acceptable (< 5%). The minimum error percentage was 0.2 % on channel 11 and the maximum error was 2% on channel 1. The readings of channel 5 and 6 were not stable, due to the open connection. Lastly, the standard deviations of the reading from each channel were very low (close to zer0).

Evaluation of digital programmable potentiometer (POT)

Two chips that had two potentiometer circuits were tested. The evaluation was based on the comparison between the expected resistance and measured resistance. The test was conducted using four resistance values. The default value of the POT was 25k ohms. The digital values of 0, 55, and 255 which represented 50k ohms, 39.6k ohms and 370 ohms respectively. The error between expected value and measured value of each

potentiometer circuit was acceptable (< 5% error) in Table 4.13. In Table 4.13, POT1-1 defined the first potentiometer circuit of the first chip, POT1-2 represent the second potentiometer circuit of the first chip, and vice versa. The maximum error was 2.8 % on POT2-1 when the potentiometer value was 55 (39.6K ohms). The minimum error occurred on POT1-2 and POT2-1 when the potentiometer was in default condition.

Table 4.12 *Result of ADC measurement*

	observation-1			observation-2			observation-3			
	Expected voltage	Measured Voltage	error percentage	Expected voltage	Measured Voltage	error percentage	Expected voltage	Measured Voltage	error percent	SD
Channel 0	1.000	0.980	2.000	1.000	0.990	1.000	1.000	0.990	1.000	0.005
Channel 1	2.500	2.470	1.200	2.500	2.480	0.800	2.500	2.480	0.800	0.005
Channel 2	5.000	4.950	1.000	5.000	4.960	0.800	5.000	4.960	0.800	0.005
Channel 3	3.300	3.290	0.303	3.300	3.280	0.606	3.300	3.280	0.606	0.005
Channel 4	4.000	3.950	1.250	4.000	3.950	1.250	4.000	3.960	1.000	0.005
Channel 5	OPEN	0.350	N/A	OPEN	0.320	N/A	OPEN	0.370	N/A	0.021
Channel 6	OPEN	0.380	N/A	OPEN	0.340	N/A	OPEN	0.330	N/A	0.022
Channel 7	0.000	0.000	N/A	0.000	0.000	N/A	0.000	0.000	N/A	0.000
Channel 8	0.000	0.000	N/A	0.000	0.000	N/A	0.000	0.000	N/A	0.000
Channel 9	0.000	0.000	N/A	0.000	0.000	N/A	0.000	0.000	N/A	0.000
Channel 10	0.000	0.000	N/A	0.000	0.000	N/A	0.000	0.000	N/A	0.000
V-ref+	5.000	4.990	0.200	5.000	4.990	0.200	5.000	4.990	0.200	0.000
V-ref-	0.000	0.000	N/A	0.000	0.000	N/A	0.000	0.000	N/A	0.000
Vref/2	2.500	2.510	0.400	2.500	2.530	1.200	2.500	2.540	1.600	0.012

Table 4.13 *Result of digital potentiometer test*

	POT1-1			POT1-2			POT2-1			POT2-2		
value	expected	measured	Error Percent	expected	measured	Error Percent	expected	measured	Error Percent	expected	measured	Error Percent
	K ohms	K ohms	%	K ohms	K ohms	%	K ohms	K ohms	%	K ohms	K ohms	%
Default	25.00	25.02	0.08	25.00	25.02	0.08	25.00	24.98	0.08	25.00	24.95	0.20
0	50.00	48.92	2.16	50.00	48.73	2.54	50.00	48.60	2.80	50.00	49.52	0.96
55	39.06	38.44	1.59	39.06	38.40	1.69	39.06	38.55	1.31	39.06	38.46	1.54
255	370.00	370.40	0.11	370.00	370.20	0.05	370.00	372.80	0.76	370.00	371.09	0.29

4.1.3 Evaluation of integrated sensor system

In this segment, the experiment was divided into two parts. Firstly, a laboratory test was conducted to access the performance of the ammonia sensor for specific concentrations. The second part was to evaluate the system in Purdue poultry farm. The measurement was taken at the outside environment at Purdue farm, the office of Purdue poultry farm and one of poultry rooms. The results then were compared among the three surroundings.

4.1.3.1 Laboratory experiment for ammonia

The first half of the experiment was conducted by testing the system whether or not was able to detect 25ppm Arsenic gas. According to the "Ammonia in poultry houses: A Literature Review" (Carlile, 2011), bird performance and profit would be affected if the level of ammonia exceeds 25ppm. Therefore, the researcher wanted to proof that there is evidence to show the E-nose integrated system has ability to detect the level of 25ppm ammonia gas.

The sample was prepared using the equation below:

$$C, ppm = \frac{10 \times C_l \times p \times V_{vol} \times R \times T}{M \times P_o \times V_o}$$ (Nakamoto, 2006; SanKarm, 2009) (Equation 4.1)

Where C_l is the concentration of ammonia liquid (wt. %), p is the density of the gas (g mL^{-1}), V_{vol} is the volume of ammonia liquid injected (μL), R is the universal gas constant (L atm $mLK^{-1}mol^{-1}$), T is the temperature inside the gas preparation chamber (K), M is the molecular weight of the analyst (g mol^{-1}), P_o is the pressure inside the gas preparation chamber, V_o is the volume of the gas preparation chamber and C is the desired concentration of gas (ppm).

The procedures are shown below:

1. Calculated the amount of solution should be inserted into gas preparation chamber.
2. Inserted the liquid using a micro-pipette.
3. Run the program and collated data.
4. Plotted the result using MATLAB script

The cycle of experiment consisted of reference air (laboratory air) that was taken into the system for 3 minutes followed by liquid injection. The holding time of gas vapor was for 8 minutes. The time for exhaust was 12 minutes.

By using the equation 4.1, 48μL of 50% ammonia solution was injected to create ammonia gas. After the amount of liquid was injected into the gas sampling chamber using a micro-pipette, the E-nose integrated system recorded the response.

During the experiment, the researcher found out that the sensor response (Vout) attained 5V soon after the gas was injected (Figure 4.16) This trend indicated the concentration might be too high for the sensor. Therefore, the test concentration in the flask was reduced to 10ppm of ammonia gas (the lowest concentration level that the sensor can detect according to the datasheet). However, the response of sensor (Vout) reached the 5V quickly (Figure 4.17)

In order to make 25ppm ammonia gas in the E-nose system's test chamber, the concentration of ammonia in gas preparation test chamber was calculated using Dilution equation.

$$C_p V_p = C_t V_t \qquad \text{(Equation 4.2)}$$

Where C_p is the concentration of the ammonia in gas preparation chamber, $V_p$is the volume of the gas preparation chamber, C_t is the concentration of the ammonia in E-nose system's testing chamber, $V_t$is the volume of the E-nose system's testing chamber.

Therefore, 25 ppm in the flake is equal to 133 ppm ammonia gas in the test chamber of E-nose system. 10 ppm in the flake equals 66 ppm ammonia gas in the test chamber. 3.8 ppm in the flake is equal to 25 ppm ammonia gas in the test chamber.

4.1.3.1.1 Raw data of sensors (VOC, NH3, temperature & humidity)

VOC sensor

Figures 4.13, 4.14 and 4.15 show the raw data (Vout and sensor resistance (R_s)) of VOC sensor with respect to time at different concentrations. The relationship of the equation between voltage and resistance is inversely proportional (Equation 3.1). That's why the shapes are upside down for Vout and R_s. Moreover, both the VOC sensors have certain sensitivity for ammonia gas because the sensor response changed while the gas sample was being injected.

Ammonia sensor

As mentioned before, Figures 4.16 and 4.17 illustrate how fast the sensor response reached the maximum level (5V) right after 133 ppm ammonia gas or 66 ppm ammonia gas was injected to the test chamber. Moreover, Comparison form Figures 4.16 to 4.18 indicated that at lower concentration (25ppm), sensor showed more trend responses on 5V.

Temperature and Humidity sensor

The temperature was reported approximately 23°C on the plots. Humidity increased while the ammonia gas was injected, and the humidity came back to normal when the air flushed the testing chamber. The ammonia solution was the mix between ammonia liquid with distilled water, so the humidity went up when the ammonia gas was injected.

4.1.3.1.2 Data processing

The following equation was implemented in this experiment below:

$$R_{ns} = \frac{R_s - R_{air}}{R_{air}} \quad \text{(Equation 4.3)}$$

Where R_{ns} is the normalized value, R_s is the resistance of sensor in sample, and R_{air} is the resistance of sensor in air.

From the Equation 4.3, as the normalized value is closer to 1, the difference between sample and reference is more significant.

Figure 4.20 shows the normalization of VOC sensors for 25 ppm in test chamber. In the three tests, plots show the pattern was identical to each other. The pattern can be explained into three parts. The first part is the air reference, which is the smallest normalized value. It happened at the initial 180 seconds. The second part is the response time, which was measured from the point where the gas was injected until the response approached forwards equilibrium in the gas environment. The sensor response in equilibrium stage was shown in the area of red circles (Figure 4.20). The average time for reaching the equilibrium was at 486.37 seconds among the three tests. The average response time of three tests was 306.36 seconds. The last part was the sensor recovery.

The sensor response for the three tests did not fully restore to the reference (air) shown in Figure 4.20. That implies that the original exhaust time (12 minutes) was too short for the VOC sensor to be fully recovered in farm environment.

The normalized sensor responses of ammonia sensor are shown in Figure 4.21. In the three tests, the trends of the response in each test are similar. The red circles and black circles (Figure 4.21) represent the equilibrium point and the point of air flushing respectively. Among the three tests, the average response time was 375.83 seconds and the average recovery time was 1270 seconds. In addition, Table 4.14 illustrates the maximum normalized value of each sensor for each test. The mean normalized response of Ammonia -1 is 0.0095 larger than the normalized response of Ammonia-2. Lastly, Table 4.15 shows the variation between VOC sensor and ammonia sensor in laboratory experiment. From each test, the variation of VOC was closer to 0 than that of ammonia sensor. That explains that the sensor response of two VOC sensors were more identical than the sensor response of the two ammonia sensors.

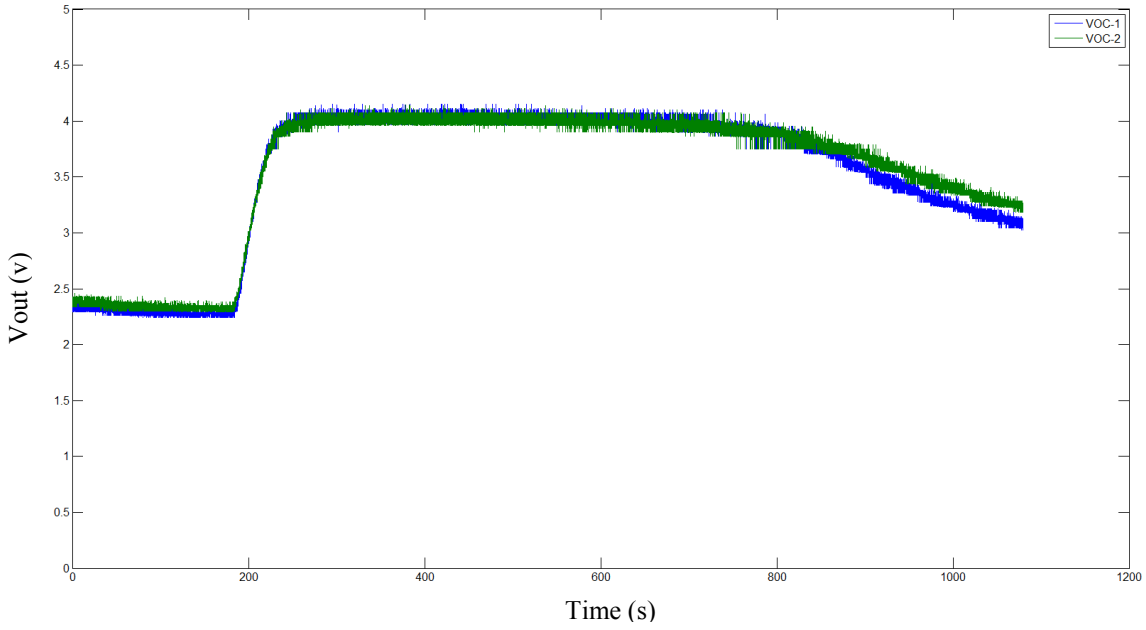

(a)

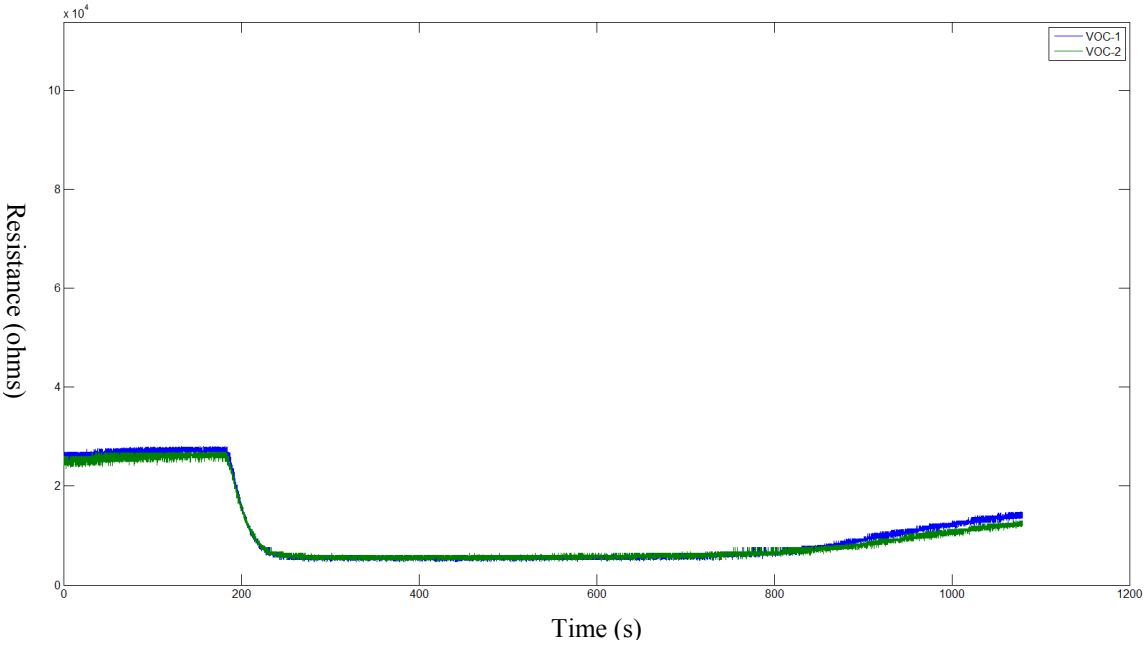

(b)

Figure 4.13 Raw data from VOC sensor (a) voltage response at 132 ppm (b) resistance response at 132 ppm

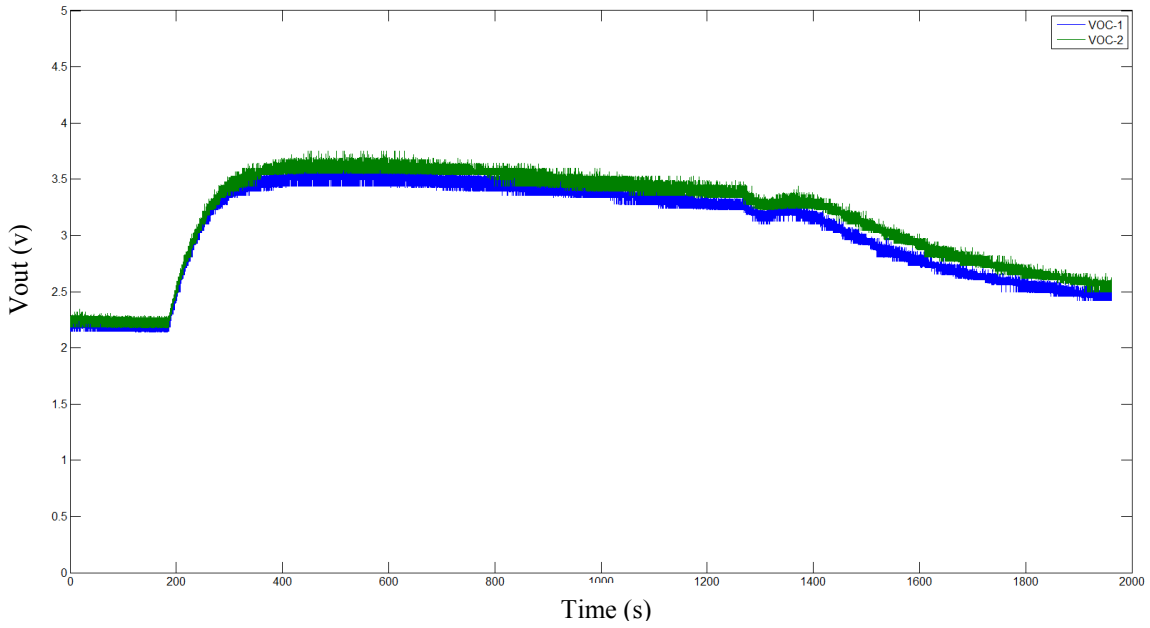

(a)

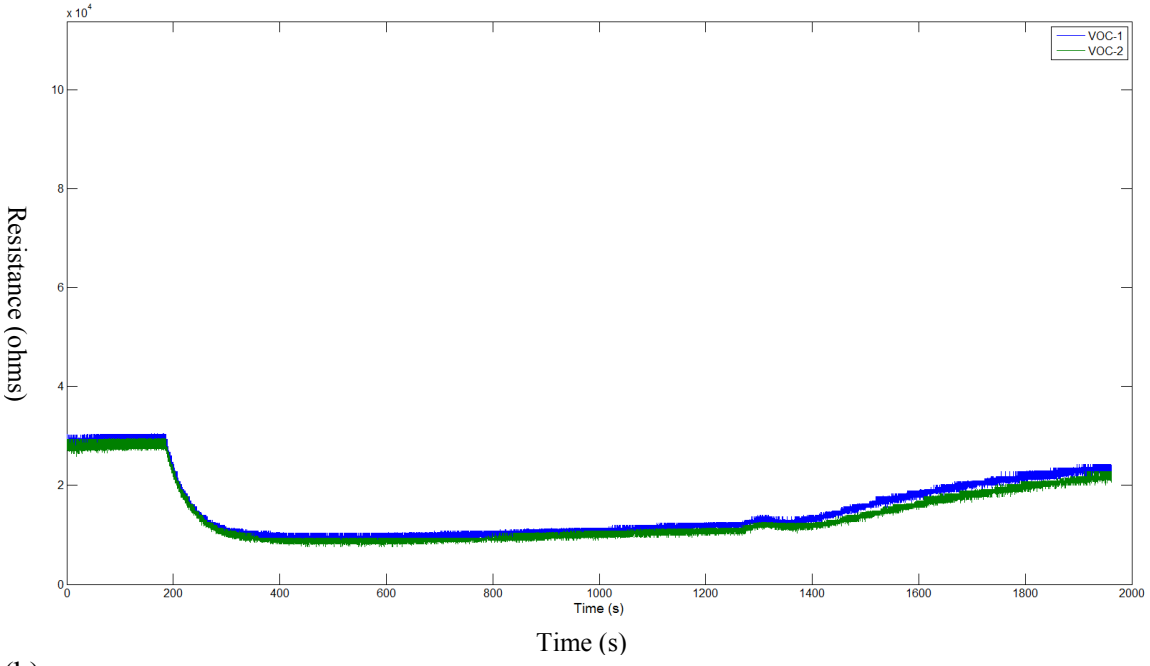

(b)

Figure 4.14 Raw data from VOC sensor (a) voltage response at 66 ppm (b) resistance response at 66 ppm

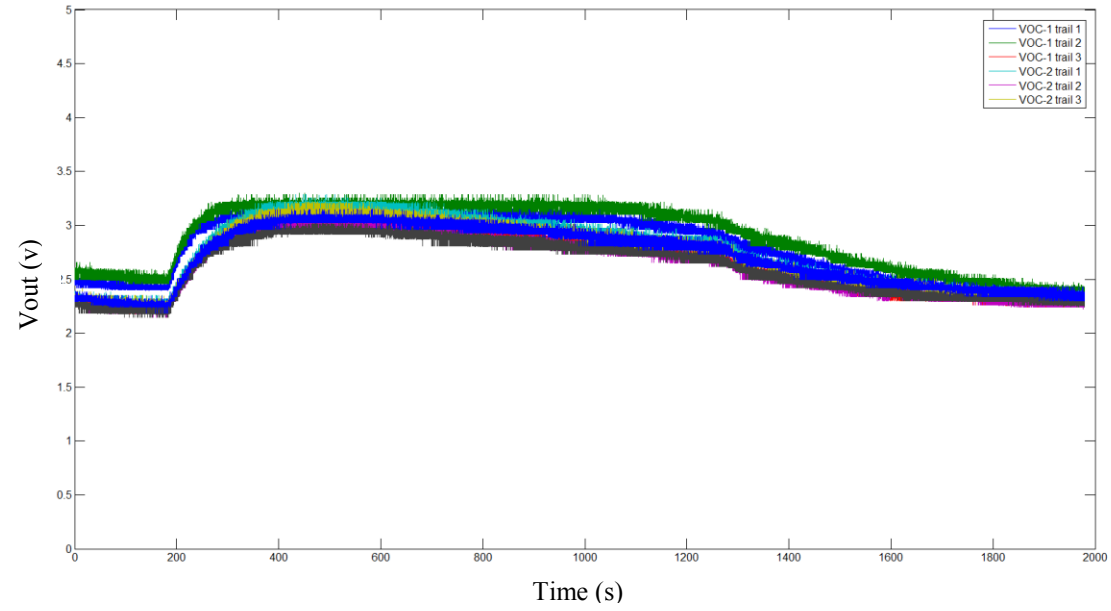

(a)

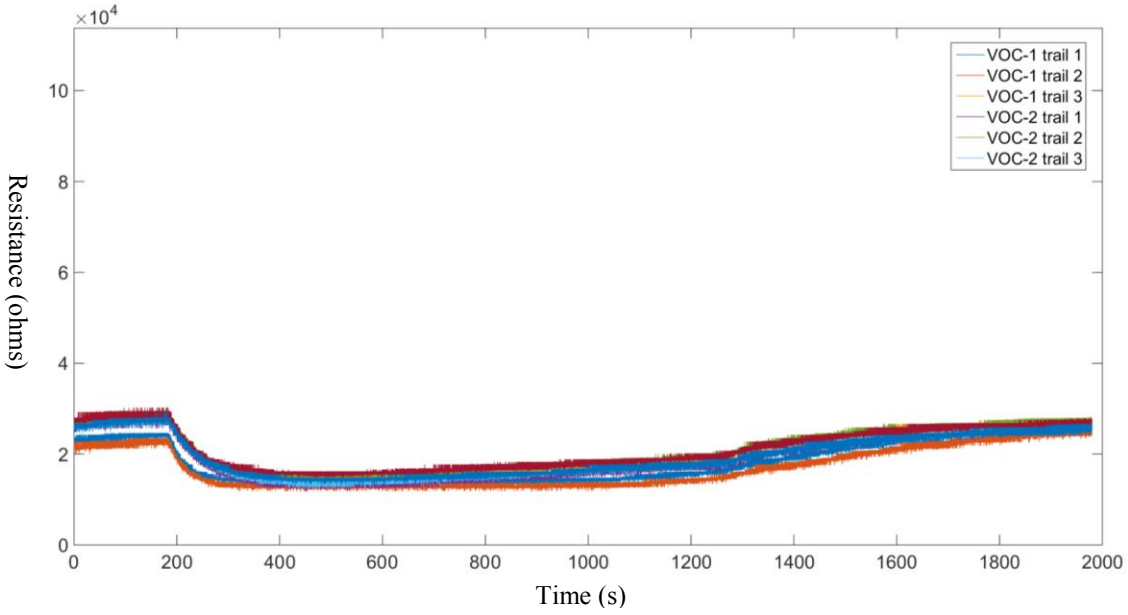

(b)

Figure 4.15 Raw data from VOC sensor (a) voltage response at 25 ppm (b) resistance response at 25 ppm

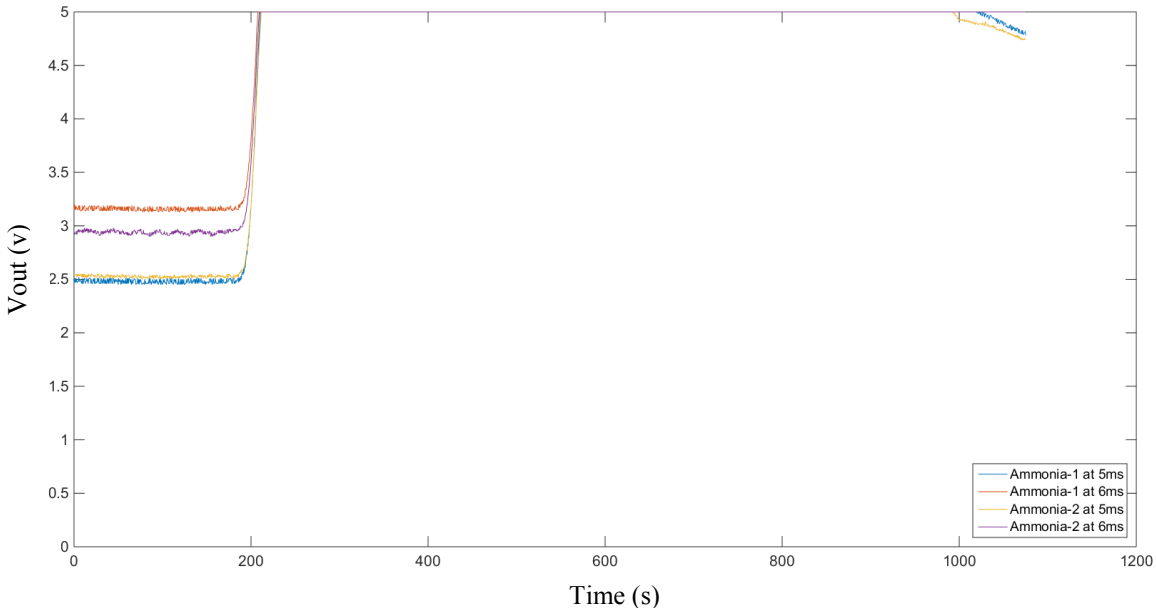

(a)

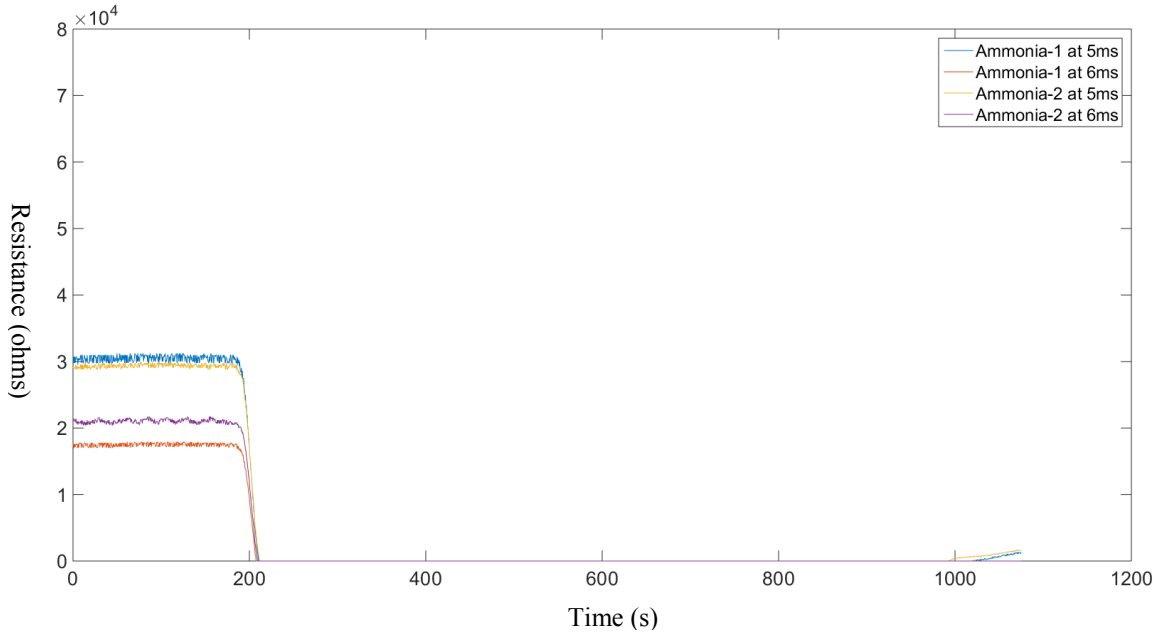

(b)

Figure 4.16 Raw data from ammonia sensor (a) voltage response at 132 ppm (b) resistance response at 132 ppm

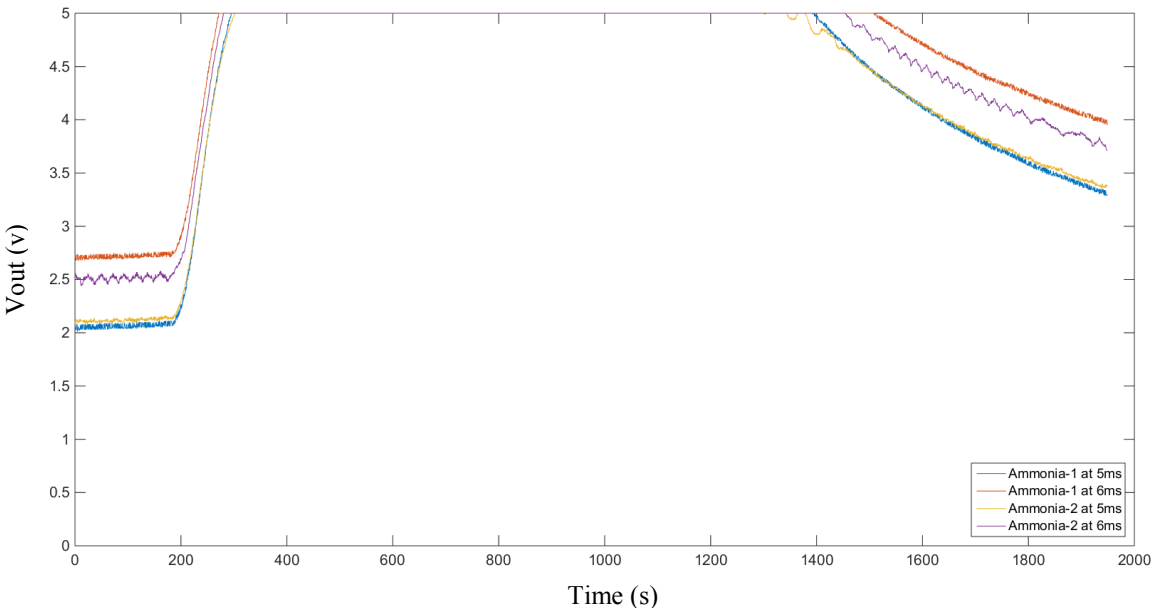

(a)

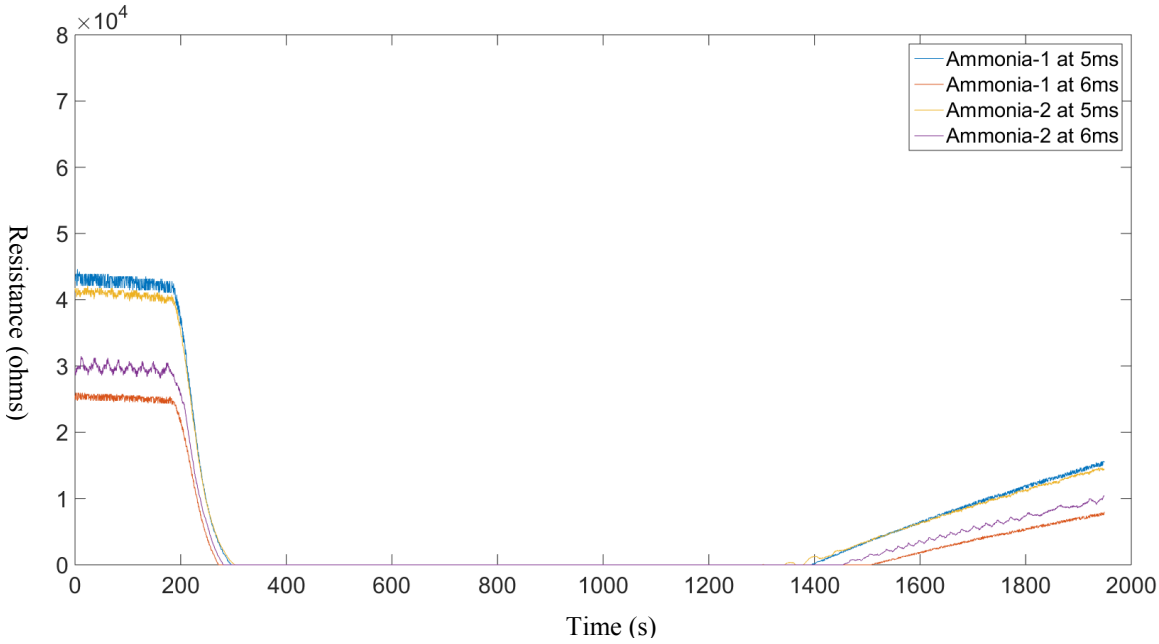

(b)

Figure 4.17 Raw data from ammonia sensor (a) voltage response at 66 ppm (b) resistance response at 66 ppm

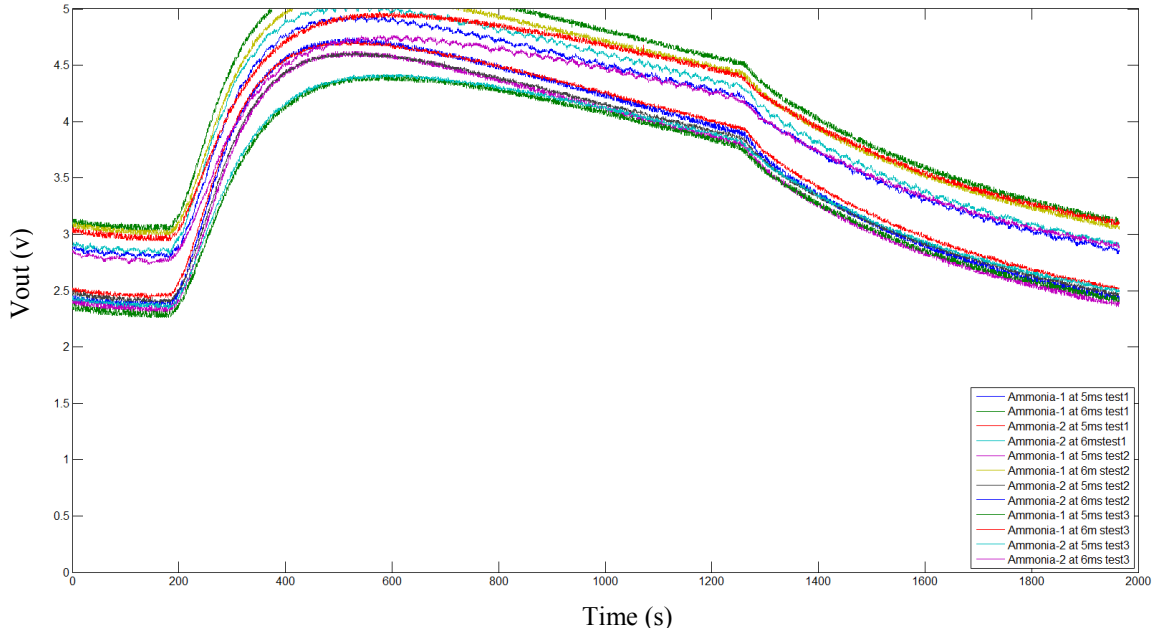

(a)

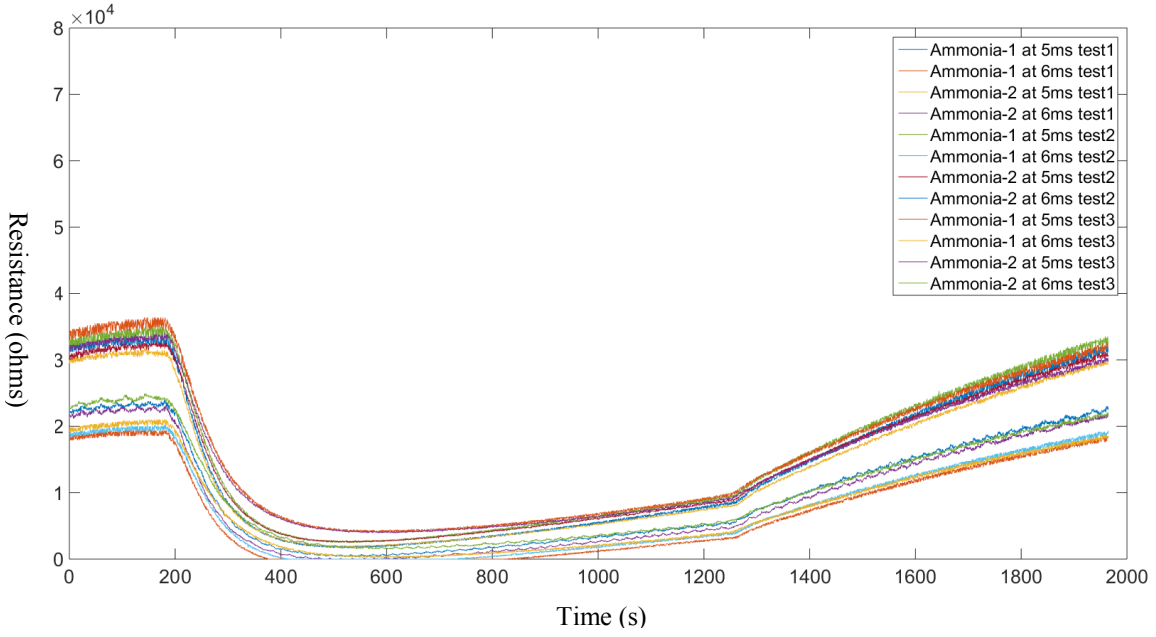

(b)

Figure 4.18 Raw data from ammonia sensor (a) voltage response at 25 ppm (b) resistance response at 25 ppm

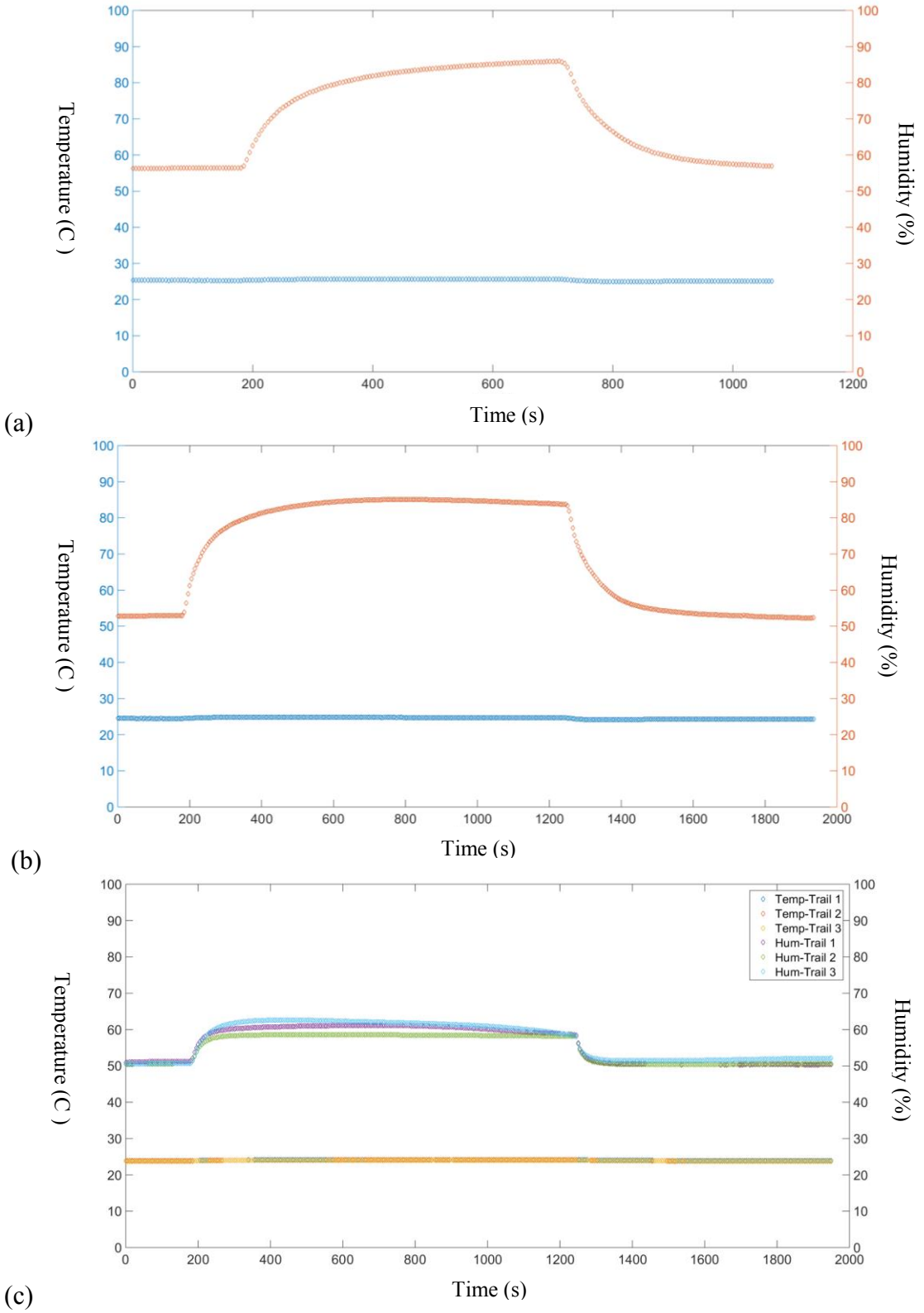

Figure 4.19 Raw data of Temperature and Humidity at (a) 132 ppm (b) 66 ppm (c) 25 ppm

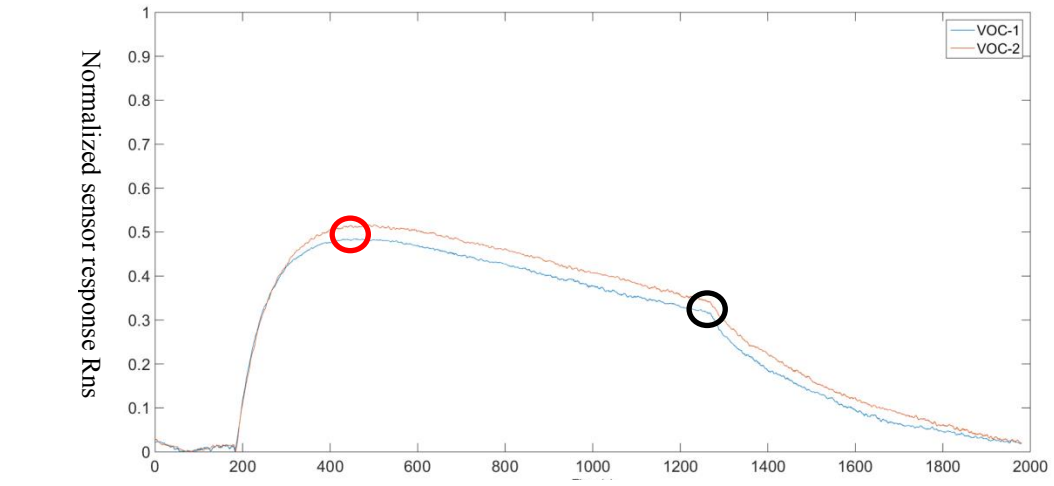

(a)

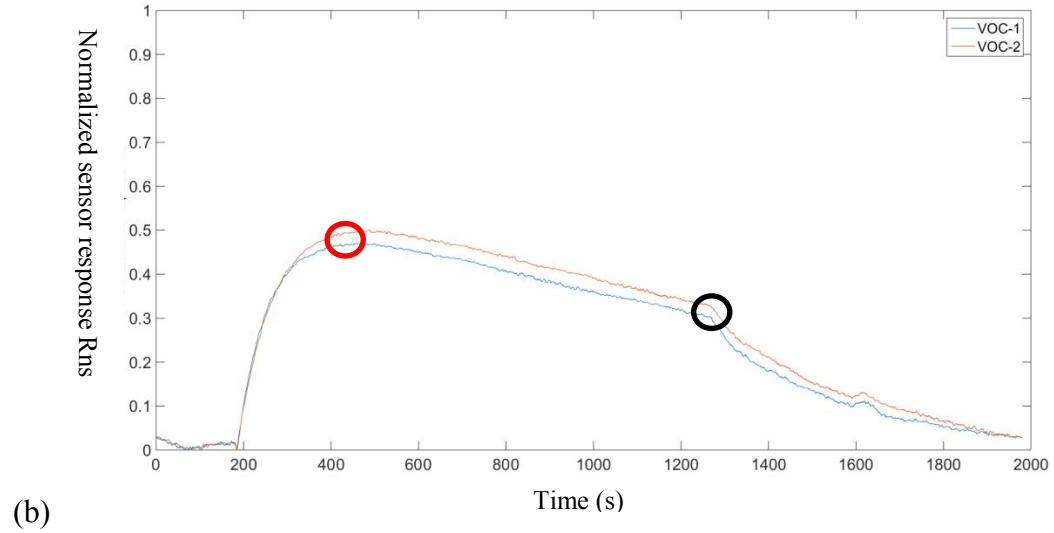

(b)

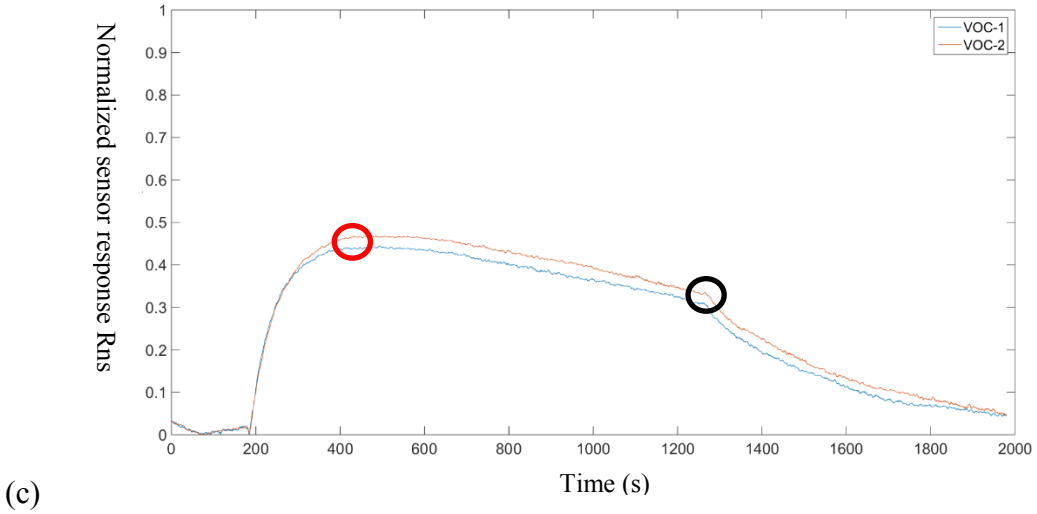

(c)

Figure 4.20 Normalization of VOC response at 25 ppm (a) Test 1 (b) Test 2 (c) Test 3

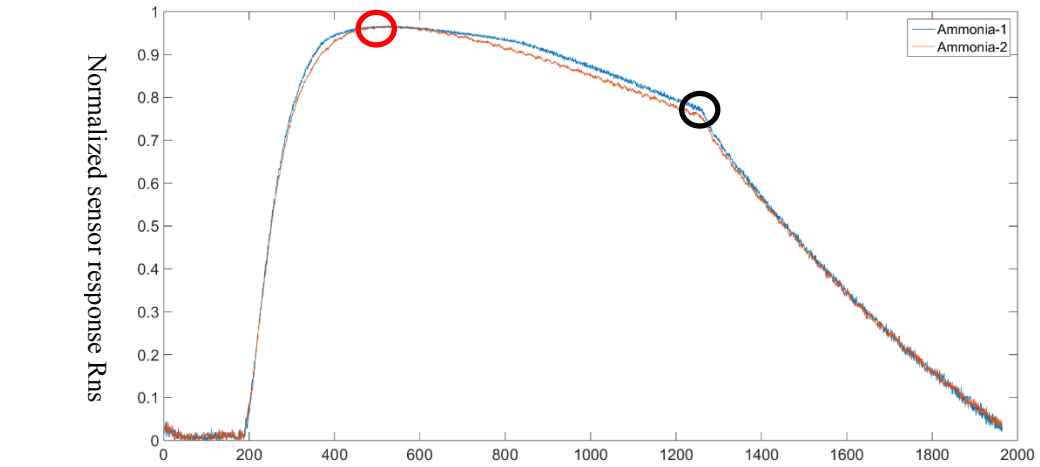

(a)

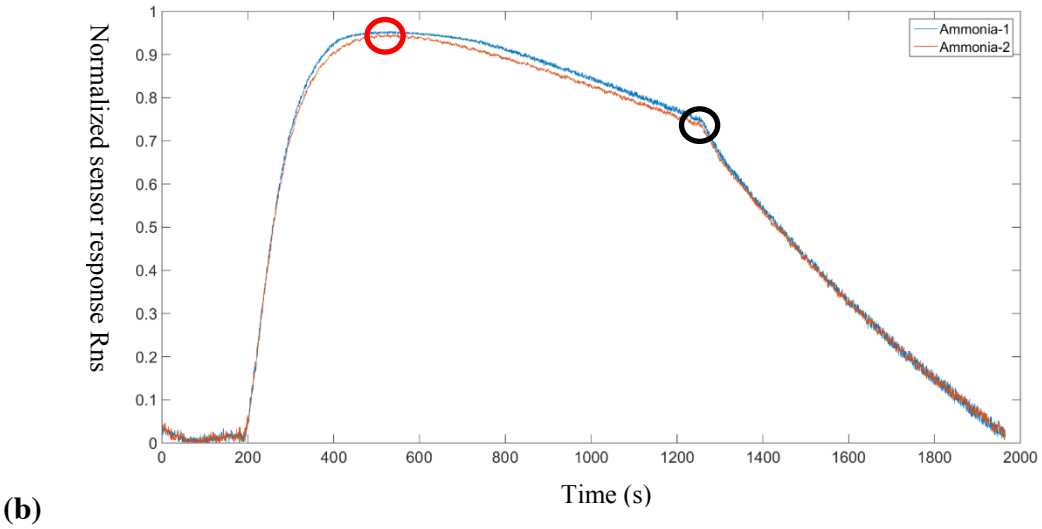

(b)

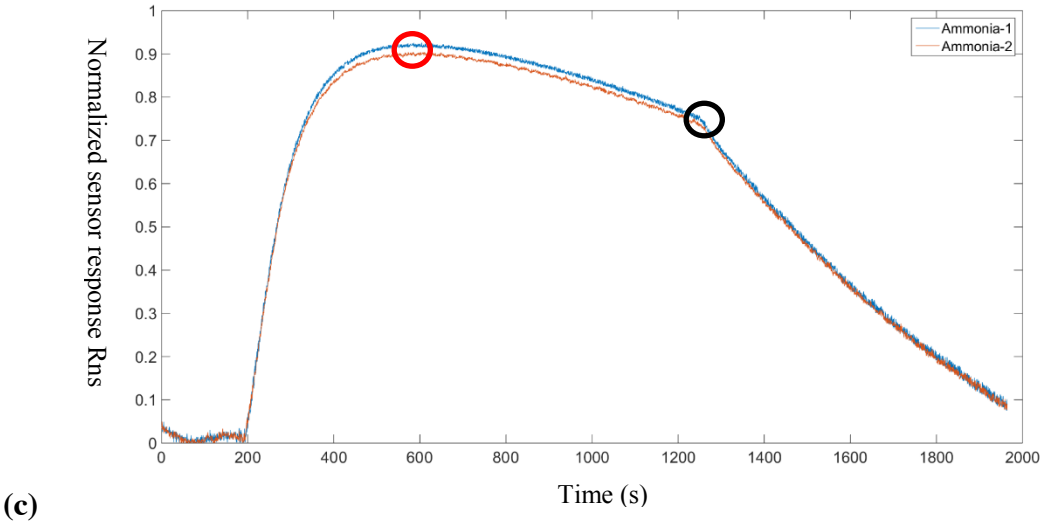

(c)

Figure 4.21 Normalization for ammonia sensor response at 25 ppm (a) Test 1 (2) Test 2 (3) Test 3

Table 4.14 *Maximum normalized sensor response for each test*

	Test 1- maximum	Test 2- maximum	Test 2- maximum
Ammonia-1	0.9678	0.9538	0.9256
Ammonia-2	0.9658	0.9477	0.9043

Table 4.15 *Variation of response of two VOC & ammonia sensors*

	Test 1	Test 2	Test 3
VOC	0.0137	0.0130	0.0116
Ammonia	0.0459	0.0452	0.0418

4.1.3.2 Air quality assessment in poultry farm

Integrated E-nose system was evaluated to assess the air quality of a typical poultry house with respect to outside air and office room air. Hence, the goal was not to determine the concentration of specific gases (NH3 or VOC). Rather, the goal was to document the change of specific patterns of selected sensors in a typical poultry (caged-chicken) house with respect to the outside air (office air or farm yard). This would allow a user to compare the air quality in a poultry house at a given time with respect to that of a standard farm house office or that of a typical farm yard. Thus, this experiment was designed with a clear practical application and use in mind. Farm yard is labelled as Refout. Poultry house is labelled as Poultry. Farm house office is labelled as Refin.

The integrated E-nose system's each sensor is programmed by default to run for 6 minute cycle (3 minutes reference air sampling and 3 minutes of target gas sampling).

For this experiment, the system was programed to use 6 minutes cycle for sampling only in the concerned environmental air (i.e. farm yard, poultry house, or farm house office). Thus, for each experiment, each observation consists of 6 minutes cycle for each sensor (Ammonia, carbon dioxide, VOC and temp/humidity). We conducted three experiments on three separate days at the Animal Science farm of Purdue University, West Lafayette. During each experiment, 5 trials were made. Thus, for three experiments, 5x3 =15 trails were conducted. It is to be noted that the integrated E-nose system contains two sensors for gas type (Ammonia and VOC).

4.1.3.2.1 Raw data of carbon dioxide, ammonia, volatile organic compound, and temperature and humidity

VOC sensor

Figures 4.22 show the sensor response for VOC-1 and VOC-2 were steady and identical in poultry room. The signal range for both sensors was about from 2.5 to 3 volts. Figure 4.23 illustrates the signal range of VOC-1 was similar to the range of VOC-2 but was shifted up 0.15 volts. The range of VOC-1 was about from 2.2 to 2.4 volts and the signal range for VOC-2 in the office was from 2.35 to 2.55 volts. In addition, the trends of two sensors were analogous in Figures 4.23. The signal was steady for 180 seconds and they went up 0.2 volts when the solenoid valve changed the direction. In Figure 4.24, the measurement was taken in the farm yard of Purdue farm. The responses of both sensors were constant except for trial 11. The signal shows there was VOC response at

beginning of the measurement. Figures 4.22, 4.23, and 4.24 also show that there were small variations among consecutive data points that projected a band pattern.

Figures 4.25, 4.26 and 4.27 show R_s for both VOC sensors. These $R_s$values were calculated from Vout shown in Equation 3.1.The $R_s$varied from 20k to 30k ohms depending on the location (Refout, Refin, Poultry). The trend of the sensor response was similar to the trend of Vout but in an inverse manner

Ammonia sensor

For ammonia sensor, Figures 4.28, 4.29 and 4.30 show the result of ammonia sensor with respect to time in the poultry room, from office and from yard respectively.

Figure 4.28 illustrates the trends of Vout from both the ammonia sensors increased during the experiment for each of 6 minute or 360 second cycle, so it was postulated that the sensors might not be reaching its equilibrium. Therefore, for ammonia sensors, 1800 seconds or 30 minutes was taken as each experiment/observation cycle. As shown in Figure 4.29, the signal responses in the farm office decreased with the time. In Figures 4.30, the sensor response from the first trial was steady but it increased at 1100 second. Then it decreased back to the initial measurement. The sensor responses for other trials were decreasing throughout the measurement (Figure 4.30). Figures 4.31, 4.32 and 4.33 show the resistance of ammonia sensors. Similar to VOC sensor, the trend of the signal in resistance was inversely proportional to the trend of the signal in voltage.

Carbon dioxide sensor

The readings were taken in the office (Refin) and the farm yard (Refout). There were 5 observations for each experiment. From Figure 4.34, the Refin and Refout were consistent during the measurement. The means of Refin and Refout are shown in Figure

4.35. The average CO_2 level of 5 observations for Refin was 531.01 ppm and the average in Refout was 375.02ppm.

Temperature and Humidity sensor

Temperature and humidity measurement were recorded in all three locations. The result is shown in Figure 4.36. The upper part of data points are the humidity values. The data points at lower part of the plot represent the temperature. Figure 4.36 (a) shows the temperature and humidity in poultry room. The humidity varied from 55% to 78% and the temperature varied from 27°C to 32°C. For the farm office (Figure 4.36 (b)), the humidity varied from 68% and 72%. The temperature reading was consistent around 23°C. As shown in Figure 4.37 (c), the humidity reading taken in outside environment of Purdue farm was varying from 57% to 81%, and the temperature was different from 25°C to 31°C. The variation within the trails is significant large because the trails was test in different days. Thus, the humidity and temperature was distinct in daily basis.

4.1.3.2.2 Data processing

The data from VOC sensor and ammonia sensor were further analyzed using the following steps:

1. Applied moving average smoothing using 10 data point as a window size for reducing the variation in raw data in VOC sensors.
2. Converted the Vout to resistance using the equations that mentioned in Equation 3.1 and Equation 3.2

3. Find normalized sensor response :

$$R_{ns} = \left|\frac{R_s - R_{refout}}{R_{refout}}\right| \quad \text{(Equation 4.4)}$$

Where R_s is the sensor resistance in poultry room and R_{refout} is the sensor reading in farm yard.

VOC sensor

Figures 4.38 through 4.43 show the normalized sensor response of samples 1, 3, 5 for VOC-1 and VOC-2 sensors. Comparing among the three tests, the trend of each test is difference. However, if the two VOC sensors were compared in the same test, the trends of VOC-1 and VOC-2 for individual test are similar (Figures 4.38, 4.39, 4.40, 4.41, 4.42 and 4.3). In the three tests measured from VOC-1, the normalized values were under 0.3. The maximum value among three tests for VOC-1 was 0.2786 in sample 3 under first test and the minimum value among three tests for VOC-1 was 0.0672 in sample 1 under third test. The maximum normalized sensor response for VOC-2 was 0.2889 in sample 3 under second test and the minimum for VOC-2 was 0.0681 in sample 1 under third test.

Figure 4.44 compared the variation for VOC-1 and VOC-2. Among the tests, the smallest variation was in second test. The standard deviation was 0.001.

Ammonia sensor

Figure 4.45 shows the normalization of ammonia with respect to time. Those three plots show the normalized sensor response was increasing along with the time. Figure 4.45(a) shows the signal was in equilibrium stage after 1600 seconds. However, Figure 4.45 (b) and (c) illustrate both sensors approached equilibrium stage in 1800 seconds. In addition, the mean response for Ammonia-1 sensor was higher than that of

Ammonia-2 among the three tests. Table 4.16 shows the variation of ammonia sensor and VOC sensor with respect to different tests.

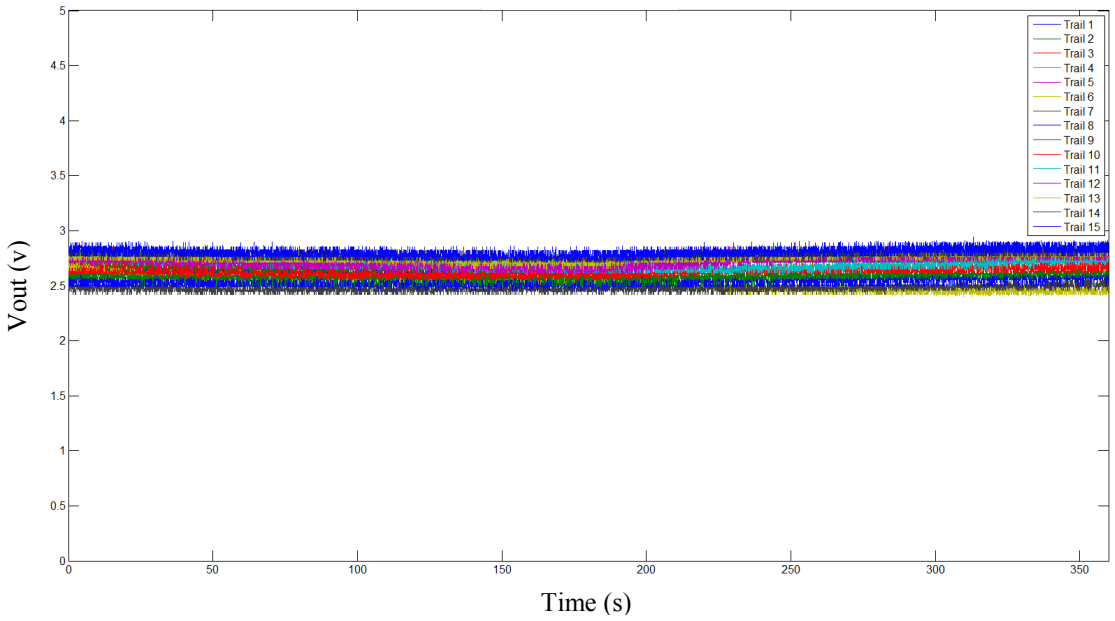

(a)

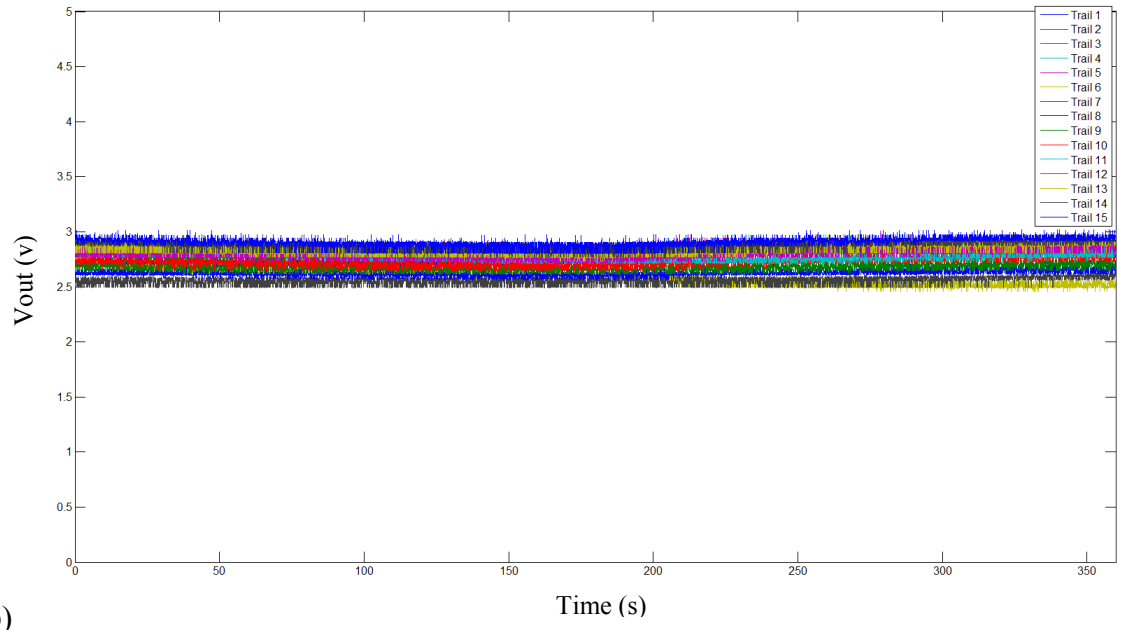

(b)

Figure 4.22 Response of VOC sensor (voltage) (a) VOC-1 at Poultry room (b) VOC-2 at Poultry room.

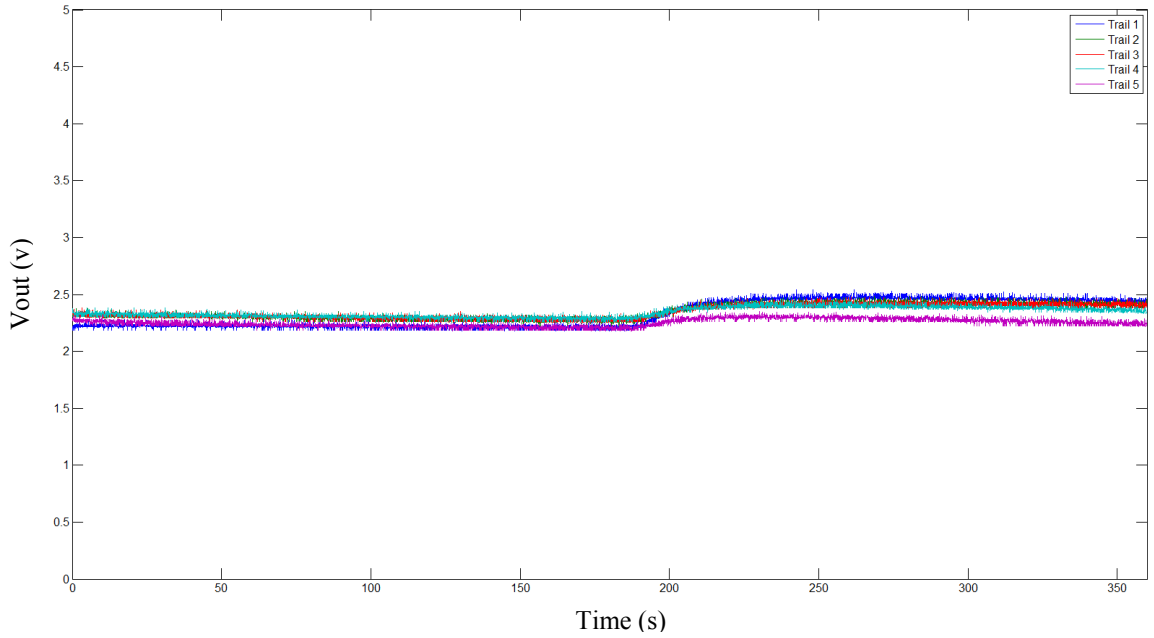

(a)

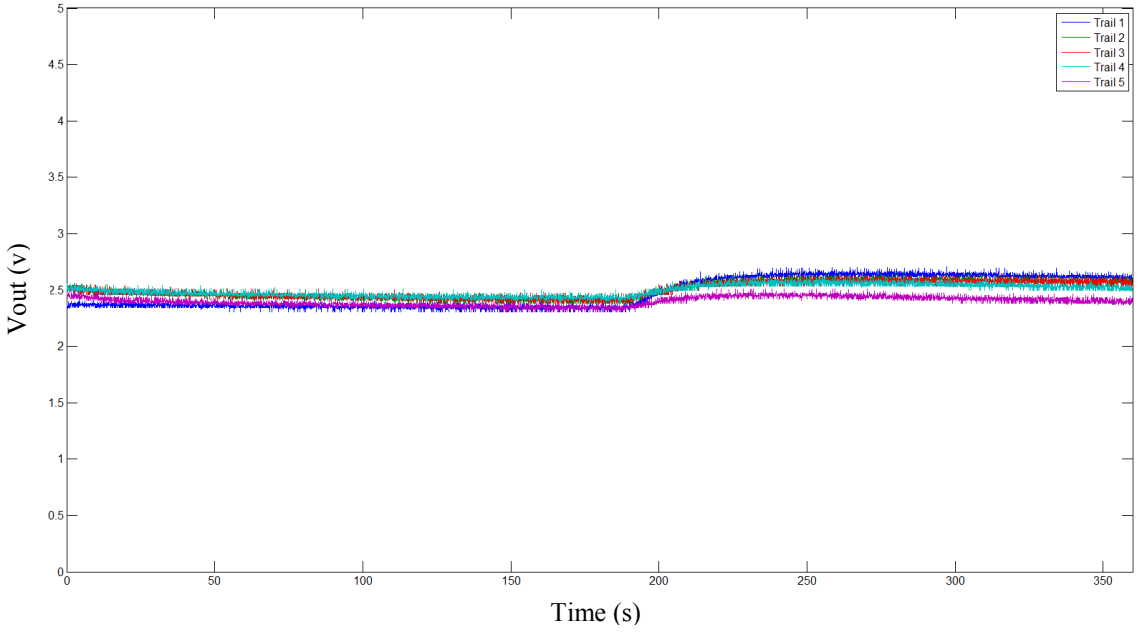

(b)

Figure 4.23 Response of VOC sensor (voltage) (a) VOC-1 at Refin (b) VOC-2 at Refin.

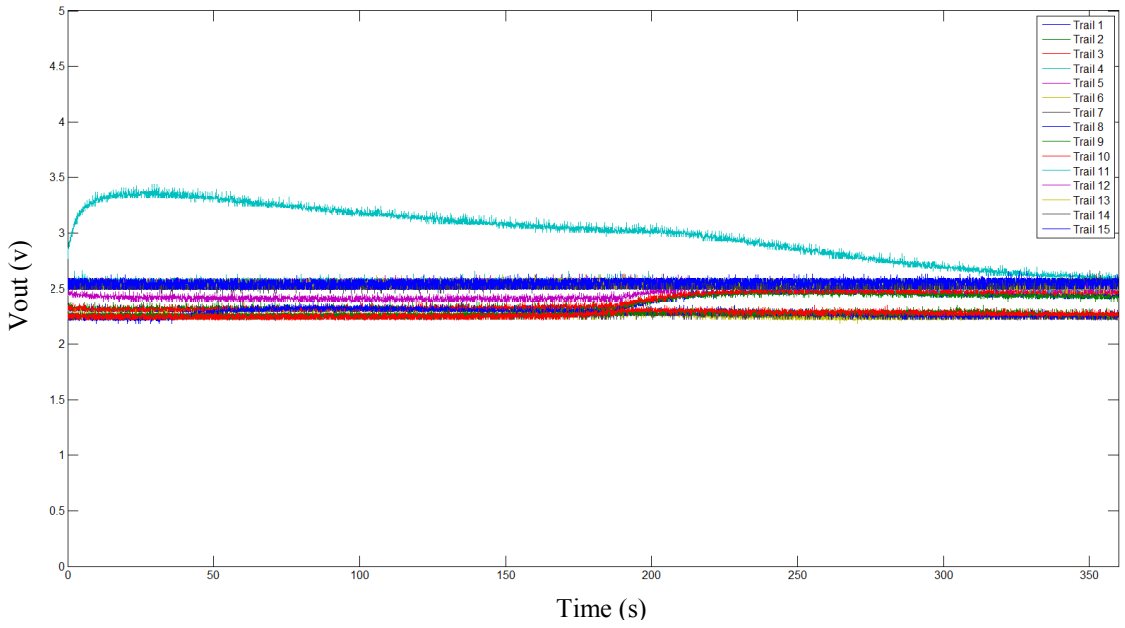

(a)

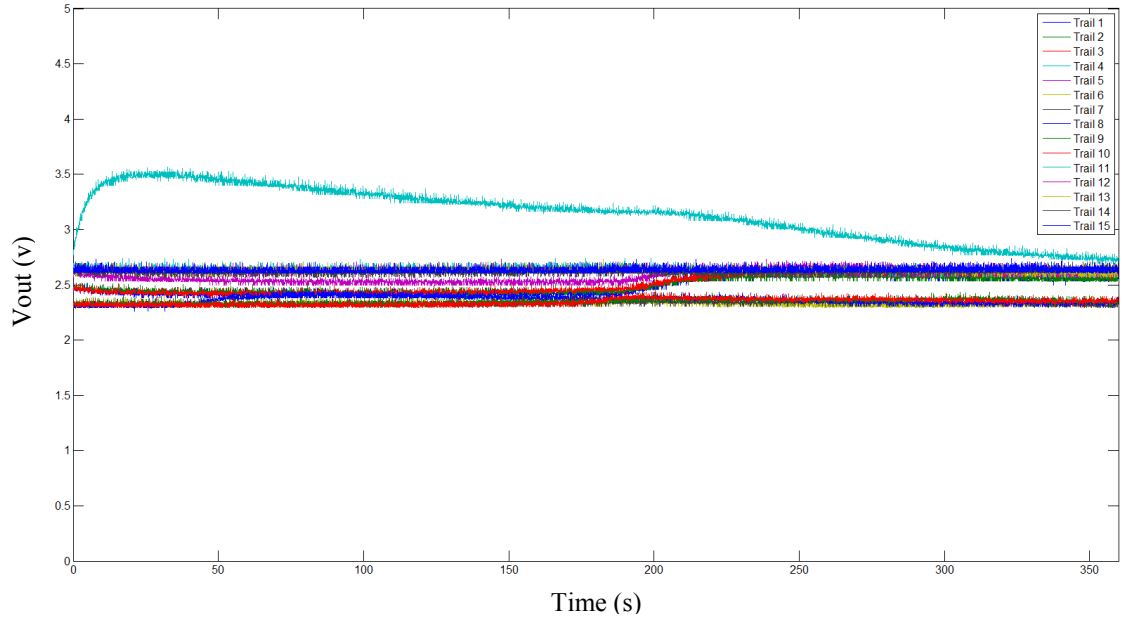

(b)

Figure 4.24 Response of VOC sensor (voltage)(a) VOC-1 at Refout (b) VOC-2 at Refout

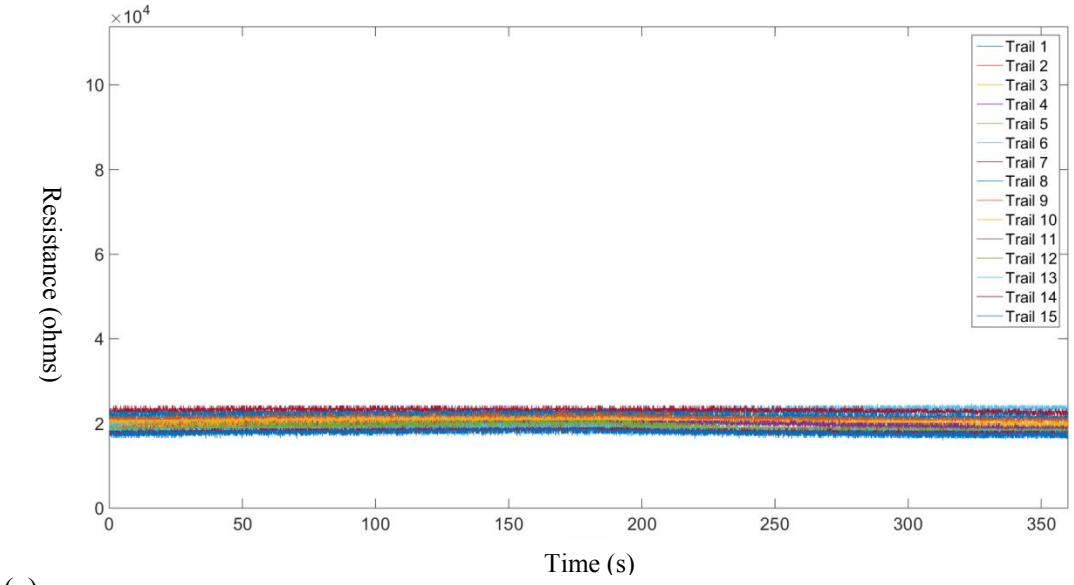

(a)

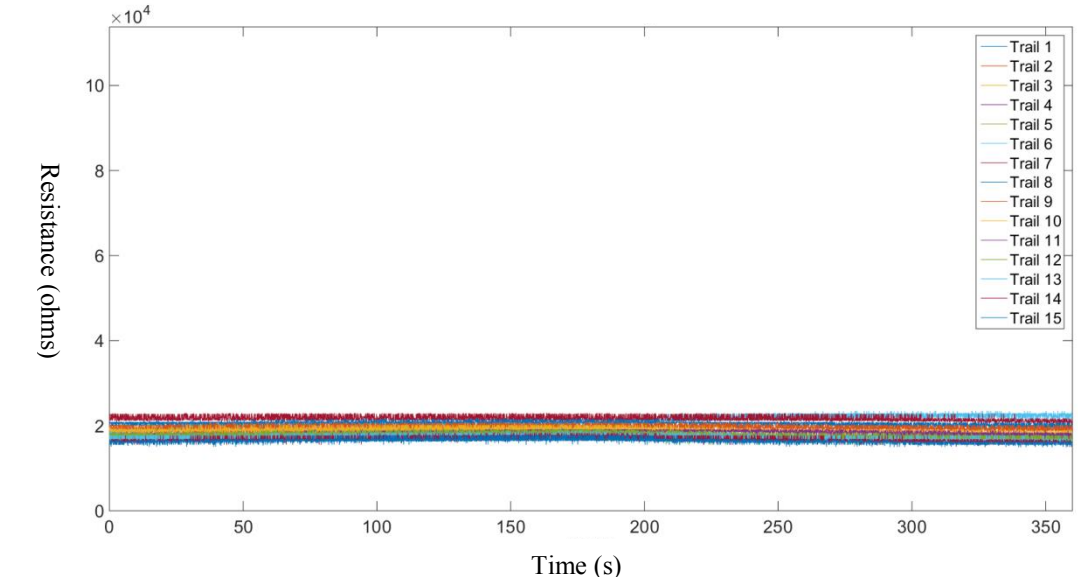

(b)

Figure 4.25 Response of VOC sensor (resistance). (a) VOC-1 at Poultry room (b) VOC-2 at Poultry room

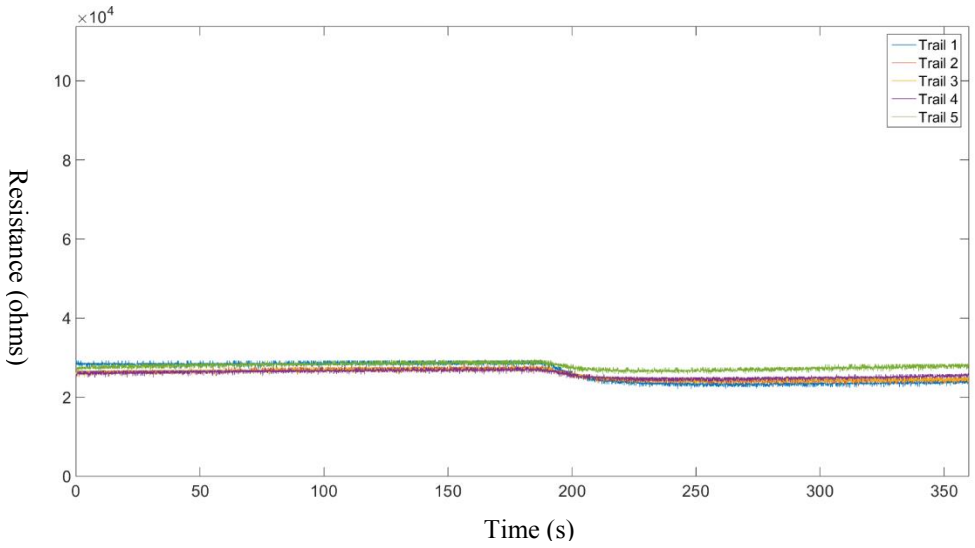

(a)

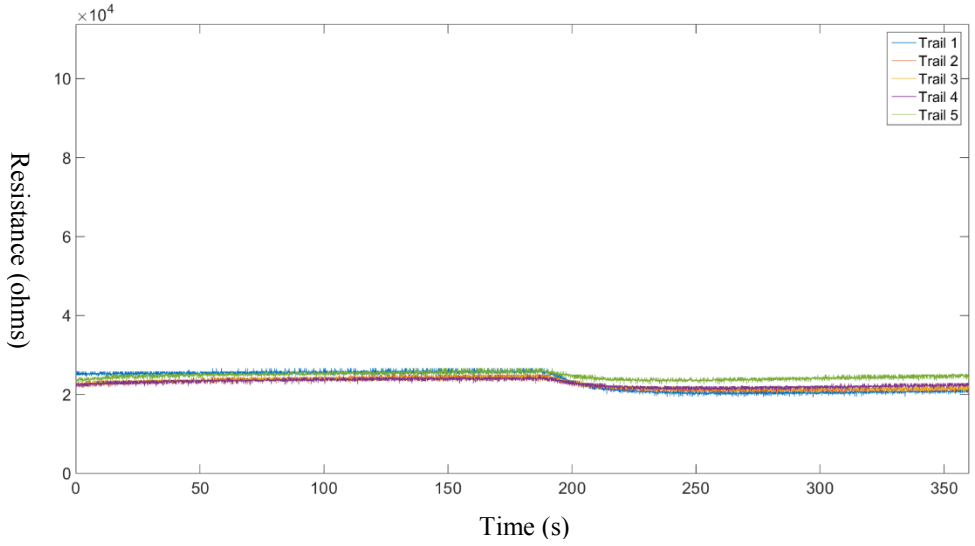

(b)

Figure 4.26 Response of VOC sensor (resistance). (a) VOC-1 at Refin (b) VOC-2 at Refin

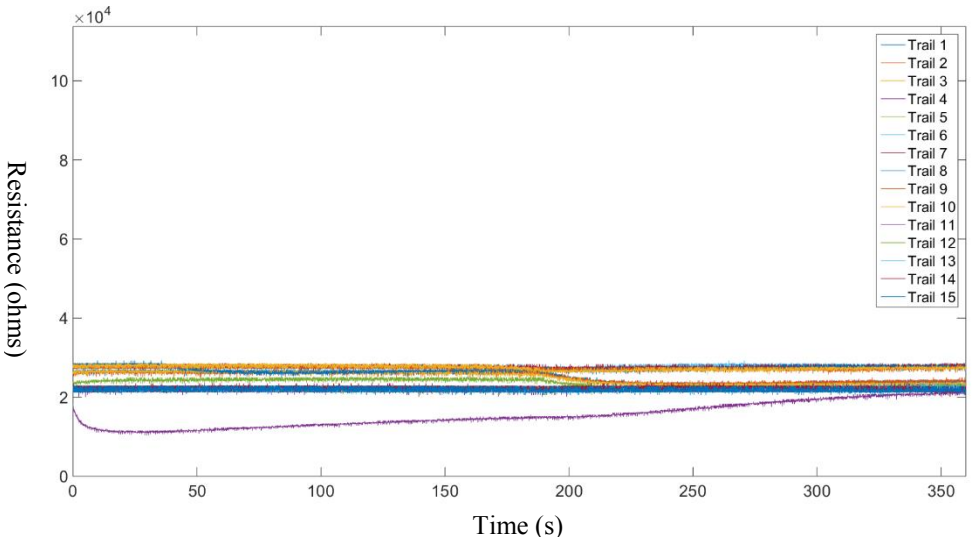

(a)

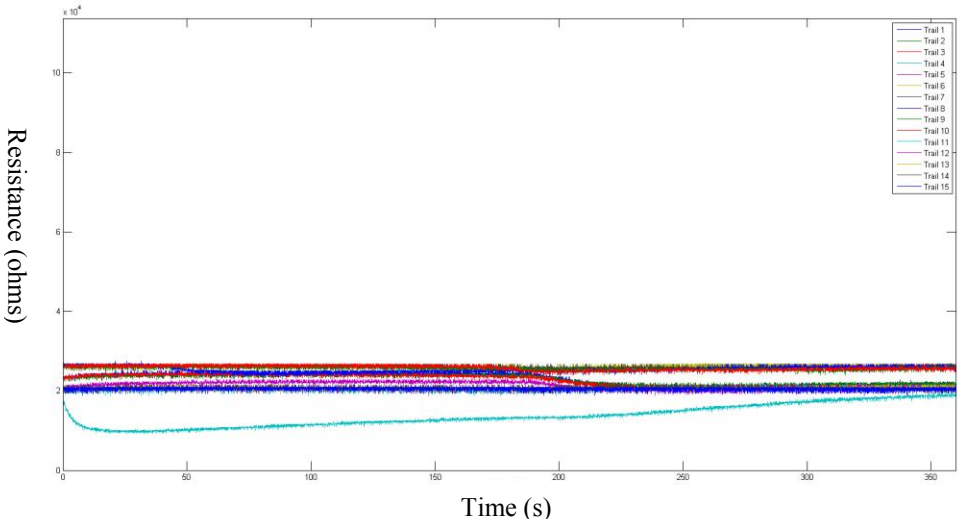

(b)

Figure 4.27 Response of VOC sensor (resistance). (a) VOC-1 at Refout (b) VOC-2 at Refout

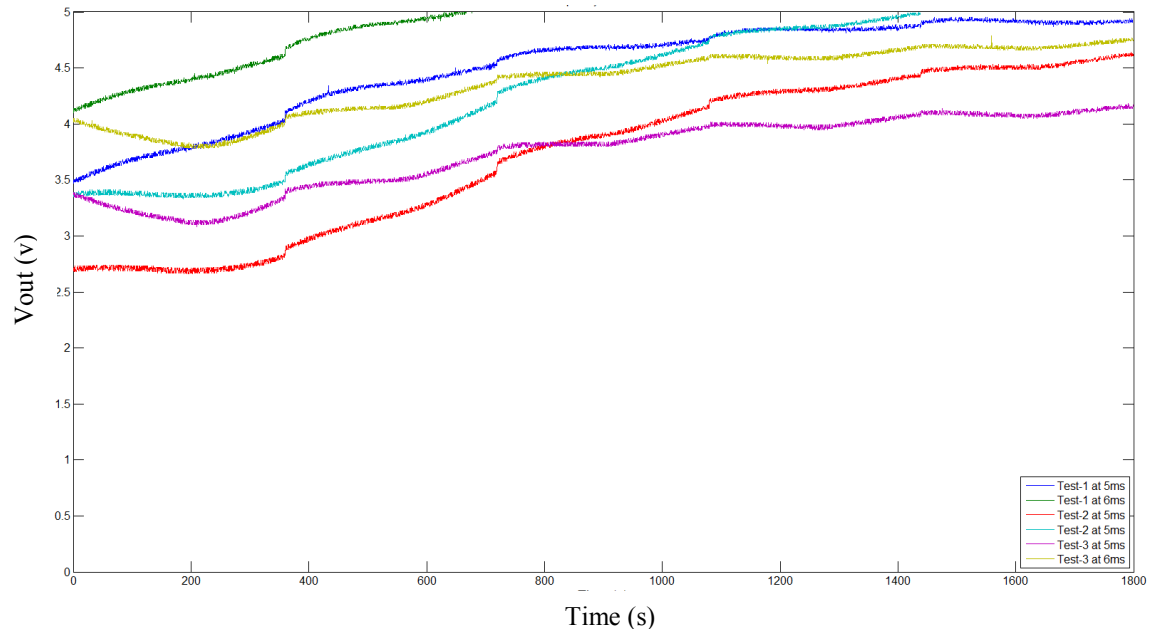

(a)

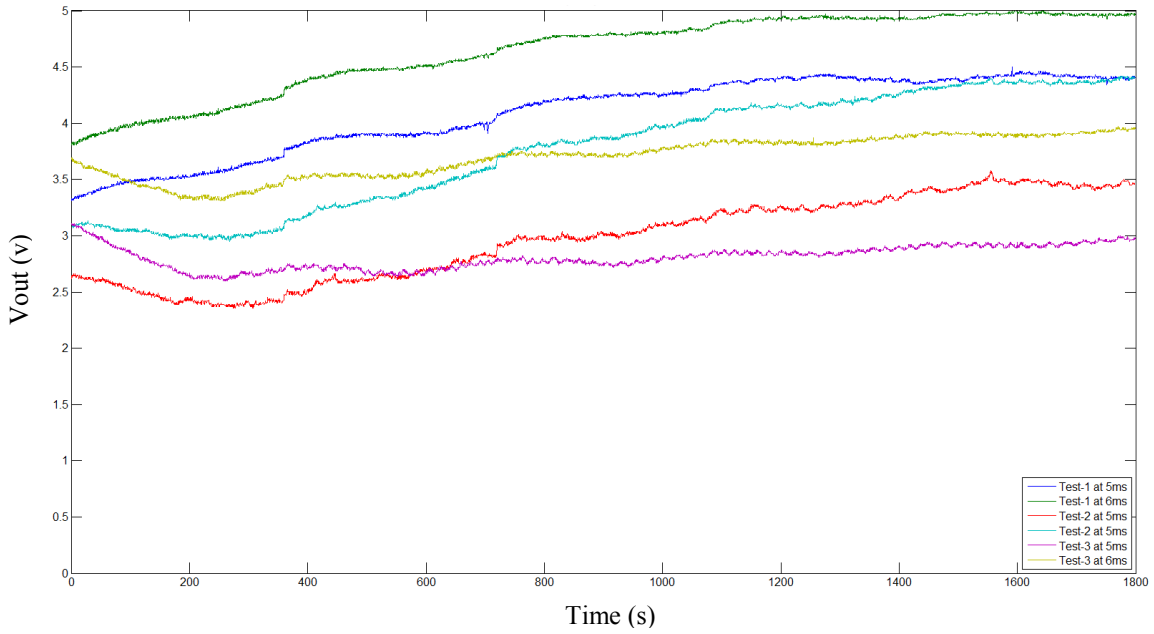

(b)

Figure 4.28 Response of ammonia sensor (voltage). (a) Ammonia-1 at Poultry room (b) Ammonia -2 at Poultry room

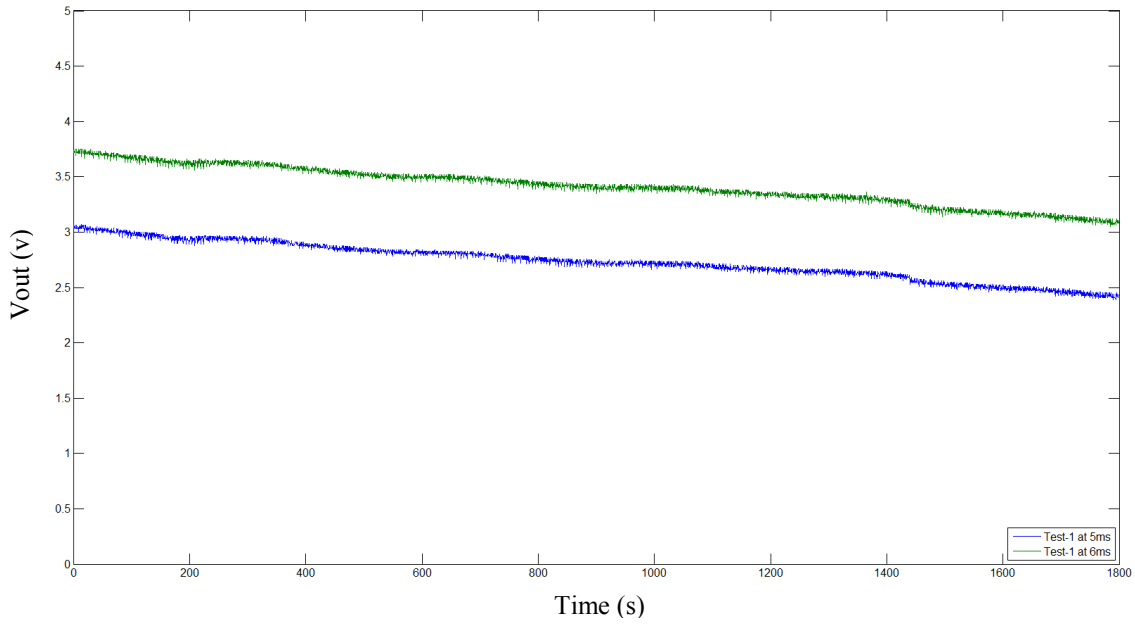

(a)

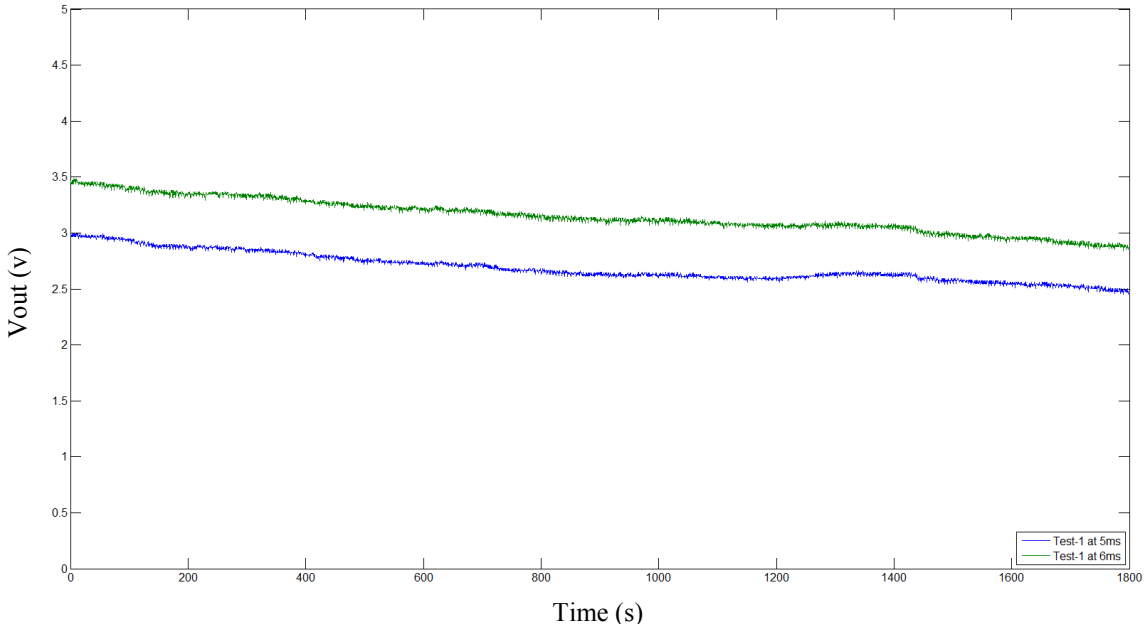

(b)

Figure 4.29 Response of ammonia sensor (voltage). (a) Ammonia -1 at Refin (b) Ammonia -2 at Refin

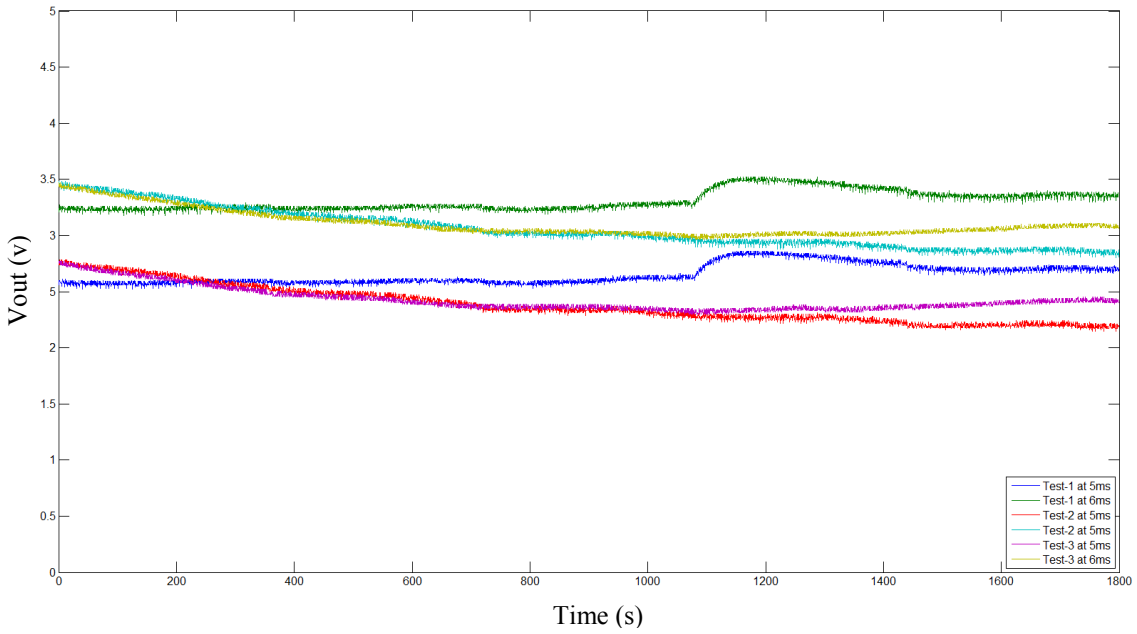

(a)

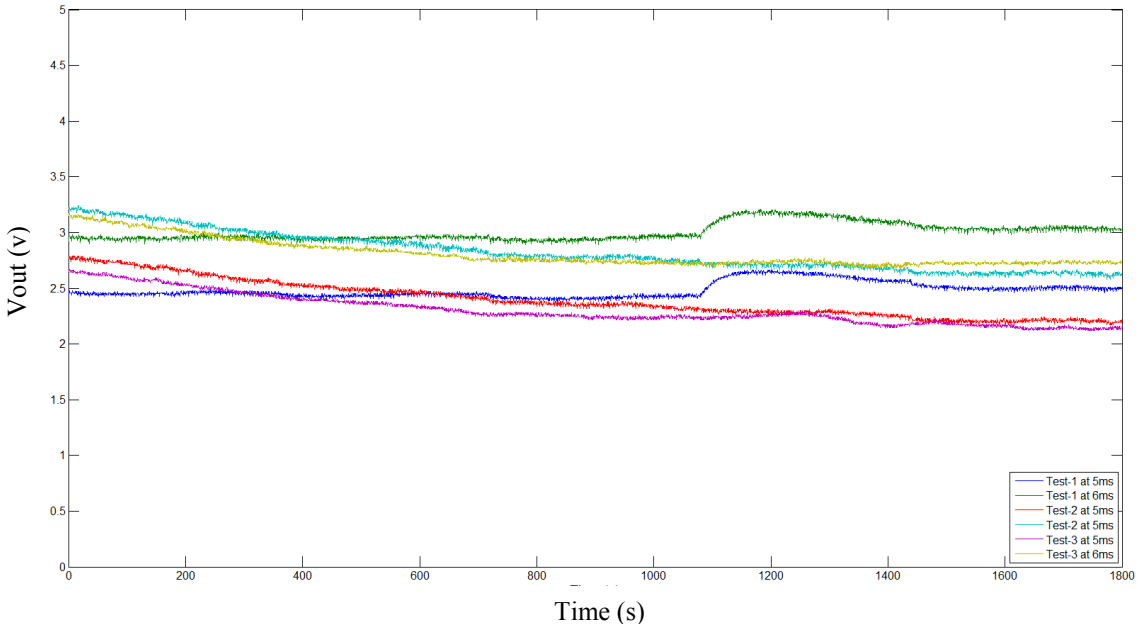

(b)

Figure 4.30 Response of ammonia sensor (resistance). (a) Ammonia -1 at Refout (b) Ammonia -2 at Refout

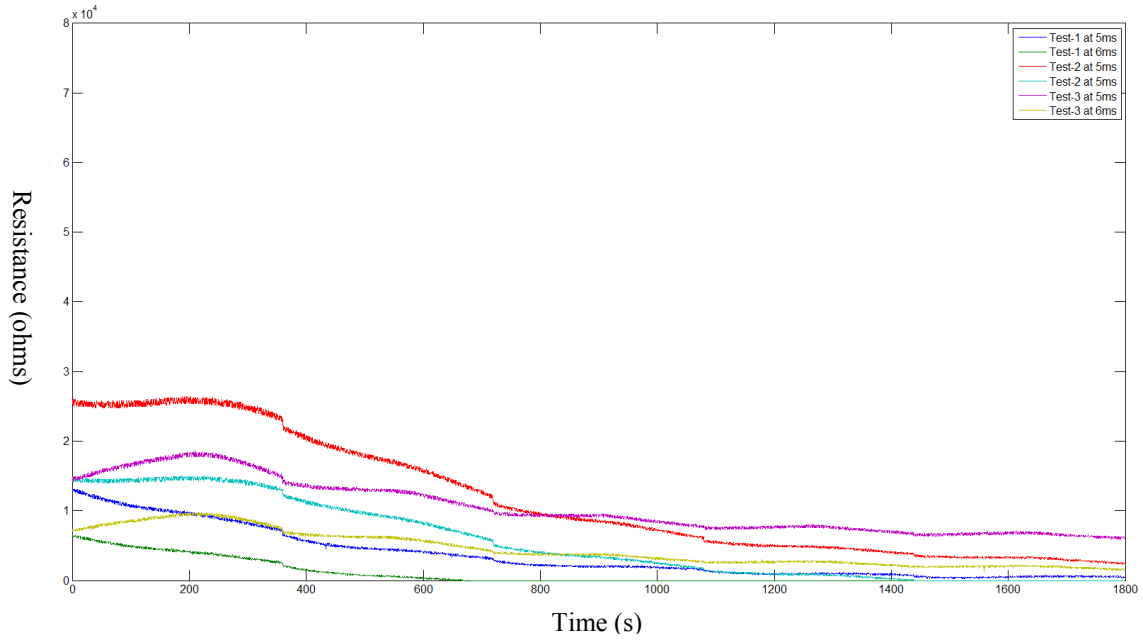

(a)

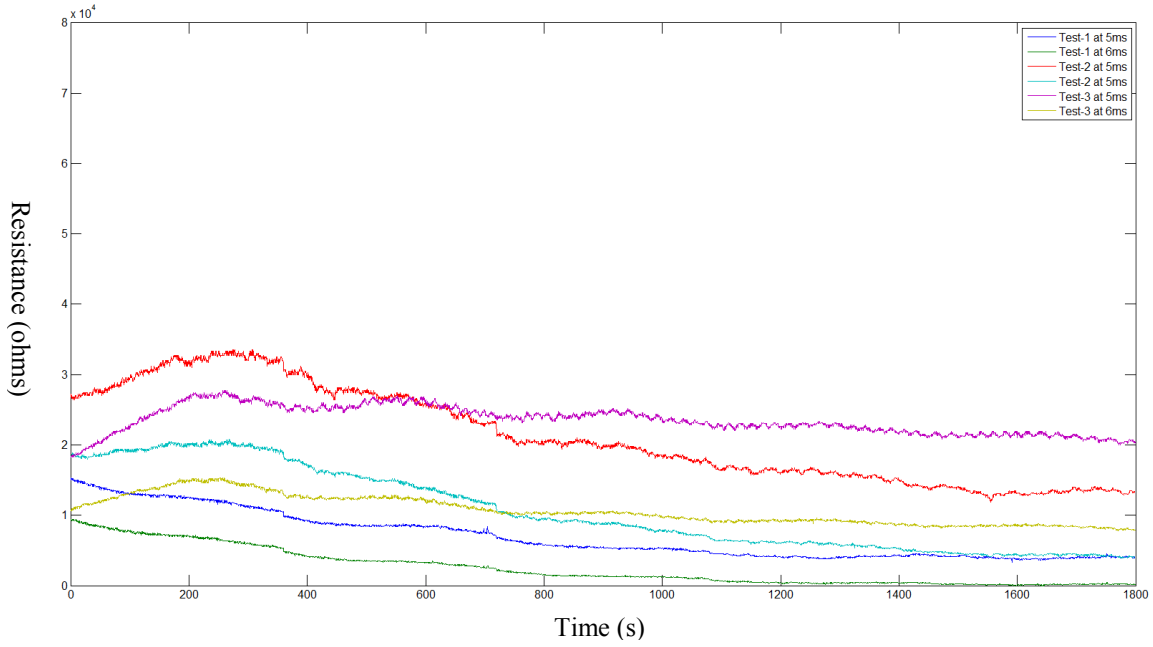

(b)

Figure 4.31 Response of ammonia sensor (resistance). (a) Ammonia-1 at poultry room (b) Ammonia -2 at poultry room

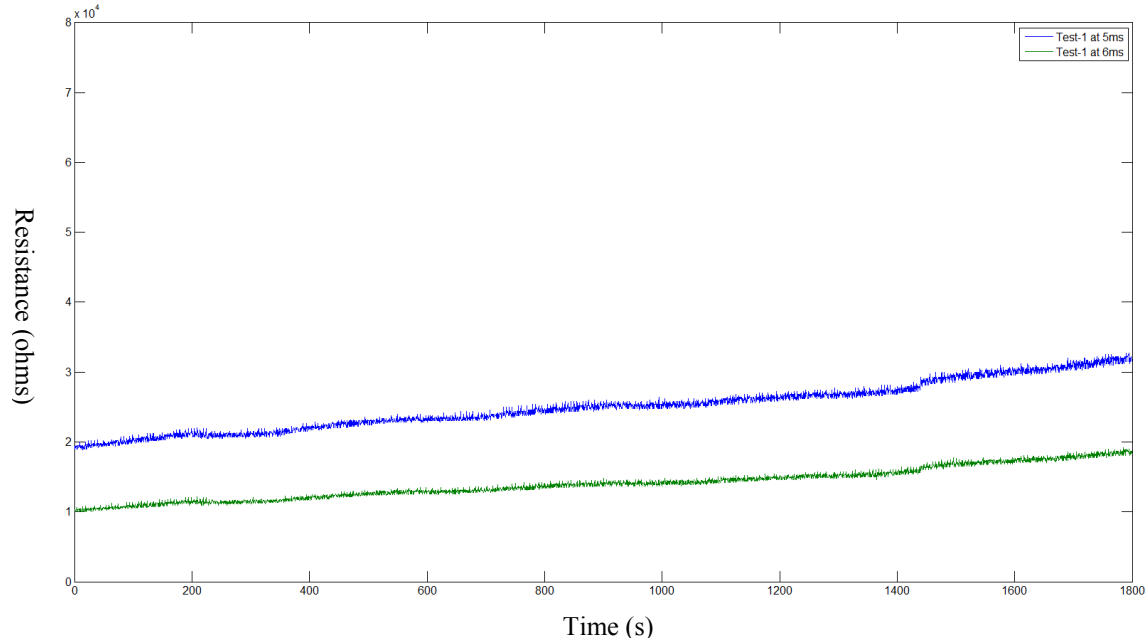

(a)

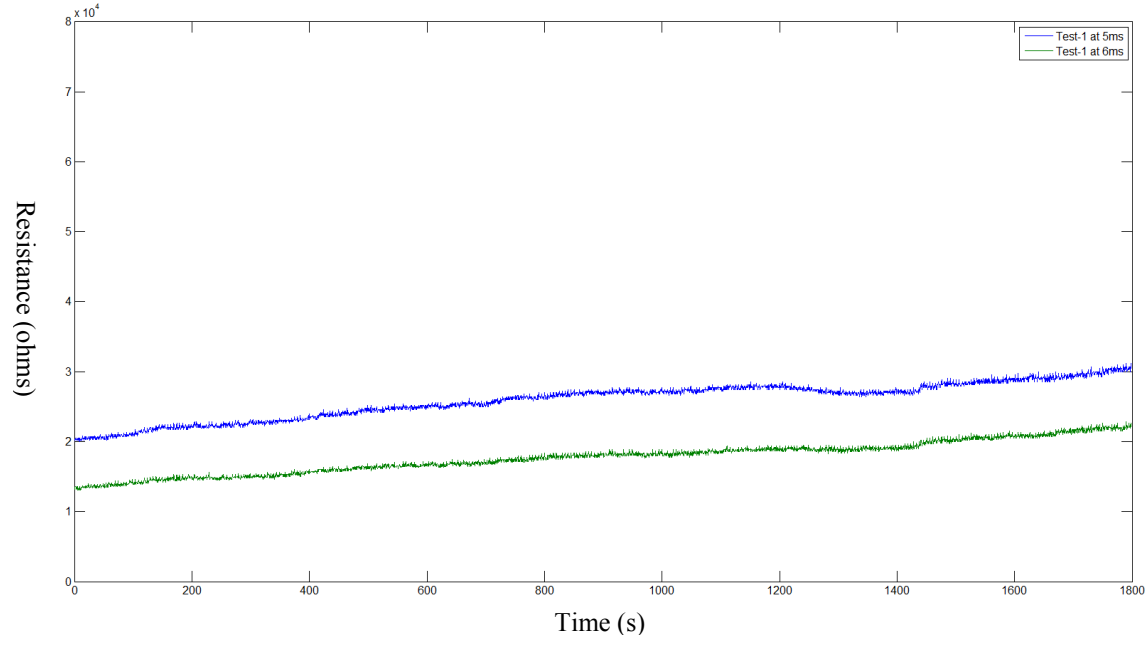

(b)

Figure 4.32 Response of ammonia sensor (resistance). (a) Ammonia -1 at Refin (b) Ammonia -2 at Refin

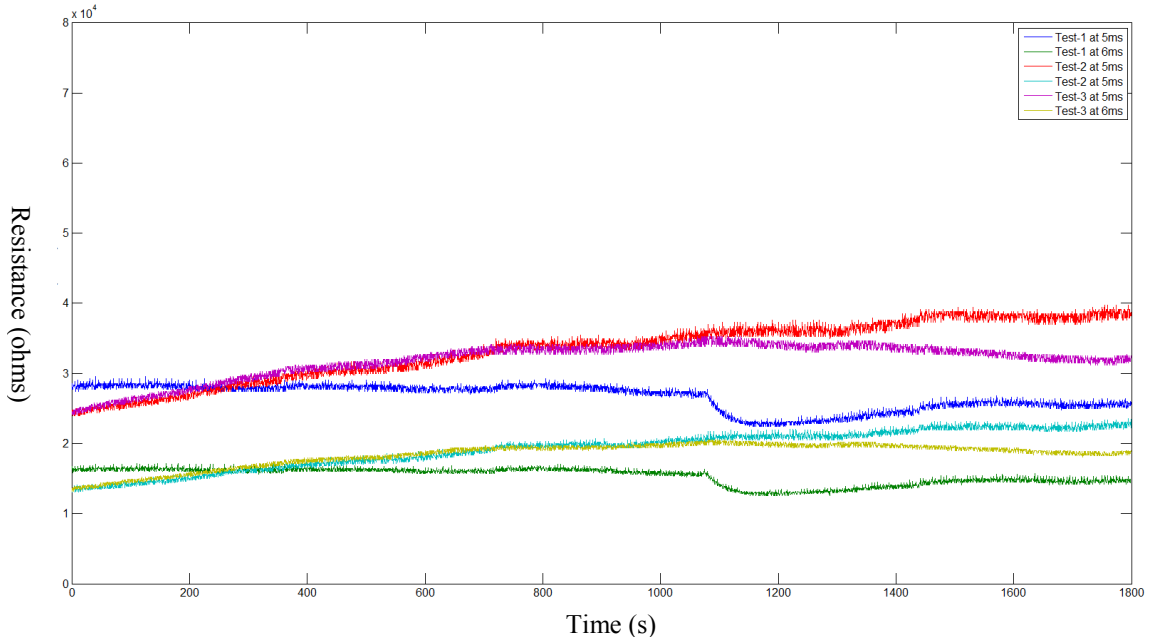

(a)

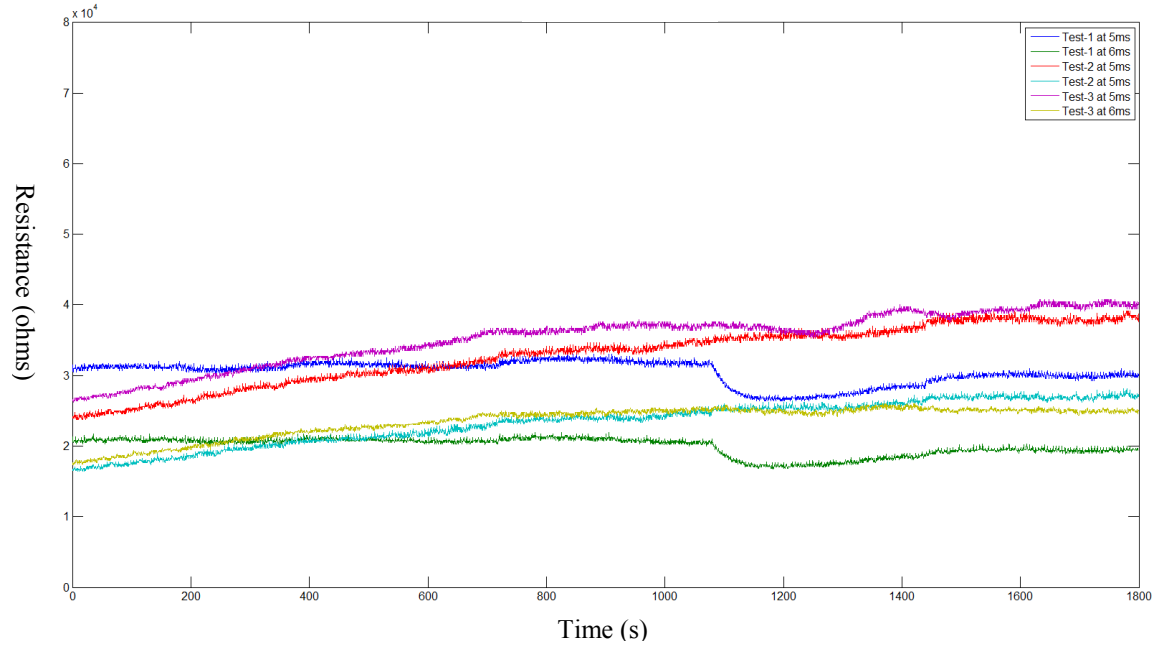

(b)

Figure 4.33 Response of ammonia sensor (resistance). (a) Ammonia -1 at Refout (b) Ammonia -2 at Refout

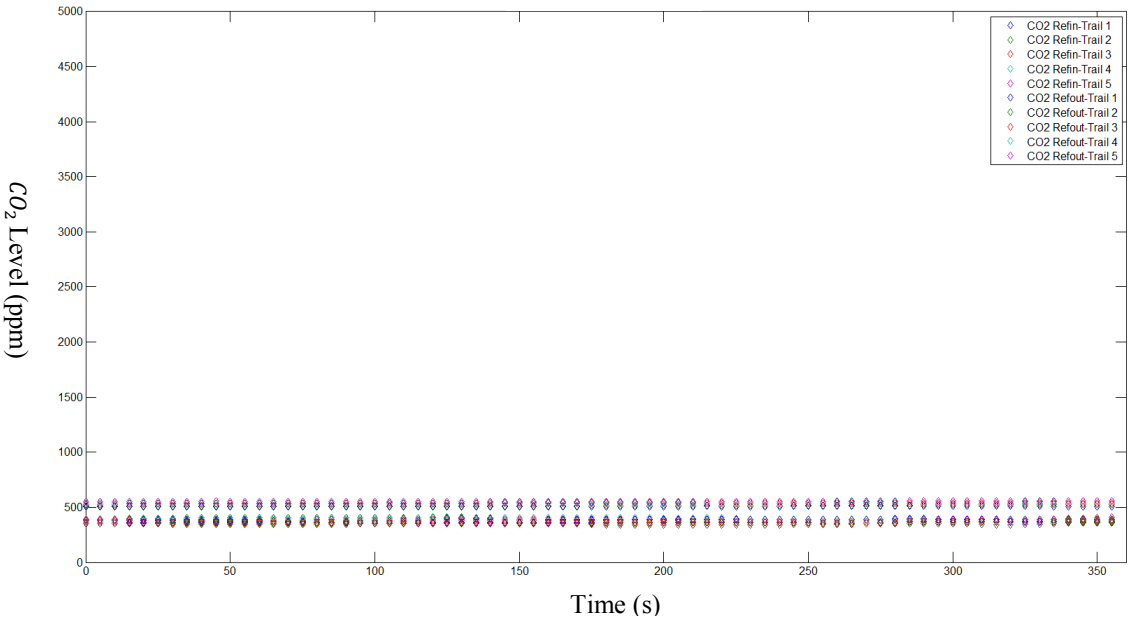

Figure 4.34 Carbon dioxide at farm office and the farm yard

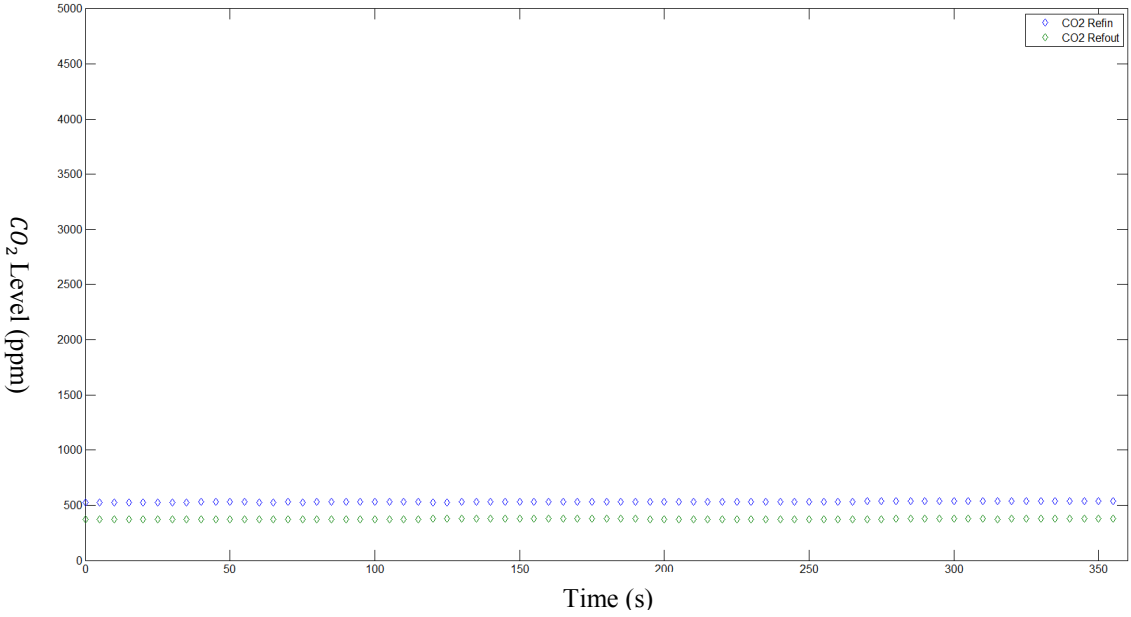

Figure 4.35 Average carbon dioxide reading at Refin and Refout

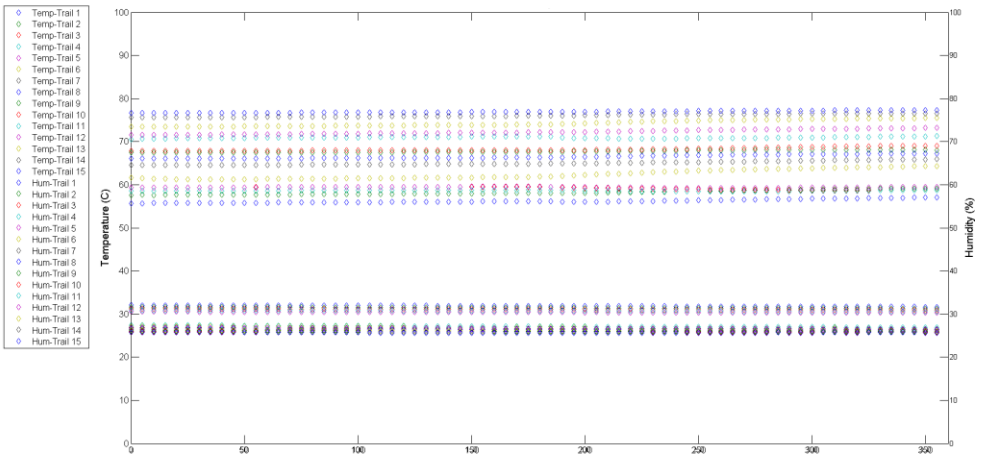

(a)

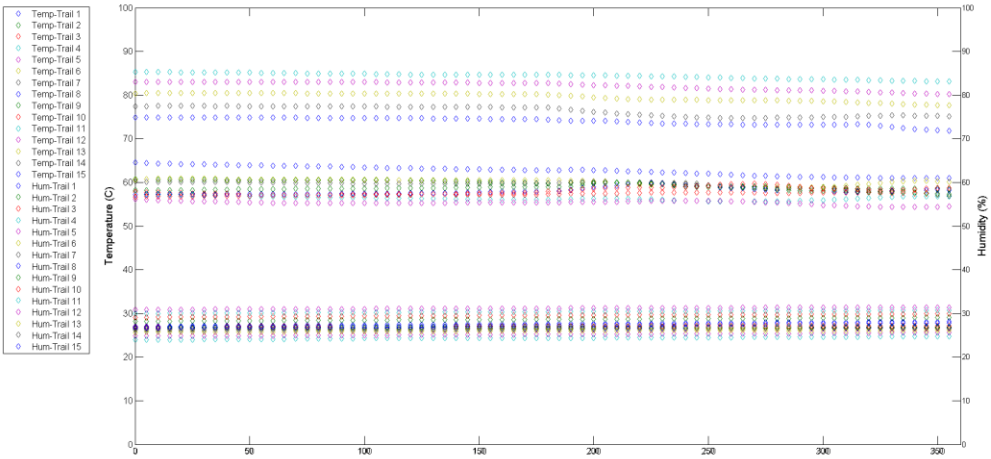

(b)

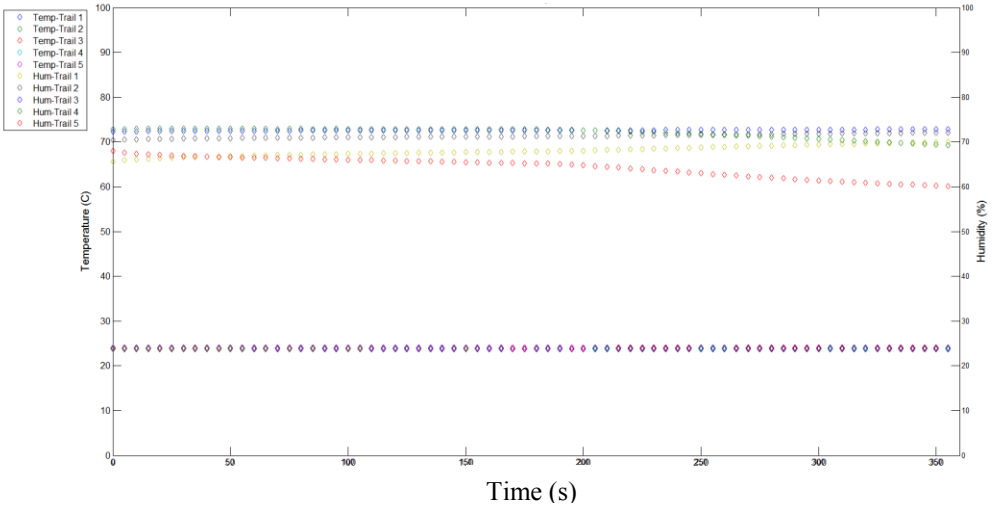

(c)

Figure 4.36 Temperature and humidity results (a) in poultry room (b) in farm office(c)in farm yard

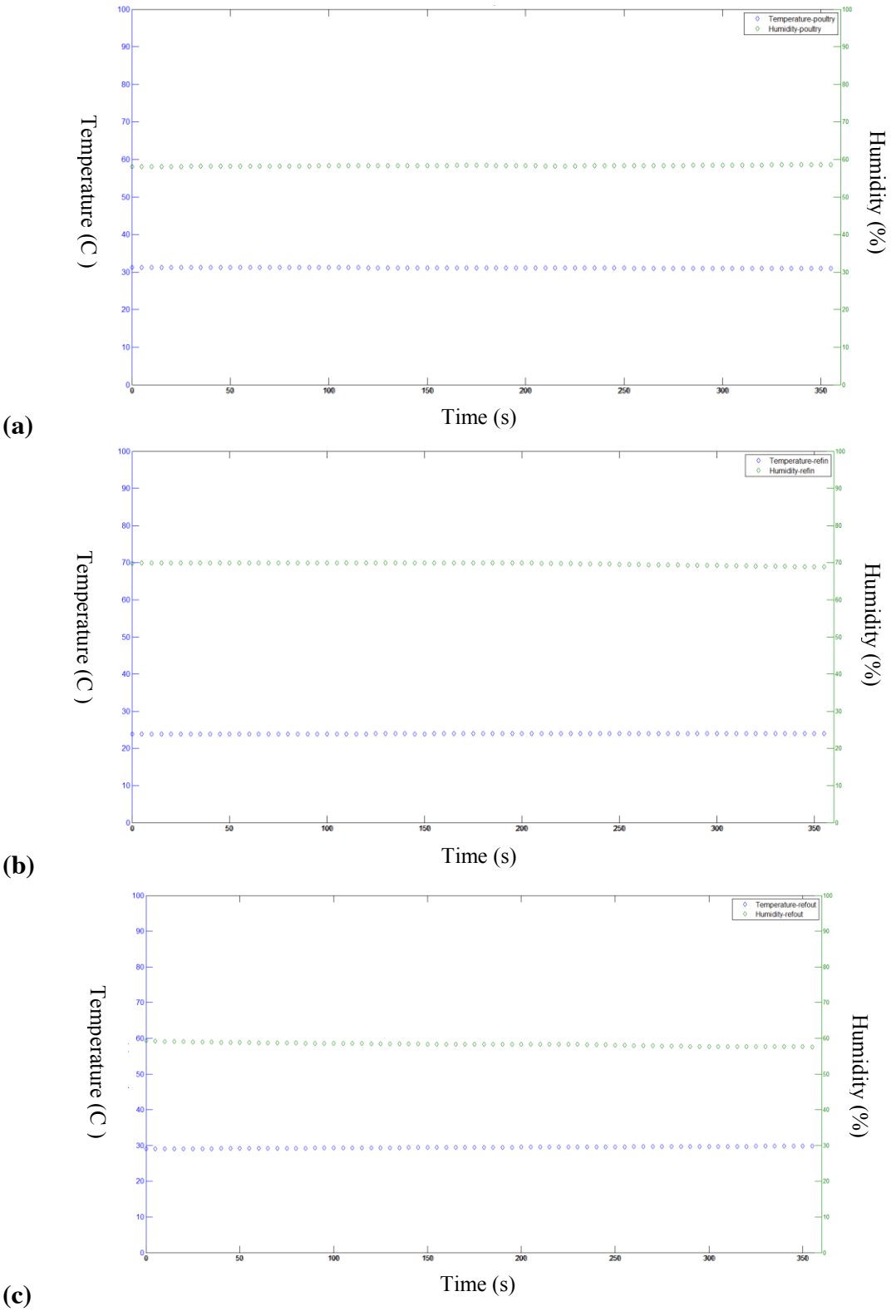

Figure 4.37 Average results of temperature and humidity (a) in poultry room (b) in farm office (c)in farm yard

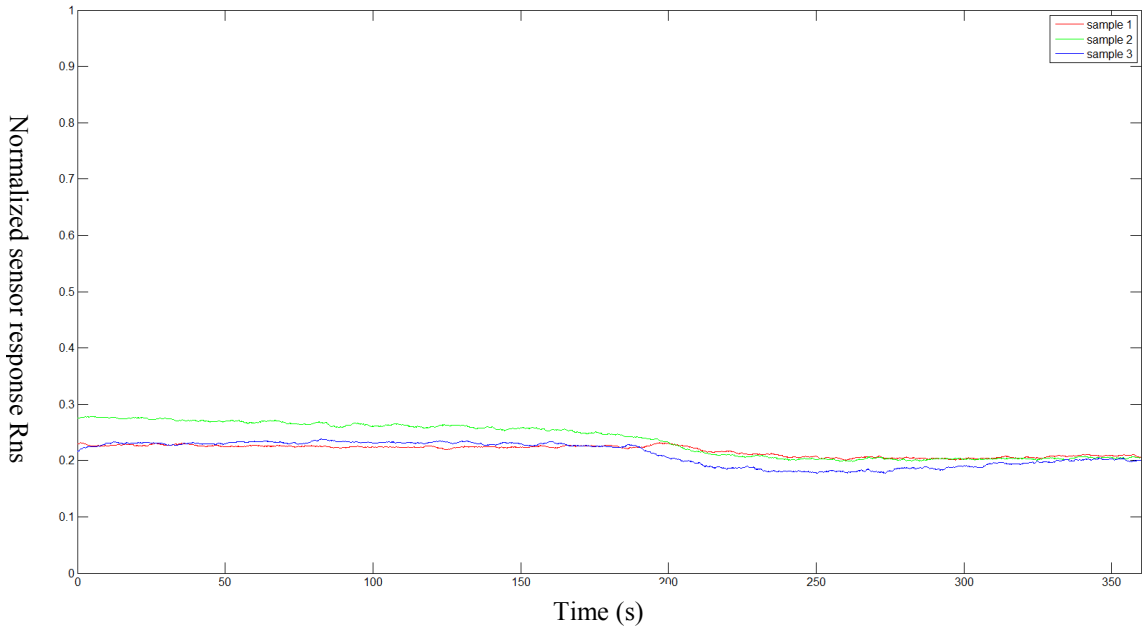

Figure 4.38 Normalization value of VOC-1under first test

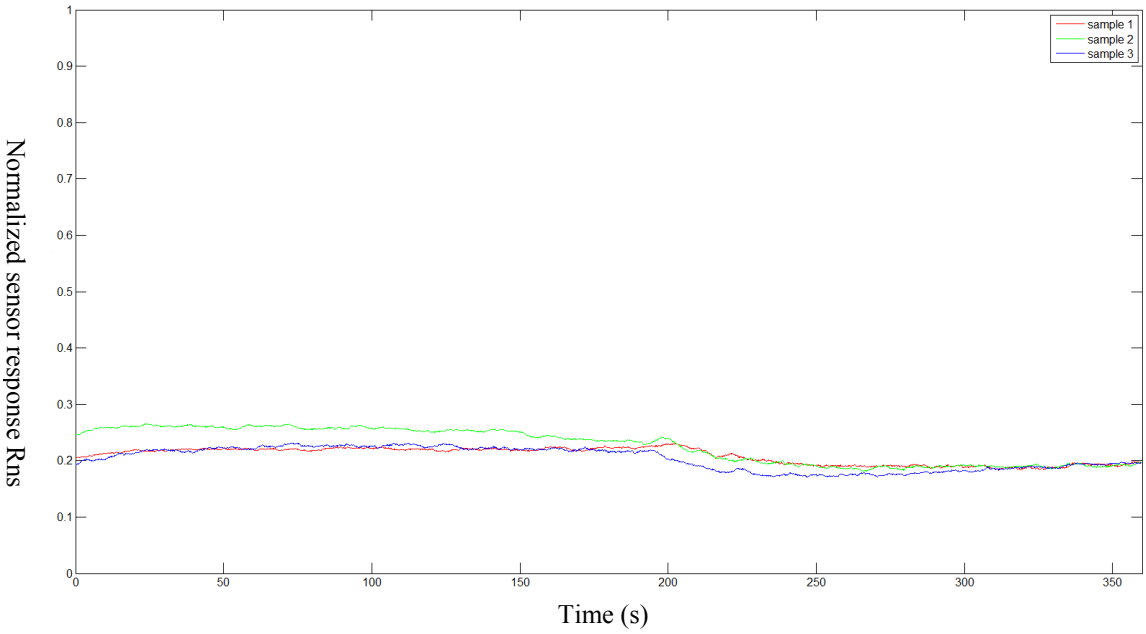

Figure 4.39 Normalization value of VOC-2under first test

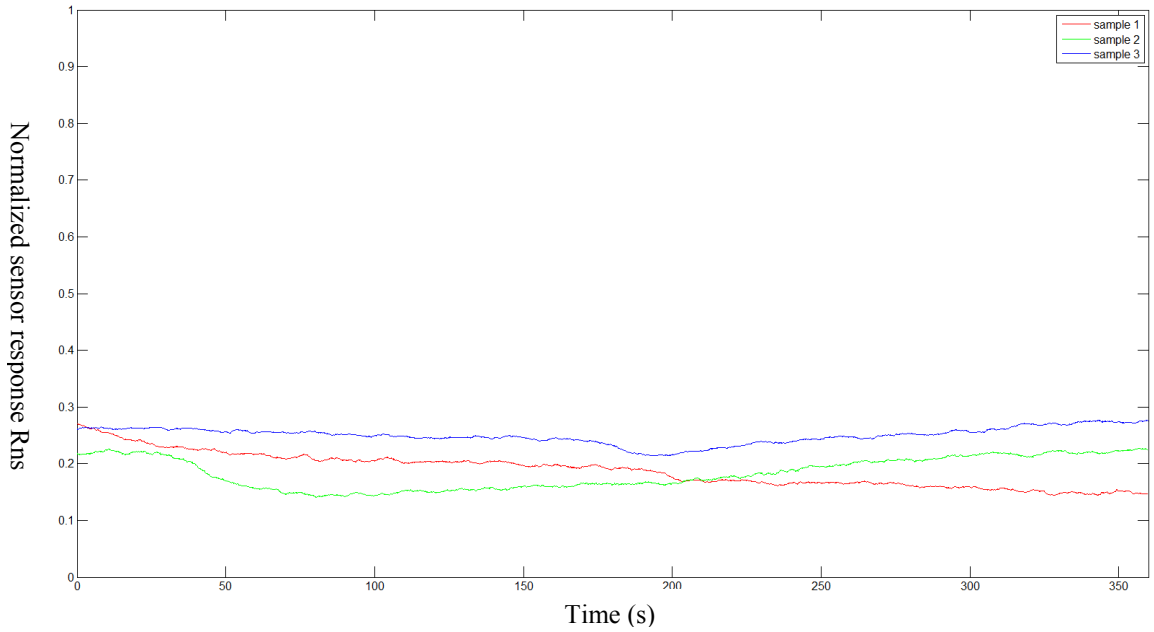

Figure 4.40 Normalization value of VOC-1under second test

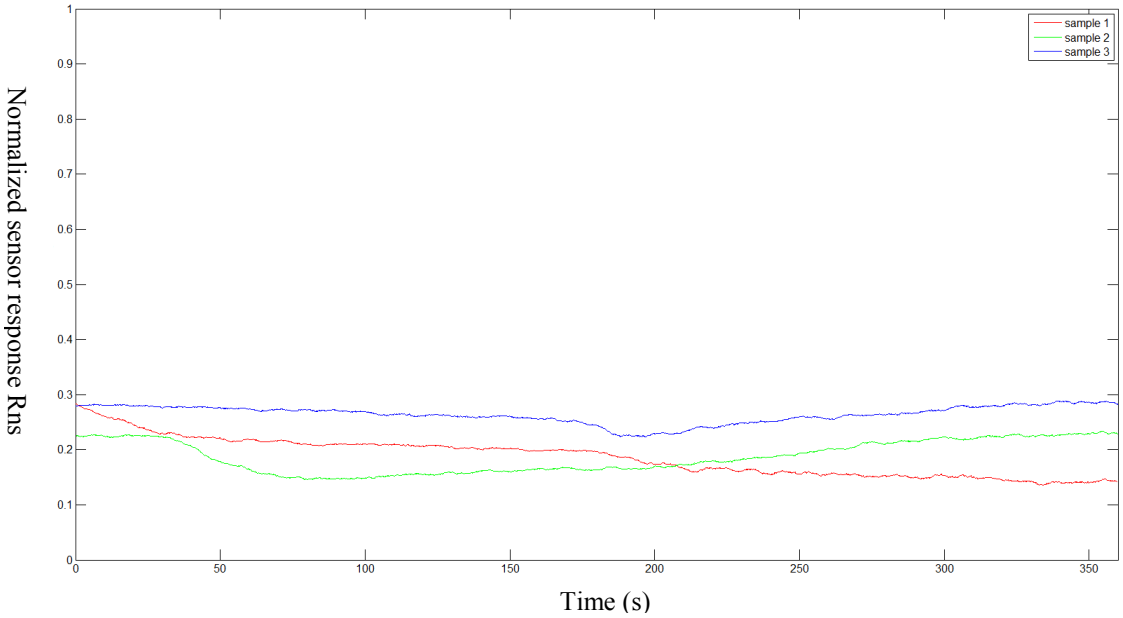

Figure 4.41 Normalization value of VOC-2 under second test

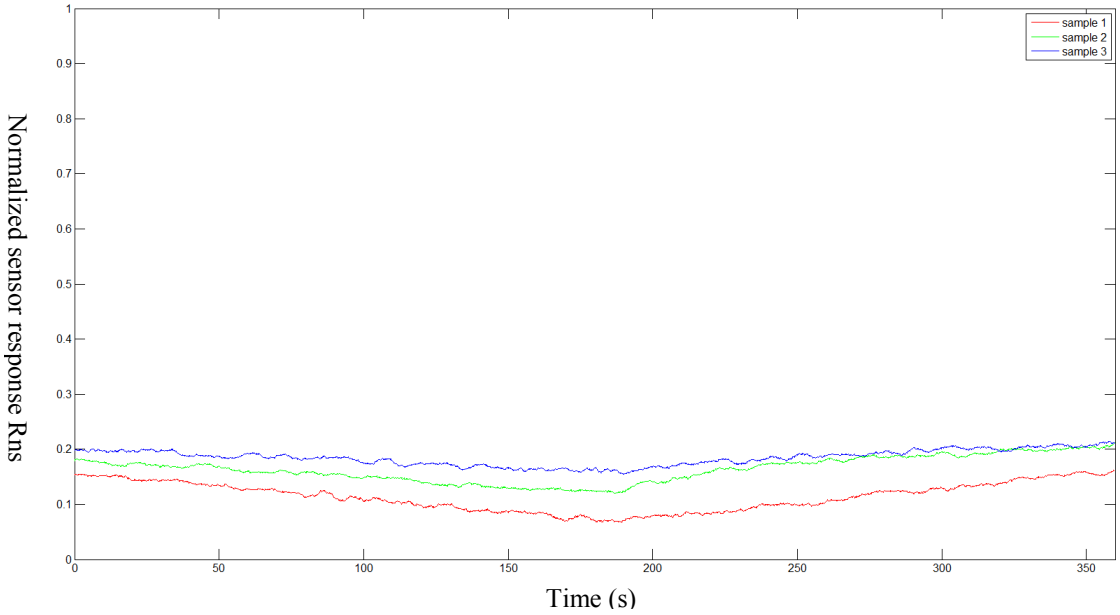

Figure 4.42 Normalization value of VOC-1under third test

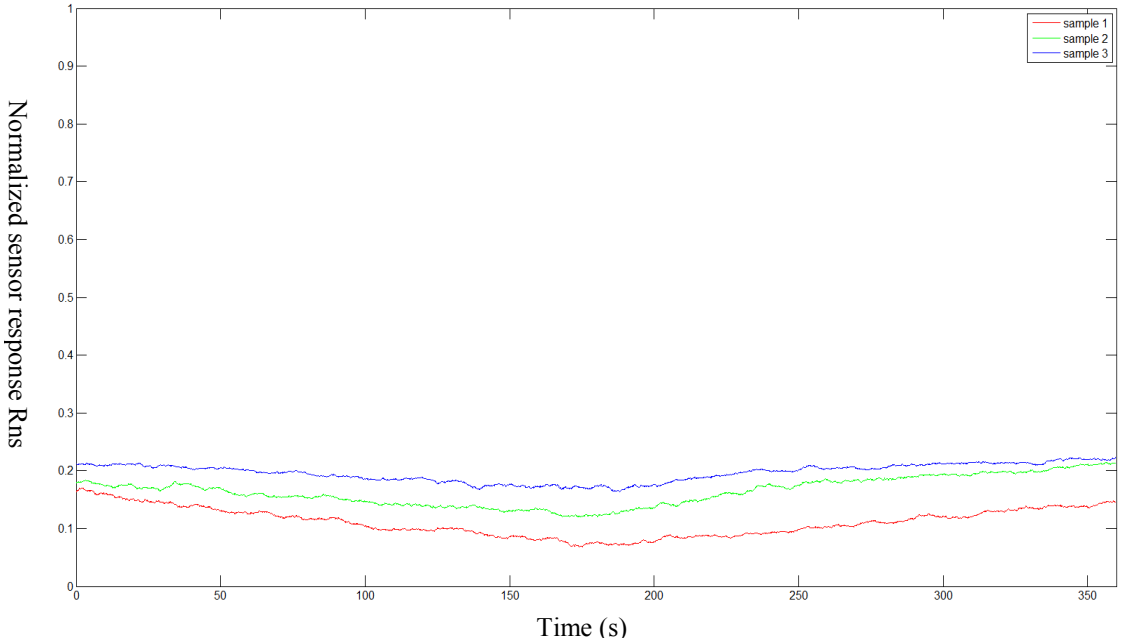

Figure 4.43 Normalization value of VOC-2 under third test

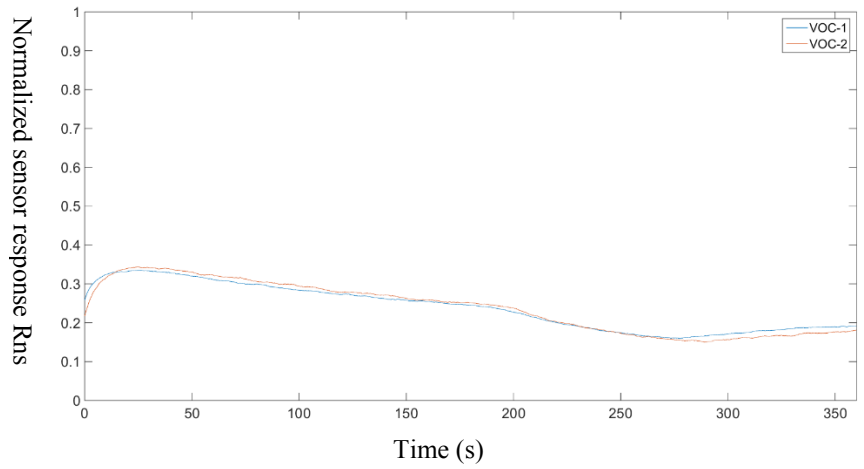

(a)

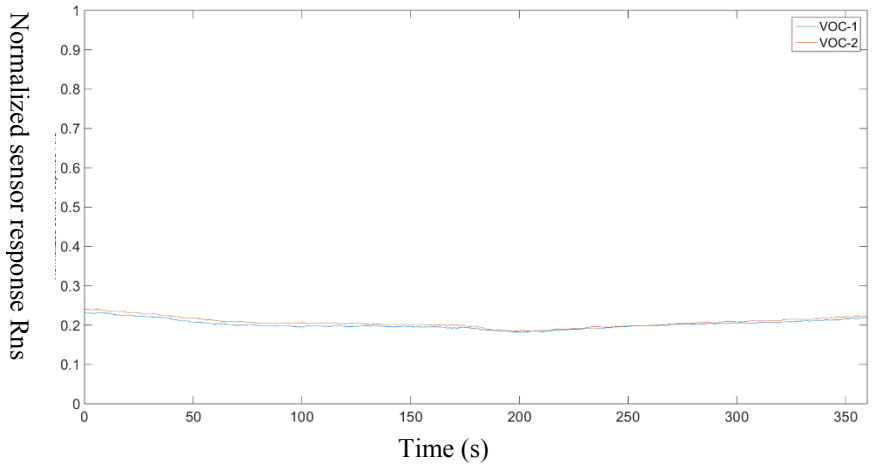

(b)

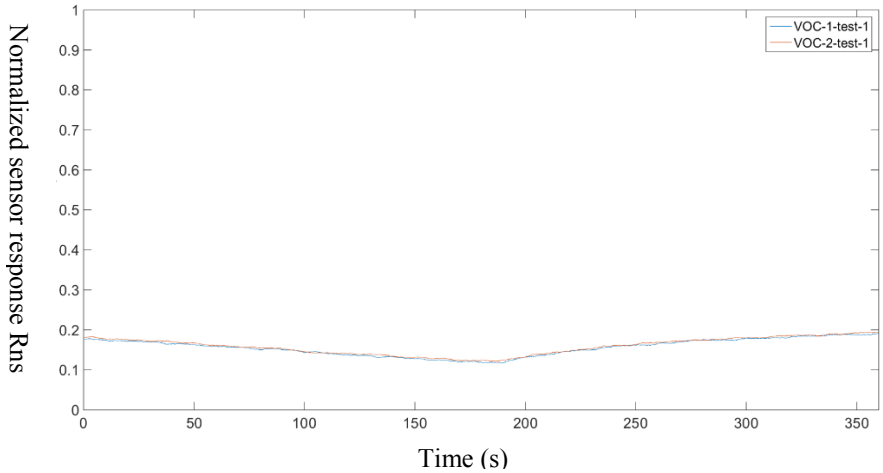

(c)

Figure 4.44 Comparison between VOC-1 and VOC-2 among tests (a) Test 1 (b) Test 2 (c) Test 3

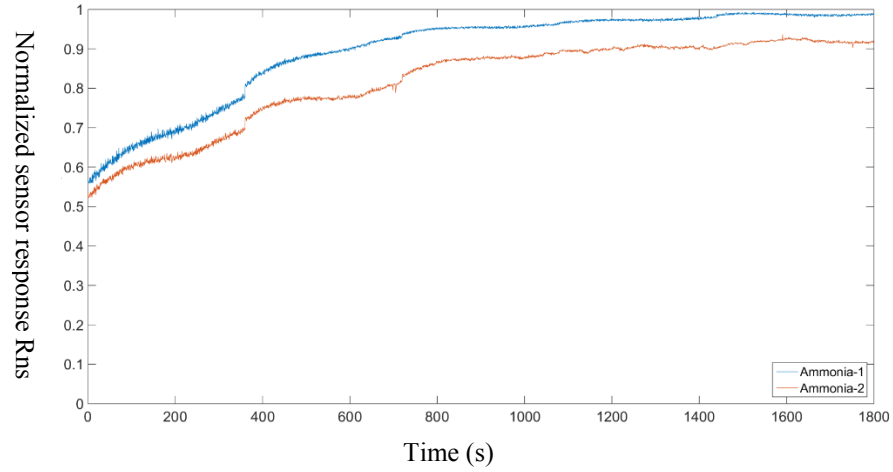

(a)

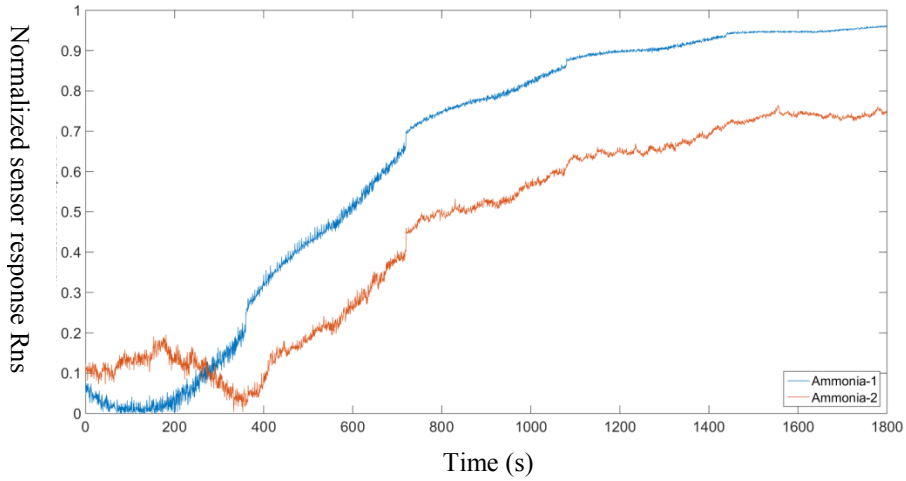

(b)

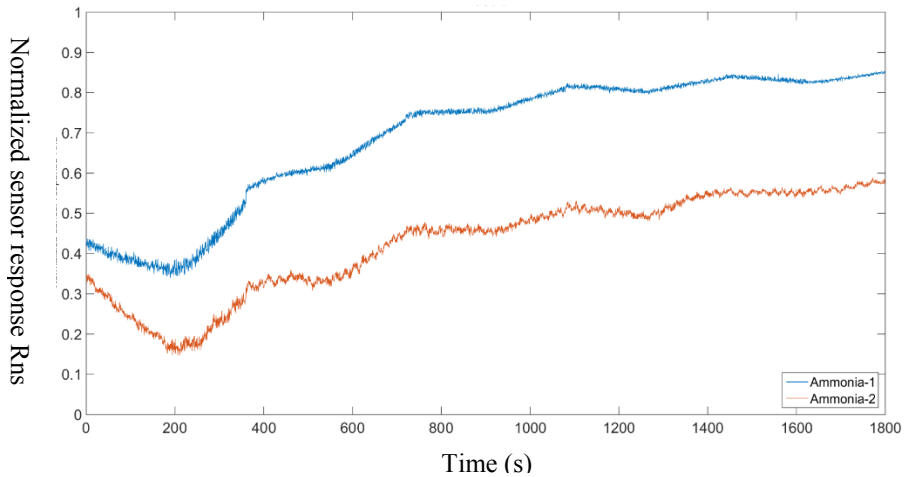

(c)

Figure 4.45 Comparison of Ammonia-1 and Ammonia-2 within tests (a) Test 1 (b) Test 2 (c) Test 3

Table 4.16 *Variation among responses of two sensors (ammonia and VOC) for poultry room*

	Test 1	Test 2	Test 3
VOC	0.0032	0.0001	0.0004
Ammonia	0.0111	0.0487	0.0182

4.2 E-tongue

There are QCM and arsenic detection using interdigitated electrode belong E-tongue. The performance of frequency counter system was evaluated to make sure the system fulfills the specifications. The result and data analysis of arsenic detection using interdigitated electrode is deliberated lastly.

4.2.1 QCM

The frequency counter of QCM was tested by using the setup described in Chapter 3. The experiment was run three times for specific accuracies, 1% and 0.005 %. The datasheet specified the amount of converting time for 1% and 0.005% are 100 micro seconds and 800 micro seconds. Table 4.17 is the result of selecting accuracy of 1% with conversion time of 100 micro-seconds. The first column of the table is the input from the function generator and the range was from 1 MHz to 15 MHz. The second column of the table is the expected value that should be displayed on microcontroller. Due to the pre-scaling, a flip flop in the circuit, the expected value was half of the input from first column. The same layout was applied to the test of 0.005% accuracy with 800 micro-seconds (Table 4.18).

The largest difference between expected and measured was 1.153% at 11 MHz and the smallest difference is 0.002% at 8 MHz for 1% accuracy (Table 4.17). For 0.005% accuracy shown Table 4.18, the maximum difference between expected and measured was 1.212% at 13 MHz, and the minimum difference was 0.001% at 2 MHz, 4 MHz and 8 MHz. Lastly, Table 4.19 illustrates the accuracy of 0.005% is more accurate than 1% because the mean of error for 0.005% was small than 1%. However, the trade-off of using higher accuracy was 700 micro-seconds longer converting time.

Table 4.17 *Result of frequency counter measurement using 1% accuracy*

Accuracy test when accuracy is 1%						
[redacted]		Observation 1	Observation 2	Observation 3	[redacted]	
Frequency	expected	Frequency counter	Frequency counter	Frequency counter	Frequency average	error
15150000	7575000	7555693.069	7555693.069	7555693.069	7555693.069	0.255
14080000	7040000	7054455.446	7054455.446	7054455.446	7054455.446	0.205
13160000	6580000	6553217.822	6547029.703	6547029.703	6549092.409	0.470
12050000	6025000	6045792.079	6045792.079	6045792.079	6045792.079	0.345
11110000	5555000	5383660.337	5544554.455	5544554.455	5490923.082	1.153
10000000	5000000	5043316.832	5037128.713	5037128.713	5039191.419	0.784
9010000	4505000	4535891.089	4529702.970	4529702.970	4531765.677	0.594
8000000	4000000	4000065.347	4000065.347	4000065.347	4000065.347	0.002
7040000	3520000	3527227.723	3527227.723	3521039.604	3525165.016	0.147
6020000	3010000	3025990.099	3019801.980	3019801.980	3021864.686	0.394
5000000	2500000	2518564.356	2518564.356	2518564.356	2518564.356	0.743
4020000	2010000	2011138.614	2017326.733	2011138.614	2013201.320	0.159
3000000	1500000	1516089.109	1516089.109	1509900.990	1514026.403	0.935
2000000	1000000	1008663.366	1004901.961	1008663.366	1007409.564	0.741
1000000	500000	502450.980	502450.980	502450.980	502450.980	0.490

Table 4.18 *Result of frequency counter measurement using 0.005% accuracy*

Accuracy test when accuracy is 0.005%						
[redacted]		Observation 1	Observation 2	Observation 3	[redacted]	
Frequency		Frequency counter	Frequency counter	Frequency counter	Frequency average	error
15150000	7575000	7500312.484	7500281.236	7500312.484	7500302.068	0.986
14080000	7040000	7000081.242	7000112.489	7000112.489	7000102.073	0.567
13160000	6580000	6500268.737	6500268.737	6500268.737	6500268.737	1.212
12050000	6025000	6000087.491	6000087.491	6000087.491	6000087.491	0.413
11110000	5555000	5500224.989	5500224.989	5500193.740	5500214.573	0.986
10000000	5000000	5000062.494	5000093.741	5000093.741	5000083.325	0.002
9000000	4500000	4500181.241	4500149.993	4500181.241	4500170.825	0.004
8000000	4000000	4000037.496	4000068.743	4000037.496	4000047.912	0.001
7040000	3520000	3500106.245	3500137.493	3500137.493	3500127.077	0.565
6020000	3010000	3000043.746	3000043.746	3000043.746	3000043.746	0.331
5000000	2500000	2500093.745	2500093.745	2500093.745	2500093.745	0.004
4000000	2000000	2000018.748	2000018.748	2000018.748	2000018.748	0.001
3000000	1500000	1500049.998	1500049.998	1500081.246	1500060.414	0.004
2000000	1000000	999993.751	999993.751	999993.751	999993.751	0.001
1000000	500000	500012.499	500012.499	500012.499	500012.499	0.002

Table 4.19 *Error comparison between 1% accuracy and 0.005% accuracy*

	Mean error
Accuracy 1%	0.494
Accuracy 0.005%	0.339

4.2.2 Arsenic detection using interdigitated electrode

The interdigitated electrode was tested among DI water (no arsenic), 10 ppb arsenic water, 50 ppb water arsenic and 100 ppb arsenic water. The voltages (peak-to-peak) were measured across the frequency range 10K Hz to 700K Hz. After plotting the voltages versus frequency, it was found out that there was more sensitive in lower frequency (10 KHz to 50 KHz). The result in lower frequency of each observation is shown in Figures 4.46 to 4.57 and the mean of treatments is shown in Figure 4.58 with respect to frequency.

For the analysis, a two sample t-test was implemented to determine whether or not to reject null hypothesis at 5% significance level. In this case, the null hypothesis was the population mean for sample *i* equals to the population mean for sample *j*. On the other hand, the alternative hypothesis was the population mean for sample *i* does not equal to the population mean for sample *j*. The result of the t-test is shown in Table 4.21. The number shown in Table 4.21 was the frequency at which there was significant difference in 5% confidence interval. Between water and different concentrations of arsenic water, the significant differences were observed in lower frequency (10K to 50K Hz).

The second comparison was the repeatability test. The plots of each treatment were shown in Figures 4.59, 4.60, 4.61, and 4.62. As shown in the Figures, the trend in

lower frequencies (10k to 50k Hz) for each observation was identical in the same treatments. The means and standard deviations for each treatment are shown in Table 4.20. Table 4.21 shows the maximum and minimum standard deviation for each treatment. The largest standard deviation among the treatments was 0.170 when measuring 10 KHz in 10ppb arsenic water.

Analysis

For further analysis, it was based on running two sample t-test for varies features. The chosen features were (1) using raw data to do t-test, (2) using Equation 4.4 with raw data and run t-test, (3) using Equation 4.5 with raw data and run t-test, (4) using Equation 4.6 to calculate standardized value and run t-test, (5) using Equation 4.4 with standardized value and run t-test, and (6) using Equation 4.5 with standardized value and run t-test. The equations to find the features are shown below.

$Ratio = \frac{ppm}{DI\ water}$ for each frequency (Equation 4.4)

$Difference\ as\ water\ reference = \frac{ppm - DI\ water}{DI\ water}$ for each frequency (Equation 4.5)

$Standalization = \frac{Data - Min}{Max - Min}$ (Equation 4.6)

Where *ppm* indicates the voltage reading of 10 ppb, 50 ppb and 100 ppb and *DI water* means the voltage reading in DI water with respect to frequency, *Data* is the voltage across the resistor, *Min* is the minimum voltage among all observations and *Max* is the maximum voltage among all observations.

The program scrip was written in MATLAB and the flow chart of the program is shown in Figure 4.63. The first part of the program was transfer the data from excel to MATLAB. The data was converted to the features with respect to frequency for

individual observation. Last part was calling the t-test against different combinations of the treatments.

The result of the analysis is shown in Tables 4.20, 4.23, 4.24, 4.25, 4.26 and 4.27. In the tables, the frequency number shown in cells represents there is significant difference between indicated treatments at the specific frequency. Comparing Tables 4.20, 4.23, and 4.24, the most appeared frequency was 50K Hz. In water versus 10ppb, water versus 50ppb, water versus 100pb and 50ppb versus 100ppb, 50K Hz had significant difference by using two sample t-test. Similarly, 50K Hz was the most frequent frequency using standardization comparing in the Tables 4.25, 4.26 and 4.27.

Comparing the results from all the features mentioned previously, all the features showed significant different for DI water versus 10, 50 and 100 ppb arsenic water for at least one frequency. In some case, there is more than one frequency where significant difference occurred. However, when the inter group(i.e. 10 ppb versus 50 ppb, 10ppb versus 100 ppb and 50 ppb versus 100ppb) was compared, most of features cannot be differentiated. Only feature 3 and feature 6 showed the significant difference when comparing between 10ppb arsenic water versus 100ppb arsenic water.

Raw data

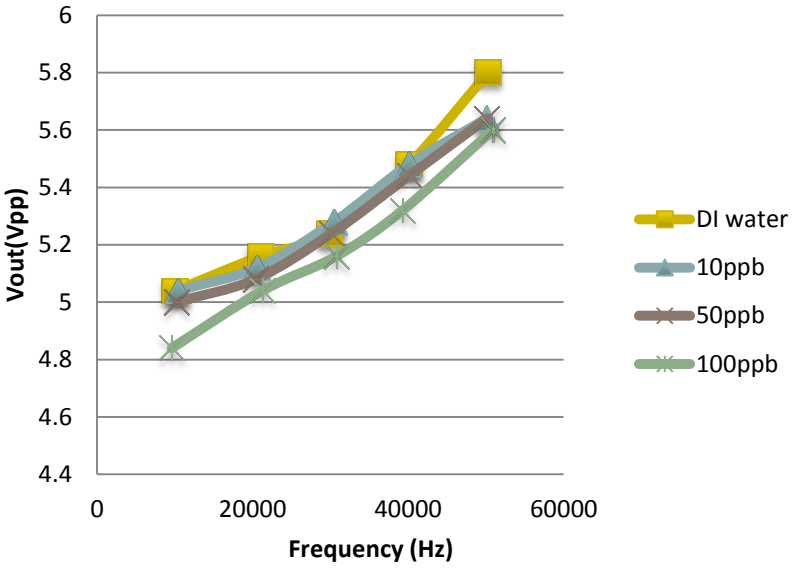

Figure 4.46 Raw data of observation 1

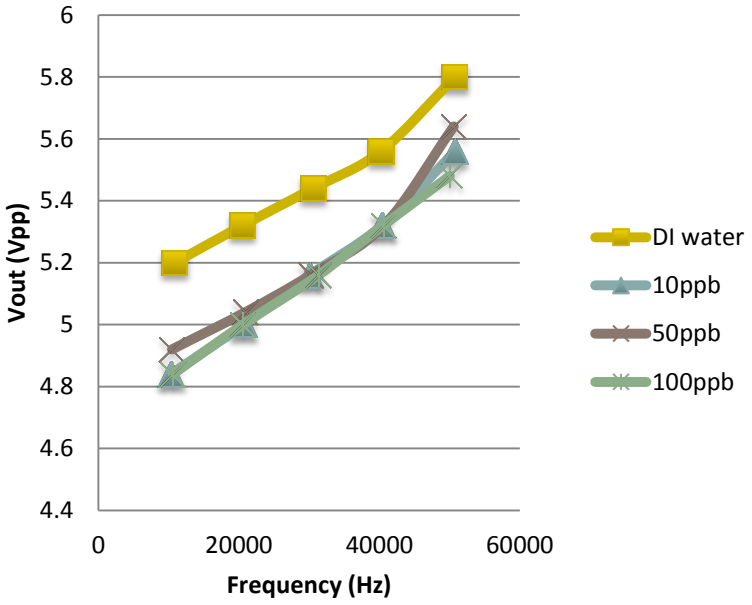

Figure 4.47 Raw data of observation 2

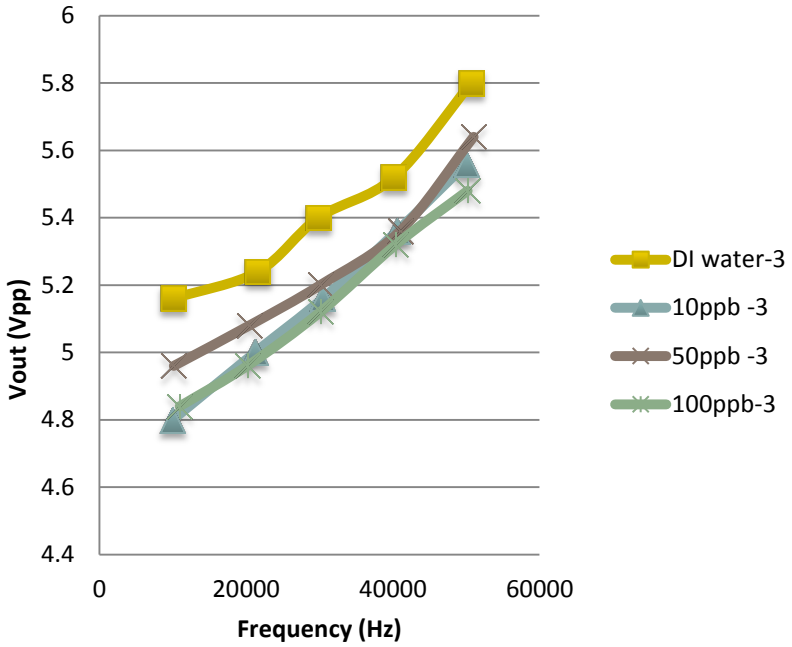

Figure 4.48 Raw data of observation 3

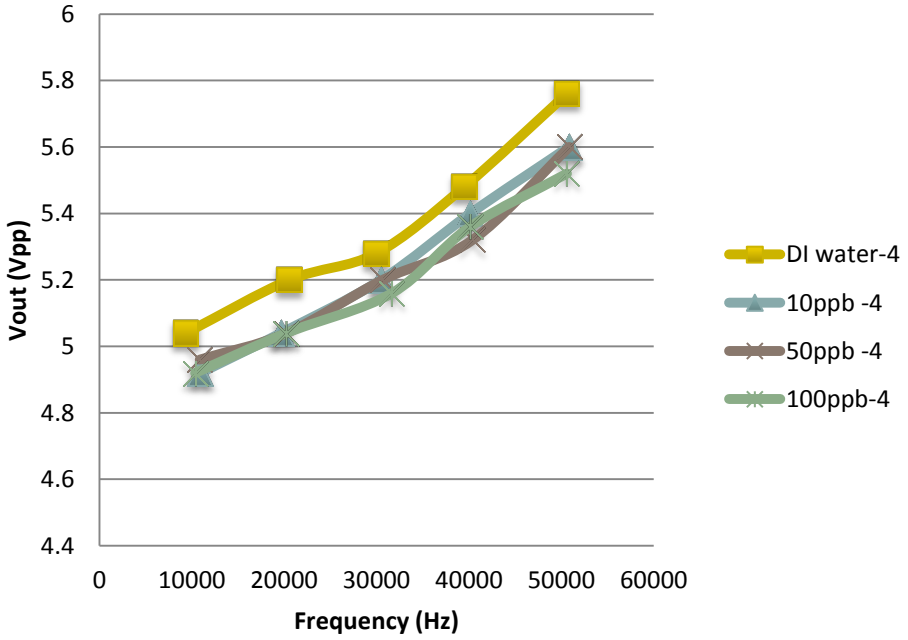

Figure 4.49 Raw data of observation 4

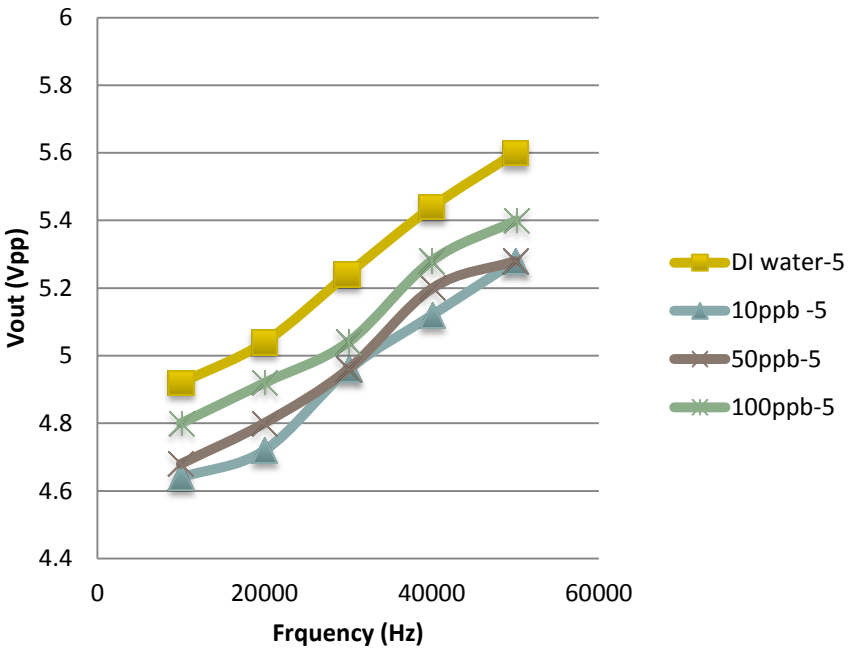

Figure 4.50 Raw data of observation 5

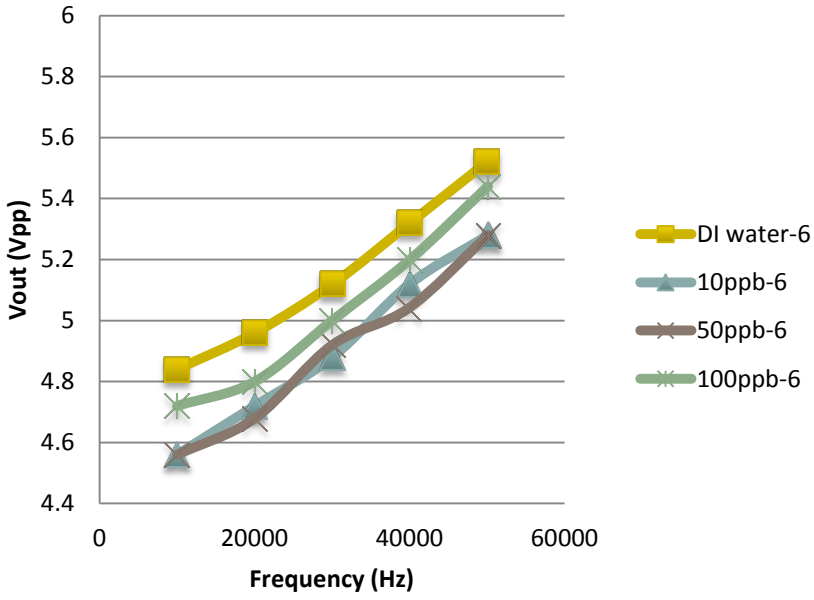

Figure 4.51 Raw data of observation 6

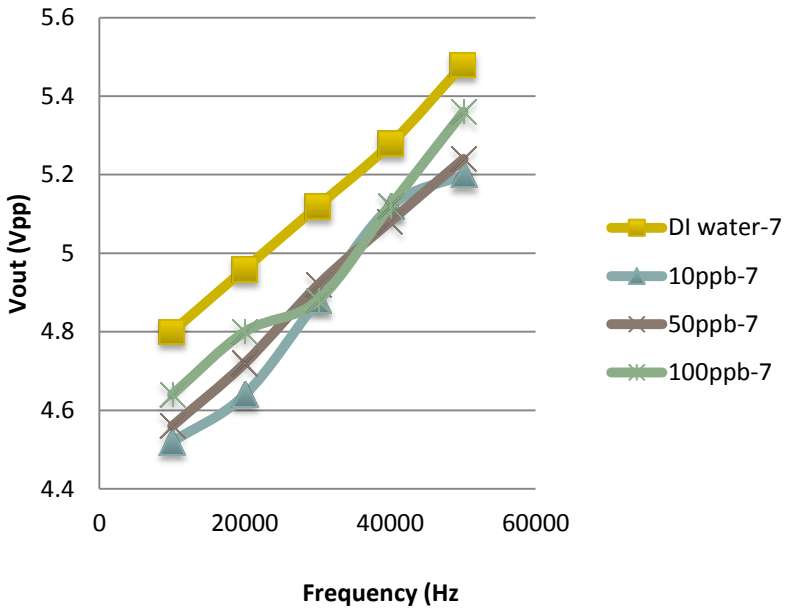

Figure 4.52 Raw data of observation 7

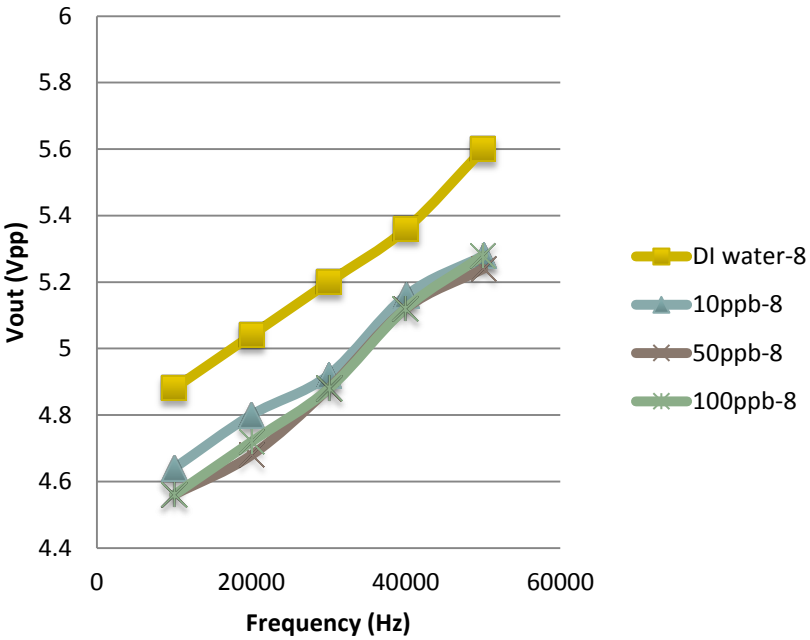

Figure 4.53 Raw data of observation 8

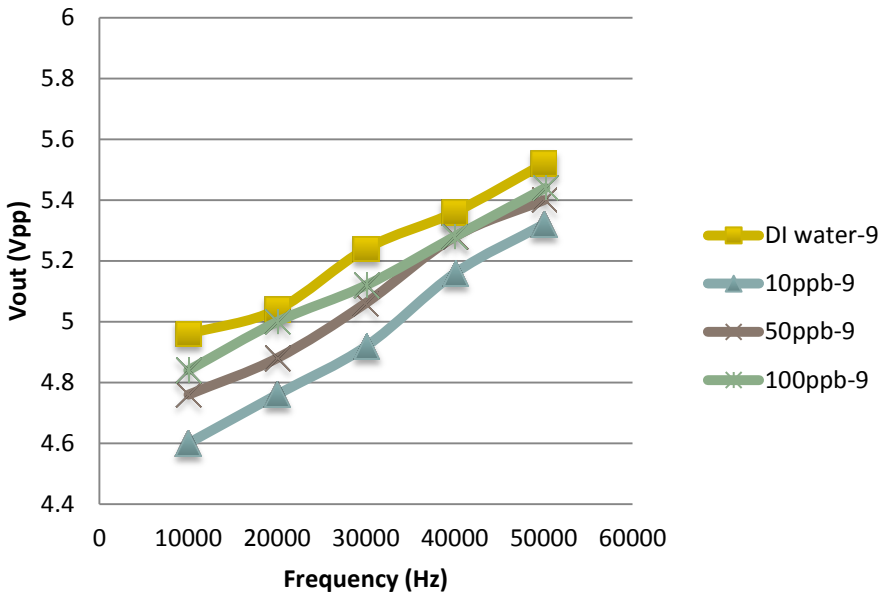

Figure 4.54 Raw data of observation 9

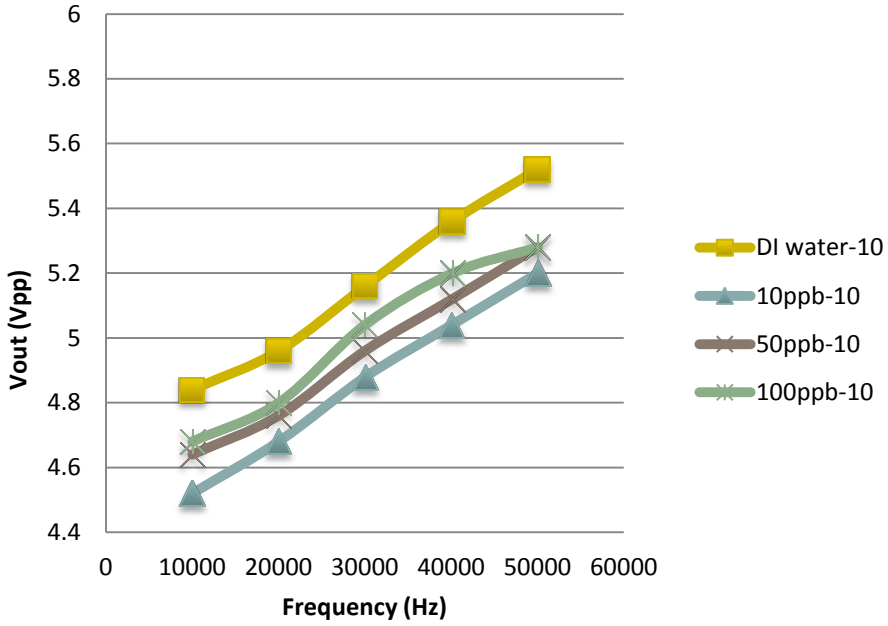

Figure 4.55 Raw data of observation 10

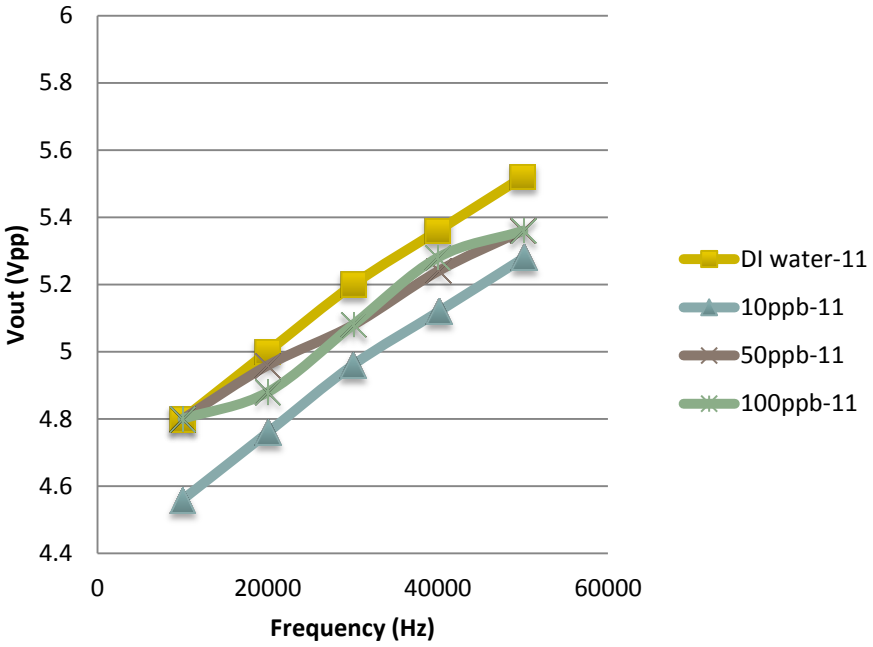

Figure 4.56 Raw data of observation 11

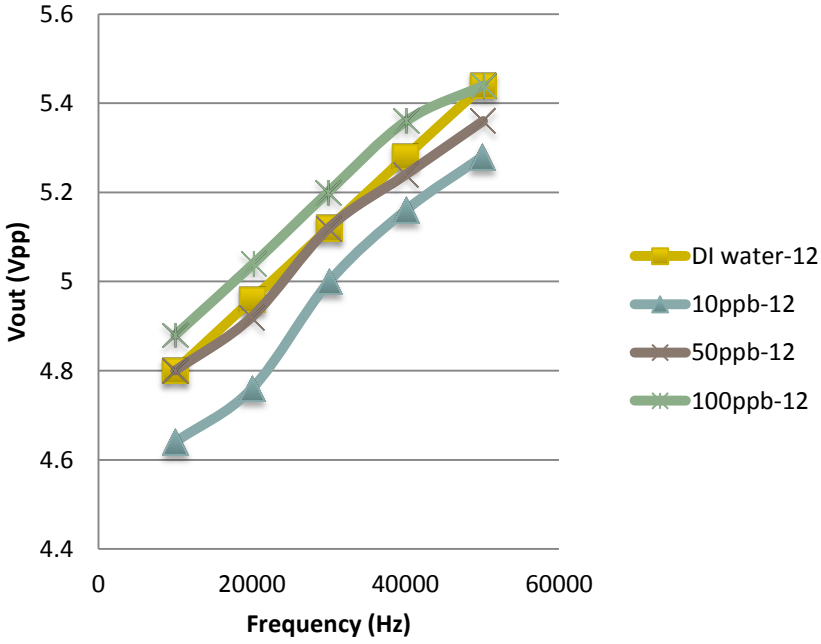

Figure 4.57 Raw data of observation 12

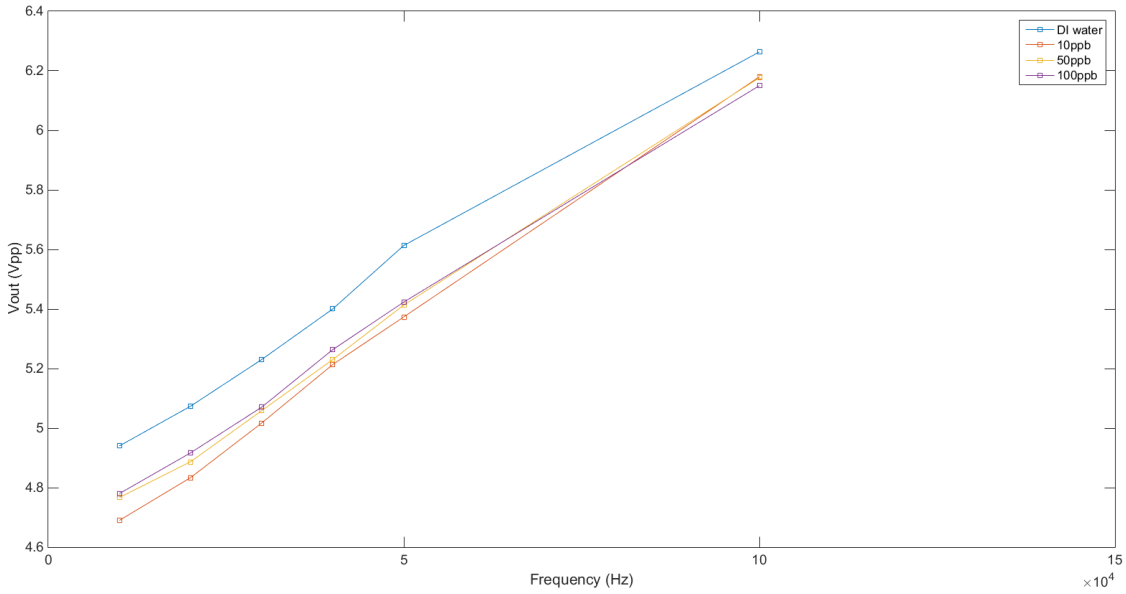

Figure 4.58 Average Vout of twelve observations with respect to frequency

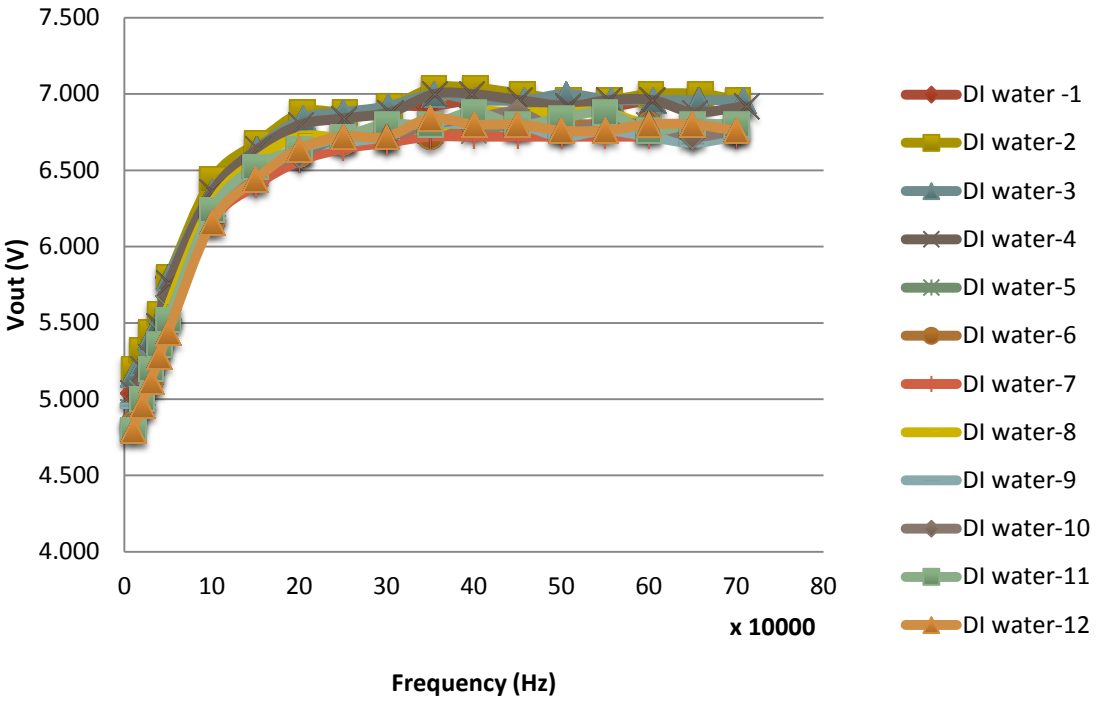

Figure 4.59 DI water measurement of 12 observations

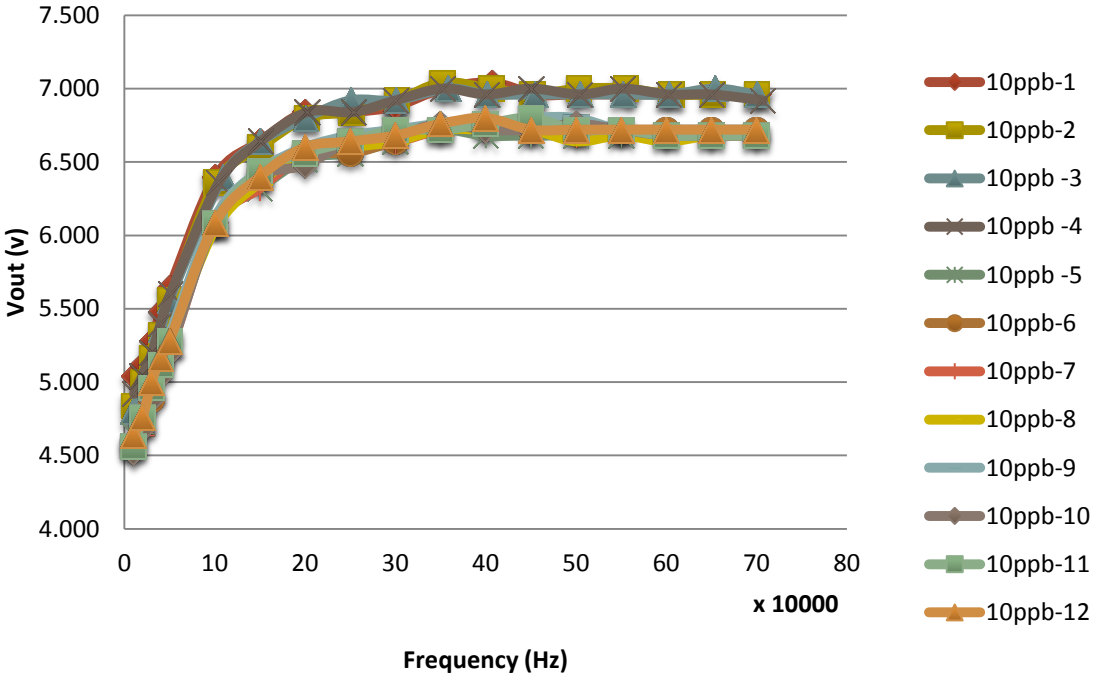

Figure 4.60 10 ppb arsenic water measurement of 12 observations

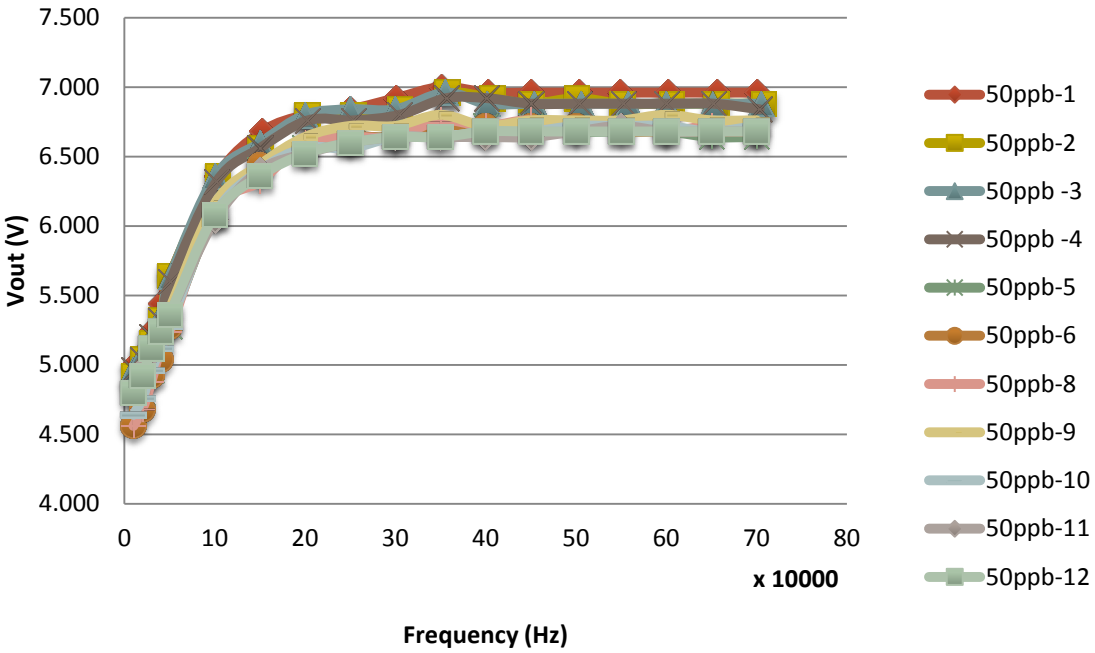

Figure 4.61 50 ppb arsenic water measurement of 12 observations

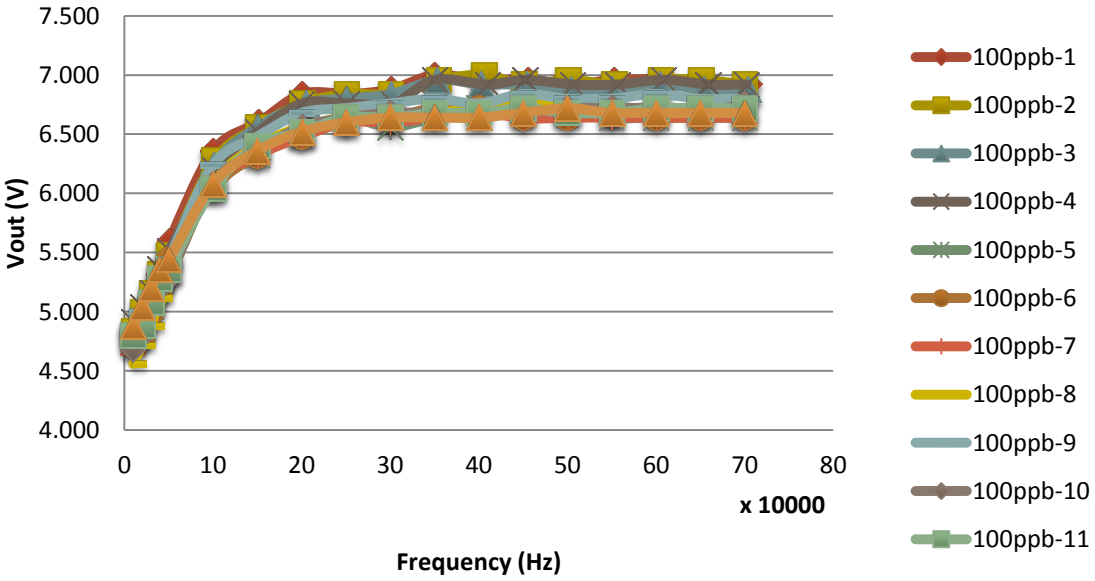

Figure 4.62 100 ppb arsenic water measurement of 12 observations

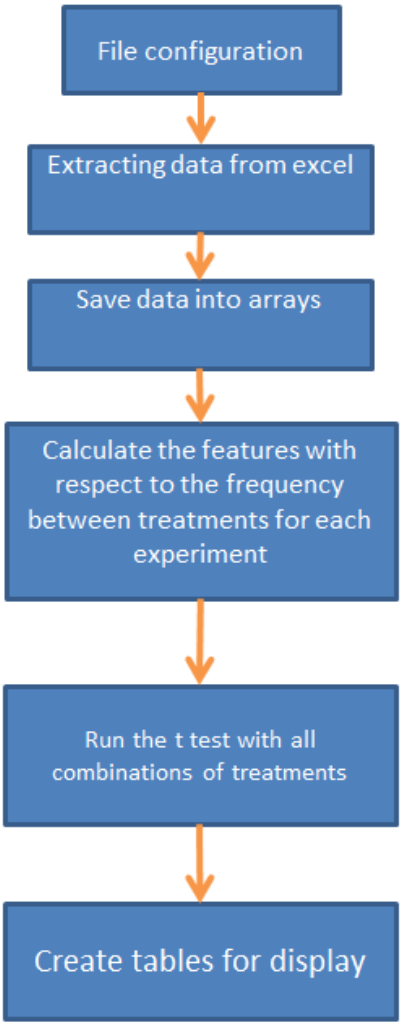

Figure 4.63 Flow chart of the analysis program

Table 4.20 *Analysis result using original value*

	water	10ppb	50ppb	100ppb
water		10k,20k,30k,40k,50k	10k,20k,30,40k,50k, 400k,450k,550k	10k,20k,30k,40k,50k,10 0k,150k,300k
10 ppb	10k,20k,30,40k,50k		No difference	No difference
50 ppb	10k,20k,30,40k,50k ,400k,450k,550k	No difference		No difference
100 ppb	10k,20k,30k,40k,50 k,100k,150k,300k	No difference	No difference	

Table 4.21 *Mean and standard deviation for each treatment (concentration)*

	DI water		10ppb		50ppb		100ppb	
Frequency	mean	SD	mean	SD	mean	SD	mean	SD
10000	4.940	0.141	4.690	0.170	4.767	0.167	4.780	0.107
20000	5.073	0.125	4.833	0.161	4.887	0.155	4.917	0.114
30000	5.230	0.104	5.017	0.143	5.058	0.127	5.070	0.107
40000	5.400	0.093	5.213	0.139	5.230	0.122	5.263	0.084
50000	5.613	0.138	5.373	0.165	5.413	0.167	5.423	0.094
100000	6.263	0.096	6.180	0.149	6.177	0.132	6.150	0.108
150000	6.530	0.092	6.467	0.127	6.463	0.110	6.433	0.105
200000	6.697	0.107	6.643	0.135	6.640	0.116	6.620	0.130
250000	6.753	0.083	6.700	0.125	6.690	0.098	6.693	0.094
300000	6.793	0.093	6.750	0.122	6.713	0.108	6.707	0.106
350000	6.847	0.114	6.827	0.137	6.790	0.136	6.780	0.147
400000	6.870	0.101	6.827	0.126	6.773	0.112	6.783	0.128
450000	6.863	0.089	6.813	0.121	6.773	0.101	6.787	0.126
500000	6.843	0.099	6.800	0.132	6.773	0.106	6.777	0.115
550000	6.850	0.087	6.800	0.134	6.770	0.101	6.770	0.120
600000	6.840	0.101	6.780	0.135	6.763	0.110	6.780	0.137
650000	6.823	0.104	6.787	0.137	6.757	0.112	6.763	0.125
700000	6.827	0.095	6.780	0.127	6.753	0.109	6.767	0.117

Table 4.*22 Maximum and minimum standard deviation for each treatment*

	DI water	10ppb	50ppb	100ppb
max	0.141	0.170	0.167	0.147
min	0.083	0.122	0.098	0.084

Table 4.23 *Analysis result using ratio of concentration to DI water*

	Ratio (ppm/water)			
	water	10ppb	50ppb	100ppb
water		10k,20k,50k	50k	No difference
10ppb	10k,20k,50k		No difference	20k
50ppb	50k	No difference		No difference
100ppb	No difference	20k	No difference	

Table 4.24 *Analysis result using difference as water reference*

	Difference as water reference (ppm-water)/water			
	water	10ppb	50ppb	100ppb
water		10k,20k,30k,50k	50k	40k
10ppb	10k,20k,30k,50k		No difference	20k
50ppb	50k	No difference		No difference
100ppb	40k	20k	No difference	

Table 4.25 *Analysis result using standardization value*

	Standardization			
	water	10ppb	50ppb	100ppb
water		10k,20k,30k,40k,50k	10k,20k,30,40k,50k,400k,450k,550k	10k,20k,30k,40k,50k,100k,150k,300k
10ppb	10k,20k,30,40k,50k		No difference	No difference
50ppb	10k,20k,30,40k,50k,400k,450k,550k	No difference		No difference
100ppb	10k,20k,30k,40k,50k,100k,150k,300k	No difference	No difference	

Table 4.26 *Analysis result in ratio using standardization value*

	Standardization-Ratio (ppm/water)			
	water	10ppb	50ppb	100ppb
water		20k,50k	No difference	No difference
10ppb	50k		No difference	10k,20k
50ppb	No difference	No difference		No difference
100ppb	No difference	10k,20k	No difference	

Table 4.27 *Analysis result of difference using standardization value*

	Standardization-Difference as water reference (ppm-water)/water			
	water	10ppb	50ppb	100ppb
water		20k,30k,50k	50k,600k	40k
10ppb	20k,30k,50k		No difference	10k,20k,300k,350k
50ppb	50k,600k	No difference		No difference
100ppb	40k	No difference	50k	

CHAPTER 5. CONCLUSIONS AND FUTURE WORK

5.1 Conclusions

This study demonstrated the process of design, adaption and development of integrated sensor system (E-nose) as well as the possibility to detect arsenic in water using interdigitated electrode sensor.

Integrated E-nose system can simultaneously sense multiple gases (i.e. NH3, VOC, $CO2$) along with temperature and humidity. The overall design was an extension E-nose work of Dr. Panigrahi's group at North Dakota State University. However, several new features have been implemented in this system. The new features include:

I. The sensing chamber has removable upper cover plate having different sensor/detectors.
II. A centralized power supply system for all the sensors and associated peripherals.
III. The main computational unit used a SOC (i.e. Beaglebone black) instead of a microcontroller.
IV. Dual sensors were used for error detection and future intelligent data analysis.
V. External ADC (Besides the main SOC) for increased flexibility with sensor.

VI. Enhanced on-board store capability (4GB in Beaglebone Black) and this can farther be extended via user defined SD card.

VII. Flexible and portable platform to be interfaced with mobile phone or portable embedded system via USB, BLE or WIFI.

The E-nose system was found sensitive for 25 ppm of ammonia gas in lab and field. The E-nose system, based on the conducted field study, responded to the change of ammonia concentration and air quality in a poultry farm and farm safety.

For E-tongue, the interdigitated dielectric sensing mode showed its capability to discriminate DI water (no arsenic) from DI water with 10, 50 or 100 ppb arsenic at 95% confidence interval. All the 6 methods provide a statistical significance for discrimination of water versus each of the three arsenic contamination levels. However, All features could not provide statistical significant difference for inter group (10ppb versus 50ppb, 50ppb versus 100ppb, or 100ppb versus 10ppb) discrimination. For the frequency counter in QCM system, it was able to measure the frequency from 1 MHz to 15 MHZ within accuracy of 0.339%.

5.2 Future work

Future work for E-nose is to implement pattern recognition technique and develop Android application. By applying pattern recognition, E-nose would be more accurate on telling the user what kind of gas is in the air and the system can be fully automatic. By developing phone application, a phone can control and monitor the E-nose system. Additionally, by implementing Bluetooth ability, the system can communicate any the device with Bluetooth enabled such as smartphone.

Future work for E-tongue is to improve on the AC source, the function generator. The one in the experiment was an old fashion. It changes the frequency by turning the knob. It was very hard for the researcher to make the same frequency for every observation. In order to solve the question, a digital function generator can work and also it can reduce variation of the experiment too.

LIST OF REFERENCES

LIST OF REFERENCES

Akyar, I. (2011). *Wide spectra of quality control*. (pp. 268-290). Croatia: InTech. Retrieved from http://www.intechopen.com

Arshak, K., Moore, E., Lyons, G. M., Harris, J., Clifford , S. (2004). A review of gas sensors employed in electronic nose applications . *Sensor Review*, *24*(2), 181-198. doi: 10.1108/02602280410525977

Beard, J. K., (2007, April 20). A simple hydrocarbon vapor detector and alarm. Retrieved from http: http://rowan.jameskbeard.com/Electronics_I_ECE_Materials/2007-04-20_Lab_6_HM.pdf

Cevoli, C., Cerretani, L., Gori, A., Caboni, M. F., Gallina Toschi, T., & Fabbri, A. (2011). Classification of pecorino cheeses using electronic nose combined with artificial neural network and comparison with gc-ms analysis of volatile compounds. *Food Chemistry*, *129*, 1315-1319. doi: 10.1016/j.foodchem.2011.05.126

Chaturvedi, A., Mishra, V. N., Dwivedi, R., & Srivastava, S. K. (2000). Selectivity and sensitivity studies on plasma treated thick film tin oxide gas sensors. *Microelectronics Journal, 31*(4), 283-290. doi: http://dx.doi.org/10.1016/S0026-2692(99)00147-0

Chiu, S. W., & Tang , K. T. (2013). Towards a chemiresistive sensor-integrated electronic nose: A review. *Sensors*, *13*, 14214-14247. doi: 10.3390/s13101421Chiu , S. W., Wang, J. H., Lin, G. T., Chang, C. L., Chen, H., & Tang, K. T. (2012, August). *Towards a chemiresistive sensor-integrated electronic nose:A review*. 2012 ieee 55th international midwest symposium, Boise. doi: 10.1109/MWSCAS.2012.6291983El

Barbri, N., Llobet, E., El Bari, N., Correig, X., & Bouchikhi, B. (2007). Application of a portable electronic nose system to assess the freshness of Moroccan sardines. *Materials Science and Engineering c*, *28*, 666-670. doi: 10.1016/j.msec.2007.10.056

Fujinaka, T., Yoshioka, M., Omatu, S., & Kosaka, T. (2008, September). *Intelligent electronic nose system for fire detection system based on neural networks*. The second international conference on advanced engineering computing and applications in sciences, Valencia. doi: 10.1109/ADVCOMP.2008.47

Gardner, J. W., Shurmer, H. V. and Corcoran, P. (1991) Integrated tin oxide odor sensors. Sensors and Actuators B 4, 109-l 15.

Gardner, J., & Bartlett, P.N. (1994). A brief history of electronic noses. Sensors and Actuators B 46-47,211-220.

Gutierrez-Osuna, R. (2002). Pattern analysis for machine olfaction:A review. *IEEE SENSRS JOURNAL*, *2*(3), 189-201. doi: 10.1109/JSEN.2002.800688

Haddi, Z., Amari, A., Alami, H., El Bari, N., Llobet, E., & Bouchikhi, B. (2010). A portable electronic nose system for the identification of cannabis-based drugs. *Sensors and Actuators B: Chemical*, *155*, 456-463. doi: 10.1016/j.snb.2010.12.047

Haugen, J. E., & Kvaal , K. (1998). Electronic nose and artificial neural network. *Meat Science* , *49*(1), 273-286.

Hao, H. C., Tang , K. T., Ku, P. H., Chao, J. S., Li, C. H., Yang, C. M., & Yao, D. J. (2009). Development of a portable electronic nose based on chemical surface acoustic wave array with multiplexed oscillator and readout electronics. *Sensors and Actuators B: Chemical*, *146*, 545-553. doi: 10.1016/j.snb.2009.12.02

Jianwen, S. (2006). An Improved Microcontroller-Based Sensorless Brushless DC (BLDC) Motor Drive for Automotive Applications. *Industry Applications, IEEE Transactions on, 42*(5), 1216-1221. doi:10.1109/TIA.2006.880888

Kanazawa, E., Sakai, G., Shimanoe, K., Kanmura, Y., Teraoka, Y., Miura, N., & Yamazoe, N. (2001). Metal oxide semiconductor N2O sensor for medical use. *Sensors and Actuators B: Chemical, 77*(1–2), 72-77. doi: http://dx.doi.org/10.1016/S0925-4005(01)00675-X

Khot, L. R. (2009). Characterization and Pattern Recognition of sensors(Doctoral dissertation).Avaliable from ProQuest Dissertations and Thesis databases.(UMI No. 3370361)

Lančok, J., Santoni, A., Penza, M., Loreti, S., Menicucci, I., Minarini, C., & Jelinek, M. (2005). Tin oxide thin films prepared by laser-assisted metal–organic CVD: Structural and gas sensing properties. *Surface and Coatings Technology, 200*(1–4), 1057-1060. doi: http://dx.doi.org/10.1016/j.surfcoat.2005.02.131

Lundstrom, I., Spetz, A., Winquist , F., Ackelid, U. and Sundgren, H. (1990) Catalytic metals and field-effect devices- a useful combination. Sensor and Actuators B1,15-20

Marchlloni, F.(2001). Recognition of olfactory signals based on supervised fuzzy C-means and k-NN algorithms. *Pattern Recognition letters*, 22, 1007-1019

Molloy, D. (2015). Exploring BeagleBone: Tools and techniques for building with embedded Linux.

Mukherjee, K., & Majumder, S. B. (2010). Reducing gas sensing behavior of nano-crystalline magnesium–zinc ferrite powders. *Talanta, 81*(4–5), 1826-1832. doi: http://dx.doi.org/10.1016/j.talanta.2010.03.042

Panigrahi, S., Balasubramanian, S., Gu, H., Logue, C. M., & Marchello, M. (2006). Design and development of a metal oxide based electronic nose for spoilage classification of beef . *Science and Actuators B* , *119*, 2-14. doi: 10.1016/J.SNB.2005.03.120

Pearce, T., Schiffman, S., Nagle, H., & Gardner, J. (2003).*Handbook of machine olfaction*. (pp. 105-158). Germany: WILEY-VCH.

Sadeghifard, S., Anjomshoa, M., & Esfandiari, E. (2011, October). *A new embedded e-nose system in smoke detection*. 2011 1st international econference on computer and knowledge engineering , Mashhad. doi: 10.1109/ICCKE.2011.6413317

Schiffman, S.S., Wyrocl, D.W., Gutierrez-Osuna R., & Nagle, H.T. (2001). *Effectiveness of an electronic nose for monitoring bacterial and fungal growth: Electronic Noses and Olfaction 2000: Proceeding of the seventh International Symposium on Olfaction and Electronic Noses*, Brighton, UK, July 2000, 173-180.

Shih, C. H., Lin, Y. J., Lee, K. F., Chien, P. Y., & Drake, P. (2010). Real-time electronic nose based pathogen detection for respiratory intensive care patients. *Sensors and Actuators B: Chemical*, *148*, 153-157. doi: 10.1016/j.snb.2010.04.025

SanKarm, S. (2009). *Novel sensing Materials-Food safety applications,* 59.

Tan, E., & Abdul Halim, Z. (2012, June). *Data acquisition system development of an electronic nose for sulphate-reducing bacteria detection*. 2012 4th international conference on intelligent and advanced system, Kuala Lumpur,Malasia doi: 10.1109/ICIAS.2012.6306079

Tang, K. T., Chiu, S. W., Pan, C. H., Hsieh, H. Y., Liang, Y. S., & Liu, S. C. (2010). Development of a portable electronic nose system for the detection and classification of fruity odors. *Sensors*, *10*, 9179-9193. doi: 10.3390/s101009179

Tang, K. T., Chiu, S. W., Chang, M. F., Hsieh, C. C., & Shyu, J. M. (2011, November). *A wearable electronic nose SoC for healthier living*. Biomedical circuits and system conference , San Diego doi: 10.1109/BioCAS.2011.6107785

Wongchoosuk, C., Lutz, M., & Kerdcharoen, T. (2009). Detection and classification of human body odor using an electronic nose . *Sensors*, *9*(9), 7234-7249. doi: 10.3390/s90907234

Zampolli, S., Elmi, I., Ahmed, F., Passini, M., Cardinali, G. C., Nicoletti, S., & Dori, L. (2004). An electronic nose based on solid state sensor arrays for low-lost indoor air quality monitoring applications. *Sensors and Actuators B*, *101*, 39-46. doi: 10.1016/j.snb.2004.02.024

Zhang, S., Xie, C., Zend, D., Zhang, Q., Li, H., & Bi, Z. (2007). A feature extraction method and a sampling system for fast recognition of flammable liquids with a portable e-nose. *Sensors and Actuators B*, *124*, 437-447. doi: 10.1016/j.snb.2007.01.013

Zhang, L., Tian, F., Liu, S., Guo, J., Hu, B., Ye, Q., Dang, L., Peng, X., Kadri, C., & Feng, J. (2012). Chaos based neural network optimization for concentration estimation of indoor air contaminants by an electronic nose. *Sensors and Actuators A:Physical*, *189*, 161-167. doi: 10.1016/j.sna.2012.10.023

Zhou, B., & Wang, J. (2010). Use of electronic nose technology for identifying rice infestation by nilaparvata lugens. *Sensors and Actuators B: Chemical*, *160*, 15-21. doi: 10.1016/j.snb.2011.07.00

APPENDICES

Appendix A Datasheets

All datasheets can be found from the following websites:

Amphenol Advanced Sensors, Figaro, KNF, Measurement Specialties INC., Microchip, Parker, and Texas Instruments.

Appendix B PCB- E-nose

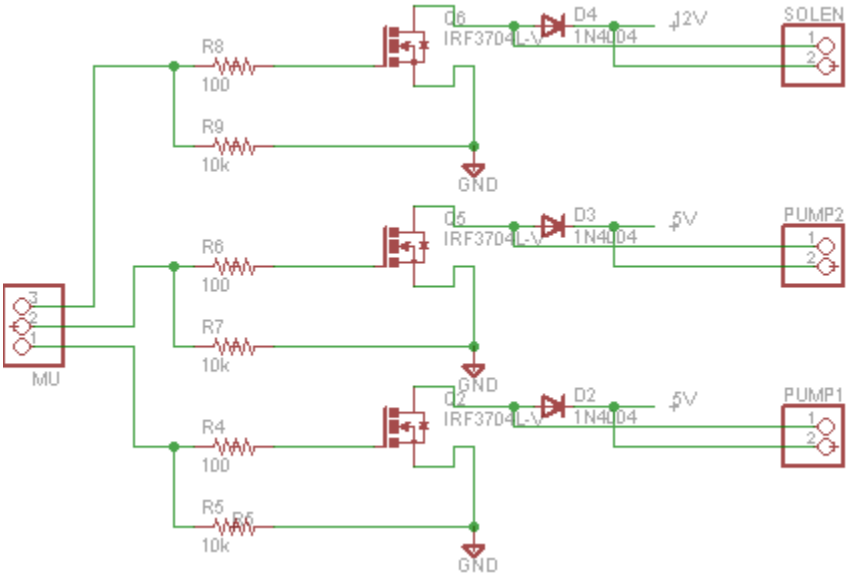

Figure B.1 PCB schematic of pump and solenoid valve drivers

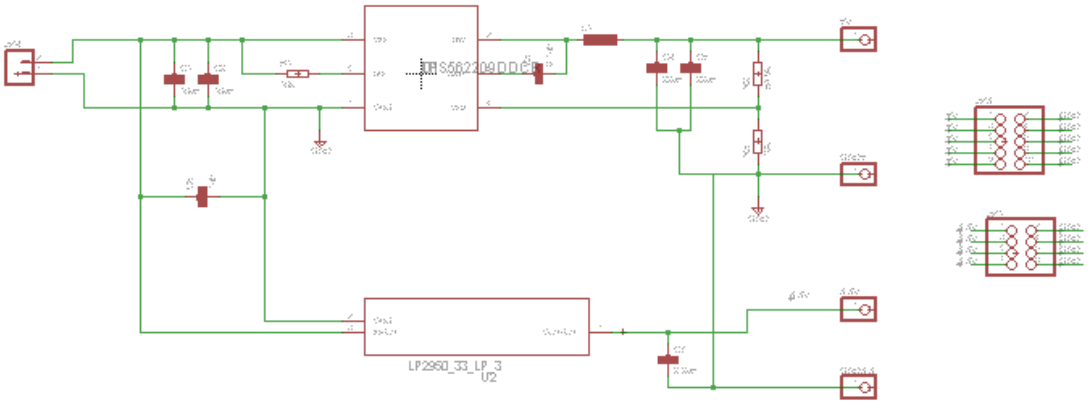

Figure B.2 PCB schematic of Centralized power system

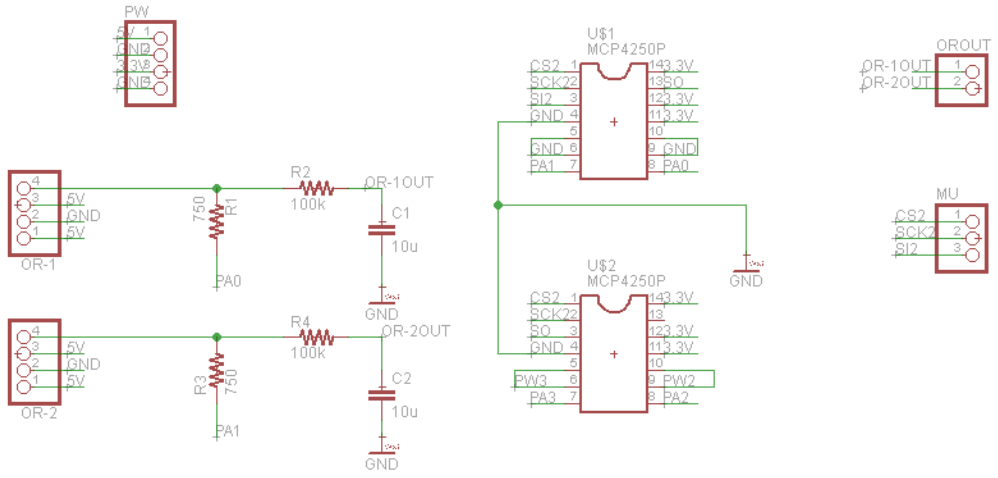

Figure B.3 PCB schematic of VOC sensor hardware acquisition

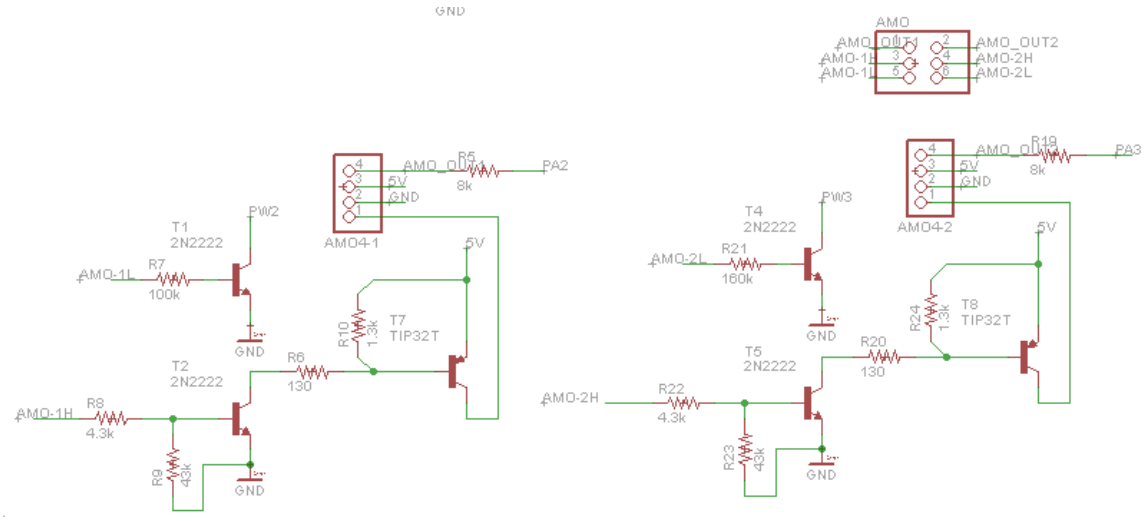

Figure B.4 PCB schematic of Ammonia sensor hardware acquisition

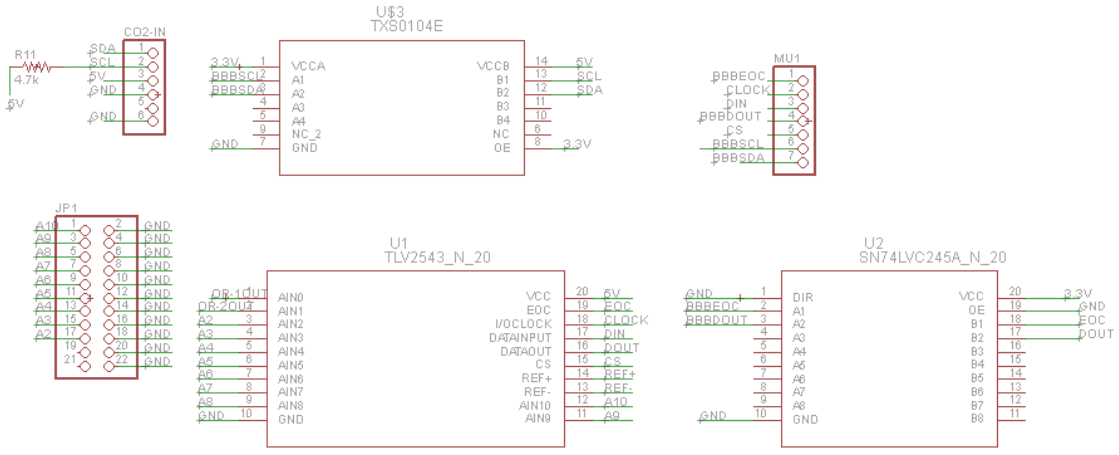

Figure B.5 PCB schematic of CO2 sensor hardware acquisition and external ADC

Appendix C BOM

Commercial Sensor System

Part	Quantity	Unit Price	Extended price
Beaglebone Black	1	$45.00	$45.00
PCBs	1	$52.35	$52.35
Electromechanical System			
Solenoid Valve	1	$131.50	$131.50
drivers	1	$5.32	$5.32
Teflon/tubing	1	$200.60	$200.60
Sensor system			
Ammonia Sensors	2	$61.90	$123.80
CO2 Sensor	1	$95.00	$95.00
Temp&Hum Sensor (HTU21D-F)	1	$14.95	$14.95
Power supply system			
TPS562209-5	1	$20.45	$20.45
LP2950-3.3	1	$14.70	$14.70
AC to 12VDC adapter	1	$26.18	$26.18
Components	1	$40.32	$40.32
Peripherals			
External ADC (TLV2543IN)	1	Sample	Free
OLED MonoChrome 128x32 display	1	$17.50	$17.50
Digital Potentiometer (MCP42050)	2	$1.65	$3.30
Transmission Bus			
point-point board	1	$2.49	$2.49
OR/NOT gate	1	$1.00	$1.00
handling & shipping			$76.88
Total			$871.34

Appendix D PCB Board Layouts

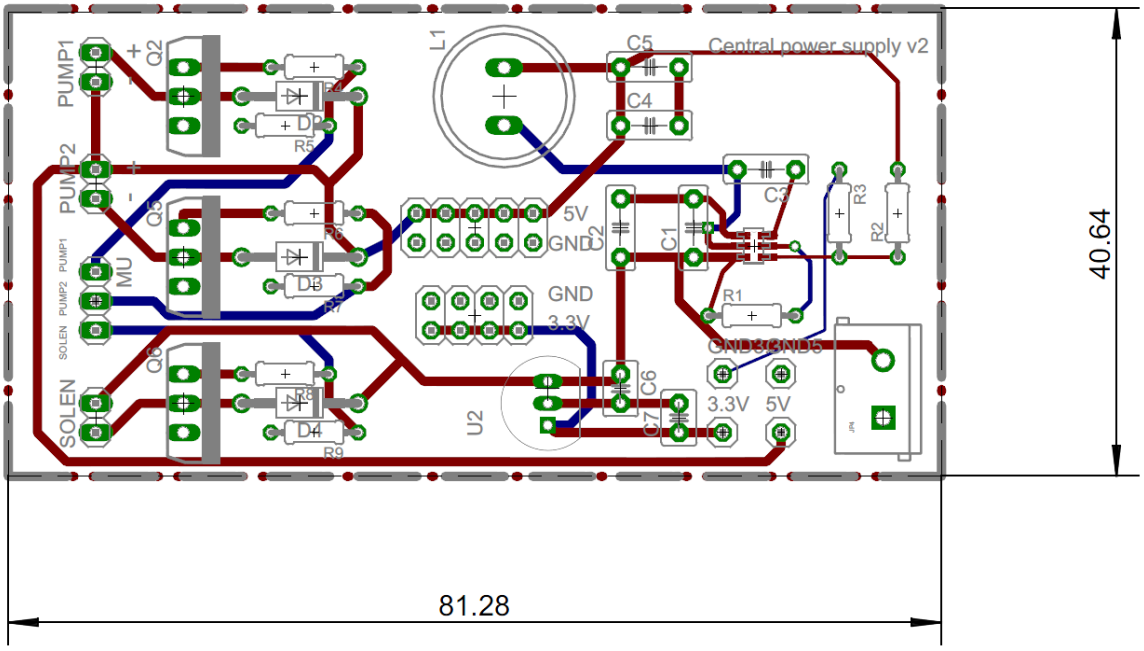

Figure D.1 PCB of centralized power supply using TPS562209

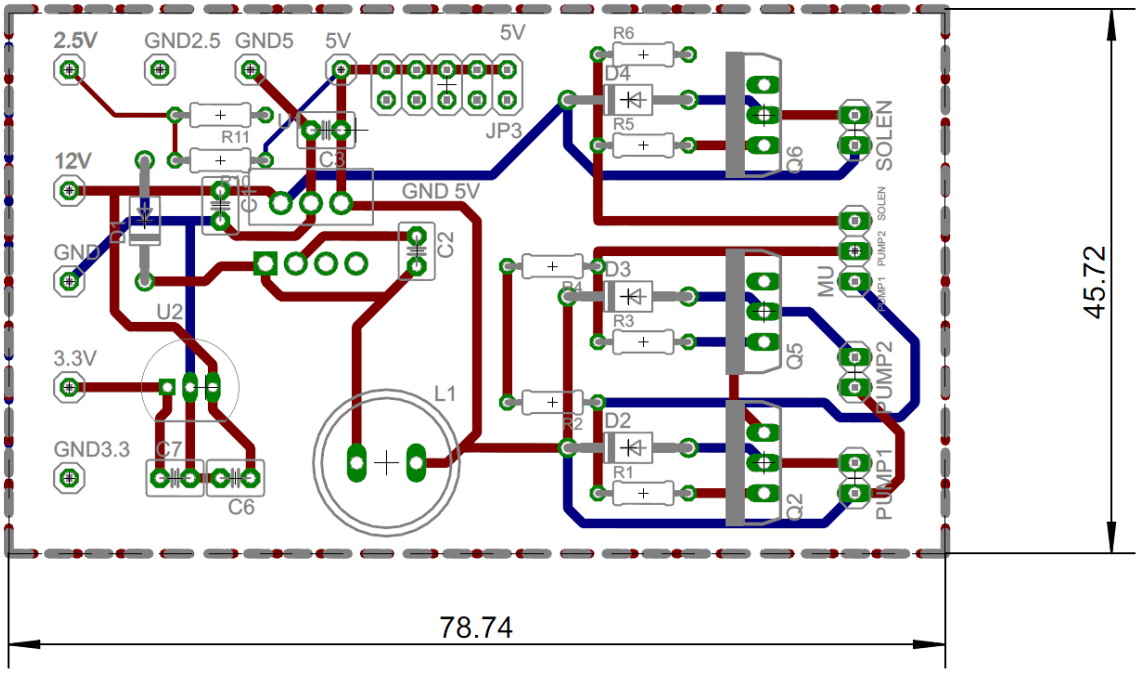

Figure D.2 PCB of centralized power supply using LM2678

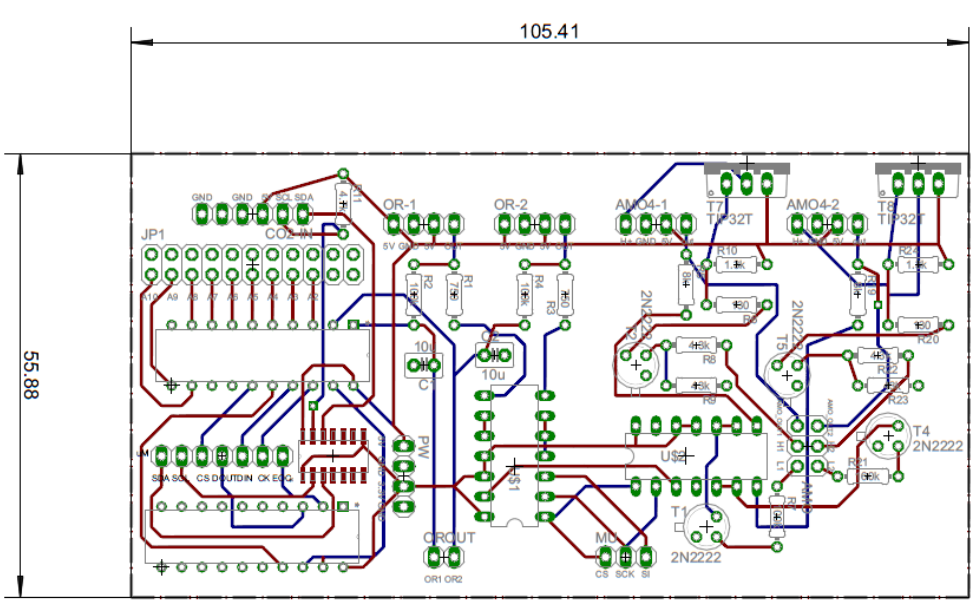

Figure D.3 PCB of sensor acquisition board

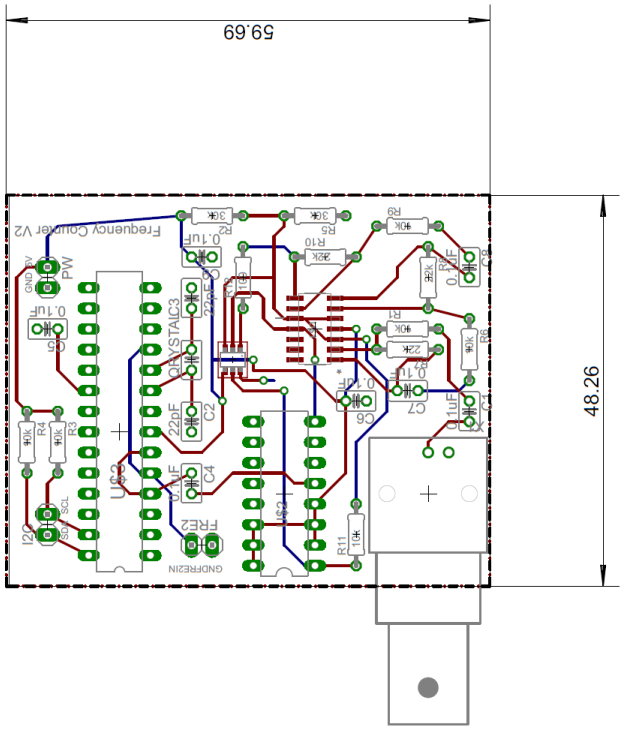

Figure D.4 PCB of QCM

Appendix E Main program for E-nose

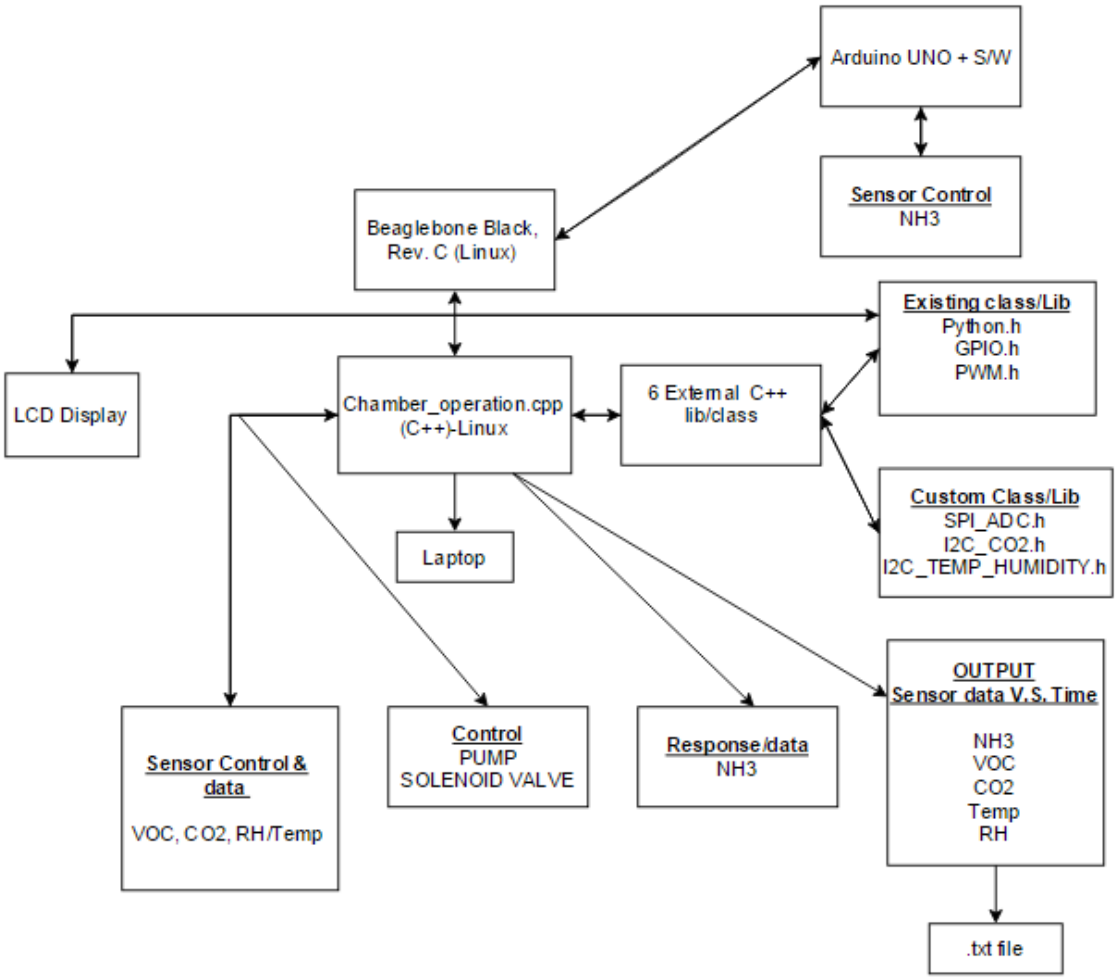

Figure E. The relationship flow chart for main program in Beaglebone black